



Technische Universität München

Robust and Precise Relative Orbit Determination for Distributed Spacecraft using GPS

Dissertation

von

Gerardo Allende Alba

Ingenieurfacultät Bau Geo Umwelt



Technische Universität München
Ingenieur fakultät Bau Geo Umwelt
Fachgebiet Satellitengeodäsie

Robust and Precise Relative Orbit Determination for Distributed Spacecraft using GPS

Gerardo Allende Alba

Vollständiger Abdruck der von der Ingenieur fakultät Bau Geo Umwelt der Technischen Universität München zur Erlangung des akademischen Grades eines

Doktor - Ingenieurs

genehmigten Dissertation.

Vorsitzender: Univ.-Prof. Dr.-Ing. habil. T. Wunderlich

Prüfer der Dissertation: 1. Priv.-Doz. Dr. rer. nat. habil. O. Montenbruck
2. Univ.-Prof. Dr. phil. nat. U. Hugentobler
3. Prof. Dr. Ir. P.N.A.M. Visser
Technische Universiteit Delft, Niederlande

Die Dissertation wurde am 14.07.2017 bei der Technischen Universität München eingereicht und durch die Ingenieur fakultät Bau Geo Umwelt am 03.10.2017 angenommen.

Abstract

In this dissertation, the implementation and evaluation of methods and algorithms for the generation of robust and precise relative orbit solutions have been analyzed. Recent experience with the GRACE and TanDEM-X missions showed the feasibility of obtaining relative navigation solutions with precision at the mm/sub-mm level. A key element to achieve such precision levels is the use of carrier phase observations from the Global Positioning System (GPS) with fixed ambiguities. However, when integer ambiguities cannot be correctly fixed, the precision of final baseline solutions is degraded. Hence, although general baseline precision requirements have been fulfilled, the performance of current algorithms may be downgraded under certain mission conditions affecting a correct integer ambiguity resolution or the estimation scheme in general. This is particularly true for mission profiles with long baselines (due to high ionospheric delays), sundry receiver characteristics (e.g. high pseudorange noise, half-cycle ambiguities) and frequent orbit control maneuvers. In this context, the robustness of schemes, characterized by the preservation of proper functionality of estimation techniques regardless of the formation-flying mission profile, started to play a fundamental role. An imperative demand of high levels of robustness for relative orbit determination systems has thus arisen as a key requirement to allow a reliable long-term generation of precise baseline products.

In a first stage of this research, a dedicated scheme for integer ambiguity resolution in the low Earth orbit (LEO) scenario has been developed. This scheme aims at improving the robustness levels of current approaches by using dedicated algorithms for the estimation and validation of float and integer ambiguities. For float ambiguity estimation, a developed sequential/batch strategy for data arrangement is used together with an a priori-constrained least-squares estimator. Integer ambiguities were estimated using the optimal integer least-squares estimator. Solution ambiguities were validated with a series of theoretical and empirical validation tests. The ambiguity resolution scheme has been complemented with a baseline determination method based on an extended Kalman filter. The proposed algorithms have been extensively tested using flight data from the GRACE, TanDEM-X and Swarm missions to validate their performance under various mission profiles. An improved robustness with GRACE data has been obtained, directly benefiting the long-term availability of precise solutions. State-of-the-art performance has been achieved for the TanDEM-X mission in short and medium-length baseline configurations. Robust functionality and performance with Swarm data in a long baseline scenario has been attained, even in the presence of half-cycle ambiguities.

In a second stage, the overall robustness of the system has been extended. A precise relative orbit determination method based on a batch least-squares estimator has been implemented. This scheme aims to provide more robustness to data gaps and orbit control maneuvers and delivers a relative orbit solution that is completely differentiable (smooth). An important feature of this proposed scheme is the added capability of orbit control maneuver estimation using differential GPS observations. The method has been validated using representative data arcs from the GRACE, TanDEM-X and PRISMA missions. Improved solution quality around

maneuver periods has been obtained for the three missions under analysis. Maneuver estimates were assessed using a proposed technique called *dummy* maneuvers insertion. An improved precision of maneuver estimates has been achieved, with potential benefits for maneuver calibration in flight dynamics operations.

Zusammenfassung

Die Implementierung und Auswertung von Methoden und Algorithmen für die Erzeugung von hochpräzisen Relativbahnbestimmungslösungen wurden in dieser Dissertation analysiert. Die jüngsten Erfahrungen mit den GRACE und TanDEM-X Raumfahrtmissionen haben die Durchführbarkeit von Relativnavigationen mit mm/sub-mm Präzision gezeigt. Ein entscheidendes Element, um einen solchen Präzisionsgrad zu erreichen, ist die Anwendung von Trägerphasenmessungen vom Global Positioning System (GPS) mit festgesetzten Mehrdeutigkeiten. Jedoch, wenn ganzzahlige Mehrdeutigkeiten nicht richtig festgesetzt sind, die Präzision von Basislinielösungen ist abgebaut. Daher, obwohl die generelle Voraussetzungen um Basisliniepräzision erfüllt wurden, die Leistung von heutigem Algorithmen kann unter bestimmten Bedingungen degradiert werden. Dies ist besonders wahr für Missionprofilen mit langen Basislinien (wegen hoher ionosphärischer Laufzeitverschiebungen), verschiedenen Empfängereigenschaften (hoch Pseudorange Rausch, Halbzyklus-Mehrdeutigkeiten) und häufigen Bahnregelungsmanövern. In diesem Kontext, die Robustheit der Systeme, die durch die Erhaltung der Funktionalität von Schätzungsmethoden ungeachtet von Missionprofilen charakterisiert werden kann, begann eine grundlegende Rolle zu spielen. Ein unerlässlicher Bedarf an hohen Robustheitsgraden für Relativebahnbestimmungssysteme hat sich als eine entscheidende Voraussetzung für eine verlässliche und langfristige Erzeugung von hochpräzisen Orbitprodukten herauskristallisiert.

In der Anfangsphase dieser Forschung wurde, ein dediziertes Verfahren für Mehrdeutigkeitsauflösung im niedrigen Erdorbit (LEO) entwickelt. Dieser Ansatz zielt auf die Verbesserung des Robustheitsgrades von aktuellen Methoden, indem er dedizierte Algorithmen für die Bestimmung und Validierung von reellwertigen und ganzzahligen Mehrdeutigkeiten anwendet. Für die Bestimmung reellwertiger Mehrdeutigkeiten wurde eine entwickelte sequenzielle/stapelweiseverarbeitete Strategie für Datenordnung angewendet, zusammen mit einem a priori-einengenden Least-Squares Schätzer. Ganzzahlige Mehrdeutigkeiten wurden mit einem optimalen Integer Least-Squares Schätzer geschätzt. Lösungsmehrdeutigkeiten wurden mit einer Reihe von theoretischen und empirischen Validierungstests überprüft. Das Mehrdeutigkeitsauflösungsverfahren wurde durch eine Extended-Kalman-Filter-basierte Basislinienbestimmungsmethode ergänzt. Die vorgeschlagenen Algorithmen sind mit Flugdaten der GRACE, TanDEM-X und Swarm Raumfahrtmissionen ausgiebig getestet worden, um ihre Leistung unter verschiedenen Missionprofilen zu bestätigen. Eine verbesserte Robustheit mit Daten der GRACE Mission wurde erhalten, die direkte Vorteile zur Verfügbarkeit von hochpräzisen Lösungen bietet. Eine state-of-the-art Leistung wurde mit Daten der TanDEM-X Mission in Konfigurationen von kurzen und mittellangen Basislinien erhalten. Robuste Funktionalität und Leistung wurden mit Daten der Swarm Mission in einem Langebasislinie-Szenario erhalten, auch in Anbetracht von Halbzyklus-Mehrdeutigkeiten.

In einer zweiten Phase wurde die gesamte Robustheit des Systems weiterentwickelt. Eine Least-Squares-basierte Methode für hochpräzise Relativbahnbestimmung wurde implementiert. Dieses Verfahren zielt darauf ab, eine höhere Robustheit gegen Datenlücken und Bahnregelungs-

manövern zu schaffen, und dazu liefert es eine Relativbahnlösung, die voll differenzierbar ist. Eine wichtige Eigenschaft dieses vorgeschlagenen Verfahrens ist die zusätzliche Möglichkeit einer Bahnregelungsmanöverschätzung durch differentielle GPS-Messungen. Die Methode wurde mit Flugdaten aus repräsentativen Phasen der GRACE, TanDEM-X und PRISMA Raumfahrtmissionen bestätigt. Eine verbesserte Qualität von Relativbahnlösungen in der Nähe der Manöverzeitpunkte wurde für die drei hier analysierten Raumfahrtmissionen erhalten. Manöverschätzungen wurden durch die Nutzung eines vorgeschlagenen Verfahrens namens *Dummy*-Manöver-Einführung beurteilt. Eine verbesserte Präzision der Manöverschätzungen wurde erhalten, die potenzielle Vorteile für Manöverkalibrierung in Flugdynamikbetrieben haben könnte.

Table of contents

Preface	xi
1 Introduction	1
1.1 Formation flying missions in low Earth orbit	1
1.1.1 GRACE	2
1.1.2 TanDEM-X	4
1.1.3 PRISMA	6
1.1.4 Swarm	7
1.2 GNSS-based space baseline determination	9
1.2.1 Precise orbit determination	9
1.2.2 Precise baseline determination	10
2 Research progress and state-of-the-art methods	13
2.1 Challenges for precise relative orbit determination	13
2.1.1 Duration of signal tracking periods	13
2.1.2 Ionospheric delays	14
2.1.3 Orbit control maneuvers	20
2.2 Previous research and milestones	21
2.2.1 Batch scheme and WL/NL ambiguity resolution	21
2.2.2 Sequential scheme and on-the-fly ambiguity resolution	22
2.3 Path for this research	24
2.3.1 A requirement on robustness	24
2.3.2 Issues, considerations and questions	24
3 Synoptic description of this research	29
3.1 Context and framework	29
3.2 Main contributions	30
3.3 Software tools and implementation	32
3.4 Description and discussion of publications	34
3.4.1 [Pub 1] Robust integer ambiguity resolution	35
3.4.2 [Pub 2] Half-cycle ambiguities and space baseline determination	39
3.4.3 [Pub 3] Robust relative orbit determination and maneuver estimation	44
3.5 Conclusions	49
4 Lessons learned and outlook	51
4.1 Considerations and open questions	52
4.2 Recommendations and outlook	54

A Methodology for integer ambiguity resolution	57
A.1 Arrangement of processing batches	57
A.2 Float ambiguity estimation	59
A.3 Integer ambiguity estimation and validation	60
A.3.1 Hypothesis test	61
A.3.2 Ratio test integer aperture estimator	64
A.3.3 (Semi-)empirical test with widelane residuals	68
A.3.4 Approaches for partial ambiguity resolution	71
A.4 Half-cycle ambiguity processing	73
References	75
Appendix A Publication 1	85
Appendix B Publication 2	105
Appendix C Publication 3	117

Preface

This cumulative dissertation has been written based on the following publications:

- Allende-Alba, G. and Montenbruck, O. (2016) *Robust and precise baseline determination of distributed spacecraft in LEO*. *Advances in Space Research* 57(1):46-63, doi: 10.1016/j.asr.2015.09.034.
- Allende-Alba, G., Montenbruck, O., Jäggi, A., Arnold, D. and Zangerl, F. (2017) *Reduced-dynamic and kinematic baseline determination for the Swarm mission*. *GPS Solutions* 21(3):1275-1284, doi: 10.1007/s10291-017-0611-z.
- Allende-Alba, G., Montenbruck, O., Ardaens, J.-S., Wermuth, M. and Hugentobler, U. (2017) *Estimating maneuvers for precise relative orbit determination using GPS*. *Advances in Space Research* 59(1):45-62, doi: 10.1016/j.asr.2016.08.039.

The first paper is introduced and described in §3.4.1 and deals primarily with the problem of developing a scheme for robust integer ambiguity resolution for precise baseline determination. The second publication is devoted to the analysis of half-cycle ambiguities in GPS carrier phase observations in the context of baseline determination for the Swarm mission. This publication is introduced and described in §3.4.2. Finally, the third publication is introduced in §3.4.3 and it is devoted to the problem of robust relative orbit determination and maneuver estimation. The published version of each paper has been reproduced in Appendices A - C applying minor re-formatting changes.

Chapter 1 provides a brief introduction to the spacecraft formation flying technology in low Earth orbit (LEO) and the space missions that have been fundamental for the development of this research. Additionally, a reference to the key elements of space baseline determination techniques using GNSS observations is provided. Chapter 2 presents a brief description of the main challenges for precise relative orbit determination in LEO and the current research progress and state-of-the-art strategies to cope with such challenges. In addition, this chapter describes some of the main issues and open research questions that serve as starting point for the present research. Chapter 3 briefly introduces the context and framework of this research and it is mainly devoted to the description of the main contributions made by this study. Each publication is summarized and discussed according to the most significant obtained results. Finally, Chapter 4 provides a posterior analysis of this research, describes the most important lessons learned and provides some recommendations for future research.

An additional chapter, denoted as Addendum, has been devoted to expand the description of the methodology for integer ambiguity resolution proposed in this research. This chapter provides (additional) results from a series of tests performed with various configurations of the proposed ambiguity validation scheme.

Chapter 1

Introduction

Spacecraft formation flying is a key concept for many current and future space missions. Among other things, it enables the implementation of spaceborne distributed instrumentation used for the scientific, engineering and commercial applications as well as the application of the on-orbit servicing technique. The main concept consists in the active control of two or more spacecraft in order to either act as a single spaceborne instrument or to execute proximity and rendezvous maneuvers. One of the main advantages of this concept is the implementation of large spaceborne instrumentation that would be otherwise too expensive or too complex to deploy if monolithic spacecraft were used. In addition, an improved resolution and coverage from the remote sensing platform is achieved (Leitner, 2002). Aside from that, this technology makes it possible to perform on-orbit spacecraft maintenance and/or substitution in future space concepts, such as distributed satellites (Long et al., 2007; Ross et al., 2004). Similarly, spacecraft formation flying represents a key element in some proposals concerning the management of space debris on Earth orbit (Peters, 2016).

This chapter provides a brief introduction to some of the basic concepts of spacecraft formation flying, including a concise description of the space missions that have been used for the analysis of concepts and methods proposed in the present work. In addition, this chapter provides a brief overview of key concepts involved in orbit and baseline determination using Global Navigation Satellite System (GNSS) observations, paving the way for the analysis of challenges in state-of-the-art and proposed solutions described in following chapters.

1.1 Formation flying missions in low Earth orbit

The formation flying technology has been explored since the dawn of the space age. One of the first and most important applications of the technology was the execution of proximity and rendezvous maneuvers for the assembly of large structures on-orbit (Vogeley and Brissenden, 1963). Along the years, the concept has evolved to incorporate various techniques and to enable different and diverse applications, ranging from gravimetry and Earth's mass distribution (Velicogna, 2009) to synthetic aperture radar (SAR) interferometry (Rosen et al., 2000).

In general, the formation flying concept does not have an agreed or commonly accepted definition. For example, the Goddard Space Flight Center (GSFC) of the National Aeronautics and Space Administration (NASA) describes such a technology as a special case of a more general category, known as *distributed space systems* (Alfriend et al., 2010) and defined as

An end-to-end system including two or more space vehicles and a cooperative infrastructure for science measurement, data acquisition, processing, analysis and distribution.

The overall complexity of the concept consists in the coordination of various spacecraft in order to perform a given task. Such a complexity unfolds mostly in requirements of very accurate positioning/navigation and orientation of the spacecraft in the formation. Depending on the characteristics of the mission, formation control can be performed ground-based, employing the ground-in-the-loop concept or fully autonomous. The latter approach has received particular attention in recent lustra as it represents a step forward for the implementation of more complex systems. The first example of an autonomous formation flying mission is the Japanese ETS-VII (Kiku-7) mission, launched in 1997 (Kawano et al., 2001). The mission consisted of two satellites (*chaser* and *target*), which successfully performed rendezvous and docking operations in relative distances ranging from 10 km to 2 m and below. Since those years, various mission concepts involving diverse formation geometries and formation control approaches have been explored and put into practice in real missions.

In general terms, it is possible to loosely classify formation-flying missions according to their coordination approach. Among the various concepts, it is possible to distinguish the trailing (or leader/follower) formation, the virtual structure, the cluster formation and the swarming technique (Alfriend et al., 2010; Graziano, 2013). Various of the formation-flying missions that have been developed so far have specific characteristics that allow to classify them in one of the aforementioned groups. However, specific mission requirements and the various spacecraft cooperation techniques are among the most common criteria to define and distinguish formation-flying missions. Particularly important for this study have been those missions for which the determination of relative orbits with high precision is of fundamental significance for the fulfillment of mission objectives. The following sections sketch some of the main scientific and technological characteristics of the four formation-flying missions that have been addressed in this study.

Although the specific details of each control approach may vary in the literature, such concepts provide a starting point in mission design stages according to specific scientific or technology demonstration goals. In this work, distinction among different missions is made only according to the specific mission profile and objectives, given the application of the presented methods and results. Due to the vast amount of information regarding each mission, the brief introduction provided in this section is given only in terms of the overall mission characteristics, formation geometries and scientific/engineering goals, intending to provide the required background for the analysis of tests and results described in following chapters.

1.1.1 GRACE

The Gravity Recovery And Climate Experiment (GRACE) mission is a joint project between the NASA and the German Aerospace Center (DLR). It was launched on March 17, 2002 and consist of two identical spacecraft (called GRACE A and GRACE B) located on the same orbit with an along-track separation of 220 (± 50) km. Each of the satellites had an initial mass of 485 kg and both were launched into a near-circular orbit with an initial altitude of about 490 km at an inclination of 89° on-board a Eurockot launch vehicle from Plesetsk, Russia. The main objective of the mission is to map the Earth's global gravity field with a spatial resolution of 400 km to 40,000 km every thirty days (Tapley et al., 2004). The mission was initially planned

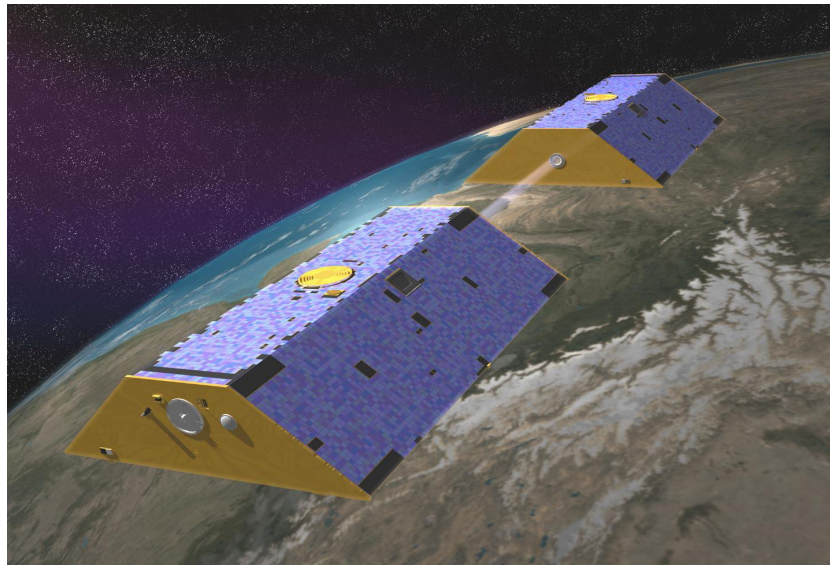


Fig. 1.1 Artist's depiction of the GRACE formation (Source: NASA/JPL)

to operate for 5 years (Tapley and Reigber, 2001; Watkins and S., 2000) but, by the time of writing, it has accomplished 15 years in orbit.

For the creation of the Earth's global gravity field map, the spacecraft make use of accurate measurements of the inter-satellite distance by means of a K/Ka-band ranging (KBR) system at the μm level (Tapley et al., 2004). In addition, each satellite carries a geodetic-class Global Positioning System (GPS) receiver for precise 3D satellite tracking and radio occultation measurements (Dunn et al., 2003) and a high precision micro-accelerometer (SuperSTAR) for the measurement of surface accelerations due to air drag and solar radiation pressure (Touboul et al., 1999). Aside from the generation of gravity field models, the estimates obtained from data gathered by the GRACE instruments provide valuable information, with unprecedented accuracy, for the specific analysis of the Earth's global mass distribution and its temporal variations (Kirschner et al., 2013). Prominent results include the study of hydrology, oceanic mass distribution and ice mass loss at the polar regions (see e.g. Morison et al. (2007); Neerem et al. (2003); Tiwari et al. (2009); Velicogna (2009)).

Attitude and formation control

Given that the GRACE spacecraft are themselves considered part of the instrumentation for the measurement of the Earth's gravity field, the attitude and orbit control system is affected in various ways. The inter-spacecraft distance should be controlled within a window of ± 50 km around a mean separation of 220 km and the attitude should be maintained within dead bands of $\leq 3\text{-}5$ mrad (Kirschner et al., 2013). During science data collection, both spacecraft are nominally maintained in a 3-axis stabilized (near Earth-pointing) orientation in order to have both KBR antennas precisely aligned at each other (Fowler et al., 2000). Two sets of six 10 mN cold gas nitrogen (GN_2) thrusters are used for attitude control (Schelke, 2000), which are used together with magnetic torque rods on each axis with maximum moment of 110 Am^2 . Each set of thrusters is connected to a GN_2 tank and the torque rods have redundant double coils (Kirschner et al., 2013).

For orbit control each of the two spacecraft has been equipped with two 40 mN GN₂ thrusters located in the anti-flight direction (Schelke, 2000). The orbit maintenance strategy has been to maximize the time between maneuvers in order to counteract the effects of conservative and non-conservative perturbations on the spacecraft trajectories. Based on the characteristics of the designed relative trajectories and the ballistic coefficients of the spacecraft (differing mainly due to the different pitch angle and orientation of each satellite to ensure a line-of-sight orientation), these maintenance maneuvers have been planned to be executed with a maximum rate of 12 maneuvers per year (Kirschner et al., 2001).

1.1.2 TanDEM-X

The TerraSAR-X mission is a German project based on a public-private partnership between the DLR and EADS Astrium GmbH and it has been targeted at the production of scientific and commercial applications (Werninghaus et al., 2004). The spacecraft was successfully launched on June 15, 2007 from Baikonur, Kazakhstan on a Russian/Ukrainian Dnepr-1 launch vehicle into a near-circular orbit at an altitude of about 515 km and an inclination of 97°. The TerraSAR-X (TSX) satellite has been equipped with an advanced high-resolution X-band Synthetic Aperture Radar (SAR) based on active phase array antenna technology. The system targets at the operation in different SAR modes and various polarizations, including Spotlight-, Stripmap- and ScanSAR (Ochs and Pitz, 2007; Werninghaus et al., 2004). The technology on board TerraSAR-X allows to combine the ability to acquire high resolution images (for detailed view analysis) and wide swath images for overview applications. Additionally, experimental modes allow applications such as moving target identification (Buckreuss et al., 2008).

The TerraSAR-X add-on for Digital Elevation Measurements (TanDEM-X or TDX) spacecraft was successfully launched on June 21, 2010 from Baikonour, Kazakhstan on a Dnepr-1 launch vehicle into a close orbit with TSX. Both spacecraft conform the TanDEM-X mission¹ and it represents an extension of the TerraSAR-X mission by coflying two satellites of nearly identical capability in close formation (Krieger et al., 2007). Both satellites act as a large single-pass SAR interferometer with the added feature of flexible baseline dimension. The primary mission objective of TanDEM-X is the generation of a worldwide, consistent, timely and high precision digital elevation model (DEM), which should be aligned with the HRTI-3 (High Resolution Terrain Information) specification (Krieger et al., 2010). By using SAR interferometry, the TanDEM-X mission enables highly precise measurements of important geophysical parameters such as surface topography, glacier movements and ground deformation and subsidence (Moreira et al. (2013) and references within).

The instrumentation in both spacecraft consist of advanced high-resolution X-band synthetic aperture radars based on active phased array technology. In addition, each spacecraft has a system of X-band horn antennas for inter-satellite phase synchronization (Krieger et al., 2013). Both spacecraft have been each equipped with a total of three GPS receiver units. A redundant pair of single-frequency receivers for onboard time synchronization and real-time GPS navigation solutions. The third unit consists of a geodetic class GPS receiver used primarily for precise orbit and baseline reconstruction (Montenbruck et al., 2011).

¹As there is not always a clear distinction in the literature concerning names, in this work the spacecraft are referred to as TSX and TDX whereas the mission as a whole is called TanDEM-X.

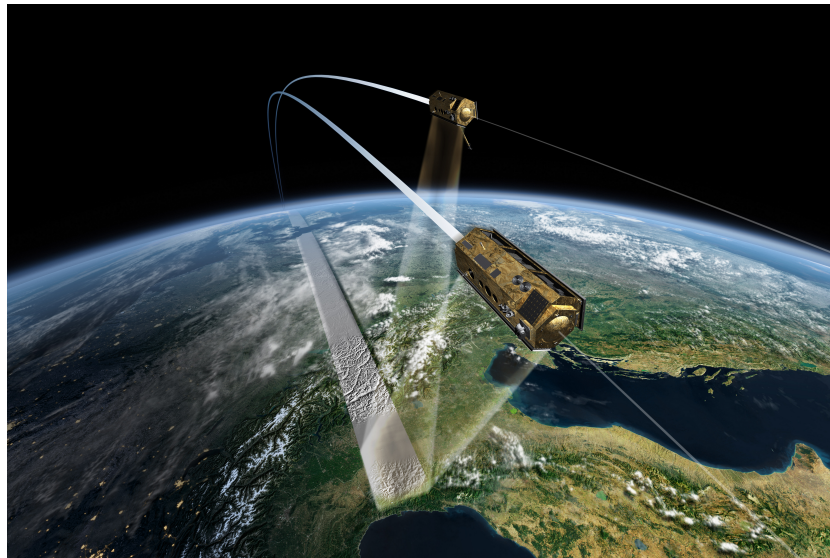


Fig. 1.2 Artist's depiction of the TanDEM-X formation (Source: DLR)

Attitude and formation control

For the acquisition of the DEM, the TanDEM-X formation requires that both satellites are operated coordinately in close formation. The chosen geometry is based on the concept of relative eccentricity/inclination vector separation (D'Amico and Montenbruck, 2006), which creates a helix-like relative motion of the spacecraft along the orbit (Kahle et al., 2012). For TSX, the attitude in the standard operational modes is controlled within 0.3 mrad and four reaction wheels with a torque capability of 0.2 Nm. Continuous wheel unloading is carried out by magnetic torque rods that are mounted parallel to the spacecraft's axes (Herman et al., 2010). When using the so-called safe mode, the TDX spacecraft uses the same strategy for attitude control (Maurer et al., 2012).

For orbit control, both the TSX and TDX spacecraft have been equipped with four 1N hydrazine (H_2N_4) thrusters, installed in the anti-flight direction. In addition, two 40mN GN_2 thrusters were added to the TDX spacecraft in order to enable fine-tuning for formation keeping (Herman et al., 2010). The TSX osculating orbit is maintained within a maximum absolute radial/cross-track distance of 250 m from a target Earth-fixed reference orbit (Arbinger et al., 2004; D'Amico et al., 2004). Orbit maneuvers to counteract luni-solar and atmospheric drag perturbations are performed 3-5 times per year (out-of-plane) except during periods of high solar activity, for which a rate of up to 3 maneuvers per week (in-plane) is necessary. For the task of formation maintenance the TDX spacecraft must execute daily in-plane maneuvers (using GN_2 thrusters) to compensate the natural eccentricity vector drift and control the along-track separation perturbed mainly by atmospheric drag. Additionally, H_2N_4 thrusters are used in TDX in order to replicate maneuvers executed by TSX as well as to perform out-of-plane maneuvers in order to counteract the natural drift of the eccentricity vector (Kahle et al., 2012).



Fig. 1.3 Artist's depiction of the PRISMA formation (Source: DLR)

1.1.3 PRISMA

The PRISMA mission emerged as an initiative of the Swedish National Space Board and OHB Sweden (Bodin et al., 2009; Persson et al., 2009). It was successfully launched on 15 June 2010 atop a Dnepr-1 rocket from the Yasny/Dombrovsky launch site, Russia. The mission comprises two spacecraft of different characteristics. The chief spacecraft is denominated Mango and consist of a three-axis-stabilized vehicle with 3D Δv maneuverability. The deputy spacecraft is called Tango and it has a three-axis attitude control system with no maneuver capabilities (D'Amico et al., 2012).

The main mission objectives are the validation and demonstration of sensors, actuators and experiments for formation flying and rendezvous. The mission has been supported by the German Aerospace Center (DLR/GSOC), the French Space Agency (CNES) and the Technical University of Denmark (DTU) with key instrumentation for formation flying, homing, rendezvous and proximity operations (Bodin et al., 2012). In particular, CNES contributed with the Formation Flying Radio-Frequency (FFRF) sensor for the execution of guidance, navigation and control (GNC) experiments (Harr et al., 2008). DTU provided the Vision-Based Sensor (VBS) which is implemented in the autonomous star-tracker with two extra rendezvous cameras (Benn and Jørgensen, 2008). DLR/GSOC contributed with the instrumentation and software of a GPS-based absolute and relative navigation system (D'Amico et al., 2009).

During the nominal mission, several GNC experiments using the aforementioned navigation sensors and systems were performed. These experiments included passive GPS-based formations and reconfigurations, three-dimensional forced motion, autonomous vision-based rendezvous, formation keeping and closed-loop experiments involving passive and forced motion within rendezvous and collision avoidance operations (Bodin et al., 2012). In addition, alternative propulsion systems were tested for the first time in space in a mission like this one. The Swedish Space Corporation (SSC) and ECAPS (a subsidiary of SSC) provided the High Performance Green Propellant (HPGP) propulsion system (Anflo and Möllerberg, 2009), which aims at providing an alternative to hydrazine propulsion systems. SSC and NanoSpace (a subsidiary of SSC) provided a micro-electro-mechanical system (MEMS)-based propulsion system (Rangsten et al., 2011), which aimed to acquire space flight qualification.

Attitude and formation control

As briefly stated previously, the Mango spacecraft is a three-axis stabilized spacecraft. It has been equipped with three propulsion systems, two of them experimental (HPGP and MEMS). The main propulsion system consists of six 1N hydrazine thrusters with an approximate Δv capability of 120 m/s. On the other hand, the Tango spacecraft has a three-axis-stabilizing, magnetic attitude control system (D'Amico et al., 2012).

Being a technology demonstration mission, PRISMA underwent several tests of formation flying strategies and configurations, using various navigation and propulsion systems. All of these operations were executed under the framework of various GNC modes, with two backbone modes known as Safe and AFF, which used GPS as primary navigation system (D'Amico et al., 2013). Similarly, among the experimental GNC modes, the so-called DLR mode was based on the GPS sensor for the execution of formation flying operations. For this research, only the mission stages within the DLR GNC mode have been relevant and they are briefly described in this section.

During the GNC DLR mode, the Spaceborne Autonomous Formation-flying Experiment (SAFE) was conducted. The main aim of this experiment was the demonstration of fuel-efficient long-term autonomous acquisition, reconfiguration and keeping of passive relative orbits in routine operations (D'Amico et al., 2013). During the SAFE, the formation is mainly operated in closed-loop mode. The GNC approach uses the method of relative eccentricity and relative inclination separation to minimize collision risk and reduce J_2 secular effects on the formation (D'Amico and Montenbruck, 2006). The SAFE is composed of two operational slots called Autonomous Formation Control (AFC) 1 and 2. The duration of both slots was 16 and 19 days, respectively. In total, 22 formation flying geometries were exercised during SAFE. The key tasks of such geometries were the acquisition, maintenance and reconfiguration over prescribed time intervals (D'Amico et al., 2012). During the first days of AFC1 and AFC2 (after verification phase), the mean along-track separation was stepwise reduced from approximately 2-5 km down to rendezvous (i.e. zero distance). These operations were followed in AFC2 by flyaround and inspection phases, where the relative eccentricity and inclination vectors are stepwise reduced to a minimum separation of 20 m (D'Amico et al., 2012).

1.1.4 Swarm

Swarm is an Earth Explorer mission from the European Space Agency (ESA) and approved as part of the Living Planet Program (Friis-Christensen et al., 2006). It was successfully launched on 22 November 2013 atop an Eurokot launch vehicle from Plesetsk, Russia. The mission comprises three spacecraft called the Earth's Magnetic Field and Environment Explorers, commonly denominated as Swarm satellites A, B and C. The planned orbit configuration consists in the deployment of two spacecraft with an east-west separation of 1° - 1.5° at an initial altitude of around 480 km and a third spacecraft in a higher orbit with an initial altitude of around 530 km (Mackenzie et al., 2014).

The main goal of the Swarm mission is to provide a highly accurate survey of the Earth's magnetic field and its temporal evolution. The three spacecraft are designed to simultaneously obtain a space-time characterization of internal field sources (core, mantle, etc.) as well as ionospheric-magnetospheric current systems (Friis-Christensen et al., 2006). The multi-spacecraft concept of the mission was developed in order to take advantage of currently obtainable instrument precision (Friis-Christensen et al., 2006). In particular, internal sources



Fig. 1.4 Artist's depiction of the Swarm formation (Source: ESA)

of the magnetic field are measured in an Earth-fixed frame, whereas external sources are ordered primarily in a local time frame. A mission with several spacecraft orbiting the Earth at different local times provides an adequate spatial coverage of the external field sources. If, in addition, the mission concept considers spacecraft in polar orbits, it is possible to obtain a reasonably dense sampling of the internal field (Friis-Christensen et al., 2008).

Each Swarm spacecraft has been equipped with scalar and vector field magnetometers to measure the direction of the magnetic field in space and its strength (Fratter et al., 2016). Additionally, to enhance the determination of the contributions to the magnetic field from ionospheric currents, the spacecraft are equipped with the Canadian Electric Field Instrument (CEFI) (Friis-Christensen et al., 2008). The core instrumentation has been complemented with an accelerometer to provide information on the state of the atmospheric/ionospheric environment (Visser et al., 2013) and geodetic-class GPS receivers for the generation of precise science orbits (van den IJssel et al., 2015).

Attitude and formation control

The Swarm spacecraft use a propulsion system based on cold gas Freon 14 (GCF_4), which is used to feed two low pressure systems. Each system consists of two pairs of 50 mN thrusters for orbit control. The first pair has been installed in anti-flight direction and the second pair on the side of the spacecraft for inclination control. In addition, these systems include eight 20 mN thrusters for attitude control (Mackenzie et al., 2014).

After the completion of the orbit acquisition phase, the three spacecraft have been placed in a constellation with Swarm A and Swarm C orbiting at an altitude of around 468 km with inclination of 87.35° and Swarm B at an altitude of 516 km with inclination of 87.75° (Sieg and Diekmann, 2016). The two lower spacecraft have been separated by a RAAN difference of 1.4 degrees. The side-by-side constellation is maintained with an along-track separation of 4-10

seconds of ascending node crossing time. The eccentricity vectors of Swarm A and Swarm C are kept close enough to ensure an altitude difference of less than 5 km. The orbit eccentricities of both orbits are enforced to be as close as possible for mitigation of collision risks (Diekmann et al., 2016). Up to mid 2016, an eccentricity threshold corresponding to an altitude difference of 67 m was applied. During a period of about 2 years of nominal operation, this threshold was exceeded only on February 2016, which required the execution of an eccentricity control maneuver (Sieg and Diekmann, 2016).

Notes on terminology

In the present study, the terms *space baseline determination* and *relative orbit determination* have been used interchangeably in almost all cases. However, the latter term has been preferred for scenarios when orbit control maneuvers are taken into account in the estimation problem and in the analysis of results. In this respect, the term precise relative orbit determination can be considered as a more general concept. This can be interchanged by the term precise baseline determination when orbit control maneuvers are either not present in the estimation problem or not a fundamental part of the orbit determination analysis.

Additionally, the term *Global Navigation Satellite System* has been used for all cases where general navigation concepts are introduced or explained (i.e. applicable for any or most of navigation systems). When referring to specific data or concepts applicable only to one particular system, the term GNSS is replaced correspondingly. This is particularly applicable for discussions involving real flight data, given that this dissertation deals only with observations from GPS receivers. Similarly, it is important to mention that the analysis carried out in this study is restricted to systems with an availability of measurements of up to two frequencies. No techniques devoted to triple-frequency observations are treated.

1.2 GNSS-based space baseline determination

Orbit and space baseline products are of primary importance for the generation of remote sensing and Earth observation products from distributed spacecraft missions. Since various years, GNSS has been identified as a key technology for the generation of real-time and offline (also known as on-ground) orbit and positioning solutions. For this study, offline products have been the primary focus of analysis, for which the precision requirements are typically more stringent in comparison with real-time systems. In order to fulfill such requirements, a variety of statistical orbit and baseline determination schemes are used together with precise GNSS observations and positioning models. This section provides a brief overview of key concepts involved in GNSS-based orbit and baseline determination.

1.2.1 Precise orbit determination

The theory of relative motion in space is built upon the framework of single spacecraft dynamics. The key element in such a theory is the description of spacecraft motion under the influence of several interactions. Although the accelerations due to conservative forces can be modeled with reasonable accuracy (for most applications), non-conservative forces impose a major difficulty for high-precision applications using purely dynamic methods for spacecraft trajectory and velocity determination. Depending on the targeted application, an alternative to a purely-

dynamic orbit determination consists in using only GNSS observations to perform a statistical adjustment of the spacecraft trajectory at specific epochs. Such an approach is called kinematic orbit determination. This method has the important advantage of being independent of any mis-modeling of the spacecraft dynamics but the major drawback of being highly influenced by the quality of observations and the spacecraft-GNSS constellation geometry (Bock et al., 2002; Colombo et al., 2002; Montenbruck et al., 2002).

An alternative approach consists in the use of both dynamical models and GNSS observations in the orbit determination scheme. The key idea is the use of statistical parameters for compensating deficiencies and/or errors in the assumed force model, an approach denoted as reduced dynamic orbit determination (Yunck et al., 1990). It can be implemented, for example, by adding process noise in the estimation scheme during the propagation of the equations of motion in order to reflect the confidence on the used dynamical model. Alternatively, un-modeled accelerations can be estimated by using available observations. The estimated corrections to the force model can be implemented as empirical accelerations (Wu et al., 1991) or more generally as pseudo-stochastic parameters (Beutler et al., 2006; Jäggi et al., 2006) along the principal directions in the orbital frame. By making use of precise observations and a high-fidelity dynamical model, the overall orbit determination scheme is strengthened, which results in an improved estimated spacecraft's trajectory.

According to the scientific or technical mission requirements, kinematic and/or reduced-dynamic orbit products can be required. Due to the achieved accuracy (typically better than 10 cm - 3D RMS), reduced-dynamic orbits have a broader range of applications, being used as precise orbit determination (POD) products. Notable examples of these orbit products include those generated for the GRACE (Jäggi et al., 2007; Kang et al., 2003; Montenbruck et al., 2005), the Jason (Bertiger et al., 2010a) and the Swarm (van den IJssel et al., 2015) missions.

For distributed spacecraft missions with precise baseline requirements, the generation of POD products is a key element as well. Particularly, precise absolute orbits are used as reference trajectories for the adjustment of precise relative orbits, an approach implemented in some state-of-art methods (e.g. Kroes (2006)). In addition, POD products are of fundamental importance for the implementation of integer ambiguity resolution schemes to be used in conjunction with precise baseline determination (PBD) methods (e.g. Jäggi et al. (2007)). Even when the baseline precision requirements are not very stringent, it is possible to generate baseline solutions directly from POD products by differencing both orbits. The advantage of such products is that some degree of common-error cancellation can be achieved and baselines with precision at the 1-2 cm (3D RMS) level can be obtained. Such benefits of POD products for the generation of PBD solutions have been extensively used in the proposed methods introduced in the present work.

1.2.2 Precise baseline determination

Founded on the experience of tools and methods for POD, during the last decade various approaches for PBD have been developed. Both kinematic and reduced-dynamic schemes have been proposed. The design of some of these first schemes for PBD has been built around the experience gathered with terrestrial relative positioning problems and they have leveraged the specific features of the first successful missions, such as GRACE (Jäggi et al., 2007; Kroes et al., 2005). In particular, PBD schemes can greatly benefit from the use of identical (or very similar) spacecraft platforms and geodetic-class GNSS receivers specially tailored for relative positioning applications.

As in the case of POD products, the implementation of a reduced-dynamic approach for PBD allows to obtain solutions with increased precision in comparison with purely kinematic and dynamic approaches. In the case of missions consisting of two similar spacecraft platforms, uncertainties in the modeling of the formation relative dynamics are constrained as a consequence of the reduced levels of relative perturbations experienced by the two vehicles, particularly from non-conservative forces. This implies that in a reduced-dynamic estimation scheme, relative empirical acceleration estimates can be similarly well constrained. The result is an improved relative trajectory modeling with direct benefits to the resulting baseline solution.

The use of geodetic-class GNSS receivers configured for relative positioning applications allows the implementation of the differential GNSS technique. An important advantage offered by such a strategy consists in an improved precision of the employed GNSS observation models due to common-error reduction and/or cancellation in the measurements. In this way, differential GNSS observations (particularly carrier phase measurements) can be used in the estimation algorithm to provide a very tight constraint to the estimated relative trajectory. Similarly, the use of differential GNSS observations allows the application of carrier phase integer ambiguity resolution methods by making use only of GNSS orbit and clock products². With successfully-fixed integer ambiguities, GNSS carrier phase observations can be used as very precise ranging observations (at the mm level), which provides even tighter constraints to the estimated relative trajectory. The result is the generation of baseline products with precision at the mm/sub-mm level.

²In contrast to single-receiver ambiguity resolution, which requires the use of other external products, such as network-calibrated biases.

Chapter 2

Research progress and state-of-the-art methods

The progress made during the development of PBD tools during the first years of the GRACE mission set important milestones in the field (Jäggi et al., 2007; Kroes et al., 2005; Svehla and Rothacher, 2004). Particularly, some of the most important challenges for precise relative orbit determination were addressed to a degree that allowed to deliver baseline solutions with the targeted precision. Further research questions arose in terms of the applicability of the proposed schemes under different mission scenarios and profiles.

The present chapter provides an overview of the challenges that must be tackled in the development of schemes for precise relative orbit determination (PROD). In addition, it introduces some of the state-of-the-art schemes that have been developed in previous research and how some of the challenges have been tackled. Finally, this chapter describes the milestones achieved by previous research and the foundation provided for the development of the proposed schemes described in Chapter 3.

2.1 Challenges for precise relative orbit determination

The low Earth orbit (LEO) scenario is particularly challenging for PROD. Aside from the inherited issues from terrestrial relative positioning problems, performing relative navigation in LEO require to face specific problems that make difficult the implementation of common schemes, particularly for integer ambiguity resolution. The present section provides a very brief introduction to some of the most important problems to tackle for PROD in LEO.

2.1.1 Duration of signal tracking periods

One of the first major differences of the LEO scenario with respect to terrestrial relative positioning problems is the duration of signal tracking periods (even assuming no cycle slips). While on Earth it is typically possible to track any given GNSS satellite for periods of 6-8 hours (Misra and Enge, 2010), in LEO these periods are, theoretically, reduced to less than 1 hour (half an orbit). In practice, tracking periods of 30-35 minutes are the among the longest to be found, depending on the data editing criteria. On average, observation spans vary between 10-15 minutes. Figure 2.1 depicts two example table excerpts of continuous tracking arcs (*passes*) as a function of GNSS satellite elevations for the GRACE and Swarm missions. In the

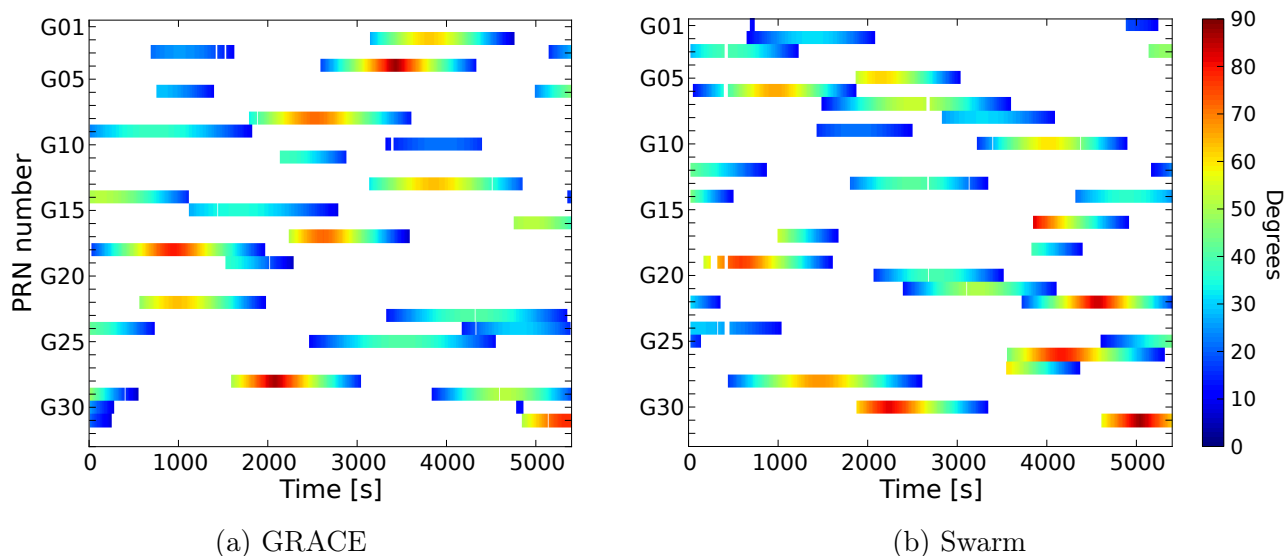


Fig. 2.1 Duration and common elevation of continuous carrier phase tracking arcs for the GRACE and Swarm missions on April 10, 2010 and February 19, 2016, respectively.

absence of detected cycle slips (simply denoted in the plots as an interruption) a few of GNSS satellite passes are about 200 epochs long. Considering 10-second epochs, this translates to ≈ 33 minutes. Although these can be considered as long arcs, some of such passes have low peak elevations (i.e. $< 20^\circ$), which may be detrimental for the positioning problem to solve, if observations with increased error levels (e.g. due to low signal-to-noise ratios) are used.

Carrier phase ambiguities are a mathematical construction of the carrier phase observation model. As such, they cannot be observed and their estimation depends to a large degree on the available number of carrier phase observations. The longer the period and number of carrier phase observations, the better the distinction of ambiguity estimates from other estimation parameters, particularly ionospheric delays. Indeed, if the observation span is short (a typical situation in LEO, as mentioned above), it is more difficult to decorrelate geometrically both parameters as they appear effectively constant¹ during such period (Richert and El-Sheimy, 2005). Even in situations when a given GNSS satellite can be observed during a longer period (in a geometrical sense), it may occur that carrier phase tracking is interrupted by cycle slips. This implies that only a reduced number of carrier phase observations can be used for estimation of a given float ambiguity. In absence of extra constraints, if the number of carrier phase observations decreases, the estimation of ionospheric delays has a larger dependence on pseudorange observations. These conditions lead to float ambiguity estimates less well determined and with increased correlation levels due to the more noisy ionospheric delay estimates, which severely complicates a successful integer ambiguity fixing.

2.1.2 Ionospheric delays

Perhaps the most influential problem for successful and robust integer ambiguity resolution (IAR) and PROD in LEO is the presence of ionospheric delays in GPS observations. Although this problem must also be tackled in relative positioning problems for terrestrial applications, the LEO scenario presents increased difficulties. Particularly, most of the models and applied

¹This is not strictly true in all cases as the ionosphere activity may change heavily even during short passes.

corrections that have been developed for terrestrial GNSS receivers are not suitable for use in LEO.

From a general perspective, the delay experienced by GNSS signals from transmitter to receiver is dependent on the total electron content (TEC) in the ionosphere along the path l from satellite s to receiver r . It is given by

$$N_{TEC} = \int_s^r n_e(l) dl \quad (2.1)$$

where $n_e(l)$ is the electron density along the signal path (Klobuchar, 1996). N_{TEC} denotes the slant TEC and it is expressed in TEC units (TECU), which is defined as $10^{16} e^-/m^2$. Thus, the change in the trajectory of the propagated signal with carrier frequency f_n from GNSS satellite i causes a delay given by

$$v_n^i = k_N \frac{N_{TEC}}{f_n^2} \quad (2.2)$$

where the constant $k_N = 40.3 \text{ m}^3/\text{s}^2$. In practice, the problem is defined by the determination of $n_e(l)$, which depends on the signal trajectory and the state of the ionosphere.

A common alternative to Eq. (2.2) is to express the slant TEC in terms of a vertical TEC (VTEC) common to all received signals and a mapping function $m(\hat{\mathbf{e}}^i)$, with $\hat{\mathbf{e}}^i$ the unit vector from receiver to GNSS satellite i . This function is, in general, direction dependent, although simplified versions with an elevation dependence only, may suffice many applications in LEO. In this way, the estimation of VTEC values provides a useful characterization of the ionosphere state at a given time and location. Much effort have been done in recent years by the international scientific community to provide useful tools for the study of ionospheric activity. One of the most renowned tools are the global VTEC maps estimated and distributed by the International GNSS Service (IGS). These maps have a spatial resolution of $2.5^\circ \times 5^\circ$ (latitude \times longitude) and a temporal resolution of 2 hours (Hernández-Pájares et al., 2009). The primary purpose of global VTEC maps is to aid terrestrial positioning applications in the modeling of ionospheric delays but they can also be used on its own for analysis and studies about ionospheric activity.

The free electrons and ions present in the ionosphere are produced by means of ionization of neutral particles. This process is caused by extreme ultraviolet radiation from the Sun and by collisions with energetic particles that reach and penetrate the Earth's atmosphere (Schunk and Nagy, 2009). Thus, aside from the state of the atmosphere and geomagnetic activity, the ionospheric delay v_n^i in Eq. (2.2) is to a large degree dependent on the solar activity. On yearly time scales, the sun has an activity cycle with a period of around 11 years. Solar activity is commonly characterized in terms of solar indices such as the sunspot number or the solar radio flux at 10.7 cm (F10.7) (Klobuchar, 1996). An example of the solar activity cycle from 2003 to 2016 in terms of sunspot number is depicted in Fig. 2.2. This period is of particular importance for this research as the data span (2007-2016) from the four missions under analysis is contained within this time frame (see Chapter 3 and Appendices). The direct dependence of v_n^i in Eq. (2.2) on the ionosphere activity implies that periods with large solar activity (i.e. with a large sunspot number) are specially stringent for the task of integer ambiguity resolution and relative positioning. Particularly, large observation errors due to high ionospheric activity have a negative impact on the precision of float ambiguity estimates, making difficult the subsequent

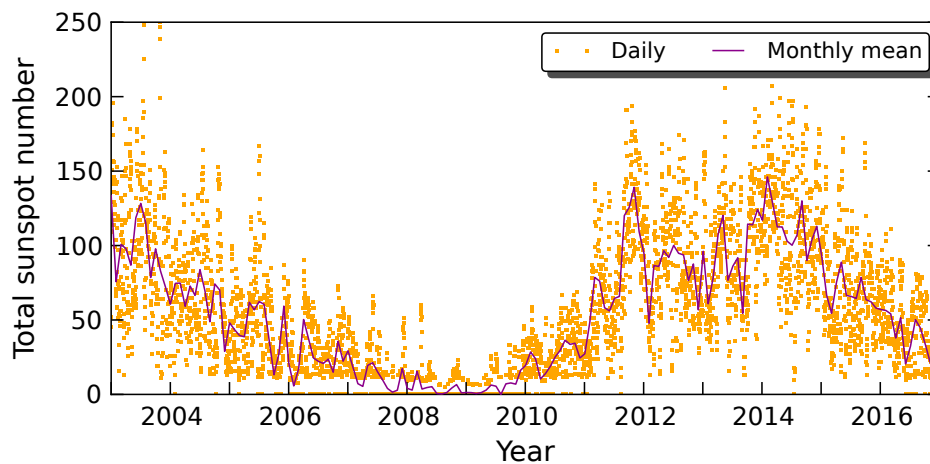


Fig. 2.2 Daily and monthly mean sunspot number from 2003 to 2016. Data source: SILSO World Data Center (2003-2016)

process of ambiguity fixing. As hinted from Fig. 2.2, periods such as the last months of year 2011 and the first 8-9 months of year 2014 have a particularly large mean sunspot number. These periods have been part of the analysis of precise baseline determination for the GRACE and Swarm missions (see Publications 1 and 2 in Appendices A and B, respectively). Due to the long baseline of GRACE, data from this mission was largely used for analysis and tests of various algorithms and configurations for integer ambiguity resolution (see Publication 1 in Appendix A).

Within the aforementioned periods of intense ionospheric activity, during October 2011 it is possible to observe in Fig. 2.2 a pronounced increment in the sunspot number. In this month, a detailed analysis of the spatio-temporal conditions of the ionosphere during a given day can be retrieved from IGS VTEC maps. As an example, Fig. 2.3 depicts the VTEC maps at four different epochs during October 22, 2011. On top of these maps, an estimated trajectory of the GRACE A spacecraft centered at the VTEC map epoch is also depicted. The estimated location of the spacecraft at this epoch is showed with a blue squared marker, giving an indication of the specific ionospheric conditions encountered by the GRACE constellation.

Ionospheric delays in GNSS measurements decorrelate in space and time when the baseline length increases and if the transmitter/receiver geometry changes rapidly between observations. This makes it difficult to reduce the impact of ionospheric delays by applying differential techniques in GNSS observations in LEO missions with long baselines. High levels of ionospheric delays may be present even at the double-difference (DD) level, which is particularly detrimental for integer ambiguity resolution. As an example, Fig. 2.4 depicts the estimates of epoch-wise DD ionospheric delays from a kinematic relative navigation estimation method during October 2011. As observed, the magnitude of ionospheric delays increase severely during the second half of the month (corresponding with the solar activity depicted in Fig. 2.2), reaching levels of various tens of a GNSS signal wavelength.

Being one of the most influential errors for precise positioning problems, along the years various strategies have been foreseen for an appropriate treatment of ionospheric delays in GNSS observations. Given that the ionosphere is a dispersive medium, it is possible to *observe* ionospheric delays in ranging measurements by using a multi-carrier system. This allows to

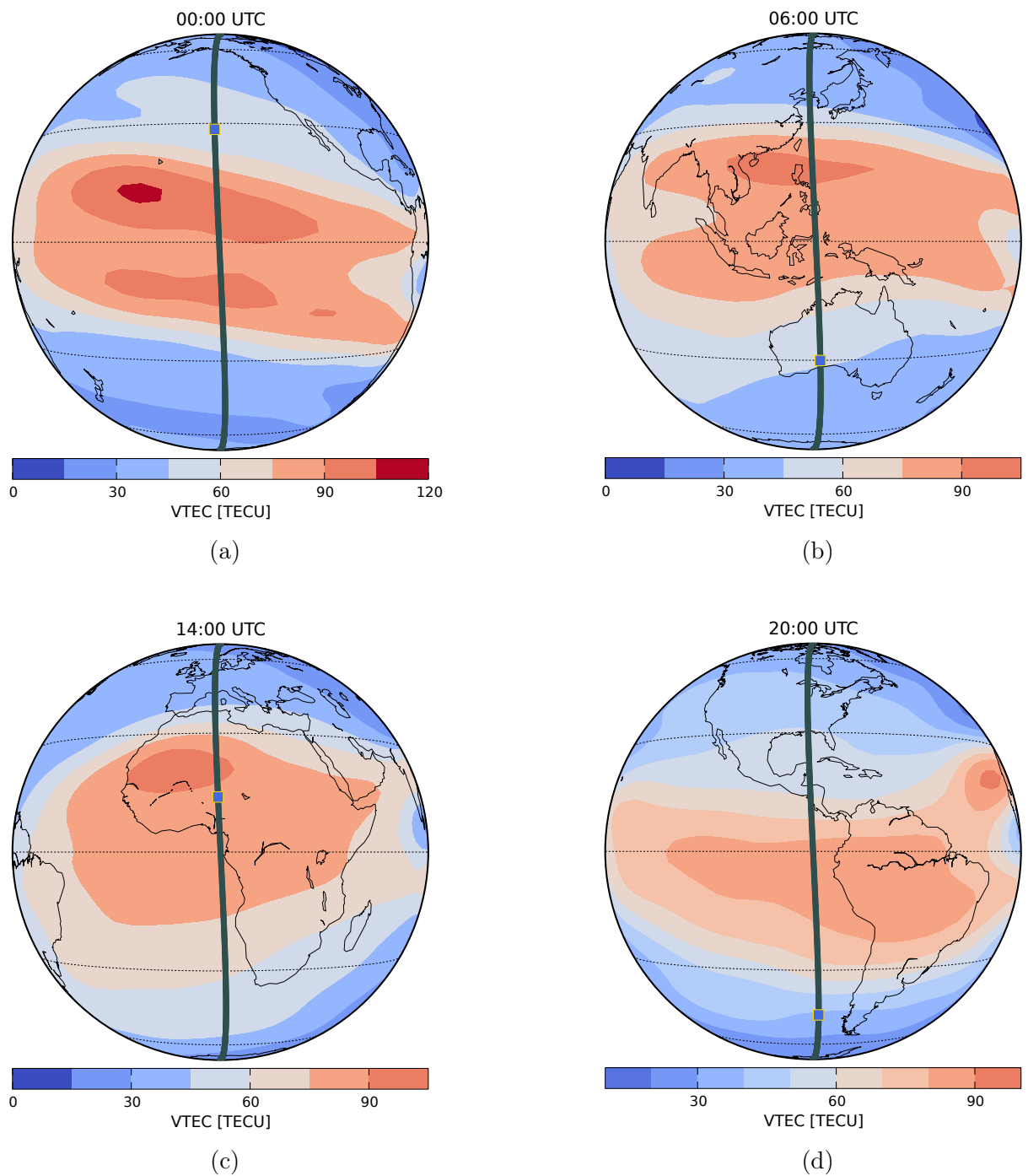


Fig. 2.3 VTEC map at four epochs on October 22, 2011. The orbit of the GRACE A spacecraft is depicted in gray and its approximate position at epoch is indicated with a blue box

reduce the impact of the ionospheric delays of different orders by combining observations (1st order) and by adding external information concerning the state of the geomagnetic field (higher orders; Liu et al. (2016)). However, for problems involving single-frequency orbit determination (Bock et al., 2009; Leung and Montenbruck, 2005) or dual-frequency integer ambiguity resolution (Kroes et al., 2005), it is necessary to consider more involved strategies to cope with ionospheric delays in GNSS observation equations.

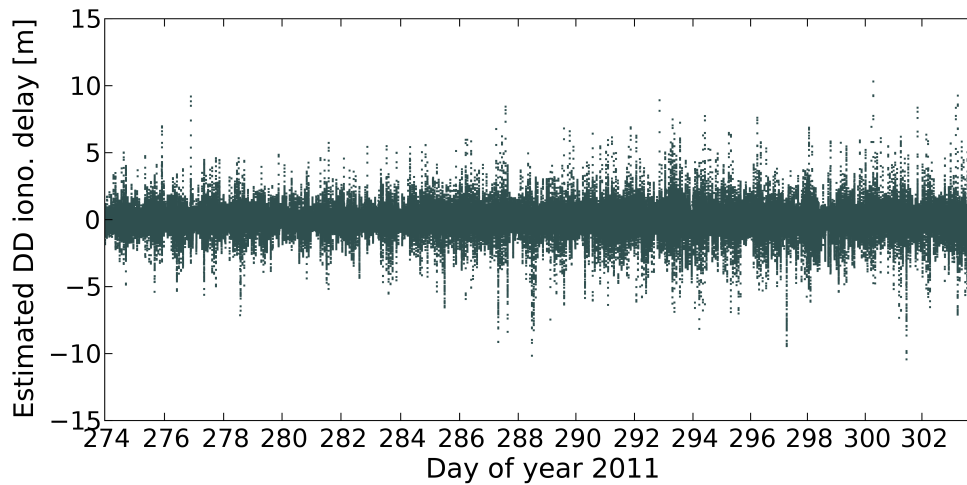


Fig. 2.4 Estimated double-difference ionospheric delays for the GRACE formation on October 2011

Several efforts have been done in recent years to produce suitable models of GNSS ionospheric delays in the context of relative positioning of spacecraft in LEO (Tancredi et al., 2011; van Barneveld et al., 2009). However, being the ionosphere a particularly difficult medium to characterize (Schunk and Nagy, 2009), such a problem has been hard to tackle and it is still under active investigation (Yang et al., 2013). In this sense, a satisfactory treatment of GNSS ionospheric delays is important for the development of robust integer ambiguity resolution methods that can be applied under a variety of space mission profiles in LEO. In general, any approach based on a so-called float ionosphere model (Richert and El-Sheimy, 2005) can be considered for most of the problems at hand. In this model (or more properly called strategy), ionospheric delays are freely estimated together with other orbital and bias parameters. The advantage of such a strategy is that, once convergence has been achieved, ionospheric delays estimates are mostly determined by carrier phase measurements. The quality of such estimates is therefore increased as more observations are considered in the estimation system. However, given that dual-frequency measurements are used, estimates of ionospheric delays and carrier phase ambiguities cannot always be properly decorrelated through the change of geometry and availability of pseudorange observations (see §2.1.1). As a consequence, L1 and L2 float ambiguity estimates will exhibit a high correlation. This information is normally encoded in the resulting variance-covariance matrix of the estimation scheme. A useful indicator of the correlation among float ambiguity estimates is given by the analysis of conditional variances (or standard deviations). These parameters are computed for each ambiguity, taking into account the values (entries in the variance-covariance matrix) obtained for previous ambiguities in the set (see Verhagen (2005) for more details in this context). As an example, Fig. 2.5 shows the so-called spectrum of ambiguity conditional standard deviations for 6 randomly-selected estimated float ambiguity sets on October 22, 2011, using the scheme described in Publication 1 (see Appendix A). These ambiguity sets have a variable length and they are composed of an equal number of L1 and L2 ambiguities. As observed, the second halves of the various spectra exhibit large conditional standard deviation values, some of them at the level of 1.5 cycles. This

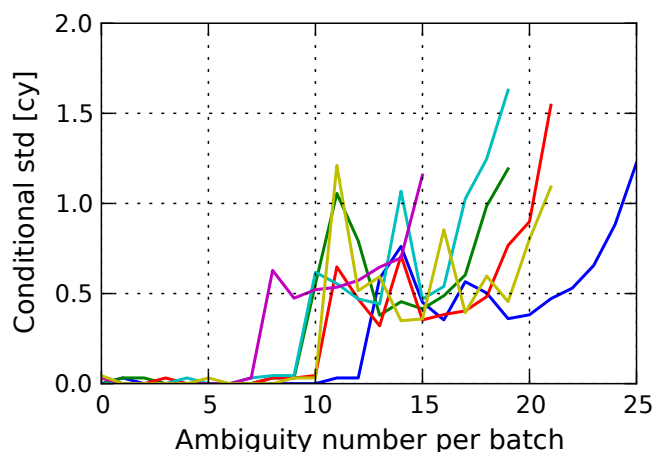


Fig. 2.5 Example spectra of conditional standard deviations of estimated ambiguities for the GRACE formation on October 22, 2011

effect mostly reveal the high correlation between L1 and L2 ambiguities to a large degree due to errors in ionospheric delay estimates (Li and Teunissen, 2011). The high correlation levels among float ambiguity estimates impose a challenge for integer ambiguity estimation methods. Particularly, simple estimators such as integer rounding and integer bootstrapping may be less suitable or less effective under such conditions and more sophisticated methods and algorithms may be required (Verhagen, 2005). However, regardless of the method employed, scenarios prone to having high ionospheric delays are generally difficult to handle given that the risk of wrong ambiguity estimation tend to rise. An increased number of wrongly-fixed ambiguities may be largely detrimental for the quality and availability of precise baseline solutions. As a consequence, missions having long baselines and/or being operated under intense solar activity are considered as particularly demanding for precise baseline determination as they jeopardize the overall robustness of the scheme and produced solutions.

A related problem to the ionospheric delays of first order described thus far is ionospheric scintillation. This phenomenon is mainly produced by irregularities in the ionosphere and causes phase, amplitude and even polarization variations on the signals traveling through this medium (Wheelon, 2001). In the particular case of carrier phase variations, ionospheric scintillation affects GNSS observations mainly in form of refraction and diffraction (Kintner et al., 2009). Although this phenomenon may appear at any latitude, there are zones with increased probability of occurrence, namely the polar regions (particularly in the northern and southern auroral ovals) and in the vicinity of the magnetic dip equator (Rawer, 1993). When the TEC increases, there exists a larger variation in the group velocity (which slows down) and phase velocity (which speeds up) of the GNSS signal. When sudden rapid phase velocity changes occur, they challenge the carrier phase tracking loops in GNSS receiver (Kintner et al., 2009). Similarly, the ionospheric irregularities can scatter radio waves passing through the medium, causing that GNSS signals reach the receiver antenna through multiple paths. Hence, these diffractive and refractive effects on GNSS signals may be interpreted as a form of space-based multipath (Kintner and Ledvina, 2005; Kintner et al., 2009). In this way, ionospheric scintillation may cause a reduced performance of carrier phase tracking loops (Buchert et al., 2015; Xiong et al., 2016), resulting in a raise in the number of cycle slips and an increment of

effective receiver noise levels (van den IJssel et al., 2016). These two effects have a negative impact both in the integer ambiguity resolution scheme and the resulting baseline products.

2.1.3 Orbit control maneuvers

An additional challenge for integer ambiguity resolution, particular to space applications, is the presence of orbit control maneuvers². The main difficulty imposed to the overall problem of precise orbit determination is that control maneuvers represent discontinuities in the spacecraft dynamics. In an orbit determination system using carrier phase observations, the estimation scheme makes use of the spacecraft (or formation) dynamics in order to provide constraints for the estimation of float ambiguities. In this way, if the presence of orbit control maneuvers introduces errors in the estimation of reference trajectories, such errors are mapped into the statistical description of float ambiguities. Thus, a successful integer ambiguity resolution in the vicinity of orbit control maneuvers becomes more difficult in such a situation.

By itself, finding a proper handling strategy of orbit control maneuvers is part of the general problem of precise orbit determination. From the point of view of relative orbit determination, this strategy must be considered together with a suitable approach to model carrier phase observations in order to achieve a successful integer ambiguity fixing. Orbit control maneuvers can be estimated by using ranging measurements (such as GPS). However, the sole use of observations may not provide enough information for a proper maneuver reconstruction. In this situation, dynamical models are used as aiding information for an enhanced maneuver detection/characterization. The joint use of observations and dynamical models have an immediate impact on the ambiguity resolution strategy. The more dynamical the strategy to be used for baseline determination, the larger the dependence of float ambiguities on reference trajectories, and the larger the risk of mis-modeling carrier phase observations due to maneuver modeling/estimation errors. On the other side, a reference trajectory with reduced stiffness may not provide the required constraints for float ambiguity estimates.

From a general standpoint, an integral strategy for maneuver handling that takes into consideration the implementation of an integer ambiguity resolution scheme is a task that has not been broadly explored in past research. One of the first successful formation-flying missions, GRACE, was designed in order to require very low maneuvering activity per year. Thus, for various of the schemes for precise baseline determination developed during this period, it was not necessary to further investigate this problem (see e.g. Jäggi et al. (2007); Kroes (2006)). With the implementation of the space interferometer TanDEM-X, the formation-flying requirements became more stringent as configurations reached baselines as short as 500 m. More intense maneuvering activity for orbit and formation control was therefore needed (up to 3 maneuvers per week during periods of high solar activity, Kahle et al. (2012)). Hence, some approaches were implemented into the existing schemes for precise baseline determination. The achieved results in tests with data from TanDEM-X showed that it was possible to achieve an overall good baseline consistency, i.e. no convergence problems due to the presence of maneuvers. However, a reduced performance in the solutions was observed in the vicinity of maneuvers under such strategies, making baseline products unsuitable for orbit assessment comparisons and for generation of remote sensing products (Jäggi et al., 2012). Further tests with missions including sometimes an almost continuous maneuver activity, such as PRISMA, showed the

²Attitude control maneuvers are equally detrimental for precise orbit determination if they make drastic changes in antenna orientation. However, such maneuvers are not directly addressed in this study.

need for an improved strategy for maneuver handling in relative orbit determination which takes into account, in addition, integer ambiguity resolution.

2.2 Previous research and milestones

Starting from the first experience with distributed spacecraft positioning and orbit determination for formation flying missions, various schemes have been proposed throughout last years. They have been developed by proposing strategies to cope with the aforementioned challenges for PROD. Some of these strategies have been based on concepts stemmed on terrestrial relative positioning problems whereas others have resulted from the accumulated experience with space baseline determination systems.

From a general point of view, the major milestone achieved by the schemes developed in previous research was the computation of precise baseline products using differential GNSS techniques and fixed carrier phase integer ambiguities. The application of such schemes to data from the GRACE mission showed that a baseline precision at the mm and sub-mm (1D RMS) level could be achieved. The milestones set by these works have been the main foundation for the present research. This section provides a brief description to the most influential schemes for the strategies proposed in the present work, developed by Kroes et al. (2005) and Jäggi et al. (2007).

2.2.1 Batch scheme and WL/NL ambiguity resolution

Some of the first results obtained for the GRACE mission in terms of precise baseline determination were obtained by Svehla and Rothacher (2004), who proposed one of the first schemes using fixed integer ambiguities, obtaining baselines with precision at the 2-3 mm level (1D RMS). These results were obtained with tailored versions of the Bernese GNSS Software (BSW, formerly known as Bernese GPS Software, Dach et al. (2015)) package. A key feature of such a scheme is the use of batch processing strategies and a least-squares (LSQ) estimator.

Further improvements on orbit modeling techniques developed by Beutler et al. (2006) and Jäggi et al. (2006) allowed to achieve baseline solutions with sub-mm precision levels in tests using GRACE data (Jäggi et al., 2007). In this scheme, the basic strategy for carrier phase integer ambiguity resolution is based on concepts developed in BSW for terrestrial relative positioning. The applied strategy is denominated as widelane/narrowlane (WL/NL) bootstrapping. It basically consists in the arrangement of pseudorange and carrier phase observations to form a DD Melbourne-Wübbena (MW) combination (commonly attributed to Melbourne (1985) and Wübbena (1985)), expressed as

$$MW_{\square_p}^{ij}(t) = \lambda_{WL} n_{\square_p, WL}^{ij} + \varepsilon_{\square_p, MW}^{ij}(t) \quad (2.3)$$

where the notation \square_p is used to denote a differential quantity between receivers. The term $n_{\square_p, WL}^{ij}$ denotes a DD widelane ambiguity for GNSS satellites i and j . Similarly, λ_{WL} indicates the wavelength of the widelane combination and $\varepsilon_{\square_p, MW}^{ij}(t)$ denotes errors and other unmodeled factors in the DD MW combination. As can be seen, this combination basically consists of an ionosphere-free and geometry-free noisy widelane ambiguity, which is computed for every epoch during overlapping GNSS satellite passes. The resulting estimate is obtained from an average of the individual epoch-wise MW estimates over the pass of common visibility of GNSS satellites i

and j . Due to the features of the widelane combination, these float widelane ambiguities can be reliably resolved by using a simple rounding estimator. Ambiguity validation strategies based on the standard deviation of float ambiguity estimates are applied in order to discard potential wrongly-fixed values (Dach et al., 2015).

The fixed DD widelane ambiguities are introduced as known parameters in a LSQ reduced-dynamic baseline determination system for the estimation of float DD narrowlane ambiguities, based on the ionosphere-free observation model, as follows

$$\Phi_{D,IF}^{ij}(t) = \rho_D^{ij}(t) + \lambda_{NL} \left[n_{D,1}^{ij} + \frac{\lambda_{WL}}{\lambda_2} n_{D,WL}^{ij} \right] + \epsilon_{D,IF}^{ij}(t) \quad (2.4)$$

where ρ_D^{ij} is the DD range between the spacecraft in the formation and GNSS satellites i and j . Similarly, λ_{NL} denotes the wavelength of the narrowlane combination, $n_{D,1}^{ij}$ is the L1 DD ambiguity and $\epsilon_{D,IF}^{ij}(t)$ denotes errors and other unmodeled factors in the DD ionosphere-free combination. In a next step, float DD narrowlane (or more properly L1) ambiguities are fixed by applying a fixing and validation scheme based on the analysis of formal errors of float estimates (Dach et al., 2015). The WL/NL bootstrapping method is very attractive as it provides essentially an ionosphere-free estimation scheme, which makes it suitable even for scenarios of long baselines.

2.2.2 Sequential scheme and on-the-fly ambiguity resolution

An alternative formulation for PBD was proposed by Kroes et al. (2005) and further expanded and analyzed by Kroes (2006) using the DLR's GPS High Precision Orbit Determination Software Tools (GHOST; Montenbruck et al. (2005); Wermuth et al. (2010)). Later, such a formulation was advanced by van Barneveld (2012) in order to allow multi-spacecraft orbit determination. The strategy is based on a sequential reduced-dynamic filtering scheme and an on-the-fly integer ambiguity resolution. This scheme has been widely used within this study for assessment and evaluation of the proposed schemes and hence a slightly more detailed description is provided in the present section.

Sequential filtering algorithms are typically more suitable for *real-time* applications due to the form in which observations are processed. Nevertheless, it is similarly possible to use them in offline applications, using complementary techniques in order to achieve an improved performance. A particularly used technique is the application of a smoother in order to improve the quality of the estimates (Brown and Hwang, 1997; Fraser and Potter, 1969; Simon, 2006). Additionally, a sequential estimation algorithm has typically a simpler formulation in comparison with batch estimators as it has a notably reduced state space.

The PBD scheme is based on an extended Kalman filter (EKF) and it is formulated using dual-frequency single-difference (SD) GNSS observations. A SD parameterization of the relative positioning problem provides additional implementation benefits in comparison with DD formulations. Particularly, SD observations profit from the cancellation and/or reduction

of common errors without considering correlations in the observation models. In this way, the state vector of the EKF is given by

$$\begin{bmatrix} \mathbf{X}_D \\ c\delta t_D \\ \mathbf{I}_D \\ \mathbf{N}_{D,1} \\ \mathbf{N}_{D,2} \end{bmatrix} = \begin{bmatrix} \mathbf{y}_D; C_{R,D}; C_{D,D}; \boldsymbol{\alpha}_D \\ c\delta t_D \\ i_D^0, \dots, i_D^{s-1} \\ n_{D,1}^0, \dots, n_{D,1}^{s-1} \\ n_{D,2}^0, \dots, n_{D,2}^{s-1} \end{bmatrix} \quad (2.5)$$

where the spacecraft relative state vector $\mathbf{y}_D = (\mathbf{x}_D, \mathbf{v}_D)$ is composed of the relative position \mathbf{x}_D and relative velocity \mathbf{v}_D of the spacecraft's center of mass. The differential receiver clock error is denoted as $c\delta t_D$. Differential solar radiation pressure and air drag coefficients are denoted as $C_{R,D}$ and $C_{D,D}$, respectively, whereas $\boldsymbol{\alpha}_D = (a_R, a_T, a_N)_D$ is the relative empirical accelerations vector in radial, along-track and cross-track directions. For the total $s - 1$ tracked GNSS satellites at estimation epoch, the state vector comprises a SD ionospheric delay vector \mathbf{I}_D and SD float ambiguity vectors $\mathbf{N}_{1,D}$ and $\mathbf{N}_{2,D}$ for L1 and L2 ambiguities, respectively

The time update of the EKF is performed by an integration of the equations of motion of each individual spacecraft (A and B). For this purpose, a reference (fixed) trajectory \mathbf{y}_A at time t_{i-1} is used in order to obtain an auxiliary estimate of the referred spacecraft $\mathbf{y}_B(t_{i-1}) = \mathbf{y}_A(t_{i-1}) + \mathbf{y}_D^+(t_{i-1})$, using the estimated spacecraft relative state vector from the previous Kalman filter update $\mathbf{y}_D^+(t_{i-1})$. A similar strategy is used for the force model parameters, where the values of the reference spacecraft are kept constant. The individual trajectories of spacecraft A and B are integrated by using a 4th-order Runge-Kutta numerical integration method, which is suitable for sequential estimation with state-updates at each measurement and short intervals (10s-30s) between observations. The integrated trajectories are then used to form a predicted spacecraft relative state vector $\mathbf{y}_D^+(t_i)$.

If orbit control maneuver(s) are executed within the propagation interval $t_{i-1} - t_i$, these must be considered in the EKF time update. In the maneuver handling approach described here, during the numerical integration of trajectories, all the executed maneuvers present within the integration interval are added in the dynamical model. Uncertainties in the spacecraft state vector are considered in the form of additional process noise, namely

$$\mathbf{P}^*(t_i) = \mathbf{P}^-(t_i) + \mathbf{Q}_m \quad (2.6)$$

where \mathbf{P}^- is the predicted state covariance matrix without considering the presence of maneuvers in the state propagation from t_{i-1} to t_i . The matrix \mathbf{Q}_m is the added process noise matrix due to maneuver execution (Montenbruck et al., 2011).

After the prediction step, the EKF performs a measurement update making use of SD pseudorange and carrier phase observations in L1 and L2 (Kroes et al., 2005). The resulting SD float ambiguity estimates are transformed by a correlation factor matrix into DD float estimates. Together with their corresponding ambiguity covariance matrix, they are used as input to an integer least-squares (ILS) estimator in order to fix them to integers. The ILS method is efficiently encoded in the LAMBDA algorithm (Teunissen, 1995), which significantly reduces the searching process of the ILS method by applying a decorrelation transformation.

The integer ambiguity solution provided by the ILS estimator is tested with an ambiguity validation scheme. It consists of theoretical tests such as the evaluation of the ILS success rate

and heuristic tests such as the evaluation of widelane and ionosphere-free ambiguity residuals. The scheme proposed by (Kroes et al., 2005) does not include any partial ambiguity resolution strategy but it does have a scheme for partial ambiguity validation, in accordance with the used heuristic validation tests. The output from this validation scheme contains fixed integer ambiguities, which are introduced into the EKF by applying an ambiguity innovation update. This process is applied whenever a new set of float ambiguities is included in the estimation scheme. If a given float ambiguity vector cannot be fixed with enough confidence, subsequent attempts are carried out for each EKF measurement update.

2.3 Path for this research

2.3.1 A requirement on robustness

The term robustness is typically used as a desirable feature to have in a system. However, the concept lacks a general definition that can be applicable without reference to specific system characteristics. From the field of complexity, Carlson and Doyle (2002) describe robustness as the maintenance of specific system characteristics that are desired even under the presence of variations in the behavior of its component parts or its environment. The overall robustness of a system can be analyzed in a general sense, even from a theoretical point of view (Fernandez et al., 2005). For the specific problem of relative orbit determination, the robustness of estimation schemes and algorithms represents the key element under consideration in this study. It can be characterized by the preservation of proper functionality of estimation techniques regardless of the formation-flying mission profile under analysis (see Publication 1 in Appendix A). Particular characteristics of such mission profiles include the baseline length, ionospheric activity and receiver characteristics.

The state-of-the-art methods introduced in §2.2 showed to be capable of coping to a certain degree with the challenges described in §2.1 in some scenarios. However, over the years, the need for increased levels of robustness of PBD schemes started to rise due to the diversity of precision and features requirements of PBD products for missions with varied profiles (e.g. real-time navigation assessment, precise baseline reconstruction). For example, even when precise baseline solutions for the GRACE mission (long baseline scenario) were obtained, some schemes exhibited a reduced robustness when the assumed estimation conditions failed (observation noise, ionospheric delay levels, etc.). Additionally, with the implementation of missions such as TanDEM-X and PRISMA, new challenges emerged, such as the incorporation of strategies for orbit control maneuver handling. Various of these challenges applied directly to real-time relative navigation systems, but they were also of key relevance for the offline generation of PBD products. As a result, the need for high levels of robustness became a demand for PBD systems so as to be effectively applied in a wider spectrum of mission scenarios. The demanded robustness shall, in addition, be incorporated without affecting the achieved precision levels of baseline products from current state-of-the-art schemes.

2.3.2 Issues, considerations and questions

The characteristics of the strategies introduced in §2.2 allowed to exploit the high inherent precision of differential carrier phase measurements and demonstrated the practical feasibility of mm-level relative navigation of Earth orbiting spacecraft. However, the experience gathered

with various mission profiles revealed some remaining issues that needed to be solved to improve the overall performance of the strategies.

Issues

The short duration of signal tracking is basically translated to a large number of GNSS satellite passes and an increased number of float ambiguities to fix. If dual-frequency L1 and L2 observation models are employed, this implies that the number of ambiguities is twice the number of passes. Under the (optimistic) assumption of few detected carrier phase cycle slips, it is expected to have 450-500 continuous tracking arcs, implying that at least 900-1000 SD float ambiguities need to be fixed for a one-day data set. This may result in increased computational burden if a complete ambiguity fixing and validation scheme is to be used. In the strategy developed by (Jäggi et al., 2007), this issue is somewhat circumvented by using a geometry-free approach for widelane ambiguity resolution. As a consequence, the resulting number of narrowlane ambiguities to fix is reduced to a half in comparison with L1/L2 ambiguity estimation schemes. On the other hand, the strategy developed by Kroes et al. (2005) is less affected by this issue as ambiguities are estimated and resolved on-the-fly using a sequential estimation scheme. Hence, the number of ambiguities to fix at every attempt is always constrained to twice the maximum number of tracked GNSS satellites at that epoch. In practice, this number is typically below 24 ambiguities for a 12-channel GNSS receiver.

Ionospheric delays in GNSS observations are a general problem affecting both terrestrial and space positioning applications. In this way, various of the ideas and strategies implemented for terrestrial applications are similarly applicable for the problem at hand. As previously mentioned, the scheme developed by Jäggi et al. (2007) makes use of ionosphere-free observation models and therefore this makes it equally suitable for mission scenarios with short and long baselines. In the sequential scheme developed by Kroes et al. (2005), observation errors due to ionospheric delays have an impact on float ambiguity estimates, being particularly large in long baseline scenarios. This increases the risk of wrongly-fixed values that have a negative impact in subsequent estimates. The experience gathered with this scheme showed that it exhibits reduced levels of robustness in scenarios with long baselines and/or intense ionospheric activity.

A major robustness issue for the sequential estimation scheme arose when processing data from the Swarm mission. One of the most important challenges in this data set was the presence of half-cycle ambiguities in carrier phase observations. Given the baseline size in this mission, in the sequential scheme employed by Kroes et al. (2005) float ambiguity estimates cannot be effectively constrained, leading to an unsuccessful ambiguity fixing. On the other hand, Jäggi et al. (2014, 2016) did not report to have used any special strategy with respect to the approach described by Jäggi et al. (2007) in order to cope with half-cycle ambiguities. Later, it was shown that such a scheme takes advantage (implicitly) of the full-cycle feature of widelane ambiguities in the GPS receivers onboard the Swarm spacecraft (see Publication 1 in Appendix A). Nevertheless, the applicability of such a scheme under more general scenarios (e.g. with half-cycle MW ambiguities) has not been tested.

As briefly stated in previous sections, the formulation of a strategy for orbit control maneuver handling is a problem that has been primarily addressed in the context of POD. In the case of PBD, in the lack of a more unified framework, the first maneuver handling strategies had to be constrained by existing estimation schemes, included integer ambiguity resolution methods. In this way, for the application of the scheme developed by Kroes et al. (2005) under the presence of maneuvers, the strategy briefly described in §2.2.2 was implemented and tested

for the TanDEM-X and PRISMA missions (Ardaens et al., 2010; Montenbruck et al., 2011). In this strategy, although the approach described by Eq.(2.6) may be suitable to reduce the impact of maneuvers on the final relative orbit products, it exhibits the major implementation problem of defining matrix Q_m (which is typically done in a heuristic way) accurately. This problem has a direct impact on the trajectory estimates, as it may lead to discontinuities around maneuver execution periods. In addition, due to the increased process noise, the estimates are more dependent on observations during such periods, thus reducing the stiffness of the resulting relative orbit. On the other hand, the batch PBD estimation scheme implemented by Jäggi et al. (2007) has the capability of direct estimation of orbit control maneuvers, which are estimated as instantaneous velocity changes at specific maneuver execution times (Jäggi et al., 2012). However, the implemented reduced-dynamic strategy in this scheme has made particularly difficult to implement a maneuver handling strategy that provides a more realistic description of satellite orbits. In particular, it has not been possible to actually observe the impact of orbit control maneuvers on integer ambiguity resolution during maneuvering periods. In a comparison of PBD solutions for the TanDEM-X mission from the BSW and GHOST packages, Jäggi et al. (2012) showed that large inter-solution discrepancies result when maneuvering periods are taken into account in the assessment. However, from this evaluation it is difficult to determine what are the actual contributions of each solution to the observed error levels.

Considerations

The experience obtained from the analysis of data from various distributed spacecraft missions has shown that some particular mission characteristics impose difficulties to the current PBD approaches. From this experience, it is possible to extract some considerations and remarks to summarize the state of the main issues to tackle towards the proposal of alternative schemes. They can be described as follows:

- i. The large number of estimated L1/L2 float ambiguities for one-day data sets may impose a high computational burden if a complete ambiguity fixing and validation scheme is considered.
- ii. The WL/NL ambiguity resolution strategy provides a workaround solution to such a problem by splitting the number of ambiguities to solve in two different stages.
- iii. The sequential baseline determination scheme resolves ambiguities on-the-fly and as a consequence the number of ambiguities to solve is always small.
- iv. The on-the-fly L1/L2 ambiguity resolution scheme has notable difficulties in coping with half-cycle ambiguities in long baselines.
- v. In the WL/NL ambiguity resolution strategy, the process of fixing MW ambiguities disregards the geometry between LEO spacecraft and GNSS satellites. This makes the scheme more dependent on pseudorange observations, which may reduce its robustness under more general cases. Additionally, an optimal integer ambiguity estimator is not used in this strategy, which theoretically has a negative impact on the achievable ambiguity fixing rate.
- vi. The sequential ambiguity resolution strategy does take into consideration the geometry between LEO spacecraft and GNSS satellites and uses an optimal integer ambiguity

estimator. However, the scheme may be very difficult to configure (filter settings, ambiguity validation thresholds, etc.) so as to work properly under general cases.

- vii. The WL/NL ambiguity resolution strategy is essentially ionosphere-free and this provides some robustness to long-baseline scenarios. However, for a successful resolution of narrowlane ambiguities, GNSS carrier phase observations must be modeled with an error levels much lower than one narrowlane wavelength.
- viii. Wrongly-fixed ambiguities are specially detrimental for the sequential estimation scheme, as they are fed into the EKF as known parameters, influencing the dynamical propagation of the reference trajectory in subsequent epochs. As a consequence, filter divergence or highly-degraded solutions may occur.
- ix. Due to its formulation, the sequential estimation scheme is unable to estimate orbit control maneuvers. Maneuver modeling provides some degree of functionality, but a degradation of baseline solutions around maneuver execution may be present.
- x. A batch relative orbit formulation provides the capability of maneuver estimation. However, considering maneuvers as instantaneous velocity changes may result in errors in baseline estimates that affect the modeling of carrier phase observations around the period of maneuver execution.

Questions

Based on the above considerations and recent progress on the field, open questions emerged that over the past years became a set of guidelines for the implementation of alternative schemes for PROD in the present work. In particular, the requirement of robustness has been considered as one of the most important elements to be taken into account in the development of such alternative schemes. Some of these open questions can be given as follows:

1. Is it possible to implement a robust scheme (i.e. based on batch processing) for float ambiguity estimation without having a large number of ambiguities to fix in one batch?
2. Can some of the advantages of a sequential estimation scheme be used for the purpose of reducing the number of ambiguities to fix?
3. How can the various sources of available information (geometry, observations, etc.) be used for float ambiguity estimation in order to improve the robustness of the scheme?
4. How can the robustness of an L1/L2 integer ambiguity resolution strategy be improved against long baselines and intense ionospheric activity?
5. How are non-ionosphere-free integer ambiguity resolution methods affected by the presence of intense ionospheric activity and/or long-baseline mission scenarios?
6. Is it possible to use more complete and/or formal integer ambiguity estimation and validation schemes (e.g. optimal estimators) so as to improve the robustness of the overall PBD method?
7. How can an integer ambiguity resolution scheme cope with the presence of half-cycle ambiguities in carrier phase observations?

8. Can the presence of half-cycle ambiguities in carrier phase observations from the Swarm mission (and similar GPS receivers) be handled before ambiguity estimation?
9. Is it possible to generate robust and precise baseline solutions for mid- and long-term analyses (e.g. 3-12 months) under general mission profiles (diverse baseline length, GPS receiver characteristics, etc.)?
10. How does the presence of orbit control maneuvers affect the estimation and resolution of integer ambiguities?
11. Is it possible to implement a PROD method that is robust to the presence of orbit control maneuvers (even under intense maneuvering activity), providing at the same time a more realistic description of the resulting satellite trajectories?
12. Is it possible to generate smooth, ambiguity-fixed PROD solutions under intense orbit control maneuvering activity?
13. How precise are maneuver estimates from a PROD scheme with respect to other maneuver estimation/reconstruction approaches?

Chapter 3

Synoptic description of this research

This chapter presents a synoptic description of the schemes and algorithms developed during the realization of this research. The chapter provides an introduction to the context into which the work here presented can be situated, based on the milestones set by previous research. Some of the main contributions to the field are also synthesized and propounded additions to the orbit determination software package used in this work are also presented. Finally, a description of the publications that conform the core part of this research is provided.

3.1 Context and framework

In order to tackle some of the issues and open questions resulting from the experience in past research, as described in §2.3.2, the schemes developed in the present research have been focused mainly in three areas, as depicted in Fig. 3.1. The various topics in these research areas are treated in some degree in each publication that shape this research. A diagrammatic representation of applied concepts and results achieved in each publication that are related to a particular research area is given by blue bars in the scheme depicted in Fig. 3.1. Naturally, the topics of relative orbit determination and integer ambiguity resolution have been the core subjects in all three publications. Various key aspects within these topics, such as estimation schemes, float ambiguity resolution and half-cycle ambiguity processing, were addressed according to specific targeted goals. The broad field of spacecraft formation flying has been only slightly addressed in Publication 3, whose main scope was devoted to the analysis of orbit control maneuvers in the PROD context.

The main foundations of the present research have been heavily based on the milestones achieved by the studies performed by Kroes et al. (2005) and Jäggi et al. (2007), as described in §2.3.2. Each of these studies is based on theoretical and heuristic foundations that give them different characteristics and levels of robustness. As described in §2.2.2, the scheme developed by Kroes et al. (2005) was one of the first strategies to make use of an optimal integer ambiguity estimation method (ILS) and applying it to the problem of PBD. Due to its implementation, this scheme provides a neat integration of baseline determination and integer ambiguity resolution strategies that makes it efficient under various mission scenarios. On the other hand, the scheme developed by Jäggi et al. (2007) demonstrated a similar performance in terms of baseline precision using a batch estimation processing scheme. This particular feature provides an inherent improvement of robustness with respect to a sequential estimation strategy.

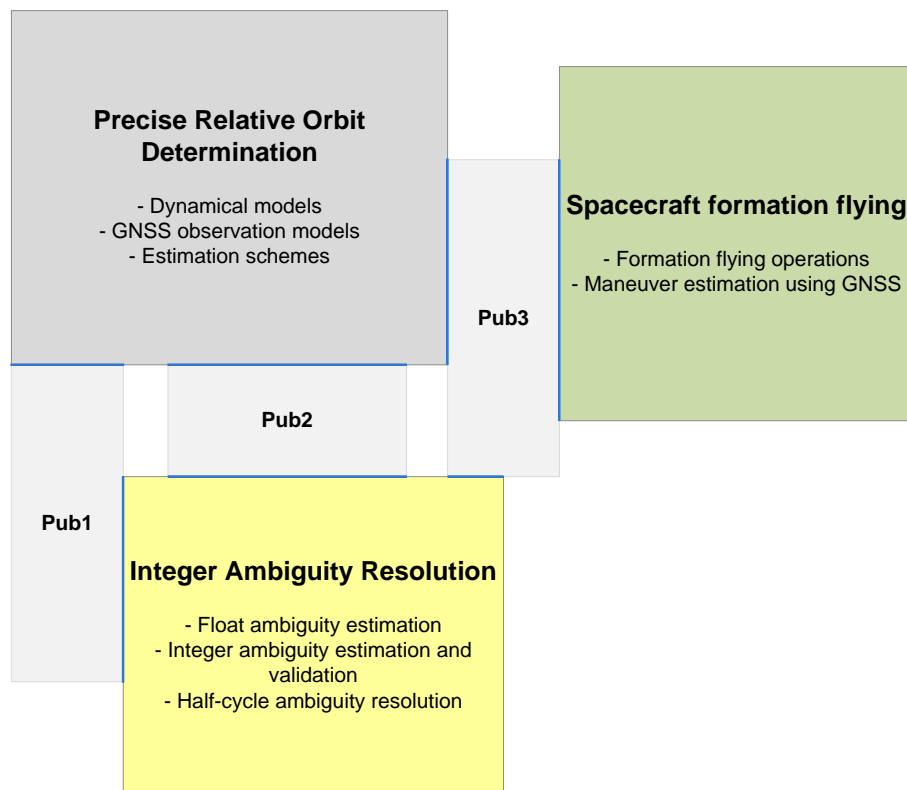


Fig. 3.1 Research context for the present study and the relation of various research areas to the three publications conforming this thesis (denoted as Pub1, Pub2 and Pub3).

From the discussion in §2.3.2, a key issue resulting from the experience of applying the aforementioned schemes with data from various distributed spacecraft missions, is an apparent reduction of robustness under more general mission scenarios. All these considerations have provided the context and framework for the development of the proposed scheme described in this work. The driving idea has been to incorporate the major strengths of strategies from previous studies in order to tackle one of the most important weaknesses of current approaches, i.e. a reduced levels of robustness. Various of these ideas have been roughly schematized in Fig. 3.2. This sketch depicts some of the most influential milestones achieved in previous research for the development of the proposed strategies for PROD. The main features of the resulting estimation system are depicted as an extension to the primary milestone about mm and sub-mm baseline precision achieved by previous research. In this sense, these features can be considered as a direct extension and/or improvement over the milestones of one or both of the depicted studies.

3.2 Main contributions

The requirement statements resulting from the issues, considerations and open questions discussed in §2.3.2 have been addressed to various degrees in the schemes developed during this study. The main tests and results obtained were conformed in the three publications that represent the major outcome of this research. From these results, it is possible to extract

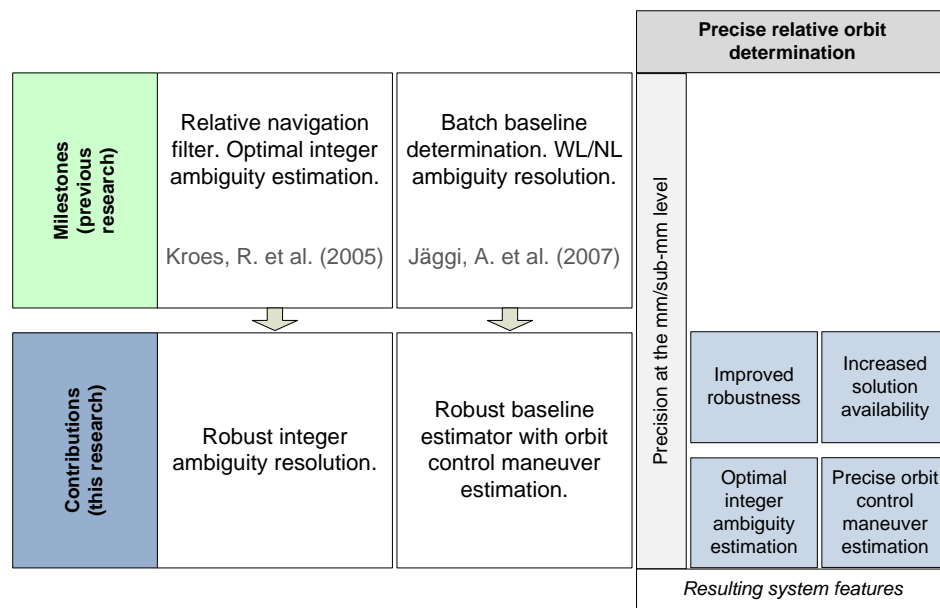


Fig. 3.2 Main research milestones achieved in previous studies as foundations for the contributions attained by this research.

key features in order to provide a synthesized overview of the achieved progress during the realization of this study. These points can be summarized as follows:

- Test and validation of proposed schemes for robust PROD using real flight data from 4 distributed spacecraft missions: GRACE, TanDEM-X, PRISMA and Swarm.
- Implementation of a data processing scheme that reduces the computational burden of integer ambiguity estimation and validation methods by using the concept of *sliding batches*.
- Development of a robust scheme for float ambiguity estimation based on an a-priori-constrained LSQ estimator using POD products as a priori information.
- Joint use of robust schemes based on batch processing for float and integer ambiguity estimation.
- Improved ambiguity validation scheme using recent concepts and ideas developed in the framework of integer aperture estimators (IAEs).
- Implementation of a robust validation scheme based in a combination of theoretical and heuristic tests.
- Improved precision and robustness of PBD products for the GRACE mission with respect to previous research.
- Analysis of the impact of mission scenarios with long baselines and intense ionospheric activity on PBD products.

- Achieved state-of-the-art precision of PBD products for the TanDEM-X mission.
- Achieved half-cycle ambiguity resolution and generation of PBD products using data from the Swarm mission.
- Improved performance of half-cycle ambiguity processing by using the proposed scheme denoted as *mixed-cycle* ambiguity resolution.
- Mid-term (3 months) generation of precise baseline products (reduced-dynamic and kinematic) for the Swarm mission.
- Inter-agency assessment of precise baseline products for the Swarm mission with products from the AIUB.
- Implementation of a robust scheme for PROD based on a batch LSQ estimator, formulated in terms of relative dynamics and differential GPS observations.
- Direct estimation of orbit control maneuvers in a PROD scheme together with extensive assessment of estimates in multi-mission tests.
- Generation of differentiable (smooth) PROD products even under intense maneuvering activity for the TanDEM-X and PRISMA missions.
- Analysis of impact of orbit control maneuvers on PROD products obtained with previous approaches.
- Improved precision of estimated orbit control maneuvers in comparison with POD-based estimates for the GRACE, TanDEM-X and PRISMA missions.

3.3 Software tools and implementation

For the implementation of algorithms in the proposed scheme for PROD, the DLR's GHOST is the primary software package that has been used during this research. GHOST is placed among various software packages for POD, e.g. the aforementioned BSW, EPOS (Uhlemann et al., 2015) and NAPEOS (Springer et al., 2012). However, it is one of the few packages that contains tools for differential GNSS processing and relative orbit determination. The core libraries and toolkit are written in C++ and organized in modules, which are used for various applications ranging from GNSS data processing to orbit determination. In particular, for POD and PROD applications, a processing chain is used in order to generate final products. Figure 3.3 depicts a schematic view of the various modules, information sources and delivered products in the generation of PROD solutions.

For each spacecraft, the first step consists in the computation of kinematic single point positioning solutions, which are used as pseudo-observations for the computation of coarse reduced-dynamic orbits. The resulting orbits are continuous and smooth with a precision at the 15-25 cm level (3D RMS). Such solutions are used for more rigorous GNSS data editing in subsequent modules, particularly for POD. As described in §1.2.1, the POD module processes GNSS pseudorange and carrier phase ionosphere-free observations and uses a batch LSQ estimator. The main output of the POD module consists of a precise reduced-dynamic orbit (with precision at the level of 5 cm 3D RMS) as well as executed maneuvers estimates.

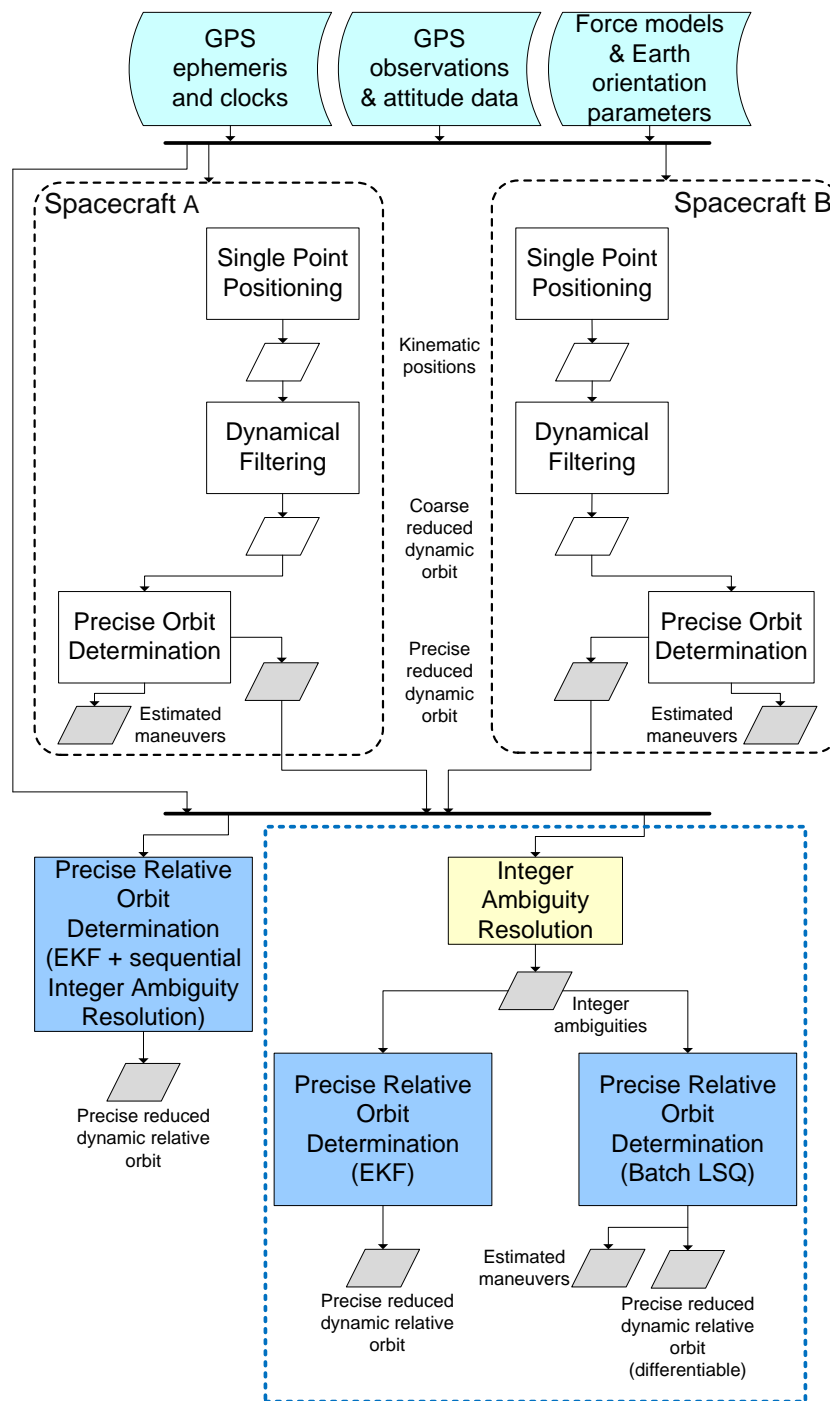


Fig. 3.3 Processing chain used in DLR’s GHOST for the generation of precise relative orbit solutions (adapted from Kroes et al. (2005) and Ardaens et al. (2010)).

The next stage in the processing chain is the generation of PROD products, which is depicted at the bottom part of Fig. 3.3. In the leftmost side, the current module for PROD is depicted. The basic structure of this module has been described in §2.2.2. Besides, the core data set, this module makes use of previously computed POD products and may require detailed information

about maneuvering activity (timing and magnitude), depending on the mission under analysis. The outcome from this module is a reduced-dynamic precise relative orbit product.

For the implementation of algorithms of the proposed PROD scheme, a set of tools and modules were developed in order to extend the current functionality of GHOST. These modules are depicted inside the blue dotted box at the bottom right part of Fig. 3.3. As they have been implemented as extended functionality, they can be considered as propounded additions to main toolset of the GHOST package. Unlike the main tool for PROD in GHOST, in the proposed scheme, the module for integer ambiguity resolution has been implemented as a standalone module. This approach was decided in order to provide some degree of flexibility for the generation of PROD solutions. Particularly, many of the auxiliary algorithms used for float and integer ambiguity estimation have been encapsulated to increase the modularity of the approach. From a system point of view, the implementation of splitted algorithms for integer ambiguity resolution and PROD eases code maintainability and does not add major difficulties in the processing chain. This module makes use of previously computed POD products and its main outcome consist of a set of files, in a custom format, containing DD integer ambiguity values and metadata referred to them.

The leftmost module inside the dotted blue box in Fig. 3.3, depicts an EKF-based scheme for PROD that makes use of integer ambiguities from the previous module. In essence, this tool is a simplified version of the main tool for PROD in GHOST, given that it makes use of GNSS ionosphere-free observation models and it does not include any integer ambiguity resolution method. From the relative determination point of view, both schemes possess similar levels of robustness. The outcome from this module is a reduced-dynamic precise relative orbit product.

Finally, the rightmost module inside the dotted blue box in Fig. 3.3, depicts a LSQ-based scheme for PROD that likewise makes use of integer ambiguities from a previous module. For this tool, POD products are not required as input. Instead, coarse reduced-dynamic orbit products are enough so as to provide functionality to the data editing algorithms included in the module. From a system point of view, this tool can be considered as the direct PROD extension of the POD module in GHOST. As such, both exhibit similar levels of robustness. Due to the characteristics of the LSQ-based PROD scheme, the delivered estimates of executed maneuvers are expected to exhibit a higher precision than their POD-based counterparts. As an additional feature of this scheme, the resulting outcome consists of a reduced-dynamic differentiable (smooth) precise relative orbit product, which may provide benefits to the analysis of data for remote sensing applications (line scanners, synthetic aperture radar, etc.). In comparison, this condition is not rigorously fulfilled by the EKF-based tool due the discontinuities caused by each measurement update (Montenbruck et al., 2005).

3.4 Description and discussion of publications

This section provides an overview of the publications that represent the major outcome from the research presented in this work. A short description of each publication is presented, briefly expanding on the theoretical background of each one and their significance within this research. Each publication is shortly presented according to a main achievement in the context of this study and a reference to the published paper is also indicated. The accepted versions of these papers have been reproduced in Appendices A, B and C.

3.4.1 [Pub 1] Robust integer ambiguity resolution

REFERENCE: Allende-Alba, G. and Montenbruck, O. (2016) *Robust and precise baseline determination of distributed spacecraft in LEO*. *Advances in Space Research* 57(1):46-63, doi: 10.1016/j.asr.2015.09.034.

Background

Precise baseline products have been a fundamental element for the generation of remote sensing products from formation flying missions in LEO. Early attempts of computing precise baselines with the CHAMP and GRACE missions showed the feasibility of achieving mm precision by making use of GPS carrier phase observations. Subsequent efforts in the introduction of more refined models and algorithms resulted in an unprecedented baseline precision at the sub-mm level using data from the GRACE mission. A key element for such a successful proof of concept was the use of GPS carrier phase observations with fixed integer ambiguities. Important features for the achievement of such precision levels were the use of an optimal integer ambiguity estimator and the implementation of robust reduced-dynamic orbit determination techniques.

The experience gained from these early studies showed the necessity of considering robustness as a primary characteristic of the baseline determination scheme. This robustness is, to large degree, inherited from the applied integer ambiguity resolution strategy. Past research showed that even if an optimal integer ambiguity estimator (i.e. ILS) is used, current schemes may produce degraded solutions due to wrong ambiguity fixing in scenarios with long baselines and/or high ionospheric activity. This reduced robustness of the scheme was similarly a consistent concern when applied in other missions profiles and with different GPS receiver characteristics.

The main aim of this paper was to improve the robustness of the float and integer ambiguity estimation strategies. Corresponding precise baseline solutions have been computed to show the impact of the proposed scheme on final products. This scheme was tested using real flight data from three formation flying missions with different mission profiles and GPS receiver characteristics.

Summary and discussion

In this paper, a strategy for precise baseline determination was presented and analyzed using data from the GRACE, TanDEM-X and Swarm missions. The core part of the strategy has been the development of a robust scheme for float and integer ambiguity estimation. Two key problems were addressed based on the scheme proposed in previous research (Kroes, 2006; Kroes et al., 2005), namely the reduction of computational burden of solving for many ambiguities in the ILS estimator and subsequent ambiguity validation scheme, and a solution for the vulnerability of the sequential (on-the-fly) integer ambiguity resolution method to challenging conditions. The first problem has been addressed by the development of a data processing technique based on the concept of *sliding batches*. In this approach, DD ambiguities are formed in localized processing batches based on a selected reference GPS satellite (with typical duration of 10-15 minutes). This allows to reduce the number of ambiguities to fix in each processing batch. The second problem has been partially addressed by making use of an estimation scheme based on the LSQ estimator, which adds robustness to the scheme by leveraging all the available GNSS observations in a given processing batch.

A key feature of the proposed strategy is the estimation of float ambiguities as a set in each processing batch, taking into account the geometrical information of the observation model. In

addition, the scheme was complemented with the inclusion of a priori information, which has been mainly derived from previously computed POD products and heuristic constraint values for ionospheric delay estimates. This feature has added robustness to the overall scheme and provides some advantages over the commonly used WL/NL ambiguity resolution strategy, as the dependence on (noisy) pseudorange observations is reduced. The use of geometric, a priori and observation information allows a more realistic model characterization for the application of the ILS estimator. The LAMBDA method has been used for the computation of the ILS estimator, which provides statistical measures over the provided solution and guarantees a theoretical optimality among admissible integer ambiguity estimators. This provides some advantage over other techniques, such as rounding or bootstrapping estimators (commonly used in WL/NL-based ambiguity resolution). Additionally, the scheme was complemented with an ambiguity validation scheme which aims at an improvement of robustness by using a combination of theoretical and heuristic validation tests. Particularly, concepts from recent advances in the theory of integer aperture estimators have been used as basis of the theoretical tests. Heuristic validation tests were built around experience from past research but some extra elements were included in order to complement the scheme. The overall integer ambiguity resolution strategy has been, in addition, complemented by the addition of a partial ambiguity resolution scheme, which has been devoted to the improvement of the ambiguity fixing rate (see Addendum).

The proposed schemes were tested with more than 2 years of data from the GRACE, TanDEM-X and Swarm missions. Differential PV maps were estimated and applied for all the missions under analysis. The improvement provided to baseline solutions with respect to absolute PV maps was tested using data from the GRACE mission over a period of 1 year. In addition, the results obtained from the GRACE mission showed an overall consistency with KBR data of 0.7 mm for periods of low and medium solar activity and of 0.8 mm for a period under intense ionospheric activity. A state-of-the-art performance was achieved for the TanDEM-X mission, achieving a consistency of kinematic and reduced-dynamic solutions of around 11 mm and 3 mm for vertical and horizontal components, respectively. The inter-product consistency with the scheme used in routine operations was of around 1.2 mm and 0.3 mm for the three components in single- and dual-frequency modes, respectively. A particular challenge for the proposed scheme was the big number of detected cycle slips in data from the TanDEM-X mission. This fact was highly detrimental for the solution of the LSQ system in each processing batch as very short GPS satellite passes are considered. It is left for further investigation to analyze whether these pass-breaks were caused by the ambiguity cycle slip detector (i.e. a high false alarm rate) or if the actual ambiguity estimation scheme must/can be improved to cope with such scenario (see Chapter 4).

Data from the Swarm mission was particularly challenging to process due to the presence of half-cycle ambiguities in GPS carrier phase observations. An initial approach was to apply a simple modification to the algorithm in order to allow GPS carrier phase observation models considering half-cycle ambiguities. With this approach, it was possible to obtain a mean fixing rate of about 89% using 30 days of data in August 2014. In an attempt to increase the performance of the algorithm, the float ambiguity estimation scheme was slightly extended in order to include a strategy for cycle type determination. The primary objective of this best-effort approach is to apply proper observation models for each ambiguity to be estimated and solved. Given that the models may be specific with full- or half-cycle ambiguities, this strategy was denominated as *mixed-cycle* ambiguity resolution. An empirical finding during these

tests was the correlation between carrier phase observations in each frequency band, namely a corresponding cycle type for ambiguities in L1 and L2. This led to the observation of full-cycle widelane ambiguities. As a direct consequence, modeling GPS carrier phase observations with the same cycle type in each frequency represented an *effective constraint* in the searching process of the LAMBDA algorithm. This resulted in a slightly improved performance of the scheme and therefore better baseline solutions. With this approach, it was possible to achieve a mean fixing rate of 93% and a consistency of reduced-dynamic and kinematic solutions of 4.0 cm, 1.7 cm and 1.1 cm in the radial, along-track and cross-track directions, respectively.

The results obtained in this paper showed the feasibility of producing baseline solutions for a variety of distributed spacecraft missions using a single scheme. For the case of GRACE and TanDEM-X, the results showed the planned capabilities of the proposed scheme and a better or similar performance with respect to state-of-the-art solutions could be obtained. For Swarm, the obtained results were part of the first efforts for precise baseline reconstruction. However, the data used for the presented tests was severely affected by ionospheric scintillation effects. This factor together with the presence of half-cycle ambiguities in observations were two limiting elements for testing the actual achievable performance in precise baseline determination for Swarm. A further improvement was achieved in Publication 2.

Individual contributions from authors

The need to improve the robustness of the heritage on-the-fly integer ambiguity resolution method and to develop a dedicated scheme for ambiguity estimation in formation flying missions was originally pointed out by Oliver Montenbruck.

The concept of data arrangement into sequential processing batches and the theoretical formulation of the estimation scheme, including the employed GNSS observation models and the incorporation of a priori information were the result of many discussions between the first author and Oliver Montenbruck.

Key contributions of the first author comprise the use of a partial ambiguity resolution strategy and various concepts of the theory of integer aperture estimators for the proposed ambiguity validation scheme. The software implementation of the proposed scheme building up on existing GHOST software components was done by the first author, who also conducted the entire data processing and basic analysis of results for all missions.

From the analysis of results from the Swarm mission, both authors jointly identified the full-cycle property of widelane ambiguities from the GPSR receivers on board the Swarm A and Swarm C spacecraft. The idea of the mixed-cycle strategy to cope with half-cycle ambiguities was developed and contributed by the first author.

The first author, finally, took care of the manuscript preparation, including the basic analysis and discussion, the creation of plots, figures and tables, while the second author contributed a review of the manuscript as well as critical discussions.

Declaration of consent


for the publication of the cumulative dissertation
of
Mr. Gerardo Allende Alba

München, August 29, 2017

The co-author hereby confirms the correctness of the declaration of contributions made by Mr. Allende Alba on the publication

Allende-Alba, G. and Montenbruck, O. (2016) *Robust and precise baseline determination of distributed spacecraft in LEO*. *Advances in Space Research* 57(1):46-63, doi: 10.1016/j.asr.2015.09.034.

The percentage of contribution by each author is estimated at:
Allende-Alba, G. (80%), Montenbruck, O. (20%)

Name of the co-author	Date	Signature
Montenbruck, O.	Aug 29, 2017	

3.4.2 [Pub 2] Half-cycle ambiguities and space baseline determination

REFERENCE: Allende-Alba, G., Montenbruck, O., Jäggi, A., Arnold, D. and Zangerl, F. (2017) *Reduced-dynamic and kinematic baseline determination for the Swarm mission*. GPS Solutions 21(3):1275-1284, doi: 10.1007/s10291-017-0611-z.

Background

A scheme for robust integer ambiguity for precise baseline determination was proposed and introduced in Publication 1. An extension of the scheme was added in order to handle carrier phase observations with half-cycle ambiguities for the Swarm mission. Although a reasonably good performance was obtained in preliminary tests with data from August 2014, some questions remained open. In particular, it was not possible to know if baselines could be determined in a consistent manner and with a precision comparable with previous formation flying missions.

During 2015 some of the tracking parameters of GPSR receivers on-board the Swarm spacecraft were modified. This was done in order to increase the robustness of receivers to ionospheric scintillation errors, which had been observed both in POD and preliminary PBD analyses. van den IJssel et al. (2016) performed a study of the impact of such changes on POD solutions computed during different periods on 2015. Such a study showed a relative improvement of solutions as a result of the configuration changes of GPSR receivers. On the other hand, a corresponding analysis for PBD was still to be performed. However, one of the main concerns was the impact of half-cycle ambiguities on baseline solutions. The present publication introduced a strategy for pre-processing of carrier phase observations from GPSR receivers in order to guarantee ambiguities of full-cycle. As a consequence, it was possible to generate precise baseline solutions using *standard* PBD schemes (assuming integer valued ambiguities). This allowed to carry out a more thorough analysis on the quality of PBD solutions for prospective applications, such as gravity field determination (Teixeira da Encarnação et al., 2016).

Summary and discussion

In this paper, an analysis of the performance of PBD schemes and resulting products for the Swarm mission was presented. The analysis was done using data from 90 days in 2016. One of the main objectives of the study was to show the feasibility of generating carrier phase observations with full-cycle ambiguities from the GPSR receivers. The resulting observations helped to improve the performance of algorithms for integer ambiguity resolution and baseline determination.

A first indicator of the enhanced performance of the IAR scheme and quality of carrier phase observations was obtained from the analysis of estimated float ambiguities. These exhibited a peaked normal frequency distribution around an integer value, in comparison with wide bi-modal or uniform distributions obtained with observations containing half-cycle ambiguities. The average ambiguity fixing rate performance was improved to 94% in comparison with values of 88%-89% reported in previous studies, where observations with half-cycle ambiguities were used.

Similarly, this study is also among the first efforts to provide a more complete analysis of the achievable performance of baseline solutions based on standard algorithms, after the

modifications in GPSR receivers performed in 2015. Reduced-dynamic and kinematic baselines were obtained and evaluated in external and inter-product assessments. In essence, it is quite difficult to obtain absolute statistical indicators about the quality of reduced-dynamic baselines, since no external reference of adequate quality is available (as was the case for the GRACE KBR system). Nevertheless, it is possible to obtain some qualitative indicators of the improvement provided by PBD solutions. In this study it was possible to show an enhanced consistency of orbits from PBD solutions in terms of satellite laser ranging residuals (SLR), in comparison with POD orbits. An additional assessment was performed by comparing differential POD (dPOD) and reduced-dynamic baseline solutions. Average RMS differences between 3 mm and 8 mm were obtained for the three orbital directions.

For the case of kinematic baselines, the assessment was based on a comparison with reduced-dynamic solutions. Given that kinematic baselines are totally dependent on observations, the evaluation of their quality is a good indicator of both the performance of the IAR scheme and the observation noise levels. As previously described in this section and analyzed in previous studies, the carrier phase observations from the GPSR receivers of Swarm have been largely affected by ionospheric scintillation. In this way, the assessment of kinematic baselines provides a hint of the quality of observations after the configuration changes of GPSR receivers on 2015. On average, RMS differences of around 18 mm and 5-6 mm were obtained in the vertical and horizontal orbital components, respectively. These values show an improvement with respect to the results obtained in Publication 1, where average RMS differences between 5 cm and 1 cm were obtained.

Of particular interest was the analysis of the spatial/geographical distribution of errors in kinematic baselines due to the previously observed effect of scintillation on kinematic absolute orbits (van den IJssel et al., 2015). For this purpose, the epoch-wise comparison of kinematic and reduced-dynamic solutions was geographically mapped using the trajectory of the Swarm A spacecraft as reference. Then, the RMS difference for each bin in a $1^\circ \times 1^\circ$ grid was computed. A map for each orbit component has been depicted in the paper. Errors in the horizontal directions are homogeneously distributed along the globe. On the other hand, the solutions in the radial direction are notably degraded in the polar regions. As the baseline determination in the radial direction is degraded by a poor geometry (larger dilution of precision values), it may be not evident that the observed differences in the polar regions may be caused by ionospheric scintillation effects. However, when vertical dilution of precision values were compared, it was found that in the polar regions such values are only moderately larger (average value of 2.9) than in mid-latitudes within the belt $\pm 60^\circ$ (average value of 2.1). The same comparison in terms of average RMS differences showed increased levels by a factor of about 2.5 in the polar regions.

To the knowledge of the authors, this study was one of the first efforts to produce precise baselines for the Swarm mission under similar conditions to previous research with other distributed spacecraft, such as GRACE and TanDEM-X. Aside from the performed inter-product assessments, a potential use of estimated baselines for applications such as gravity recovery, calls for a more exhaustive evaluation of the achievable product quality. This assessment was carried out by making use of products obtained from an independent software package, i.e. BSW from the Astronomical Institute of the University of Bern. This package has a mature tool set for several precise positioning applications. Precise reduced-dynamic and kinematic baselines are computed using different approaches than those used in the GHOST package, which provides a degree of independence for baseline assessment.

In the comparison of reduced-dynamic solutions, it was found that the biases were well confined below 1 mm, which gives an indication of low systematic errors in solutions from both software packages. Average standard deviations of around 1.8 mm and 1.2 mm were obtained for the difference of the vertical and horizontal orbital components, respectively. The obtained values suggest that the baseline precision is slightly worse in comparison to what was obtained with previous missions, e.g. TanDEM-X (Jäggi et al., 2012). Key factors contributing to this performance are the slightly larger observation errors (as a result of configuration changes in receivers) and the limited number of tracking channels in the GPSR instruments.

The assessment of kinematic baselines showed a similar situation in terms of inter-solution average biases, i.e. they were confined below 1 mm. The largest biases (around 0.5 mm on average) were found in the radial direction, which indicates a possible discrepancy in the used values for center of gravity and antenna reference points of each spacecraft. Although every effort was made in order to use a consistent set of configuration values in both software packages, it was not possible to achieve a successful reduction of inter-product biases in the radial direction. Possible explanations include the lack of a ground-based antenna phase center calibration, which in turns limits the capability to precisely separate the coordinates of antenna reference points and antenna phase center offsets. The root cause of such biases is still unknown and under investigation. On the other hand, standard deviations of around 17 mm and 5-6 mm were found for the vertical and horizontal orbital components, respectively. These values are consistent with the inter-product assessment with reduced-dynamic solutions obtained with GHOST.

Individual contributions from authors

The concept of half-cycle ambiguity correction in the generation of carrier phase observations for the RUAG GPS receiver was developed by Oliver Montenbruck in discussion with Franz Zangerl. Based on this concept, RINEX observation files with full-cycle carrier phase ambiguities were generated for the SWARM satellites by the first author, who also performed the processing and generation of ambiguity-fixed PBD solutions using his previously developed precise baseline determination software. The generation of independent baseline solutions using the BSW tools was performed by Adrian Jäggi and Daniel Arnold. The analysis and interpretation of results from the inter-agency assessment of baseline solutions was done by the lead author in discussion with his partners.

The contributions of the first author to the paper were: the generation of plots and tables, the discussion of results from the inter-product and inter-agency baseline assessments, the conception of the paper structure and the elaboration of the first version. Oliver Montenbruck wrote the section on signal tracking concepts with support from Franz Zangerl. Finally, all co-authors contributed to the improvement of the paper through their comments, suggestions and corrections about the contents and language.

Declaration of consent



for the publication of the cumulative dissertation
of
Mr. Gerardo Allende Alba

München, August 29, 2017

The co-authors hereby confirm the correctness of the declaration of contributions made by Mr. Allende Alba on the publication

Allende-Alba, G., Montenbruck, O., Jäggi, A., Arnold, D. and Zangerl, F. (2017) *Reduced-dynamic and kinematic baseline determination for the Swarm mission*. GPS Solutions 21(3):1275-1284, doi: 10.1007/s10291-017-0611-z.

The percentage of contribution by each author is estimated at:
Allende-Alba, G. (65%), Montenbruck, O. (15%), Jäggi, A. (10%), Arnold, D. (5%), Zangerl, F. (5%)

Name of the co-author	Date	Signature
Montenbruck, O.	Sep. 13, 2017	
Jäggi, A.		
Arnold, D.		
Zangerl, F.	30.8.2017	

Declaration of consent

for the publication of the cumulative dissertation
of
Mr. Gerardo Allende Alba

München, August 29, 2017

The co-authors hereby confirm the correctness of the declaration of contributions made by Mr. Allende Alba on the publication

Allende-Alba, G., Montenbruck, O., Jäggi, A., Arnold, D. and Zangerl, F. (2017) *Reduced-dynamic and kinematic baseline determination for the Swarm mission*. GPS Solutions 21(3):1275-1284, doi: 10.1007/s10291-017-0611-z.

The percentage of contribution by each author is estimated at:

Allende-Alba, G. (65%), Montenbruck, O. (15%), Jäggi, A. (10%), Arnold, D. (5%), Zangerl, F. (5%)

Name of the co-author	Date	Signature
Montenbruck, O.		
Jäggi, A.	29.8.2017	a. Jäggi
Arnold, D.	29.8.2017	D. Arnold
Zangerl, F.		

3.4.3 [Pub 3] Robust relative orbit determination and maneuver estimation

REFERENCE: Allende-Alba, G., Montenbruck, O., Ardaens, J.-S., Wermuth, M. and Hugentobler, U. (2017) *Estimating maneuvers for precise relative orbit determination using GPS*. *Advances in Space Research* 59(1):45-62, doi: 10.1016/j.asr.2016.08.039.

Background

An important factor of the robustness of a PROD system is the employed estimation scheme. Sequential algorithms, such as the family of Kalman filters, are particularly suitable for many application scenarios. They are attractive due to the generally good computational performance and the small size of the state space. In the field of orbit determination, sequential estimation algorithms have been successfully used both in real-time and offline applications. Nevertheless, such algorithms are particularly vulnerable to some nuisances present in orbit determination problems, such as data gaps and orbit control maneuvers.

Data gaps are mostly referred to a loss of track of every GNSS satellite in view for a given period, which may go from some minutes to various orbits. These may be caused by a temporal failure in a GNSS receiver or by an uncontrolled or unstable spacecraft attitude, causing a continuous change in orientation of the GNSS receiver antenna and hence a constant loss of track of GNSS satellites. This scenario represents a serious handicap in the performance of a sequential estimation scheme. In the particular case of an extended Kalman filter, the prediction step is based on the propagation of a reference trajectory using a dynamical model complemented with pseudo-stochastic parameters, such as empirical accelerations. This prediction is based only on the previous filter state. When observations are not available, it is not possible to estimate such corrections and therefore the orbit error increases with time.

Orbit control maneuvers represent a discontinuity in the orbit dynamics and as such they must be considered for trajectory propagation in the EKF prediction step. For maneuver handling in some sequential estimation schemes, it is necessary to rely on external information. As an example in the context of real-time navigation, D'Amico et al. (2009) proposed the inclusion of both estimated and external information from on-board accelerometers into the orbit prediction step to minimize the impact of maneuvers. For the case of precise baseline determination, Montenbruck et al. (2011) used a scheme in which maneuver information is reconstructed from telemetry data and process noise is added to the state covariance matrix to account for the respective uncertainties.

In order to complement the robustness of the overall scheme proposed in Publication 1, in this publication a PROD method based on a LSQ estimator is developed. Given that the LSQ estimator makes use of a complete set of GNSS observations in order to adjust the trajectory as a whole, the scheme is more tolerant to the presence of data gaps. However, the major benefit derived from this implementation is the capability of direct estimation of orbit control maneuvers. By making use of measurements taken before and after a maneuver execution, it is possible to observe the changes in the spacecraft trajectory and hence to estimate the magnitude and direction of the changes.

In this publication, a batch PROD method is introduced and discussed. The maneuver estimation capability has been particularly emphasized due to the characteristics of the implemented reduced-dynamic strategy. The proposed scheme has been tested with different mission

profiles and maneuver execution rates, using real flight data from the GRACE, TanDEM-X and PRISMA missions.

Summary and discussion

This study is focused on the description of a PROD scheme based on a batch LSQ estimator, making a particular emphasis on the orbit control maneuver estimation capability. The estimation scheme is based on the reduced-dynamic approach, in which empirical accelerations are estimated using GNSS observations and used to adjust the resulting trajectory. The strategy followed in the described study is based on the concurrent adjustment of absolute and relative trajectories within the same algorithm. This aims at the definition of a *congruent grid* intervals for absolute and relative empirical accelerations in order to apply consistent corrections to the corresponding trajectories under adjustment. In this case, a congruent grid of intervals is achieved when the defined duration, starting and ending points of intervals for estimation of empirical accelerations in each trajectory match as close as possible. In the absence of maneuvers, this is achieved by using the same parameters for the definition of intervals in both trajectories. When maneuvers are present, these intervals are matched taking into account the ending points of intervals for maneuver estimation.

The aforementioned strategy for empirical acceleration estimation already provides the proper framework for maneuver estimation, too. In this study, maneuvers are considered as constant thrust arcs in the local spacecraft's radial, along-track and cross-track components across the maneuver duration interval. This approach considers the maneuver duration and the maneuver start time as known parameters. These values can be retrieved from telemetry data. However, they also possess inherent uncertainties due to the several delays stemming from the on-board computer, thrusters, etc., leading to subtle errors in the final orbit solutions around the maneuver center of burn. A correction to this time can be performed by either changing the start time or the duration of the maneuver. In this study, it was attempted to extend the maneuver estimation algorithm in order to include an estimation of maneuver start time. The approach was initially implemented in POD and the estimated time was subsequently introduced as known value into the PROD algorithm. Although this approach worked most of the time correctly with only maneuver per day, it was less effective in scenarios with a higher maneuver execution rate.

The PROD scheme described in this study is generally suited for processing GNSS carrier phase observations with float and fixed ambiguities. While float ambiguity solutions are obtained as the *default* option, the computation of fixed ambiguity solutions require extra considerations. Common WL/NL ambiguity resolution strategies make use of a PROD scheme that concurrently solves for narrowlane float (and integer) ambiguities. In such schemes, a particular problem to consider is the effect of executed maneuvers on the estimated ambiguities, which has a direct dependency on the applied reduced-dynamic and maneuver handling strategies. Following the results obtained in Publication 1, the PROD algorithm described in this study uses the IAR strategy introduced in such that paper. The key advantage of this approach is its kinematic nature, namely the float ambiguity estimation process is not affected by the presence of maneuvers, aside from minor effects possibly caused by multipath in the observations. Similarly, this strategy assumes that reference trajectories are smooth during maneuver execution periods, which is an attainable requisite for the used POD products.

The presented algorithms have been tested using real flight data from the GRACE, TanDEM-X and PRISMA missions. These are representative examples of distributed spacecraft missions

with diverse formation control strategies and maneuver execution rates. The assessment of results has been divided into an evaluation of the quality of resulting baselines and of the accuracy/precision of maneuver estimates.

For the case of the GRACE mission, the same data set used in a recent study (Ju et al., 2017) was chosen in order to have an immediate comparison with such results. Given the sparsity of maneuver execution for GRACE, a set of 10 days distributed from 2004 to 2012 were selected. The results show an average precision of KBR residuals of 0.54 mm for days with available KBR data for assessment. Additionally, it has been possible to analyze the impact of using different values (or estimates) of center of burn time. Estimated values of start time of burn have been included into the PROD scheme in order to apply corrections in the range of 0.04-0.9 s. The corresponding improvement of the baseline precision in the vicinity of a maneuver has been at the level of 4-5 mm.

For the TanDEM-X mission a data set of 10 days during January 2014 was selected. During this period the baseline dimension of the formation was around 500 m. In this way, it was possible to perform an assessment using various baseline solutions in single- and dual-frequency modes. In addition to the schemes under test, baseline solutions using the PBD strategy used in the operative software (described in §2.2.2) have been used for comparative assessment. An important result presented in this study was to show the improvement provided by maneuver estimation in the resulting baseline. This contrasts with the approach under comparison, in which the state covariance matrix is increased in order to accommodate the uncertainty during the period of maneuver execution (Montenbruck et al., 2011). A consequence of this strategy is that the orbit loses stiffness during such periods and the solution is much more dependent on the observations. From the different comparisons, it was possible to use relative orbits obtained from the approach introduced in this study as reference in order to improve the performance of the aforementioned approach.

A similar set of tests were performed with the PRISMA mission. For such tests, two 5-days sets during September 2010 and March 2011 were selected. Similar to the TanDEM-X mission, baseline solutions using a sequential estimation scheme were degraded in the vicinity of a maneuver execution period. Indeed, the situation with PRISMA was worse. Due to a higher maneuver rate, the resulting baselines could be degraded for various minutes (or even a complete orbit) around periods with intense maneuvering activity. Similar to TanDEM-X, improved relative orbit products using the introduced PROD scheme could be obtained. Such products were used in order to improve the performance of the sequential estimation scheme.

The second assessment task was devoted to the evaluation of precision/accuracy of estimated maneuvers. Due to the lack of a reference, an assessment of estimated maneuvers is typically performed by means of inter-solution comparisons. Reconstructed maneuvers using telemetry data have been used in this comparison, as they are obtained from data independent of GNSS. The study focused in the comparison of POD and PROD (float and fixed ambiguity) solutions with respect to telemetry-reconstructed maneuvers. This comparison method yields an assessment of relative errors of maneuver estimates. For the GRACE and TanDEM-X mission, the obtained inconsistency was below 3%. For PRISMA, a much larger uncertainty was obtained among the estimates from the different methods. Due to the very small magnitude of some maneuvers, the relative errors obtained from this assessment could not provide any insight into the actual precision of estimated maneuvers from POD and PROD.

The evaluation of absolute errors in maneuver estimates was achieved by using a concept denominated as *dummy* maneuvers. In this approach, a set of maneuvers are introduced into

the estimation algorithm during true-maneuver-free periods. In this way, it is possible to take into account the value of the maneuver being executed (in this case zero) and compare the estimates with respect to this reference. The technique can be used to apply a set of various maneuvers, allowing in this way a statistical analysis of estimates. Overall, these statistical tests hints at the expected accuracy/precision of estimated maneuvers from POD and PROD. Representative maneuver duration sets were used for each test case. Due to the availability of data and maneuver-free periods, a different number of dummy maneuvers were used for these tests in the different missions. In total 250, 110 and 140 maneuvers were included in the analysis with the GRACE, TanDEM-X and PRISMA missions. In a broad sense, considering the execution of maneuvers ranging from 0.5-1 mm/s to 10-20 cm/s, the presented PROD algorithm is capable of delivering estimates with rough error levels in the range of 10% to 0.1-0.01%. However, it was not possible to observe any significant improvement in PROD solutions using fixed ambiguities with respect to those obtained using float ambiguities. A further analysis of this finding has been left for future analysis (see Chapter 4).

Individual contributions from authors

The development and implementation of a batch LSQ estimator for baseline estimation that supports the calibration of orbit maneuver and copes with known deficiencies of the previously employed EKF scheme was done by the first author following an initial suggestion by Oliver Montenbruck. The first author, furthermore, contributed the scheme for relative orbit determination making use of previously-fixed integer ambiguities as well as the concept of estimating the start time of a maneuver burn in the relative orbit determination system. He was also in charge of the overall data analysis.

The tests and analysis of results for the TanDEM-X mission were done by the first author with support of Martin Wermuth who prepared all relevant data sets and auxiliary operations information. The tests and analysis of results using data from the PRISMA mission were done by the first author with the support of Jean-Sébastien Ardaens, who also contributed tools for telemetry-based maneuver reconstruction from the PRISMA mission.

The concept of dummy maneuvers as a tool of performance assessment of the relative orbit determination system was suggested by Oliver Montenbruck. It was implemented and applied for all three missions by the first author, who also evaluated and interpreted the respective results. A general analysis of the first set of results presented in the paper was carried out during discussions between Urs Hugentobler and the first author.

Main contributions of the first author to the manuscript preparation include the generation and discussion of results, plots and tables, the conception of the paper structure and the elaboration of the first version. All co-authors contributed to the improvement of the initial writing and structure through comments, suggestions and corrections of contents and language.

Declaration of consent

for the publication of the cumulative dissertation
of
Mr. Gerardo Allende Alba




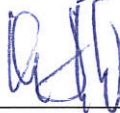
München, August 29, 2017

The co-authors hereby confirm the correctness of the declaration of contributions made by Mr. Allende Alba on the publication

Allende-Alba, G., Montenbruck, O., Ardaens, J.-S., Wermuth, M. and Hugentobler, U. (2017) *Estimating maneuvers for precise relative orbit determination using GPS*. Advances in Space Research 59(1):45-62, doi: 10.1016/j.asr.2016.08.039.

The percentage of contribution by each author is estimated at:

Allende-Alba, G. (70%), Montenbruck, O. (15%), Ardaens, J.-S. (5%), Wermuth, M. (5%), Hugentobler, U. (5%)

Name of the co-author	Date	Signature
Montenbruck, O.	29.8.2017	
Ardaens, J.-S.	1.9.2017	
Wermuth, M.	31.8.2017	
Hugentobler, U.	11.9.2017	

3.5 Conclusions

The present research has been mainly devoted to the development of robust methods and algorithms for PROD. A key feature to obtain precise relative orbit products is the use of GNSS carrier phase observations with fixed ambiguities. However, challenging conditions and mission scenarios may threaten a successful integer ambiguity fixing. When wrongly-fixed ambiguities are used, PROD solutions may be (largely) degraded, rendering them unusable for the intended application. From the perspective of final PROD products, the robustness of the method is to a large degree dependent on the robustness of the IAR scheme. Current methods based on sequential algorithms may be too vulnerable to harsh positioning conditions, such as long baselines and intense ionospheric activity. Methods based on WL/NL ambiguity resolution techniques may be prone to errors due to a large dependency on pseudorange observations and/or lack of strong ambiguity validation methods.

Publication 1 was devoted to the problem of developing a robust scheme for IAR which could reduce the susceptibility of unsuccessful ambiguity fixing. The key idea was to attempt to reduce the influence of sources of potential error and use as much information as possible for the task to solve. The float ambiguity estimation scheme has been based on a batch scheme that uses both the observations and observational geometry. A priori information from POD products and heuristic knowledge has been included in the scheme in order to make a more efficient use of available observations. Integer ambiguity estimation has been carried out by using the ILS method, regarded as optimal among admissible integer estimators. The algorithm has been complemented with a robust ambiguity validation scheme which makes use of theoretical and heuristic tests. The overall proposed strategy has been tested with data from the GRACE, TanDEM-X and Swarm missions and compared with solutions obtained with a current PBD scheme. The results show that an improved robustness and precision has been achieved for PBD solutions of the GRACE mission. A comparable performance to state-of-the-art solutions has been achieved for the TanDEM-X mission. In the case of the Swarm mission, unlike the alternative PBD scheme, the proposed strategy was able to provide precise baseline solutions. These could be computed even under harsh ionospheric conditions and the presence of half-cycle ambiguities in carrier phase observations. These results suggested the feasibility of generating PBD solutions for a variety of formation flying by using a single (robust) scheme.

From the various missions considered for test, the Swarm mission is the most recent and it imposed various challenges with respect to previous ones. Some particular problems could be partly tackled in Publication 1, but some open questions remained to be answered. Publication 2 was devoted to explore the achievable precision and quality of baselines under to the conditions present in the Swarm mission. A key feature of the study carried out in Publication 2 was the generation of carrier phase observations with full-cycle ambiguities only. Combined with configuration changes in GPSR receivers implemented during 2015, the availability of *standard* carrier phase observations called for an analysis of precise baseline solutions. As these solutions were among the first to be obtained under conditions comparable to previous formation flying missions, a thorough assessment was performed. Inter-product evaluations with reduced-dynamic and kinematic solutions showed a consistency comparable with previous results obtained for the GRACE and TanDEM-X missions. Emphasis has been made on the analysis of kinematic baseline solutions due to their total dependency on carrier phase observations. An analysis of the spatial distribution of differences showed increased error levels in the polar regions, which have been attributed to ionospheric scintillation effects (also in accord to previous POD

analyses). An inter-agency assessment using solutions from independent software tools revealed similar results in terms of quality of kinematic and reduced-dynamic baselines.

Once some degree of robustness of the IAR scheme could be attained, the next step was to extend such robustness to the actual relative orbit determination scheme. Particularly, it was deemed necessary to tackle the robustness problems of sequential estimation algorithms (explicitly extended Kalman filters) by implementing a batch LSQ estimator. Such a method could add robustness to the scheme to data gaps and outages and at the same time it added the capability of direct estimation of orbit control maneuvers. This particular asset was the main topic of Publication 3. The advantages of the introduced PROD method are twofold. First, the resulting relative orbit trajectories are smooth and differentiable along the complete data arc, even during maneuver execution. Second, the resulting maneuver estimates are obtained using differential GNSS measurements and relative spacecraft dynamics. This allowed to improve the precision of estimates in comparison with single-spacecraft POD solutions. The introduced scheme was tested using real flight data from the GRACE, TanDEM-X and PRISMA missions. The assessment of PROD solutions was performed by using external tools (GRACE) and by means of inter-product comparisons using solutions from current PROD algorithms (TanDEM-X and PRISMA). In these test cases, it was possible to show that the introduced PROD scheme provided solutions with improved quality. For the assessment of maneuver estimates, telemetry-reconstructed maneuvers were used a consistency check. This method provided a useful resource to obtain indicators about the relative precision of estimates, mostly for the GRACE and TanDEM-X missions. Indicators about absolute errors of maneuver estimates were obtained from a statistical analysis using the concept of *dummy* maneuvers.

Chapter 4

Lessons learned and outlook

This study was dedicated to the analysis of robustness on precise relative orbit determination systems for distributed spacecraft in LEO. One of the fundamental goals of this research has been to increase the robustness of such systems while keeping or enhancing the achieved precision provided by state-of-the-art schemes. The proposed strategies were focused on the improvement of robustness of both the integer ambiguity resolution strategy and the actual relative orbit determination scheme.

The development of the integer ambiguity resolution method was primarily centered on finding strategies to leverage the use of an optimal integer ambiguity estimator and a composite ambiguity validation scheme. Previous research done by Kroes et al. (2005) showed the suitability of this approach for ambiguity resolution in relative orbit determination systems. However, in such a scheme, the tight integration of the integer ambiguity resolution and sequential baseline determination schemes showed in practice a difficulty of selecting proper data weights and ambiguity validation thresholds that can be used in a variety of scenarios.

One of the first decisions in the development of the proposed scheme was to split the integer ambiguity resolution and relative orbit determination problems into two implementations. The major reason for this was to allow specific control of the various configuration settings for each problem. Hence, the specific challenges for each problem could be tackled in a more direct way. The proposed scheme was developed as a sequential/batch integer ambiguity resolution system to exploit key advantages of each strategy type. The creation of processing batches is performed in a sequential way in order to leverage the advantage of small space states. In turn, each data processing batch is solved using a batch estimation scheme, which allows the use of more observations in the estimation problem.

In the tests with data from the GRACE mission from 2007, 2009 and 2011, it was possible to observe that the overall scheme could perform with good levels of robustness in long-term analyses. In comparison with the on-the-fly ambiguity resolution scheme, this added robustness increased the availability of solutions of high precision in long-term analyses. As an example, the analysis of GRACE data on 2009 showed an increase of availability of more than 25% of solutions with a 1D precision better than 1 mm. Further tests with data from the TanDEM-X and Swarm missions from 2014 showed a similar or improved performance of the proposed scheme with respect to the state-of-the-art scheme developed by Kroes et al. (2005). A particular feature of the developed scheme is the ability to handle half-cycle ambiguities even in a long baseline scenario. Such an approach was initially tested using data from the Swarm mission from August 2014. Using two strategies to tackle the presence of half-cycle ambiguities, it was possible to achieve mean ambiguity fixing rates between 89 and 93%.

A further development with Swarm data could be achieved with a strategy for half-cycle ambiguity resolution during the generation of carrier phase observations. This strategy allowed to process carrier phase observations with full-cycle ambiguities only in the baseline determination system. A particular improvement over previous analyses with Swarm (e.g. Jäggi et al. (2016) and Publication 1 in Appendix A) was the achieved consistency among kinematic and reduced-dynamic solutions. A major enhancement with respect to the schemes developed in Publication 1 was the reduced computational burden for integer ambiguity resolution. An assessment with products from the AIUB provided an indication of the achieved precision of reduced-dynamic and kinematic solutions.

To improve the robustness of the relative orbit determination system proposed by previous research by Kroes et al. (2005), a batch estimation scheme was developed. The implemented scheme included the feature of maneuver estimation. In comparison with an EKF-based strategy, the formulation of a batch estimation scheme increases the robustness of the system to the presence of big data gaps and orbit control maneuvers. The assessment of solutions for the GRACE mission using KBR data showed the feasibility of generation of continuous and smooth baseline solutions even around maneuver execution periods. Further tests with data from the GRACE, TanDEM-X and PRISMA missions and the introduced technique of dummy maneuvers suggested the key advantages of maneuver estimation on baseline solutions.

From a general perspective, the achieved robustness of the PROD scheme was fundamentally based on the use of batch processing algorithms. A key characteristic of a such strategy is the employment of all available observations in a given data arc to solve the estimation problem as a whole. However, setting up an estimation system which makes use of this approach results in algorithms of increased complexity and computational burden. As a consequence, the overall system becomes more prone to implementation errors. In this way, although the proposed PROD scheme could achieve some degree of robustness so as to work under different mission conditions, this was done at the expense of an increased (and sometimes undesirable) complexity.

4.1 Considerations and open questions

During the development and tests of proposed algorithms in this research, it was possible to gather information that can be considered for further investigations. These considerations are given here as reference. The respective discussion and/or results related to such considerations and open questions are indicated with reference to the publications reproduced in the appendices.

Impact of ionospheric delays in integer ambiguity resolution

- i. In the proposed scheme for integer ambiguity resolution, the weighting factors for a priori information for differential ionospheric delay estimation has been chosen in a heuristic way. This selection is based on the scenario under analysis, considering the baseline length and expected ionospheric conditions (Publications 1 and 2).
- ii. Tests with data from GRACE suggest that under good carrier phase tracking conditions (i.e. low number of cycle slips), it is suitable to apply very loose constraints to the a priori information for differential ionospheric delay estimates (e.g. 10 m). In this case, a larger time span is used for estimation, allowing a change in geometry between the GNSS constellation and the formation in LEO. The longer the duration of the DD

observation, the higher the decorrelation between ionospheric delays and float ambiguities. The resulting estimates of ionospheric delays are mostly determined by carrier phase observations (Publication 1).

- iii. When intense ionospheric conditions are present, high error levels in GNSS observations may hinder a precise estimation of differential ionospheric delays and float ambiguities. In this situation, tighter constraints on a priori information for ionospheric delays may be suitable to aid the estimation of float ambiguities (Publication 1).
- iv. The aforementioned strategy may also be helpful in scenarios with bad carrier phase tracking conditions (i.e. short passes). In this case, slightly tighter constraints on differential ionospheric delays may aid to increase the precision of float ambiguity estimates and the resulting ambiguity fixing rate. This approach is more suitable for short or medium-length baselines (Publication 1, §4.3).
- v. On the other hand, care must be taken when considering very *optimistic* a priori constraints on differential ionospheric delays. This implies that a fixed (or quasi-fixed) model is applied and the impact of GNSS observations on the corresponding estimates is reduced. The resulting estimates are largely dependent on the quality of the a priori information. If such information is not accurate, this may result in wrong float ambiguity estimates and associated covariance matrix (Publication 1, §4.3).

Float ambiguity estimation and integer ambiguity resolution

- i. A key element in the scheme for float ambiguity estimation is the inclusion of a priori information. In a theoretical sense, the provided a priori information should be decorrelated from observations (Publication 1, §2.3).
- ii. Under bad carrier signal tracking conditions, the performance of the proposed scheme may be degraded. One of the main causes is an increase in the number of ambiguities with very short observation periods to solve in each batch. This results in many computed values with a lower bound of ILS ambiguity success rate below an acceptable threshold (Publication 1, §4.3).
- iii. The application of semi-heuristic tests together with theoretical tests has shown to strengthen the ambiguity validation scheme and provides it more robustness for a generality of cases (Publication 1, §2.5).
- iv. The proposed scheme can handle half-cycle ambiguities through a direct estimation and using the proposed strategy of mixed-cycle ambiguity resolution. However, the latter method makes use of a best-effort scheme for cycle type determination. Its performance may result to be sub-optimal under a generality of cases (Publication 1, §4.4.1).

Relative orbit determination and maneuver estimation

- i. The proposed relative orbit determination system makes use of the concept of matching grid of empirical accelerations for absolute reference and relative trajectories. This allows the computation of relative empirical accelerations with proper time bounds and duration (Publication 3, §2.2).

- ii. The aforementioned approach allows the estimation of orbit control maneuvers when both spacecraft perform maneuvers (as in the case of the TanDEM-X formation). However, due to the formulation of the estimation scheme, maneuvers of the selected reference spacecraft are estimated independently from the relative trajectory (Publication 3, §2.2).

General open questions

1. How to characterize in a more theoretical form the a priori information used for float ambiguity estimation, particularly for differential ionospheric delays? (Publication 1, §2.3).
2. Can the improvement of dynamical models used for POD solutions (employed as a priori information) positively influence the quality of float ambiguity estimates? Can also the use of other data sources, such as accelerometers, have a good impact on such estimates? (Publication 1, §2.3).
3. What is the root cause of the apparent *long-wave* variations of precision of PBD solutions for GRACE, exhibited in the analysis of years 2007 and 2009? (Publication 1, §4.2.1).
4. What is the main cause of the large number of detected pass-breaks in the analysis of carrier phase data from the TanDEM-X mission? (Publication 1, §4.3.1).
5. How to characterize and quantify in a more complete way the errors in kinematic baseline solutions for Swarm attributed to ionospheric scintillation? (Publication 2, §*Kinematic baselines*).
6. How to include in an effective way the estimation of start time of maneuver in a relative orbit determination system with few performance penalties? Do the resulting benefits in terms of solution quality justify such an approach? (Publication 3, §2.3).
7. How to dissect the exhibited large relative errors in the comparison of telemetry-reconstructed and POD/PROD-estimated maneuvers for PRISMA for maneuver magnitudes and duration below 5 mm/s and 1 s, respectively? (Publication 3, §4.2.1).
8. Can the estimation of empirical accelerations during maneuvering periods improve the precision of estimates of long-duration maneuvers (e.g. 600 s)? (Publication 3, §4.2.2).
9. Why PROD solutions mostly improve maneuver estimates in the radial direction for tests cases with duration of 600 s for GRACE and TanDEM-X? (Publication 3, §4.2.2).
10. Why maneuver estimates from ambiguity-fixed PROD solutions are not significantly improved in comparison with those from float PROD solutions? (Publication 3, §4.2.2).

4.2 Recommendations and outlook

Based on the results obtained in this research, some recommendations for improvements and/or further advancements on the proposed schemes are given below.

- An improvement of the quantitative characterization of robustness of the proposed schemes could be carried out in further long-term analyses with various distributed spacecraft missions.
- The proposed scheme for float ambiguity estimation is, in principle, extensible to include more complex approaches for ionospheric delay modeling/estimation. One strategy could consist in pre-computing values for each estimation epoch using sophisticated models such as NeQuick (Di Giovanni and Radicella, 1990; Nava et al., 2008). Then, such values could be fed into the scheme as a priori information. However, a major challenge in this approach would be a proper statistical characterization of such pre-computed values that is required by the estimation scheme.
- More methods for selection of reference GNSS satellites for the formation of processing batches could be used. Currently, only two have been implemented and they have been used in a complementary way. A comparative study of the advantages and weaknesses of various possible methods may help for the analysis of more mission scenarios.
- One of the factors that affect the performance of the proposed method for float ambiguity estimation is the presence of short passes. These may result either from true carrier phase cycle-slips or from loss of individual observations from the receiver (i.e. without actual tracking interruption). Within the proposed scheme, simple algorithms were implemented to attempt a correction of miss-detected pass-breaks. These algorithms exhibited an acceptable performance in tests with data from PRISMA and Swarm. However, a more robust and complete scheme for cycle-slip and/or pass-break correction that can be applied for more general mission scenarios could be implemented.
- With the availability of more signals from multi-GNSS spaceborne receivers, the proposed scheme can be adapted to process such new signals. In particular, a dual-frequency dual-constellation scheme could be one of the most suitable approaches to follow. In this case, the number of ambiguities to fix in each batch would not increase dramatically so as to have a major impact on the computational performance. Additionally, using signals from two constellations already provides major benefits for differential ionospheric delay estimation and consequently an improved ambiguity fixing performance could be expected.
- The integer ambiguity validation scheme makes use of the fixed-failure rate ratio test approach (see §A.3.2) in order to determine the threshold μ_{RTIA} in Eq. (A.6). Such value is obtained by using generic look-up tables (Verhagen and Li, 2012). Although such approach exhibits an acceptable performance (see tests in §A.3.2), further analyses could be focused on the computation of look-up tables that consider more specific scenarios. Corresponding tests could be performed to compare both approaches. In addition, different integer aperture estimators could be implemented in substitution or as a complement to the ratio test integer aperture estimator (see e.g. Wang and Verhagen (2015); Wang et al. (2014)).
- Future theoretical improvements in the field of integer aperture estimators could be leveraged to enhance the proposed ambiguity validation scheme. A desirable scenario would be to reduce the number of free-thresholds (i.e. to be selected by hand) and substitute them by more formal methods.

-
- The implemented scheme for partial ambiguity resolution is based on the analysis of iterative solutions from the ILS estimator. More efficient methods could be implemented, based on recent research on the field (see e.g. Nardo et al. (2016) and Brack (2015)).
 - A further improvement on the strategy for mixed-cycle ambiguity resolution could be carried in the stage of cycle type determination. In principle, the problem can be framed in the signal detection theory (Kay, 1998), which may allow the implementation of more formal methods.
 - The batch relative orbit determination system estimates a reference trajectory in a POD scheme. However, it would be possible to enhance this strategy by adjusting both the absolute reference and relative orbits to differential GNSS observations. In this case, it is expected that the precision of the reference trajectory can be improved due to the use of fixed ambiguities. For the case of an EKF-based scheme, such an approach has been implemented by van Barneveld (2012).
 - An evaluation of the impact on the precision of maneuver estimates if (relative) empirical accelerations are estimated during maneuvering periods could be carried out. A similar approach has been recently proposed by Ju et al. (2017), but a more complete analysis of this strategy in multi-mission tests (with different maneuvering execution rates and duration) is yet to be performed.

Addendum

Methodology for integer ambiguity resolution

The integer ambiguity resolution strategy introduced in Publication 1 has been roughly described as a two-steps method consisting in dedicated schemes for float and integer ambiguities estimation. In a first stage, float ambiguities are estimated using an a priori-constrained LSQ method. Integer ambiguities are later resolved by using a scheme consisting of ILS and integer aperture estimators with additional semi-empirical and empirical ambiguity validation tests. Although the overall flow of the algorithms has been described in Publication 1, some details regarding specific design decisions can be detailed in order to better analyze their impact on the final results. This addendum provides a more in-depth description of the implemented algorithms in the introduced methodology for integer ambiguity resolution. The details provided in the present addendum may be useful as starting point for further developments of the proposed scheme. Similarly, the additional obtained results may have some relevance for prospect alternative proposals and/or improvements to the research presented in this dissertation.

A.1 Arrangement of processing batches

As described in §2.1, one of the main difficulties in the integration of IAR and PBD algorithms into a single system lies in the amount of dual-frequency ambiguities that need to be resolved in a robust way. The scheme introduced in Publication 1 describes an algorithm which aims at the reduction of the computational burden of the integer ambiguity estimator by arranging data in sliding batches. The first step consists in the creation of a pass table (continuous tracking arcs) of mutually tracked GNSS satellites. In this way, a SD carrier phase observation is assigned to each pass. This table contains implicitly the cycle slips detected in the data editing process. As a side process, the same table is used as the base for the computation of MW ambiguities of SD observations, which are later used in the ambiguity validation scheme.

Following the creation of pass tables, a set of reference GNSS satellites are defined in order to be used for the formation of DD code and carrier phase observations. The algorithm performs an epochwise selection of a reference GNSS satellite based on a given criterion. The implemented strategies consist in a selection based on either finding the satellite with the largest tracking arc or with the highest elevation. From a theoretical point of view, the selection criteria should have little impact on the overall performance of the integer ambiguity resolution algorithm.

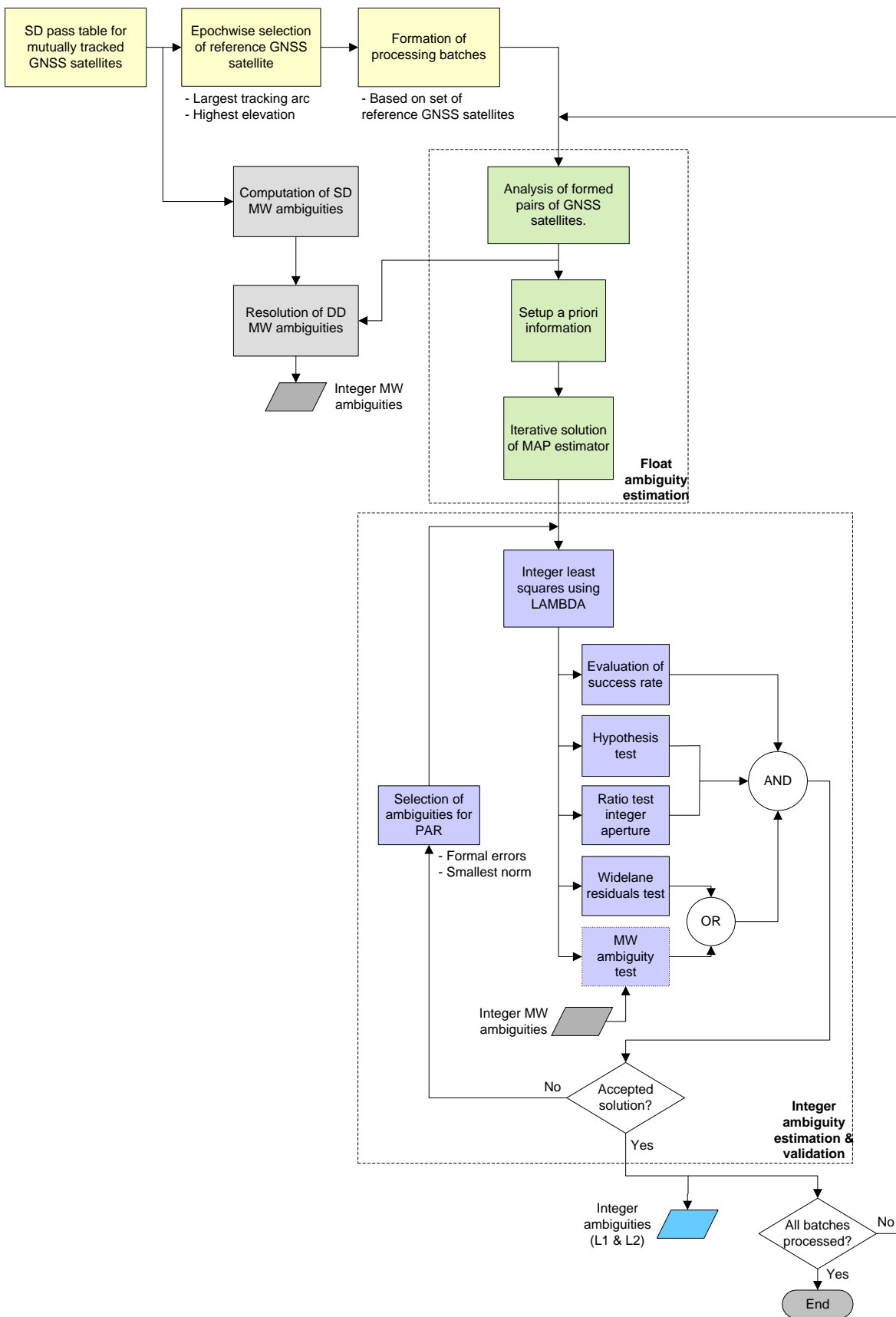


Fig. A.1 Block diagram of the proposed scheme for integer ambiguity resolution.

Nevertheless, the experience from the analysis of real flight data reveals that having the flexibility of selecting the observation model by picking any of the two aforementioned strategies may prove to be useful for a detection and discard of some wrongly fixed ambiguities. Such a flexibility may be useful mainly in long-term analyses (e.g. one year or more of data) as it allows to re-attempt some specific days with degraded solutions using a single *standard* set of ambiguity validation thresholds, which may be difficult to tune to achieve a satisfying solution.

Once the GNSS reference satellites have been selected and defined, the algorithm proceeds to the creation of the so-called processing batches (i.e. blocks of pairs of GNSS satellites) which are used as the basis for the arrangement of processing data and the computation of float ambiguity solutions. For the generation of these processing batches, care must be taken to consider the most accurate information regarding the validity periods of the carrier phase ambiguities. This task is performed by taking into account the previously created pass tables, which (as previously mentioned) contain implicit information regarding the detected cycle slips in carrier phase observations. In this way, a processing batch may contain repeated pairs of GNSS satellites but with different validity periods, as one or more cycle slips can be detected in data from the referred (i.e. not reference) satellite. Data gaps impose a particular difficulty to this scheme given that the expected periodicity of the availability of measurements is broken and this situation must be properly handled to store the correct validity periods of ambiguities. Further processing may be executed previous to the formation of batches in order to attempt to identify mis-detected cycle slips and/or true data gaps and improve the overall performance of the algorithm. Such strategies have been implemented resulting from the experience with data from different missions. They can be specified as optional pre-processing steps to the standard algorithm flow. A block diagram of the described arrangement of processing batches is given in Fig. A.1, which depicts a schematic view of the overall proposed integer ambiguity resolution scheme.

A.2 Float ambiguity estimation

The algorithms used for batch arrangement may result in DD pairs of GNSS satellites with very few epochs or available (healthy) observations to be used in the float ambiguity estimation scheme. Thus, references to formed DD pairs which have such features are discarded before setting up the main estimation scheme. The resulting (valid) DD pairs are employed for the specification of the data to be used. Similarly, they are considered for the computation of float DD MW ambiguities (using the formed per-pass SD ambiguities) which are resolved to integers (see §A.3.3) and later used in the integer ambiguity validation scheme.

The basic structure of the float ambiguity estimator is described in Publication 1. It is based on the theory of Bayesian statistics and belongs to the family of schemes denominated as Maximum A Posteriori (MAP) estimator. For every processing batch, the estimation vector is defined as

$$\begin{bmatrix} \mathbf{X}_D \\ \mathbf{I}_D^D \\ \mathbf{N}_{D,1}^D \\ \mathbf{N}_{D,2}^D \end{bmatrix} = \begin{bmatrix} \mathbf{x}_{D,0}, \dots, \mathbf{x}_{D,l-1} \\ (\iota_D^{i1}, \dots, \iota_D^{im-1})_0; \dots; (\iota_D^{i1}, \dots, \iota_D^{in-1})_{l-1} \\ n_{D,1}^{i1}, \dots, n_{D,1}^{ik-1} \\ n_{D,2}^{i1}, \dots, n_{D,2}^{ik-1} \end{bmatrix} \quad (\text{A.1})$$

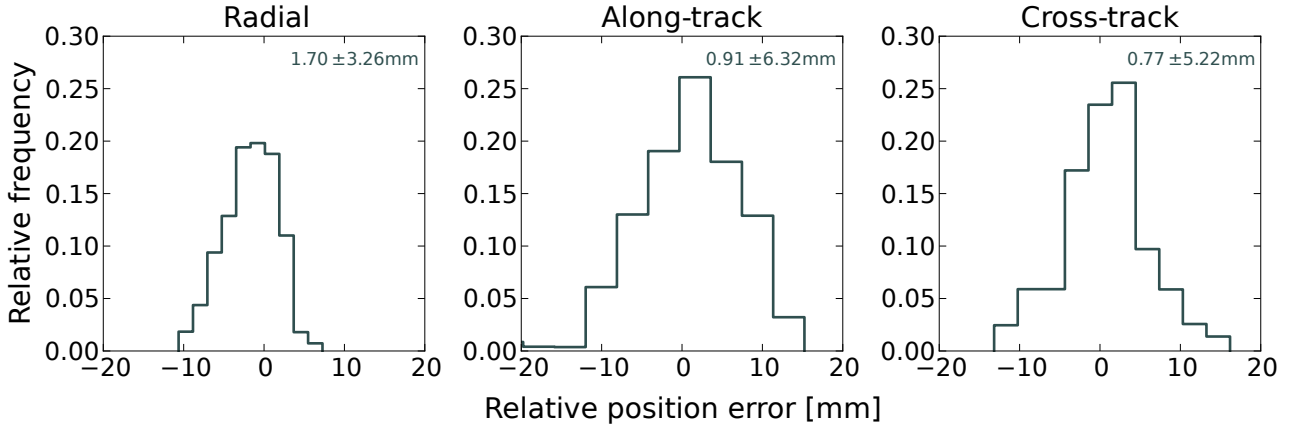


Fig. A.2 Frequency distribution of dPOD solution errors on October 7, 2011 in the radial, along-track and cross-track directions, using an ambiguity-fixed solution as reference.

where \mathbf{X}_D is the vector of relative spacecraft positions \mathbf{x}_D for a total of l epochs in the processing batch. Considering GNSS satellite i as reference, \mathbf{I}_D^p depicts the vector of DD ionospheric delays i_D^{ij} with varying number m and n of tracked GNSS satellites at each epoch in the processing batch. Finally, $\mathbf{N}_{D,1}^D$ and $\mathbf{N}_{D,2}^D$ denote the k -dimensional vectors of DD ambiguities $n_{D,1}^{ij}$ and $n_{D,2}^{ij}$ in L1 and L2, respectively.

If the errors in observations and a priori information are considered to be normally distributed, the scheme takes the closed form of an a priori-constrained LSQ estimator, which can be solved numerically using standard linear algebra methods (Strang and Borre, 1997). As developed in Publication 1, the algorithm describes a kinematic positioning estimator, which employs a priori information taken from previously computed POD solutions and empirical values for estimation of differential ionospheric delays. The assumptions on the distribution of errors of observations and a priori information can be analyzed by using POD solutions. For the case of a priori relative positions, an assessment of difference of POD (dPOD) solutions provides an indication of the errors in the assumed values. As an example, Fig. A.2 depicts the frequency distribution of errors of the dPOD solution on October 7, 2011, using an ambiguity-fixed baseline solution as reference. As can be observed, the assumption of normally-distributed errors can be considered as a good approximation to be used in the estimation scheme. Similarly, an indication of the error distribution of observations can be obtained by analyzing the residuals of POD solutions from each spacecraft. Figure A.3 depicts the frequency distribution of pseudorange and carrier phase ionosphere-free residuals for GRACE A and GRACE B on October 7, 2011. As shown, the observation errors also exhibit a normal distribution. The depicted quantities include errors mostly due to multipath, GNSS clock and ephemeris errors and receiver thermal noise.

A.3 Integer ambiguity estimation and validation

Following the estimation of float ambiguities, these must be fixed to their most probable integer value using an integer ambiguity estimator. As described in Publication 1, for this study the ILS estimator has been chosen given that it is an optimal estimator. The LAMBDA algorithm has been used in order to efficiently compute the integer ambiguity solution.

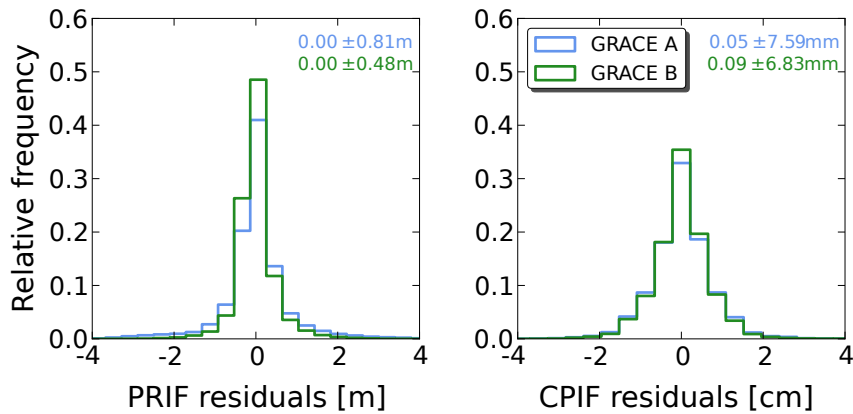


Fig. A.3 Frequency distribution of pseudorange and carrier phase ionosphere-free (PRIF and CPIF, respectively) residuals for GRACE A and GRACE B on October 7, 2011.

Although, the ILS estimator provides an optimal solution to the integer ambiguity estimation problem, the ambiguity validation problem is still an open problem in ongoing research. Publication 1 makes use of validation tests based on a combination of theoretical and heuristic (or semi-empirical) tests. The present section is devoted to a more in-depth analysis to such an ambiguity validation approach. For this analysis, a series of tests using real flight data were conducted in order to explore the impact of different validation approaches and thresholds on the final relative navigation solutions. In particular, these tests make use of data from the GRACE mission on October 2011 due to the possibility of solution assessment using KBR data, a mission profile with a long baseline and the challenges presented to the problem of correct integer ambiguity resolution during this period.

An important feature to analyze during the presented tests is the impact of validation tests when the imposed lower bound threshold on the ILS success rate ($P_{s,ILS}$) is not stringent (e.g. lower than 99%). The direct implication of this approach is that the detection of wrongly fixed ambiguities is more dependent on the subsequent validation tests. Theoretical studies recommend that only solution vectors with a high ILS success rate (or lower bound) should be accepted and used (Verhagen, 2005). However, in tests using real data, less stringent thresholds (e.g. between 80% and 95%) are typically used as a strategy to increase ambiguity fixing rates, in accord with the relative positioning scenario. For all the tests analyzed in the present section, a threshold on the lower bound of the ILS success rate of 80% is used. An overview of the configuration parameters and validation thresholds used for integer ambiguity resolution in the present section is shown in Table A.1.

A.3.1 Hypothesis test

A fundamental approach for the integer ambiguity validation problem can be based on general hypothesis test theory (Teunissen, 2007). Similarly, the analysis can be performed in terms of

Table A.1 Statistics, configuration parameters and validation thresholds for integer ambiguity resolution in the test case using GRACE data from October 2011.

Float ambiguity estimation			
Priors		GNSS observations	
State	Value	Type	Value
Relative position	$\sigma_x = 0.01$ m	Pseudorange	$\sigma_P = 0.50$ m
DD ionospheric delay	$\sigma_i = 1.00$ m	Carrier phase	$\sigma_\phi = 0.01$ m
DD ambiguities L1, L2	$\sigma_n \rightarrow \infty$		
Integer ambiguity resolution			
Validation		Partial resolution	
Test/Parameter	Standard configuration	Criterion	Standard method
Success rate ILS (§A.3)	$P_{s,ILS} = 0.80$	Selection of ambiguity set ^{*d}	Analysis of ambiguity formal errors
Ellipsoidal integer aperture ^{*a} (Eq.(A.5))	$\mu_{ELA}^2 = 100$		
Ratio test integer aperture ^{*b} (Eq.(A.6))	Fixed $P_f = 0.001$		
Widelane ambiguity residuals ^{*c} (§A.3.3)	$T_{WL} = 0.25$ cy		
Formal error MW ambiguities (§A.3.3)	$\bar{\sigma}_{MW} = 0.10$ cy		
Interval to search for integer MW ambiguities (§A.3.3)	$\hat{a}_{MW} \pm 3\bar{\sigma}_{MW}$		
Hamming distance between best ILS solutions (Pub. 1, Eq.(2))	$D_h = 0$		

* Variable configuration tests: ^a §A.3.1. ^b §A.3.2. ^c §A.3.3. ^d §A.3.4.

model selection/comparison. In this way, the two hypothesis (or models) to compare can be expressed as

$$\mathcal{M}_f : y = A\hat{a} + B\hat{b} + e, \hat{a} \in \mathbb{R}^q, \hat{b} \in \mathbb{R}^p, e \in \mathbb{R}^q \quad (\text{A.2a})$$

$$\mathcal{M}_i : y = A\hat{n} + B\hat{b} + e, \hat{n} \in \mathbb{Z}^q, \hat{b} \in \mathbb{R}^p, e \in \mathbb{R}^q \quad (\text{A.2b})$$

In this case, the null hypothesis is given by the float model \mathcal{M}_f and implies that ambiguities \hat{a} are real numbers. The alternative hypothesis is given by the integer/fixed model \mathcal{M}_i which

considers ambiguities \hat{n} as integer values. Other non-ambiguity parameters are contained in vector b (e.g. epochwise relative position vector and differential ionospheric delays in the models introduced in Publication 1).

Given that the integer ambiguity solution \hat{n} is directly dependent on the float solution \hat{a} , it is not possible to perform a model comparison by means of a direct evaluation of \mathcal{M}_f and \mathcal{M}_i . Instead, the probabilistic analysis of the ambiguity acceptance test must be done in terms of the ambiguity residuals $\hat{\varepsilon} = \hat{a} - \hat{n}$ and/or their distribution $f_{\hat{\varepsilon}}(x)$ (Wang, 2015). Such an analysis leads to the definition of the so-called acceptance and rejection regions which determine which ambiguity solutions should be discriminated. Acceptance regions are also called aperture (denoted as Ω) and they are always a subset of the ILS pull-in regions (Verhagen, 2005). In this way, ambiguity acceptance tests based on this principle can be generalized into the so-called integer aperture estimators (IAEs), which represent a unified framework for integer ambiguity estimation and validation (Teunissen, 2003).

One interesting feature of IAEs is their hybrid nature, i.e. the output of the estimator can be defined as

$$\hat{a}_{IAE} = \hat{a} + \sum_{n \in \mathbb{Z}^q} (n - \hat{a}) \omega_n(\hat{a}) \quad (\text{A.3})$$

with the function $\omega_n(\hat{a})$ given by

$$\omega_n(\hat{a}) = \begin{cases} 1 & \text{if } \hat{a} \in S_n \\ 0 & \text{if } \hat{a} \notin S_n \end{cases} \quad (\text{A.4})$$

where S_n is (generally) the ILS pull-in region. Thus, the IAE will have as output the float solution \hat{a} if $\hat{a} \notin \Omega_n$ or the fixed solution n if $\hat{a} \in \Omega_n$.

One of the simplest estimators in this class is the ellipsoidal IAE, whose principles derive directly from the hypothesis test and the analysis of ambiguity residuals. The ellipsoidal integer aperture (EIA) region is defined as (Teunissen, 2003)

$$\Omega_{EIA,n} = \Omega_{EIA,0} + n = \{a \in S_n \mid \|a - n\|_{Q_{\hat{a}}}^2 \leq \mu_{EIA}^2\} \quad (\text{A.5})$$

which is an ellipsoid defined by the distance between the float and integer ambiguity solution vectors in the space with metric $Q_{\hat{a}}$ (variance-covariance matrix of the estimated float ambiguity vector). The size of the aperture is defined by the parameter μ_{EIA} . Figure A.4 depicts an example of $\Omega_{EIA,n}$ shown as a subset of the ILS pull-in region.

The parameter μ_{EIA} can be used for the computation of the success and failure rate of the EIA estimator (Verhagen, 2005; Wang, 2015). However, in the present work, the EIA estimator has been mainly used as a hypothesis (complementary) test within a multi-step validation scheme (see Fig. A.1). In this way, the selection of the aperture parameter μ_{EIA} is done in function of an expected confidence in the float solution. The larger the value selected for μ_{EIA} , the larger the confidence in the integer solution, which effectively reduces the probability of false alarm but increases the probability of failure (see e.g. Wang (2015)). The selection of μ_{EIA} is performed in a heuristic way and a more formal probabilistic characterization of the overall validation test scheme is left to the analysis of the ILS success rate and a subsequent test using a second integer aperture estimator (see §A.3.2).

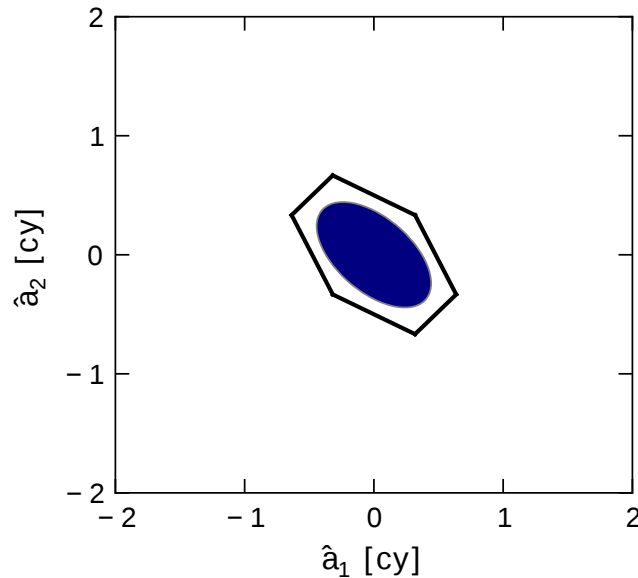


Fig. A.4 Aperture region of the ellipsoidal integer aperture estimator (blue) as a subset of the ILS pull-in region (black contour).

In order to observe the impact of different possible threshold values for μ_{EIA} , various tests have been run, analyzing as key indicators the integer ambiguity fixing rate and the final baseline precision. Figure A.5 depicts the results obtained with values $\mu_{EIA}^2 = 25, 50, 200, 300$ in comparison with a value $\mu_{EIA}^2 = 100$ corresponding to a *standard* configuration. Values roughly lying on the diagonal line indicate a similar performance for both values under comparison, whereas off-diagonal values show an improved performance in favor of either configuration. As depicted, threshold values below 100 appear more stringent in terms of the confidence on the resolved integer ambiguities. Although the probability of failure is effectively reduced for such configuration values, the ambiguity fixing rate is decreased and, in consequence, the final baseline precision is slightly reduced. In comparison, the achieved performance with configuration values above 100 is very similar, which indicates that although the probability of failure is increased, the precision of baseline solutions is not degraded for most of the days. In terms of the so-called integer test (Verhagen, 2005), threshold values above 50-100 are obtained in case of very low levels of significance and/or a large number of degrees of freedom n of an $F(n, \infty)$ distribution for a test statistic $\|a - n\|_{Q_a}^2/n$. In this sense, by using high threshold values, the test gives a large tolerance margin to the evaluated integer ambiguity solution. In the proposed validation scheme, the implementation of this hypothesis test in terms of the ellipsoidal integer aperture estimator allows a more prompt interpretation of thresholds values and facilitates its selection according to any given scenario under analysis.

A.3.2 Ratio test integer aperture estimator

The ratio test was introduced with the aim of testing whether a given integer ambiguity solution is more likely than any other candidate solution (Euler and Schaffrin, 1991). As shown by Teunissen and Verhagen (2009) it is possible to interpret the ratio test within the framework of

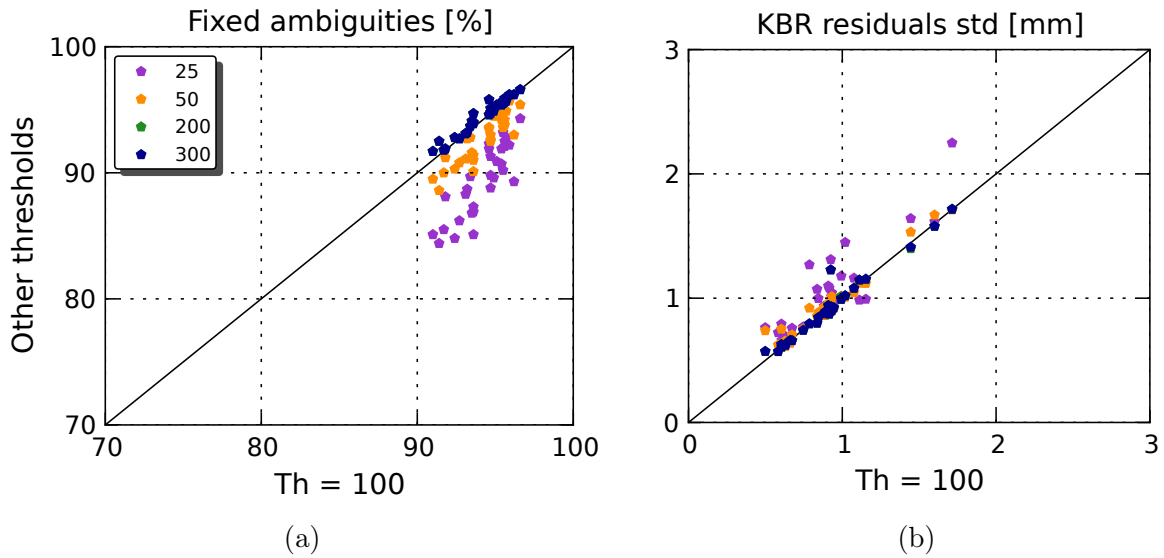


Fig. A.5 Comparative assessment of various threshold values for the hypothesis test/ellipsoidal integer aperture estimator using data from the GRACE mission in October 2011. The horizontal axes show the results using standard configuration settings.

IAEs (hence called ratio test integer aperture - RTIA - estimator), with the acceptance region defined as

$$\Omega_{RTIA} = \{a \in \mathbb{R}^n \mid \|a - n_2\|_{Q_a}^2 \geq \mu_{RTIA}(\|a - n_1\|_{Q_a}^2)\} \quad (\text{A.6})$$

where the relation between the best (n_1) and second best (n_2) ILS ambiguity solutions are compared against the free parameter μ_{RTIA} (known as critical value or aperture parameter). The acceptance region of the RTIA estimator consists of the overlapping region of a series of hyper-ellipsoids with centers and size defined by the parameter μ_{RTIA} and the metric Q_a (Teunissen and Verhagen, 2011). An example of a two-dimensional problem is shown in Fig. A.6, where the RTIA region is shown as a subset of the ILS pull-in region.

One feature of IAEs is that they allow to quantify the confidence in the outcome of the integer ambiguity resolution by means of the definition of the probabilities of success (s), failure (f) and rejection (u) given by (Teunissen and Verhagen, 2009)

$$P_s = P(\hat{a}_{IAE} = n) = \int_{\Omega_n} f_{\hat{a}}(x) dx \quad (\text{A.7a})$$

$$P_f = \sum_{z \in \mathbb{Z}^q \setminus \{n\}} P(\hat{a}_{IAE} = z) = \sum_{z \in \mathbb{Z}^q \setminus \{n\}} \int_{\Omega_z} f_{\hat{a}}(x) dx \quad (\text{A.7b})$$

$$P_u = 1 - P_s - P_f \quad (\text{A.7c})$$

where $f_{\hat{a}}(x)$ is the probability density function (PDF) for the float ambiguity solution vector \hat{a} (assumed to be normally distributed). The probability that the IAE accepts the ILS solution is given by $P_{fix} = P_s + P_f$, whereas the probability of rejection (i.e. giving the float solution as output) is given in terms of the probability of false alarm (P_{fa}) and the probability of detection

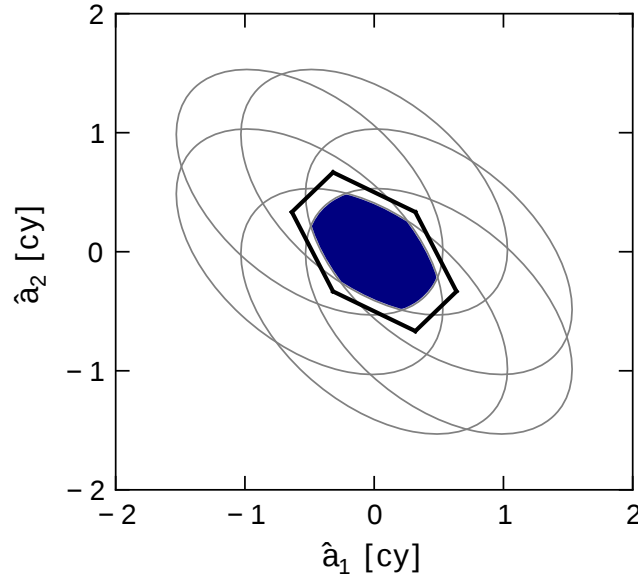


Fig. A.6 Aperture region of the ratio test integer aperture estimator (blue) as a subset of the ILS pull-in region (black contour).

(P_d), namely $P_u = P_{fa} + P_d$. The corresponding relations with the ILS success and failure rate ($P_{s,ILS}$ and $P_{f,ILS}$, respectively) can be expressed as $P_{s,ILS} = P_s + P_d$ and $P_{f,ILS} = P_f + P_d$ (Verhagen and Teunissen, 2013).

The probabilities given by Eq.(A.7) have a direct dependence on the shape and size of the aperture region Ω_n and on the PDF for \hat{a} . Thus, any change on such parameters will affect the computation of probabilities. Given that the shape of Ω_n and the PDF for \hat{a} are directly dependent on the form of the ratio-test and the measurement scenario, respectively, only by changing the value of μ_{RTIA} it is possible to change the size of Ω_n and, in this way, to affect the probabilities of the IAE (Teunissen and Verhagen, 2009).

When the parameter $\mu_{RTIA} > 1$, the aperture region is a subset of the ILS pull-in region (i.e. when $P_u \neq 0$), which results in a probability of failure $P_f < P_{f,ILS} = 1 - P_{s,ILS}$. Hence, by choosing a value for μ_{RTIA} it is possible to have control over P_f , i.e. the probability of incorrect integer estimation (Teunissen and Verhagen, 2009). In other words, it is possible to set a given desired P_f and select the corresponding μ_{RTIA} based on that value, an approach denominated as fixed failure rate ratio test (FFRT; Teunissen and Verhagen (2009); Verhagen and Teunissen (2013)). A key advantage of such an approach is that the determination of the aperture parameter is based on the metric $Q_{\hat{a}}$, i.e. it is model-driven. This strategy contrasts with a common way of using the ratio test, where a fixed critical value is selected based on heuristic arguments according to the problem at hand (see e.g. Han and Rizos (1996), Kroes (2006) and Parkins (2011)), but it does not provide any tool to control the ambiguity fixing failure rate. On the other hand, the computation of μ_{RTIA} based on a fixed value of P_f is not trivial, given it would require the *inversion* of the integral equation that relates both terms. In an attempt to overcome such difficulties, a proposed strategy is based on the computation of look-up tables based on Monte Carlo simulations, which can be readily used, provided that the number of ambiguities to evaluate and $P_{f,ILS}$ are specified, for a given fixed failure rate P_f (the

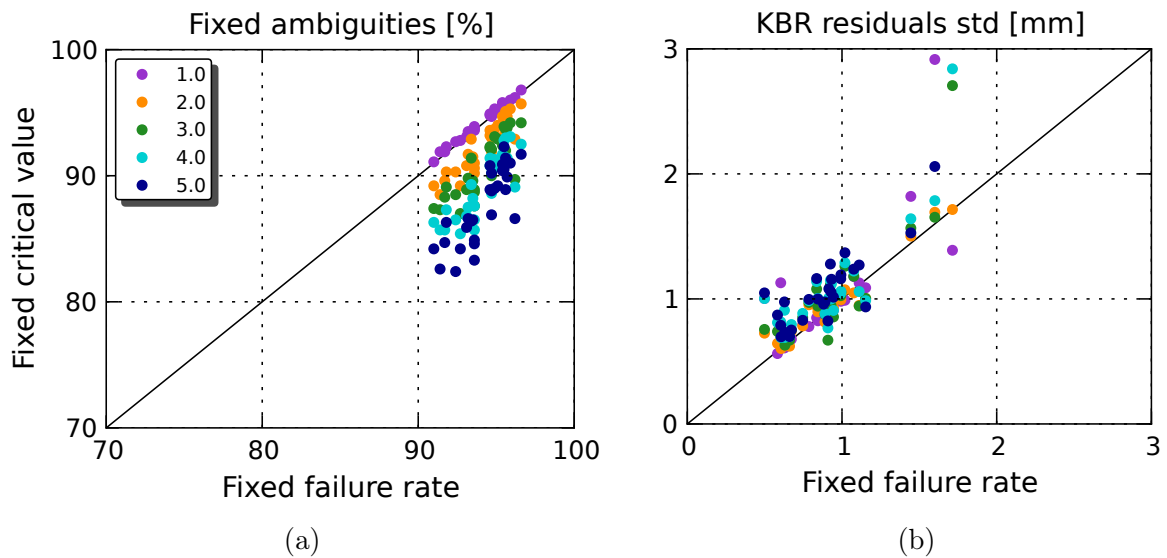


Fig. A.7 Comparative assessment of threshold values and strategies for the ratio test integer aperture estimator using data from the GRACE mission on October 2011. The horizontal axes show the results using standard configuration settings.

interested reader is referred to Teunissen and Verhagen (2009) and Verhagen and Teunissen (2013) for details). The algorithm described in Publication 1 makes use of this strategy based on the look-up table method described by Verhagen and Teunissen (2013) and implemented in Verhagen and Li (2012).

As briefly described in §A.3.1, one of the main aims of the used RTIA estimator is to provide a basis for a probabilistic analysis of the overall ambiguity validation scheme. From a general perspective, it forms part of a series of theoretical tests, which includes an evaluation of the ILS success rate and a hypothesis test/EIA estimator, as schematized in Fig. A.1. In terms of the use of various IAEs, the described strategy is similar to the approach proposed by Ji et al. (2010), in which a combination of EIA and RTIA estimators shows an improved performance of the integer ambiguity process altogether (using aperture parameters chosen empirically).

An important step in the selection of the approach used for the RTIA estimator is to analyze the impact of different configurations on the final baseline solutions. For this purpose, a series of tests were executed, aiming at comparing the RTIA estimator using fixed critical values (various configurations) and using the fixed-failure rate approach. Figure A.7 depicts a comparison of results using fixed critical values of 1.0 to 5.0 and using the FFRT approach with $P_f = 0.001$ (considered as *standard* configuration). Depicted are the integer ambiguity fixing rates and the precision of baseline solutions for the days under analysis.

In terms of ambiguity fixing rates, it is possible to observe that fixed critical values above 3.0 appear to be conservative and very stringent in comparison. Commonly used values (in the range 2.0-3.0) perform better and provide reasonable fixing rates above 85% for all days. A critical value of 1.0 performs slightly better than the FFRT approach, which is somehow expected given that such aperture values imply that the ratio test accepts all the ILS solutions.

The analysis of the achieved baseline precision shows closely similar results for all the configurations of fixed critical values. In particular, it is noticeable that although values above 3.0 were shown to be conservative in terms of ambiguity fixing rates, the resulting baseline precision for most of the days is only slightly worse in comparison with critical values below

3.0. As previously stated, the configuration using the least stringent critical value of 1.0 results in higher ambiguity fixing rates with respect of the FFRT approach. However, in terms of baseline precision, the performance obtained using such a value is slightly degraded on some days. Similarly, it is possible to observe that the performance of the ambiguity validation scheme is very similar when using critical values of 1.0 – 2.0 and the FFRT approach. This provides an indication of the strength of the observation models computed for each one of the processing batches. From a general perspective, it is possible to notice that the FFRT approach performs better (on average) than any of the configurations using fixed critical values. This result suggests that some of the theoretical assumptions regarding the used FFRT look-up table method (error distribution of estimates, computed $P_{f,ILS}$, use of generic look-up tables, etc.) may also have a good justification from a practical point of view. Nonetheless, these results should always be interpreted according to the specific characteristics of the ambiguity validation strategy described throughout this chapter.

The topic of IAEs is a very active research area and important theoretical results have been obtained in the past few years. In particular, the so-called difference test integer aperture (DTIA) estimator (based on the difference test proposed by Tiberius and de Jonge (1995)) has received much attention, as it has been suggested in recent studies that it achieves higher success rates than the RTIA estimator (Wang et al., 2014). A key problem under investigation is to find suitable methods for the determination of aperture parameters. Although the fixed failure (FF) approach provides a theoretical framework for this task, it is highly demanding in terms of computational burden. Various strategies have been foreseen in order to either try to reduce the complexity of the FF approach or to improve the overall scheme for the determination of aperture parameters. Aside from the aforementioned look-up table method and improvements to the FFRT scheme (Hou et al., 2016a), other approaches have been recently proposed for the DTIA estimator, including the threshold function method (Wang and Verhagen, 2015; Wang et al., 2014) and the instantaneous and controllable approach (iCON, Zhang et al. (2015)). Such theoretical explorations have been accompanied by some experimental tests (Li et al., 2016; Wang et al., 2017) with some mixed results with respect to the predicted outcomes from simulation tests.

A.3.3 (Semi-)empirical test with widelane residuals

As stated before, one of the key features in the ambiguity validation scheme described in this chapter is the combination of various tests in order to increase the robustness of the final integer ambiguity solution vector. In particular, theoretical validation tests, such as those described in §A.3.1 and A.3.2, have been complemented with (semi-)empirical/heuristic validation methods (see Fig. A.1). Similar strategies have been explored in past studies in the same context of space baseline determination (e.g. Kroes et al. (2005)). The key idea and description behind these additional tests have been explained in Publication 1. Basically, they take advantage of the decorrelation property of the widelane combination/transformation (Teunissen, 1997) in order to validate whether the fixed values in the widelane ambiguity space are *likely correct* according to a certain (user-defined) threshold T_{WL} .

Aside from the strategy of widelane residuals check test, a complementary test within this framework has been implemented in the actual integer ambiguity validation algorithm. This test consists in the evaluation of widelane residuals using MW ambiguities that can be computed directly from the observations. According to the data arrangement described in §A.1, the batches and DD are formed according to a certain criterion of reference GNSS satellite.

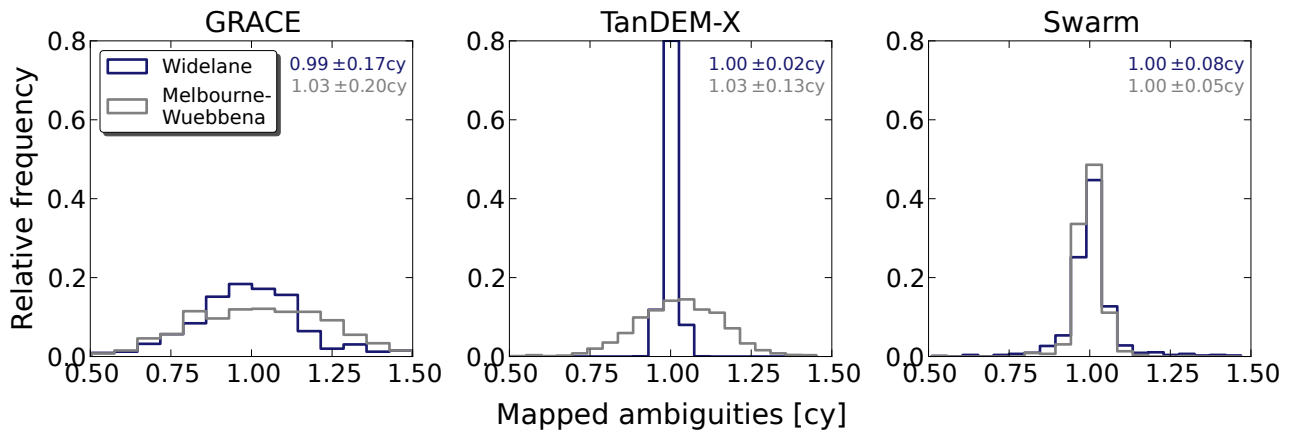


Fig. A.8 Frequency distribution of estimated widelane and MW ambiguities mapped into the interval [0.5-1.5] for the GRACE, TanDEM-X and Swarm missions on October 7, 2011, January 10, 2014 and March 20, 2016, respectively.

With this approach, only overlapping GNSS satellite passes are used in order to compute float ambiguities. In contrast, if the requirement of a geometry-based observation model is dropped, SD MW ambiguities can be directly computed from the observations for each GNSS satellite pass. Hence, as more observations are (typically) used for this task, uncertainty over the computed ambiguity can be reduced (a clear nuisance here is the increased dependency on pseudorange observations). Subsequently, DD MW ambiguities can be computed by making use of information stemming from the process of formation of GNSS satellite pairs (see Fig. A.1). A subtle detail worth mentioning is that such a strategy relies on the assumption of constant (or stable) widelane biases during the observation period of a given GNSS satellite, which is reasonable for spaceborne receivers in LEO but may not be valid in general (Bertiger et al., 2010b).

Due to the properties of the widelane combination, the estimated float DD MW ambiguities can be reliably solved to integers by using a rounding estimator. This process can be controlled by analyzing the available statistical information from the estimates. Explicitly, the user can define a maximum tolerable standard deviation $\bar{\sigma}_{MW}$ of the PDF (assumed to be normal) for each float ambiguity in order to evaluate the quality of the estimate. If the statistical properties of the estimate are accepted, a second user-defined threshold k_i is used in order to define an interval (a credible interval in the Bayesian sense) for the search of an integer ambiguity candidate. If a candidate is found within the interval $\hat{a}_{MW} \pm k_i \bar{\sigma}_{MW}$, the float ambiguity is fixed to such a value and declared as solved. With a set of integer DD MW ambiguities available, the complementary test in this stage of the validation scheme consist of a simple comparison of integer widelane ambiguities from the ILS estimator and integer MW ambiguities from the aforementioned strategy. The total outcome of the widelane residuals test consists in the acceptance of the resolved widelane integer ambiguity if it is within (user-defined) bounds with respect to the widelane float ambiguity or if it is equal to the resolved MW integer ambiguity (see Fig. A.1).

The fundamental reason for the inclusion of the complementary MW test (i.e. as second sub-test) is to attempt to decrease the ambiguity rejection rate or, equivalently, to increase the ambiguity fixing rate (with a corresponding increase of the failure rate). As with previous tests,

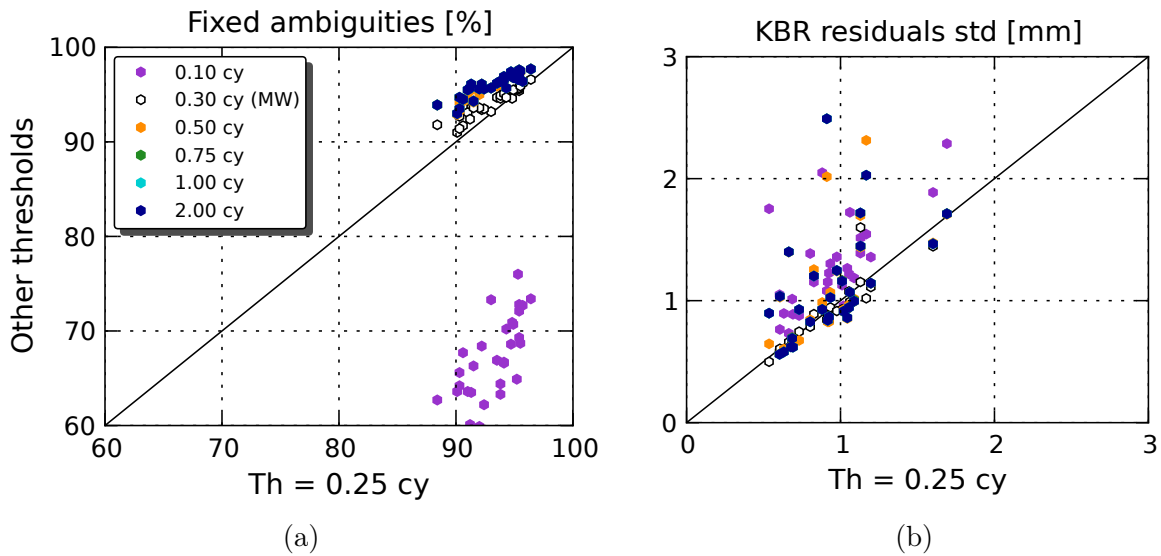


Fig. A.9 Comparative assessment of various threshold values for the widelane residuals test using data from the GRACE mission in October 2011. The horizontal axes show the results using standard configuration settings.

the analysis of the impact of different configurations for the widelane residuals test on the final solutions is carried out by the means of the execution of a series of trials. In this case, two configurations are considered as standard: using a threshold of 0.25 widelane cycles for the first sub-test, with and without considering the inclusion of the second sub-test. This configuration is compared with a set of threshold values ranging from 0.1 to 2 widelane cycles, without considering the second sub-test. Given that these thresholds are selected in a heuristic way, any given fixed configuration may have a different impact depending on the data set on which it is applied. As an example, Fig. A.8 depicts the frequency distribution of estimated widelane and MW ambiguities (mapped into the interval [0.5-1.5]) for the GRACE, TanDEM-X and Swarm missions on October 7, 2011, January 10, 2014 and March 20, 2016, respectively. As can be seen, validation thresholds T_{WL} between 0.1 and 0.2 widelane cycles may be stringent in the case of GRACE, but they may be considered suitable for TanDEM-X and Swarm. For example, a validation threshold of 0.1 widelane cycles can be roughly translated to ambiguity acceptance rates below 68% for GRACE in this example data set. In comparison, for TanDEM-X and Swarm, such a validation threshold may result in ambiguity acceptance rates above 90% and 70%, respectively.

The results of the aforementioned tests with different validation thresholds in terms of ambiguity fixing rates and final baseline precision are shown in Fig. A.9. As observed, a very stringent threshold of 0.1 cycles results in a severe degradation of ambiguity fixing rates. As a consequence, the resulting baseline precision is also demeaned. A very interesting result is the comparison of the two standard configurations. As depicted, the inclusion of the MW sub-test effectively provides a slight increase in the ambiguity fixing rate with respect to the configuration using only the first sub-test. Similarly, in terms of baseline precision, the results obtained with the configuration using both sub-tests appears to be slightly better in comparison.

Starting from threshold values of 0.5 cycles, the widelane residuals test is more and more relaxed and the ambiguity fixing rates increase in all cases. Particularly, for values of 1.0 and 2.0 cycles, the test can be considered as superfluous, given that practically all the solutions

accepted in the various theoretical tests are not discriminated by the widelane residuals test at all. Naturally, the first consequence of a more relaxed validation test is a reduction in the false alarm rate. This leads to solutions with slightly improved precision for some days but with degradation on some others as a consequence of a corresponding increase of the ambiguity failure rate. This argument suggests a similar (or equal) behavior of the ambiguity validation scheme with threshold values above 0.5 cycles, as observed in Fig. A.9. In general, these trials suggest that the configuration including the two sub-tests appears to deliver the most satisfactory results (on average). Therefore, this configuration has been the chosen one in other diverse scenarios, such as those described in Publications 1, 2 and 3. More comparative trials could be helpful in order to better determine the range of applicability and successful performance of this proposed strategy.

From this series of trials, it is possible to grasp the importance of the inclusion of (semi-) empirical validation tests into the overall integer ambiguity validation scheme. Even though the justification for the inclusion of these tests may be purely driven by experience with certain type of positioning scenarios, it is possible to imagine that the concept of combining theoretical and heuristic validation tests can be well adapted for a diversity of problems. The major drawback of such a strategy is the lack of a systematic way of determining the most suitable thresholds to use other than the realization of several trials or use the experience from the analysis of similar scenarios.

A.3.4 Approaches for partial ambiguity resolution

An important step in the integer ambiguity resolution process is the selection of float ambiguities to fix based on the available statistical information. According to the specific problem scenario, it is not always possible to resolve the complete *initial* solution vector from the process of float ambiguity estimation due to low success rates caused by estimates with poor precision. Therefore, a given criterion is used in order to discriminate such float ambiguities and resolve the remaining ones. This strategy is commonly known as partial ambiguity resolution (PAR). It is currently a very active research area, mainly driven by the modernization, expansion and implementation of existing and new GNSS. Recent studies have explored complex scenarios and theoretical constructions for PAR, addressing some of the key issues in the strategy, including GNSS satellite selection (Verhagen et al., 2011), fast ambiguity resolution with PAR (Zhang et al., 2016), data-driven PAR (Hou et al., 2016b), PAR using GPS and Galileo (Nardo et al., 2016) and extensions to the theory of IAEs to include PAR (Brack, 2015; Brack and Günther, 2014).

The strategy described in Publication 1 follows a less formal approach and it was implemented driven by the architecture of the overall integer ambiguity resolution algorithm. The key idea is to decide *a posteriori* whether to execute PAR or not based on the outcome of the theoretical tests. If the solution under test is not accepted, a series of float ambiguities are discarded iteratively according to a given criterion, until a solution is accepted or all the float ambiguities have been discarded (worst case with very poor observation models). The *standard* criterion for the selection of the subset of ambiguities to fix consists in the evaluation of the formal error of float ambiguities. The estimates with the largest formal errors are discarded and the remaining subset of ambiguities is used as input to the ILS estimator for the computation of a new integer ambiguity vector.

As stated, the rationale behind the aforementioned strategy has a more heuristic than theoretical justification, but it proved to be a reasonable strategy for most of the tests carried

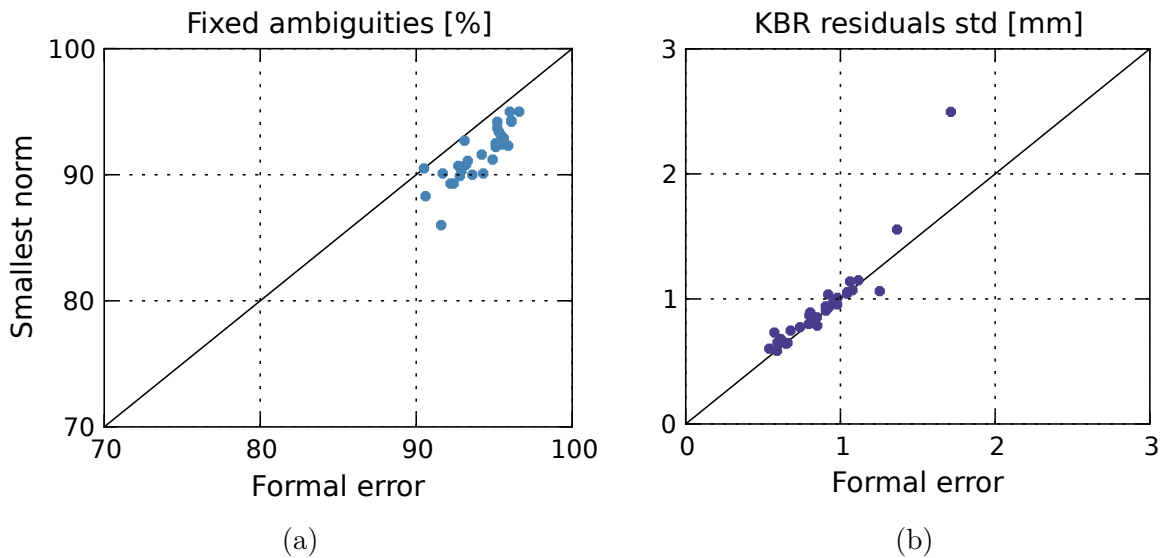


Fig. A.10 Comparative assessment of tested approaches for partial ambiguity resolution using data from the GRACE mission on October 2011. The horizontal axes show the results using standard configuration settings.

out under different baseline determination scenarios. Nonetheless, a degree of reliability on this approach may be quantified if it is compared with some other (perhaps more theoretical) methods. For this purpose, a second strategy for ambiguity selection for PAR was implemented and integrated into the ambiguity validation scheme. Such a strategy is based on the proposed method by Verhagen et al. (2011). It consists in the iterative search and selection of the subset of ambiguities that deliver the smallest norm between integer and float ambiguities solution vectors in the space with metric $Q_{\hat{a}}$. In this way, the ambiguity selection is more data-driven, as a float ambiguities solution is required for this evaluation. Although more appealing from the theoretical point of view, one major drawback of this approach is that many iterative executions of the ILS algorithm must be done just for the selection of the ambiguity subset to fix and validate.

Similar to the tests performed for the evaluation of different configurations for ambiguity validation tests, the two aforementioned strategies have been compared through a series of tests. The results are shown in Fig. A.10. In terms of ambiguity fixing rates, the selection method based on the evaluation of formal errors appears to outperform slightly the selection method based on the evaluation of the smallest norm of ambiguity solutions. However, in terms of the achieved baseline precision, the advantage of the former method is only marginal with respect to the latter one, as both strategies appear to deliver solutions with virtually the same precision. In this case, the apparent major advantage of the standard selection method over its counterpart can be expressed in terms of computational burden and algorithm performance. On the other hand, having good theoretical foundations on the applied methods is always desirable, which appears to be the major asset of the selection method based on the smallest norm. In any case, more formal PAR methods may be implemented and integrated into the overall ambiguity resolution strategy in order to search an improvement to both the theoretical foundations and the performance of the scheme.

A.4 Half-cycle ambiguity processing

All of the aforementioned strategies and algorithms for integer ambiguity estimation and validation have as a fundamental pre-requisite for functionality that the GNSS receivers generate ambiguities only at full-cycles. This may seem, after all, a basic or even obvious requirement for the successful execution of integer ambiguity resolutions methods. However, depending on the GNSS receiver characteristics and configurations, full-cycle carrier phase ambiguities are not always part of the design requirements. Hence, in some GNSS receivers, resulting half cycles from carrier phase tracking loops may not be corrected in the generation of observations. In its standard configuration, this was the case of the GPSR receivers onboard the Swarm spacecraft. At a first glance, it may appear that none of the developed methods for integer ambiguity resolution may be applied. However, from the basic carrier phase observation model, it is possible to deduce that an exactly equivalent model can be expressed in the case of half-cycle ambiguities if a corresponding correction factor is applied to the complete bias. In this case, half-cycle ambiguities can simply be multiplied by a factor of two and the *integer-ness* of the ambiguity is recovered. The price to pay is that the apparent effective wavelength of the bias is reduced by a half, which imposes some extra challenges for a successful integer ambiguity fixing. In particular, the precision requirements for modeling carrier phase observations become more stringent in order to be able to estimate well-defined float ambiguities.

This simple approach can be readily implemented and tested with the aforementioned framework for ambiguity estimation and validation. However, due to the increased required precision in the observation models, it is expected to have a degraded performance in comparison with processing full-cycle ambiguities only. On the other hand, the application of full-cycle ambiguity models even when half-cycle ambiguities are present in the observations may lead to highly degraded baseline solutions due to a reduced ambiguity fixing rate and increased number of wrongly-fixed ambiguities. These concepts have been tested with flight data from the Swarm mission as shown in Publications 1 and 2.

Even when the half-cycle ambiguity approach appears to work reasonably well under the conditions of precise modeling of carrier phase observations, it has a particular drawback. Assuming still that no half-cycle correction is applied to any constructed carrier phase measurement, it is expected to have an statistically equal number of half- and full-cycle ambiguities in the observations. This implies that roughly 50% of carrier phase observations do not require the aforementioned ambiguity factor correction. In such a case, observations with full-cycle ambiguities could be modeled with a proper model in order to increase the probability of successful fixing. This was driving idea for the development of the so-called *mixed-cycle* ambiguity resolution strategy, introduced in Publication 1. Starting from the flow diagram depicted in Fig. A.1, the expanded framework to include such a strategy is shown in Fig. A.11. Although the diagram depicts an algorithm extension for each individual batch, in practice it was easier to implement an extension at the general level, namely, for all batches at once. Due to the independence among the processing batches, these two strategies are equivalent.

The key idea depicted in Fig. A.11 is to apply a best-effort scheme for a cycle-type determination of each individual float ambiguity to be resolved. In a first run, all the float ambiguities are modeled as being full-cycle. Then, float widelane ambiguities are formed with these estimates and they are used for the subsequent cycle-type resolution of ambiguities in L1 and L2. If the estimated ambiguities have a low uncertainty, it is possible to apply a simple statistical testing in order to decide if they are of half-cycle or full-cycle types. As

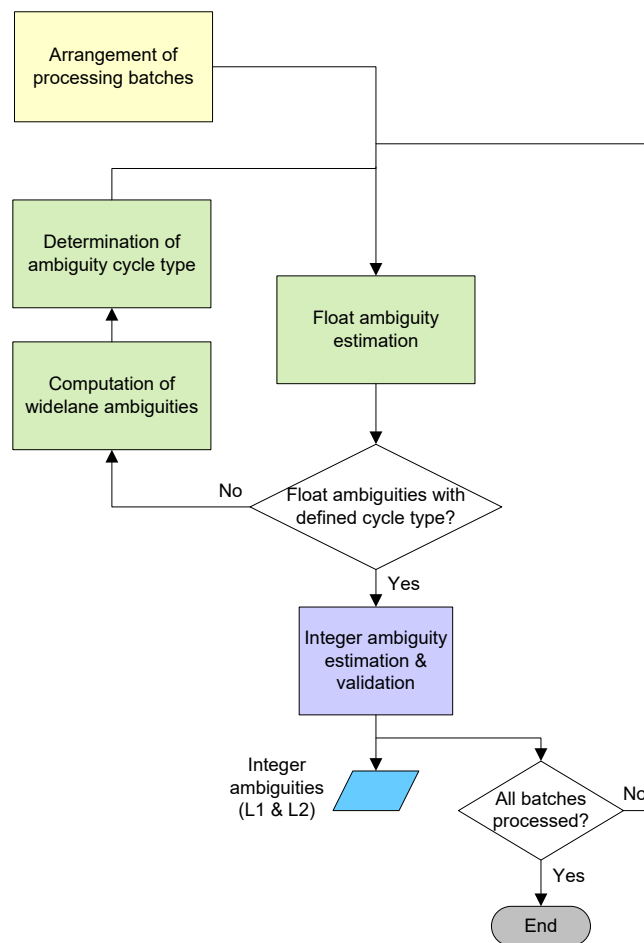


Fig. A.11 Block diagram of the strategy for mixed-cycle ambiguity resolution.

shown in Publication 1, an empirical finding made during the first tests with Swarm data was that widelane ambiguities were mostly of full-cycle type. This fact in turn helped to ease the cycle-type determination of individual ambiguities in L1 and L2 and provided an implicit constraint for a second run of float ambiguity estimation (see Fig. A.11). This effective constraint was then used in the ILS method by the LAMBDA algorithm, helping to improve the ambiguity fixing rate, as shown in the results included in Publication 1.

References

- K.T. Alfriend, S.R. Vadali, P. Gurfil, J.P. How, and L.S. Breger. *Spacecraft formation flying: dynamics, control and navigation*. Elsevier, 1st edition, 2010.
- K. Anflo and R. Möllerberg. Flight demonstration of new thruster and green propellant technology on PRISMA satellite. *Acta Astronautica*, 65(9-10):1238–1249, 2009.
- C. Arbinger, S. D’Amico, and M. Eineder. Precise ground-in-the-loop orbit control for low Earth observation satellites. In *Proceedings of the 18th international symposium on spaceflight dynamics*, pages 333–338, Munich, Germany, October 2004.
- J.-S. Ardaens, O. Montenbruck, and S. D’Amico. Functional and performance validation of the PRISMA precise orbit determination facility. In *Proceedings of the ION international technical meeting*, pages 490–500, San Diego, CA, Jan 2010.
- M. Benn and J.L. Jørgensen. Short range pose and position determination of spacecraft using a micro-advanced stellar compass. In *3rd international symposium on formation flying, missions and technologies*, Noordwijk, The Netherlands, April 2008. ESA/ESTEC.
- W. Bertiger, S. D. Desai, A. Dorsey, B. J. Haines, N. Harvey, and D. Kuang. Sub-centimeter precision orbit determination with GPS for ocean altimetry. *Marine Geodesy*, 33(1):363–378, 2010a. doi: 10.1080/01490419.2010.487800.
- W. Bertiger, S.D. Desai, B. Haines, N. Harvey, A.W. Moore, S. Owen, and J.P. Weiss. Single receiver phase ambiguity resolution with GPS data. *Journal of Geodesy*, 84(5):327–337, 2010b. doi: 10.1007/s00190-010-0371-9.
- G. Beutler, A. Jäggi, U. Hugentobler, and L. Mervart. Efficient satellite orbit modeling using pseudo-stochastic parameters. *Journal of Geodesy*, 80(7):353–372, 2006. doi: 10.1007/s00190-006-0072-6.
- H. Bock, G. Beutler, and U. Hugentobler. Kinematic orbit determination for Low Earth Orbiters (LEOs). In *Vistas for Geodesy in the New Millennium. International Association of Geodesy Symposia*, volume 125. Springer, Berlin, Heidelberg, 2002. doi: 10.1007/978-3-662-04709-5_50.
- H. Bock, A. Jäggi, R. Dach, S. Schaer, and G. Beutler. GPS single-frequency orbit determination for low earth orbiting satellites. *Advances in Space Research*, 43(5):783–791, 2009. doi: 10.1016/j.asr.2008.12.003.
- P. Bodin, R. Larsson, F. Nilsson, C. Chasset, R. Noteborn, and M. Nylund. PRISMA: an in-orbit test bed for guidance, navigation and control experiments. *Journal of Spacecraft and Rockets*, 46(3):615–623, 2009. doi: 10.2514/1.40161.

- P. Bodin, R. Noteborn, R. Larsson, T. Karlsson, S. D'Amico, J.-S. Ardaens, M. Delpech, and J.-C. Berges. The PRISMA formation flying demonstrator: overview and conclusions from the nominal mission. In *35th Annual AAS Guidance and Control Conference*, Breckenridge, Colorado, February 2012.
- A. Brack. On reliable data-driven partial GNSS ambiguity resolution. *GPS Solutions*, 19(3): 411–422, 2015. doi: 10.1007/s10291-014-0401-9.
- A. Brack and C. Günther. Generalized integer aperture estimation for partial GNSS ambiguity fixing. *Journal of Geodesy*, 88(5):479–490, 2014. doi: 10.1007/s00190-014-0699-7.
- R.G. Brown and P.Y.C. Hwang. *Introduction to Random Signals and Applied Kalman Filtering*. Jhon Wiley and Sons, New York, 1997.
- S. Buchert, F. Zangerl, M. Sust, M. André, A. Eriksson, J.-E. Wahlund, and H. Opgenoorth. SWARM observations of equatorial electron densities and topside GPS track losses. *Geophysical Research Letters*, 42(7):2088–2092, 2015. doi: 10.1002/2015GL063121.
- S. Buckreuss, R. Werninghaus, and W. Pitz. The German satellite mission TerraSAR-X. In *IEEE Radar Conference, RADAR '08*, Rome, Italy, May 2008.
- J. M. Carlson and J. Doyle. Complexity and robustness. *Proceedings of the National Academy of Sciences*, 99(1):2538–2545, 2002. doi: 10.1073/pnas.012582499.
- O.L. Colombo, S. B. Luthcke, D. D. Rowlands, D. Chin, and S. Poulouse. Filtering errors in LEO trajectories obtained by kinematic GPS with floated ambiguities. In *Proceedings of the 15th International Technical Meeting of the Satellite Division of ION*, pages 1863–1871, Portland, OR, September 2002.
- R. Dach, S. Lutz, P. Walser, and P. Fridez. *Bernese GNSS Software Version 5.2. User manual*, 2015. Bern Open Publishing.
- S. D'Amico and O. Montenbruck. Proximity operations for formation-flying spacecraft using and eccentricity/inclination vector separation. *Journal of Guidance, Control and Dynamics*, 29(3):554–563, 2006. doi: 10.2514/1.15114.
- S. D'Amico, C. Arbinger, M. Kirschner, and S. Campagnola. Generation of an optimum target trajectory for the TerraSAR-X repeat observation satellite. In *Proceedings of the 18th international symposium on spaceflight dynamics*, Munich, Germany, October 2004.
- S. D'Amico, J.-S. Ardaens, and O. Montenbruck. Navigation of formation flying spacecraft using GPS: the PRISMA technology demonstration. In *ION GNSS conference*, Georgia, USA, September 2009.
- S. D'Amico, J.-S. Ardaens, and R. Larsson. Spaceborne autonomous formation flying experiment on the PRISMA mission. *Journal of Guidance, Control and Dynamics*, 35(3):834–850, 2012. doi: 10.2514/1.55638.
- S. D'Amico, P. Bodin, M. Delpech, and R. Noteborn. In *Distributed Space Missions for Earth System Monitoring*, chapter *PRISMA*, pages 599–637. Springer, 2013.
- G. Di Giovanni and S. M. Radicella. An analytical model of the electron density in the ionosphere. *Advances in Space Research*, 10(11):27–30, 1990.

- F.J. Diekmann, I. Clerigo, G. Albin, L. Maleville, A. Neto, D. Patterson, A.P. Niño, and Sieg D. A challenging trio in space 'routine' operations of the swarm satellite constellation. In *Proceedings of the Living Planet Symposium*, Prague, Czech Republic, May 2016.
- C. Dunn, W. Bertiger, Y. Bar-Sever, et al. Instrument of GRACE: GPS augments gravity measurements. *GPS World*, 14:16–28, February 2003.
- H.-J. Euler and B. Schaffrin. In *Kinematic systems in geodesy, surveying, and remote sensing*, volume 107 of *International association of geodesy symposia*, chapter *On a measure for the discernibility between different ambiguity solutions in the static-kinematic GPS-mode*, pages 285–295. Springer New York, 1991. doi: 10.1007/978-1-4612-3102-8_26.
- J.C. Fernandez, L. Mounier, and C. Pachon. In *Testing of Communicating Systems. TestCom 2005. Lecture Notes in Computer Science*, volume 3502, chapter *A Model-Based Approach for Robustness Testing*, pages 333–348. Springer Berlin, Heidelberg, 2005. doi: 10.1007/11430230_23.
- W. Fowler, Bettadpur S., and B.D. Tapley. Mission planning for the twin GRACE satellites. *Advances in the Astronautical Sciences*, 105 II:987–997, 2000.
- D. Fraser and J. Potter. The optimum linear smoother as a combination of two optimal filters. *IEEE Transactions on Automatic Control*, 14(4):387 – 390, 1969. doi: 10.1109/TAC.1969.1099196.
- I. Fratter, J.-M. Léger, F. Bertrand, T. Jager, G. Hulot, L. Brocco, and P. Vigneron. Swarm absolute scalar magnetometers first in-orbit results. *Acta Astronautica*, 121:76–87, April-May 2016. doi: 10.1016/j.actaastro.2015.12.025.
- E. Friis-Christensen, H. Lühr, and G. Hulot. Swarm: a constellation to study the earth's magnetic field. *Earth, Planets and Space*, 58(4):351–358, 2006. doi: 10.1186/BF03351933.
- E. Friis-Christensen, H. Lühr, D. Knudsen, and R. Haagmans. Swarm - an Earth observation mission investigating geospace. *Advances in Space Research*, 41(1):210–216, 2008. doi: 10.1016/j.asr.2006.10.008.
- M.D. Graziano. In *Distributed space missions for Earth system monitoring*, chapter *Overview of distributed missions*, pages 375–386. Springer/Microcosm Press, 2013.
- S. Han and C. Rizos. Validation and rejection criteria for integer least-squares estimation. *Survey Review*, 33(260):375–382, 1996. doi: 10.1179/sre.1996.33.260.375.
- J. Harr, M. Delpéch, T. Grelier, D. Seguela, and S. Persson. The FFIORD experiment - CNES RF metrology validation and formation flying demonstration on PRISMA. In *3rd International Symposium on Formation Flying, Missions and Technologies*, Noordwijk, The Netherlands, April 2008. ESA/ESTEC.
- J. Herman, D. Fischer, D. Schulze, S. Löw, and M. Licht. AOCS for TanDEM-X. Formation flight at 200 m separation in low-Earth orbit. In *SpaceOPS conference*, Huntsville, AL, April 2010.
- M. Hernández-Pájaras, J.M. Juan, J. Sanz, R. Orus, A. García-Rigo, J. Feltens, A. Komjathy, S.C. Schaer, and A. Krankowski. The IGS VTEC maps: a reliable source of ionospheric information since 1998. *Journal of Geodesy*, 83(3):263–275, 2009. doi: 10.1007/s00190-008-0266-1.
- Y. Hou, S. Verhagen, and J. Wu. An efficient implementation of fixed failure-rate ratio test for GNSS ambiguity resolution. *Sensors*, 16(7):945, 2016a. doi: 10.3390/s16070945.

- Y. Hou, S. Verhagen, and J. Wu. A data driven partial ambiguity resolution: two step success rate criterion, and its simulation demonstration. *Advances in Space Research*, 58(11): 2435–2452, 2016b. doi: 10.1016/j.asr.2016.07.029.
- A. Jäggi, U. Hugentobler, and G. Beutler. Pseudo-stochastic orbit modeling techniques for low Earth orbiters. *Journal of Geodesy*, 80(1):47–60, 2006. doi: 10.1007/s00190-006-0029-9.
- A. Jäggi, U. Hugentobler, H. Bock, and G. Beutler. Precise orbit determination for GRACE using undifferenced or doubly differenced GPS data. *Advances in Space Research*, 39(10): 1612–1619, 2007. doi: 10.1016/j.asr.2007.03.012.
- A. Jäggi, O. Montenbruck, Y. Moon, M. Wermuth, R. König, G. Michalak, H. Bock, and D. Bodenmann. Inter-agency comparison of TanDEM-X baseline solutions. *Advances in Space Research*, 50(2):260–271, 2012. doi: 10.1016/j.asr.2012.03.027.
- A. Jäggi, C. Dahle, D. Arnold, U. Meyer, and H. Bock. Kinematic space-baselines and their use for gravity field recovery. In *40th COSPAR scientific assembly*, Moscow, Russia, 2014.
- A. Jäggi, C. Dahle, D. Arnold, H. Bock, U. Meyer, G. Beutler, and J. van den IJssel. Swarm kinematic orbits and gravity fields from 18 months of GPS data. *Advances in Space Research*, 57(1):218–233, 2016. doi: 10.1016/j.asr.2015.10.035.
- S. Ji, W. Chen, X. Ding, Y. Chen, Ch. Zhao, and C. Hu. Ambiguity validation with combined ratio test and ellipsoidal integer aperture estimator. *Journal of Geodesy*, 84(10):597–604, 2010. doi: 10.1007/s00190-010-0400-8.
- B. Ju, D. Gu, T.A. Herring, G. Allende-Alba, O. Montenbruck, and Z. Wang. Precise orbit and baseline determination for maneuvering low earth orbiters. *GPS Solutions*, 21(1):53–64, 2017. doi: 10.1007/s10291-015-0505-x.
- R. Kahle, B. Schlepp, A. Saika, M. Kirschner, and M. Wermuth. Flight dynamics operations of the TanDEM-X formation. In *SpaceOPS conference*, Stockholm, Sweden, June 2012. American Institute of Aeronautics and Astronautics. doi: 10.2514/6.2012-1275094.
- Z. Kang, P. Nagel, and R. Pastor. Precise orbit determination for GRACE. *Advances in Space Research*, 31(8):1875–1881, 2003. doi: 10.1016/S0273-1177(03)00159-5.
- I. Kawano, M. Mokuno, T. Kasai, and T. Suzuki. Result of autonomous rendezvous docking experiment of engineering test satellite-VII. *Journal of Spacecraft and Rockets*, 38(1):105–111, 2001. doi: 10.2514/2.3661.
- S.M. Kay. *Fundamentals of statistical signal processing*, volume 2: Detection theory. Prentice Hall, 1998.
- P.M. Kintner and B.M. Ledvina. The ionosphere, radio navigation and global navigation satellite systems. *Advances in Space Research*, 35(5):788–811, 2005. doi: 10.1016/j.asr.2004.12.076.
- P.M. Kintner, T. Humphreys, and J. Hinks. GNSS and ionospheric scintillation. *GNSS Solutions*, pages 22–30, July/August 2009.
- M. Kirschner, O. Montenbruck, and Bettadpur S. Flight dynamics aspects of the GRACE formation flying. In *16th international symposium on spaceflight dynamics*, December 2001.
- M. Kirschner, F.H. Massmann, and M. Steinhoff. In *Distributed Space Missions for Earth System Monitoring*, chapter GRACE, pages 547–574. Springer/Microcosm Press, 2013.

- J.A. Klobuchar. In *Global Positioning System: Theory and Applications*, volume 1, chapter *Ionospheric effects on GPS*, pages 485–515. American Institute of Aeronautics and Astronautics, 1996.
- G. Krieger, A. Moreira, H. Fiedler, I. Hajnsek, M. Werner, M. Younis, and M. Zink. TanDEM-X: A satellite formation for high-resolution SAR interferometry. *IEEE transactions on geoscience and remote sensing*, 45(11):3317–3341, 2007. doi: 10.1109/TGRS.2007.900693.
- G. Krieger, I. Hajnsek, K.P. Papathanassiou, M. Younis, and A. Moreira. Interferometric Synthetic Aperture Radar (SAR) missions employing formation flying. In *Proceedings of the IEEE*, volume 98, pages 816–843, 2010. doi: 10.1109/JPROC.2009.2038948.
- G. Krieger, M. Zink, M. Bachmann, B. Bräutigam, D. Schulze, M. Martone, P. Rizzoli, U. Steinbrecher, J. Walter, F. De Zan, I. Hajnsek, K. Papathanassiou, F. Kugler, M. Rodriguez Cassola, M. Younis, S. Baumgartner, P. López-Deckker, P. Prats, and A. Moreira. TanDEM-X: a radar interferometer with two formation-flying satellites. *Acta Astronautica*, 89:83–98, August–September 2013. doi: 10.1016/j.actaastro.2013.03.008.
- R. Kroes. *Precise Relative Positioning of Formation Flying Spacecraft Using GPS*. PhD thesis, Technische Universiteit Delft, 2006.
- R. Kroes, O. Montenbruck, W. Bertiger, and P. Visser. Precise GRACE baseline determination using GPS. *GPS Solutions*, 9(1):21–31, 2005. doi: 10.1007/s10291-004-0123-5.
- J. Leitner. Distributed space systems: mission concepts, systems engineering, and technology development. In *Systems engineering seminar*, Systems engineering seminar. NASA-GSFC, April 2002.
- S. Leung and O. Montenbruck. Real-time navigation of formation-flying spacecraft using global-positioning-system measurements. *Journal of Guidance, Control and Dynamics*, 28(2): 226–235, 2005. doi: 10.2514/1.7474.
- B. Li and P.J.G. Teunissen. High dimensional integer ambiguity resolution: a first comparison between LAMBDA and Bernese. *Journal of Navigation*, 64(S1):192–210, 2011. doi: 10.1017/S038346331100035X.
- T. Li, J. Zhang, M. Wu, and J. Zhu. Integer aperture estimation comparison between ratio test and difference test: from theory to application. *GPS Solutions*, 20(3):539–551, 2016. doi: 10.1007/s10291-015-0465-1.
- Z. Liu, Y. Li, J. Guo, and F. Li. Influence of higher-order ionospheric delay correction on GPS precise orbit determination and precise positioning. *Geodesy and Geodynamics*, 7(5):369–376, 2016. doi: 10.1016/j.geog.2016.06.005.
- A.M. Long, M.G. Richards, and D.E. Hastings. On-orbit servicing: a new value proposition for satellite design and operation. *Journal of Spacecraft and Rockets*, 44(4):964–976, 2007. doi: 10.2514/1.27117.
- R. Mackenzie, R. Bock, D. Kuijper, P. Ramos-Bosch, D. Sieg, and G. Ziegler. A review of Swarm flight dynamics operations from launch to routine phase. In *Proceedings of the 24th International Symposium on Space Flight Dynamics*, May 2014.
- F. Maurer, S. Zimmermann, F. Mrowka, and H. Hofmann. Dual satellite operations in close formation flight. In *SpaceOPS conference*, Stockholm, Sweden, June 2012.

- W.G. Melbourne. The case for ranging in GPS-based geodetic systems. In *Proceedings of the 1st International Symposium on Precise Positioning with the Global Positioning System*, pages 373–386, Rockville, MD, April 1985.
- P. Misra and P. Enge. *Global Positioning System: Signals, Measurements, and Performance*. Ganga-Jamuna Press, revised 2nd edition, 2010.
- O. Montenbruck, T. Ebinuma, E. Glen Lightsey, and S. Leung. A real-time kinematic GPS sensor for spacecraft relative navigation. *Aerospace Science and Technology*, 6(6):435–449, 2002. doi: 10.1016/S1270-9638(02)01185-9.
- O. Montenbruck, T. van Helleputte, R. Kroes, and E. Gill. Reduced dynamic orbit determination using GPS code and carrier measurements. *Aerospace Science and Technology*, 9(3):261–271, 2005. doi: 10.1016/j.ast.2005.01.003.
- O. Montenbruck, M. Wemuth, and R. Kahle. GPS based relative navigation for the TanDEM-X mission - first flight results. *NAVIGATION*, 58(4):293–304, 2011. doi: 10.1002/j.2161-4296.2011.tb02587.x.
- A. Moreira, P. Prats-Iraola, M. Younis, G. Krieger, I. Hajnsek, and K.P. Papathanassiou. A tutorial on synthetic aperture radar. *IEEE Geoscience and Remote Sensing Magazine*, 1(1): 6–43, 2013. doi: 10.1109/MGRS.2013.2248301.
- J. Morison, J. Wahr, R. Kwok, and C. Peralta-Ferriz. Recent trends in arctic ocean mass distribution revealed by GRACE. *Geophysical Research Letters*, 34(7), 2007. doi: 10.1029/2006GL029016.
- A. Nardo, B. Li, and P.J.G. Teunissen. Partial ambiguity resolution for ground and space-based applications in a GPS+Galileo scenario: a simulation study. *Advances in Space Research*, 57(1):30–45, 2016. doi: 10.1016/j.asr.2015.09.002.
- B. P. Nava, P. Coison, and S. M. Radicella. A new version of the nequick ionosphere electron density model. *Journal of Atmospheric and Solar-Terrestrial Physics*, 70(15):1856–1862, 2008. doi: 10.1016/j.jastp.2008.01.015.
- R.S. Neerem, J.M Wahr, and E.W. Leuliette. Measuring the distribution of ocean mass using GRACE. *Space Science Reviews*, 108(1):331–344, July 2003. doi: 10.1023/A:1026275310832.
- S. Ochs and W. Pitz. The TerraSAR-X and TanDEM-X satellites. In *3rd International Conference on Recent Advances in Space Technologies*, Istanbul, Turkey, June 2007. doi: 10.1109/RAST.2007.4283999.
- A. Parkins. Increasing GNSS RTK availability with a new single-epoch batch partial ambiguity resolution algorithm. *GPS Solutions*, 15(4):391–402, 2011. doi: 10.1007/s10291-010-0198-0.
- S. Persson, S. Veldman, and P. Bodin. PRISMA - a formation flying project in implementation phase. *Acta Astronautica*, 65(9-10):1360–1374, 2009. doi: 10.1016/j.actaastro.2009.03.067.
- T.V. Peters. Formation flying guidance for space debris observation, manipulation and capture. In *Astrodynamics Network AstroNet-II. Astrophysics and Space Science Proceedings*, volume 44, 2016. doi: 10.1007/978-3-319-23986-6_16.
- P. Rangsten, H. Johansson, M. Bendixen, K. Jonsson, J. Bejhed, and T.-A. Grönland. MEMS micropropulsion components for small spacecraft. In *25th Annual AIAA/USU Conference on Small Satellites*, Logan, UT, August 2011.

- K. Rawer. *Wave Propagation in the Ionosphere*. Springer Science & Business Media, 1993.
- T. Richert and N. El-Sheimy. Ionospheric modeling - the key to GNSS ambiguity resolution. *GPS World*, pages 35–40, June 2005.
- P.A. Rosen, S. Hensley, I.R. Joughin, F.K. Li, S.N. Madsen, E. Rodriguez, and R. Goldstein. Synthetic aperture radar interferometry. In *Proceedings of the IEEE*, volume 88, pages 333–382, 2000. doi: 10.1109/5.838084.
- J. Ross, D. Musliner, T. Kreider, J. Jacobs, and M. Fisher. Configurable spacecraft control architectures for on-orbit servicing and upgrading of long life orbit platforms. In *IEEE Aerospace Conference Proceedings*, Big Sky, MT, March 2004. doi: 10.1109/AERO.2004.1368057.
- M. Schelke. The GRACE cold gas attitude and orbit control system. In *Proceedings of the 3rd international conference on spacecraft propulsion*, Cannes, France, October 2000.
- R. W. Schunk and A. F. Nagy. *Ionospheres. Physics, plasma physics, and chemistry*. Cambridge, 2nd edition, 2009.
- D. Sieg and F. J. Diekmann. Options for the further orbit evolution of the swarm mission. In *Proceedings of the Living Planet Symposium*, Prague, Czech Republic, May 2016.
- SILSO World Data Center. The international sunspot number. *International Sunspot Number Monthly Bulletin and online catalogue*, 2003-2016. URL <http://www.sidc.be/silso/>.
- D. Simon. *Optimal State Estimation - Kalman, H and nonlinear approaches*. John Wiley and Sons, New York, 2006.
- T. Springer, M. Otten, and C. Flohrer. Spreading the usage of NAPEOS, the ESA tool for satellite geodesy. In *EGU 2012-7099-2*, Geophysical Research Abstracts 14, Vienna, Austria, April 2012.
- G. Strang and K. Borre. *Linear Algebra, Geodesy, and GPS*. Wellesley-Cambridge Press, 1997.
- D. Svehla and M. Rothacher. CHAMP and GRACE in tandem: POD with GPS and K-band measurements. In *Joint CHAMP/GRACE science meeting*, Postdam, Germany, July 2004.
- U. Tancredi, A. Renga, and M. Grassi. Ionospheric path delay models for spaceborne gps receivers flying in formation with large baselines. *Advances in Space Research*, 48(3):507–520, 2011. doi: 10.1016/j.asr.2011.03.041.
- B.D. Tapley and C. Reigber. The GRACE mission: status and future plans. In *Fall meeting of the American Geophysical Union*, San Francisco, CA, December 2001.
- B.D. Tapley, Bettadpur S., M. Watkins, and C. Reigber. The gravity recovery and climate experiment: mission overview and early results. *Geophysical Research Letters*, 31(9):L09607, 2004. doi: 10.1029/2004GL019920.
- J. Teixeira da Encarnação, D. Arnold, A. Bezděk, C. Dahle, E. Doornbos, J. van den IJssel, A. Jäggi, T. Mayer-Gürr, J. Sebera, P.N.A.M. Visser, and N. Zehentner. Gravity field models derived from swarm GPS data. *Earth, Planets and Space*, 2016.
- P.J.G. Teunissen. The least-squares ambiguity decorrelation adjustment: a method for fast GPS ambiguity resolution. *Journal of Geodesy*, 70(1-2):65–82, 1995.

- P.J.G. Teunissen. On the GPS widelane and its decorrelating property. *Journal of Geodesy*, 71(9):577–587, 1997.
- P.J.G. Teunissen. Integer aperture GNSS ambiguity resolution. *Artificial Satellites - Journal of Planetary Geodesy*, 38(3):79–88, 2003.
- P.J.G. Teunissen. In *GPS for Geodesy*, chapter *GPS carrier phase ambiguity fixing concepts*, pages 263–335. Springer, 2007.
- P.J.G. Teunissen and S. Verhagen. The GNSS ambiguity ratio-test revisited: a better way of using it. *Survey Review*, 41(312):138–151, 2009. doi: 10.1179/003962609X390058.
- P.J.G. Teunissen and S. Verhagen. Integer aperture estimation - a framework for GNSS ambiguity acceptance testing. *Inside GNSS*, pages 66–73, March-April 2011.
- C.C.J.M. Tiberius and P. de Jonge. Fast positioning using the LAMBDA method. In *Proceeding of the 4th international conference differential satellite systems*, number 30, Bergen, Norway., 1995.
- V.M. Tiwari, J. Wahr, and S. Swenson. Dwindling groundwater resources in northern india, from satellite gravity observations. *Geophysical Research Letters*, 36(18), 2009. doi: 10.1029/2009GL039401.
- P. Touboul, E. Willemenot, B. Foulon, and V. Josselin. Accelerometers for CHAMP, GRACE and GOCE space missions: synergy and evolution. *Bullettino di Geofisica Teorica ed Applicata*, 40(3-4):321–327, September-December 1999.
- M. Uhlemann, G. Gendt, M. Ramatschi, and Deng Z. GFZ global multi-GNSS network and data processing results. In *Proceedings International Association of Geodesy Symposia*, pages 1–7. Springer, 2015. doi: 10.1007/1345_2015_120.
- P.W.L. van Barneveld. *Orbit determination of satellite formations*. PhD thesis, Technische Universit at Delft, 2012.
- P.W.L. van Barneveld, O. Montenbruck, and P.N.A.M. Visser. Epochwise prediction of GPS single differenced ionospheric delays of formation flying spacecraft. *Advances in Space Research*, 44(9):987–1001, 2009. doi: 10.1016/j.asr.2009.07.006.
- J. van den IJssel, J. Encarna o, E. Doornbos, and P.N.A.M. Visser. Precise science orbits for the Swarm satellite constellation. *Advances in Space Research*, 56(6):1042–1055, 2015. doi: 10.1016/j.asr.2015.06.002.
- J. van den IJssel, B. Forte, and O. Montenbruck. Impact of Swarm GPS receiver updates on POD performance. *Earth, Planets and Space*, 68:85, 2016. doi: 10.1186/s40623-016-0459-4.
- I. Velicogna. Increasing rates of ice mass loss from the Greenland and Antarctic ice sheets revealed by GRACE. *Geophysical Research Letters*, 36(19):L19503, 2009. doi: 10.1029/2009GL040222.
- S. Verhagen. *The GNSS integer ambiguities: estimation and validation*. PhD thesis, TU Delft, 2005.
- S. Verhagen and B. Li. *LAMBDA - Matlab implementation. Version 3.0*. TU Delft and Curtin University, 2012.
- S. Verhagen and P.J.G. Teunissen. The ratio test for future GNSS ambiguity resolution. *GPS Solutions*, 17(4):535–548, 2013. doi: 10.1007/s10291-012-0299-z.

- S. Verhagen, P.J.G. Teunissen, H. van der Marel, and B. Li. GNSS ambiguity resolution: which subset to fix. In *IGNSS Symposium, International Global Navigation Satellite Systems Society*, Sydney, Australia, November 2011. University of New South Wales.
- P.N.A.M. Visser, E. Doornbos, J. van den IJssel, and J. Teixeira da Encarnação. Thermospheric density and wind retrieval from Swarm observations. *Earth, Planets and Space*, 65(11): 1319–1331, 2013. doi: 10.5047/eps.2013.08.003.
- A.W. Vogeley and R. F. Brissenden. In *Guidance and Control II*, chapter *Survey of rendezvous progress*, page 805. American Institute of Aeronautics and Astronautics, 1963.
- L. Wang. *Reliability control of GNSS carrier-phase integer ambiguity resolution*. PhD thesis, Queensland University of Technology, 2015.
- L. Wang and S. Verhagen. A new ambiguity acceptance test threshold determination method with controllable failure rate. *Journal of Geodesy*, 89(4):361–375, 2015. doi: 10.1007/s00190-014-0780-2.
- L. Wang, S. Verhagen, and Y. Feng. Ambiguity acceptance testing : A comparison of the ratio test and difference test. In *Proceeding of the China Satellite Navigation Conference (CSNC)*, volume 2. Springer Berlin, Heidelberg, 2014.
- L Wang, Y. Feng, and J. Guo. Reliability control of single-epoch RTK ambiguity resolution. *GPS Solutions*, 21(2):591–604, 2017. doi: 10.1007/s10291-016-0550-0.
- M. Watkins and Bettadpur S. GRACE mission: challenges of using micro-level satellite-to-satellite ranging to measure the earth’s gravity field. In *International Symposium on Space Dynamics*, Biarritz, France, June 2000.
- M. Wermuth, O. Montenbruck, and T. van Helleputte. GPS High precision Orbit determination Software Tools (GHOST). In *4th International Conference on Astrodynamics Tools and Techniques*, Madrid, Spain, May 2010.
- R. Werninghaus, W. Balzer, S. Buckreuss, P. Mittermayer, P Mühlbauer, and W. Pitz. The TerraSAR-X mission. In *Proceedings of EUSAR*, Ulm, Germany, May 2004.
- A.D. Wheelon. *Electromagnetic Scintillation*, volume 1: Geometrical Optics. Cambridge University Press, 2001.
- S.C. Wu, T.P. Yunck, and C.L. Thornton. Reduced-dynamic technique for precise orbit determination of low Earth satellites. *Journal of Guidance, Control and Dynamics*, 14(1): 24–31, 1991.
- G. Wübbena. Software developments for geodetic positioning with GPS using TI 4100 code and carrier measurements. In *Proceedings of the 1st International Symposium on Precise Positioning with the Global Positioning System*, pages 403–412, Rockville, MD, April 1985.
- C. Xiong, C. Stolle, and H. Lühr. The Swarm satellite loss of GPS signal and its relation to ionospheric plasma irregularities. *Space Weather*, 14(8):563–577, 2016. doi: 10.1002/2016SW001439.
- Y. Yang, Y. Li, A.G. Dempster, and C. Rizos. Ionospheric path delay modelling for spacecraft formation flying. In *International Global Navigation Satellite Systems Society Symposium*, Queensland, Australia, July 2013.

-
- T.P. Yunck, S.C. Wu, Wu J.T., and C.L. Thornton. Tracking of remote satellites with the global positioning system. *IEEE Transactions of Geoscience and Remote Sensing*, GE-28(1): 108–116, 1990.
- J. Zhang, M. Wu, T. Li, and K. Zhang. Instantaneous and controllable integer ambiguity resolution: review and an alternative approach. *Journal of Geodesy*, 89(11):1089–1108, 2015. doi: 10.1007/s00190-015-0836-y.
- S. Zhang, L. Zhao, X. Li, and B. Cheng. A sequential and partial ambiguity resolution strategy for improving the initialization performance of medium-baseline relative positioning. *Earth, Planets and Space*, 68, 2016. doi: 10.1186/s40623-016-0411-7.

Appendix A

Publication 1

Robust and precise baseline determination of distributed spacecraft in LEO

Gerardo Allende-Alba, Oliver Montenbruck

Deutsches Zentrum für Luft- und Raumfahrt (DLR), German Space Operations Center (GSOC), Münchner Straße 20, 82234 Weßling, Germany

Abstract

Recent experience with prominent formation flying missions in Low Earth Orbit (LEO), such as GRACE and TanDEM-X, has shown the feasibility of precise relative navigation at millimeter and sub-millimeter levels using GPS carrier phase measurements with fixed integer ambiguities. However, the robustness and availability of the solutions provided by current algorithms may be highly dependent on the mission profile. The main challenges faced in the LEO scenario are the resulting short continuous carrier phase tracking arcs along with the observed rapidly changing ionospheric conditions, which in the particular situation of long baselines increase the difficulty of correct integer ambiguity resolution. To reduce the impact of these factors, the present study proposes a strategy based on a reduced-dynamics filtering of dual-frequency GPS measurements for precise baseline determination along with a dedicated scheme for integer ambiguity resolution, consisting of a hybrid sequential/batch algorithm based on the maximum-a-posteriori and integer aperture estimators. The algorithms have been tested using flight data from the GRACE, TanDEM-X and Swarm missions in order to assess their robustness to different formation and baseline configurations. Results with the GRACE mission show an average 0.7 mm consistency with the K/Ka-band ranging measurements over a period of more than two years in a baseline configuration of 220 km. Results with TanDEM-X data show an average of 3.8 mm consistency of kinematic and reduced-dynamic solutions in the along-track component over a period of 40 days in baseline configurations of 500 m and 75 km. Data from Swarm A and Swarm C spacecraft are largely affected by atmospheric scintillation and contain half cycle ambiguities. The results obtained under such conditions show an overall consistency between kinematic and reduced-dynamic solutions of 1.7 cm in the along-track component over a period of 30 days in a variable baseline of approximately 60 to 175 km. An analysis of one orbital period excluding a region where errors due to atmospheric scintillation occur, shows a consistency between kinematic and reduced-dynamic solutions of 3 mm in the along-track direction.

Keywords: Precise baseline determination; Spacecraft formation flying; Integer ambiguity resolution; GRACE; TanDEM-X; Swarm

1. Introduction

The formation flying technology is a fundamental concept for many current and future Earth-observation space missions. An essential requirement for the operation of distributed instrumentation in space is the precise determination of relative position of spacecraft in the formation. For this purpose, since many years, the Global Positioning System (GPS) has been an indispensable tool for a wide range of space navigation applications. Recent experience with prominent formation flying missions in LEO with requirements of highly precise relative orbit determination, such as the Gravity Recovery and Climate Experiment (GRACE) and the TerraSAR-X add-on for Digital Elevation Measure-

ment (TanDEM-X) mission, has shown the feasibility of relative navigation at millimeter and sub-millimeter levels using GPS carrier phase measurements with fixed integer ambiguities (Jäggi et al., 2007, 2012; Kroes et al., 2005; Montenbruck et al., 2011-2012).

One of the main challenges for integer ambiguity resolution methods in LEO is given by the typical duration of continuous tracking arcs for a given GPS satellite. Unlike receivers on Earth's surface, they are always restricted to less than one hour and commonly to less than half an hour if cycle slips are detected in the carrier phase measurements. This imposes a difficulty in the processing algorithm if, for example, a reduced-dynamic batch estimator is used for simultane-

ous relative orbit adjustment and ambiguity resolution. The resulting number of ambiguities that need to be considered (which is typically of the order of 1000 to 2000 for one-day data sets in dual-frequency processing) may result in very large computing times if a complete integer ambiguity resolution framework is considered (e.g. including searching algorithms, validation tests and partial ambiguity resolution).

In an effort to overcome these difficulties, current algorithms use approaches that include the wide-lane/narrowlane (WL/NL) resolution technique (see e.g. Jäggi et al., 2007) and ambiguity resolution using a reduced-dynamic adjustment in a sequential algorithm (see e.g. Kroes et al., 2005). However, these approaches may be prone to produce solutions with reduced precision and/or availability at some baseline configurations (i.e. if large residual ionospheric delays are expected) or in the presence of some measurement characteristics (e.g. large error levels in pseudoranges) due to partial disregard of orbit geometry information in ambiguity resolution.

Based on a general concept from the field of complexity (Carlson and Doyle, 2002) and adapted to the context of precise baseline determination, the present study describes the term robustness as the preservation of the functionality of techniques and the availability of solutions, regardless of the baseline length, levels of ionospheric activity and receiver characteristics. Thus, the present study addresses the problem of robust and precise baseline determination, i.e. the generation of baseline solutions with high levels of precision and availability for various mission profiles. The proposed schemes aim to cope the difficulties for robust ambiguity resolution in the LEO scenario by introducing algorithms for efficient use of observations in a float ambiguity estimator, and by making use of an optimal method for integer ambiguity resolution.

The main contributions of this study comprise the exploration of methods for float and integer ambiguity estimation and validation through extensive use of flight data. The major difficulties for precise relative navigation in LEO are described and key concepts and advantages of using a priori information in the overall ambiguity estimation scheme are introduced. Some concepts and strategies for half cycle integer ambiguity resolution are also introduced. Such contributions aim at the possibility of a consistent, long-term generation of precise GPS-based space baseline products. Applications that may benefit from these products include gravity field determination, monitoring of ground deformation from space and generation of digital elevation and topographic models.

The paper starts with a general description of the problem of integer ambiguity resolution, including a short description of precise orbit determination (POD) of single-satellite orbits (which is a key element in the subsequent algorithms) and a description of schemes for float ambiguity estimation and integer ambiguity

resolution and validation. Following is a description of the method for precise baseline determination using ambiguity-fixed carrier phase measurements, including estimated differential antenna phase pattern corrections. The proposed schemes are validated under a diversity of conditions by performing tests using data from different periods of the GRACE, TanDEM-X and Swarm missions. The obtained solutions and the particular details of data and methods used for each of them is described, including the assessment of the estimated baseline precision.

2. Carrier phase integer ambiguity resolution

Since many years, it has been recognized that the use of carrier phase measurements with correctly fixed ambiguities is the key to achieve highly precise relative navigation solutions of space vehicles (Švehla and Rothacher, 2004). Subject to proper receiver design (Psiaki and Mohiuddin, 2007), the ambiguities in carrier phase measurements from a single GPS receiver are restricted to an integer number of cycles, but due to the presence of other biases in the transmission/reception chain, the resulting ambiguity in the undifferenced carrier phase is a float number (Misra and Enge, 2006). These additional biases can be reduced or eliminated by using single- and double- differences of carrier phase measurements (SD and DD, respectively) between receivers and GPS satellites. In particular the resulting ambiguity from a DD is of integer nature, which allows the application of methods for integer ambiguity resolution. In recent years, ambiguity resolution techniques at the single-receiver level have been developed (Bertiger et al., 2010a); however, the present study focuses on ambiguity resolution at the DD level.

2.1. Single-satellite precise orbit determination

A key element in the complete baseline determination processing chain is single-satellite POD. Aside from being used as reference trajectories for relative dynamics propagation, as further described in Section 3.1, they can be used to provide valuable information for float ambiguity estimation. For this study, the reference absolute orbits were computed using the GPS High-precision Orbit Determination Software Tools (GHOST; Montenbruck et al., 2005). The estimation scheme consists of a least-squares adjustment of 24-h pseudorange and carrier phase measurements batches in a reduced-dynamic approach (Wu et al., 1991). The estimated parameters include the initial state vector of the spacecraft's center of gravity, piece-wise constant empirical accelerations (10 min intervals), drag and radiation pressure coefficients as well as epoch-wise receiver clock offsets. The scheme makes use of ionosphere-free (IF) combinations in order to eliminate ionospheric delays of 1st order in the measurements. Pass-by-pass carrier phase biases are included as part of the estimation parameters. A summary of the used models and schemes is included in Table 1. The precise GPS orbits and 30 s

Table 1 Summary of GHOST processing standards for precise orbit and baseline determination.

Item	Precise Orbit Determination	Baseline Determination
GPS measurement model	Undifferenced ionosphere-free pseudorange and carrier phase observations, corrected for approximate receiver clock offset; 5° cut-off elevation w.r.t. horizon; phase center offset and variations of receiver antenna	Single-difference ionosphere-free pseudorange and carrier phase observations at synchronized measurement epochs; 5°/10° cut-off elevation w.r.t. local horizon; differential phase center offset and variations of receiver antenna
Gravitational forces	Phase center offset and variations of transmitter antenna; phase wind-up; CODE GPS orbits and 30 s clock solutions in ITRF2005 ^a /IGS05 and ITRF2008 ^b /IGS08-IGb08 reference frames	UT/CSR GGM01S model ^c (100x100); relativity; solid-Earth tides; polar tide; ocean tides (UT/CSR TOPEX_3.0) ^d ; luni-solar third body acceleration using analytical ephemerides ^e
Non-gravitational forces	Jacchia-Gill atmospheric density model ^f with daily F _{10.7} and 3-hours K _p values; Cannon ball solar radiation pressure model with conical Earth shadow model (umbra, penumbra) ^e	Empirical accelerations in radial, along-track and cross-track direction at 10 min intervals
Numerical integration	Constant thrust arcs (estimated)	Empirical accelerations in radial, along-track and cross-track direction with exponential time correlation
Reference frames	Variable-order Shampine-Gordon DE method ^g	Constant thrust arcs (modeled)
Estimation	EME2000; IAU 1976 precession (Lieske model); IAU 1980 nutation (Wahr model) ^h ; Earth orientation from IERS igs96p02 solution; spacecraft body frame orientation relative to EME2000 based on star sensor attitude determination	4 th -order Runge-Kutta method
	Batch least-squares	Extended Kalman filter/smoothen

^a Altamimi et al. (2007).

^b Altamimi et al. (2011).

^c Tapley et al. (2003).

^d UT/CSR Ocean Tide Models (2001).

^e Montenbruck and Gill (2005).

^f Gill (1996).

^g Shampine and Gordon (1975).

^h McCarthy (1996).

clock products used for POD and throughout this study were obtained from the Center for Orbit Determination in Europe (CODE; Dach et al., 2009).

2.2. Pre-processing and data arrangement

In principle, an estimation method based on pseudorange and carrier phase measurements only can be used to provide float ambiguity estimates. However, this technique may be too vulnerable to the presence of high error levels in observations, and fails to take advantage of the fact that all measurements from visible satellites at a given epoch (or continuous tracking arc) form a consistent set (Misra and Enge, 2006). The proposed estimation scheme exploits this idea, aiming at an improvement of the quality of float ambiguity estimates by effectively applying geometry-based constraints.

The algorithm starts with the arrangement of data into a set of sequential batches defined by the selection of common-tracked reference GPS satellites. Every batch has a duration equal to the continuous tracking arc of the selected reference satellite. This allows to process a manageable number of float ambiguities without imposing a risk of large computational burden in the subsequent ambiguity fixing algorithms. For the purpose of choosing a reference, several satellite selection algorithms have been proposed over the years (see e.g. Kihara and Okada, 1984; Li et al., 1999; Park 2001) although most of them are more suitable for either real-time navigation or receivers on Earth's surface. Due to their relatively good trade-off between performance and computational complexity, two semi-optimal algorithms have been considered in this study. These algorithms are either selection by pass duration

(denoted as scheme A) or selection by common-highest elevation (denoted as scheme B). Fig. 1 depicts the concept of formation of batches based on these schemes, where an excerpt of common-continuous phase tracking arcs of the two GRACE spacecraft on 1 February 2009 is depicted. As an example, both schemes select satellite G14 as reference at the beginning of the data arc, followed by a batch where schemes A and B select satellites G15 and G28, respectively. Considering 10 s epochs, it is shown that for receivers with very few to zero detected cycle-slips per pass, an average of 3 to 5 batches are expected to be formed in around one orbital period (≈ 100 min). In order to ensure good ambiguity discernibility, a set of thresholds (typically 5 to 10 data points) are specified in order to exclude from a given batch those DD pairs with few common-tracking epochs (e.g. G31-G14 and G15-G14 in Fig. 1). If a given continuous tracking arc has a larger duration, these excluded satellites are considered in a subsequent batch.

In general, scheme A accommodates a larger number of observations per batch and it has been the preferred method in this study. Scheme B has been chosen only for those data sets in which the formed DD pairs by scheme A complicate a successful ambiguity fixing. A thorough comparison of the performance of both schemes within the overall estimation algorithm under general conditions has not been addressed in this study and it is left for further analysis.

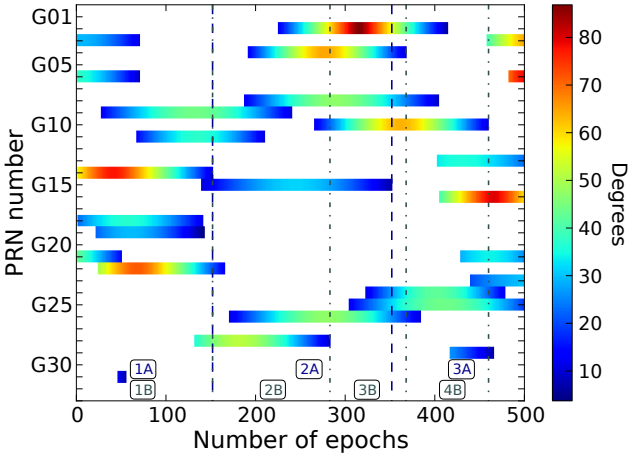


Fig. 1 Duration and common elevation of continuous carrier phase tracking arcs of the two GRACE spacecraft during the first 500 epochs (at 10 s sampling) on 1 February 2009. The duration of formed batches using schemes A and B is indicated by dashed and dash-dotted lines, respectively. The identification of every batch by number and scheme is displayed in squares.

2.3. Maximum-a-posteriori estimator

The main purpose of the formation of sequential batches is the assurance of an adequate number of observations as well as a sufficient geometric diversity (arc length) for float ambiguity estimation. However, in the scenario of GPS-based navigation in LEO, the presence of rapidly-changing ionospheric delays in the measurements complicates a concurrent precise estimation of spacecraft positions and ambiguities in a standard least-squares adjustment, particularly if the carrier phase continuous tracking arc is short. In this context, estimation schemes that include a priori information may be helpful as they do not need asymptotic assumptions, i.e. a large sample size is not required in order to provide valid estimates (Jaynes and Bretthorst, 2003). Thus, the present study proposes the implementation of an a priori constrained least-squares method for float ambiguity estimation. This scheme seeks to make a more efficient use of observations by including suitable a priori information, aiming at an overall improvement of the quality of float ambiguity estimates.

The observations used in the proposed estimator consist of GPS DD dual-frequency pseudorange and carrier phase measurements for each of the processing batches, which are modeled as

$$P_{[1]}^{ij} = \rho_{[1]}^{ij} + i_{[1]}^{ij} + \epsilon_{[1]}^{ij} \quad (1a)$$

$$P_{[2]}^{ij} = \rho_{[2]}^{ij} + \frac{f_1^2}{f_2^2} i_{[1]}^{ij} + \epsilon_{[1]}^{ij}$$

$$\Phi_{[1]}^{ij} = \rho_{[1]}^{ij} - i_{[1]}^{ij} + \lambda_1 n_{[1]}^{ij} + \epsilon_{[1]}^{ij} \quad (1b)$$

$$\Phi_{[2]}^{ij} = \rho_{[2]}^{ij} - \frac{f_1^2}{f_2^2} i_{[1]}^{ij} + \lambda_2 n_{[2]}^{ij} + \epsilon_{[1]}^{ij}$$

where the notation $\square_{[1]}^{ij}$ indicates a DD between GPS satellites i and j and two receivers denoted by brackets [and]. If any, the character inside the brackets gives a reference to an observable quantity or frequency thereof. Here, $\rho_{[1]}^{ij}$ represents the DD of geometric ranges between both receivers and the i -th and j -th GPS satellites, $i_{[1]}^{ij}$ is the DD ionospheric delay for every epoch in the estimation batch and $n_{[1]}^{ij}$ and $n_{[2]}^{ij}$ denote the DD float carrier phase ambiguities in each frequency. Similarly, λ denotes the carrier wavelength, and ϵ and ϵ indicate thermal noise and other non-modeled errors in the pseudorange and carrier phase measurements, respectively. These errors are assumed normally distributed with properties further described in Section 4.1 for each of the GPS receivers under test.

For every processing batch, the parameters to be adjusted in the proposed estimator comprise dual-frequency DD float ambiguities as well as epochwise relative positions between the spacecraft's centres of gravity and DD ionospheric delays. The a priori information included in the system consists of constraints on the spacecraft relative positions, which are obtained from pre-processed differential POD (dPOD) solutions, with representative accuracies discussed in Section 4.1. For the case of differential ionospheric delays, heuristic constraints have been applied based on previous studies or suitable ionospheric models (e.g. van Barneveld et al., 2009; Tancredi et al., 2011).

The proposed estimation scheme belongs to the general framework of a maximum-a-posteriori (MAP) estimator (Stone, 2013) and it is henceforth denoted as such in the present study. In essence, it describes a kinematic relative orbit determination algorithm with orbital constraints from dynamical models used in a previous POD processing. By constraining kinematic positions, the estimator makes a more efficient use of observations for float ambiguity estimation, which translates into more precise estimates and a more effective integer ambiguity search in the subsequent algorithm.

2.4. Integer aperture estimator

The solution vector from the MAP estimator is statistically characterized by a posterior covariance matrix which encodes all the information from the model and the constraints given by the a priori information. This solution is used in a second stage for the resolution to integer values by using an integer estimation scheme. Among the several options, the integer least-squares (ILS) method is regarded as optimal, as it is possible to show that it has the largest success rate (denoted as $P_{s,ILS}$) of all admissible ambiguity estimators (Teunissen, 1999). The ILS method is efficiently encoded in the LAMBDA algorithm (Teunissen, 1995), which realizes the minimization condition by searching the solution after applying a decorrelation procedure using the so-called Z -transformation.

The (best) solution vector resulting from the ILS algorithm must be validated before it can be further

used for the computation of the so-called fixed solution. An integral framework of the resolution and validation steps of integer ambiguity resolution is given by the so-called integer aperture (IA) estimators (Teunissen, 2003; Verhagen, 2004). This approach takes the float solution as input and decides whether to map it to an integer solution or leave it as is. In the context of IA estimators, it can be shown that the so-called ratio test is an IA estimator (Teunissen and Verhagen, 2009). This method allows to control the rate of accepting a wrongly fixed ambiguity (failure rate) by controlling the size of the aperture region, an approach referred to as the fixed-failure rate ratio test (FFRT; Verhagen and Teunissen, 2013). Thus, the size of the aperture region is a function of the covariance matrix of the MAP solution vector, meaning that the decision of accepting or rejecting an ILS solution vector is model-driven, which is suitable for the proposed scheme, due to the different possible observation models in every processing batch, as described in Section 2.2. The present study makes use of the FFRT look-up table method (Verhagen and Li, 2012; Verhagen and Teunissen, 2013), considering a lower bound for the ILS success rate given by the bootstrapping estimator (i.e. $P_{s,B} \leq P_{s,ILS}$).

2.5. Heuristic validation tests

The key idea of theoretical validation tests is to evaluate the complete solution vector, given that a total decorrelation of the ILS estimates is not possible due to the characteristics of the Z -transformation (Teunissen, 1995). Even though these tests represent the backbone of the validation scheme for the ILS solution vector, their performance depends on assumptions and/or approximations that might not be good enough when actual flight data is processed (e.g. distribution for errors and estimates). Hence, in order to increase the confidence on the computed solution, an additional set of heuristic tests based on the concept of partial ambiguity validation (PAV) have been included in the present study. An approach of this concept uses the idea of taking advantage of the decorrelating property of the WL transformation (Teunissen, 1997) in order to compare pairs of float ambiguities with their counterpart in the ILS solution vector and decide the validity of the solution based on this comparison. This idea has been tested already in previous studies in the contexts of precise relative navigation and real-time relative navigation (see e.g. Kroes, 2006; Tancredi et al., 2013).

2.6. Partial ambiguity resolution

In many cases, the full MAP solution vector cannot be fixed with enough confidence and is rejected by the IA estimator. In this situation, a suitable approach is the application of partial ambiguity resolution (PAR), in which a subset of ambiguities from the original MAP solution vector is used to re-compute a solution and evaluate it using the IA estimator.

Several theoretical models and methods have been proposed in recent studies for the selection of the best subset of ambiguities to be fixed (see e.g. Hou and Verhagen, 2014; Verhagen et al., 2011). The approach followed in the present study is based on the analysis of the posterior formal errors of the MAP solution vector, discarding iteratively the ambiguities of one satellite with the largest value from the (sub)set, if the test in the IA estimator fails. In case of acceptance of a solution vector, the resulting integer ambiguities are flagged as valid and subsequently used in the precise baseline determination process.

This iterative form of PAR may be computationally demanding due to the number of executions of the ILS algorithm. A heuristic argument to reduce the computational burden can be given by defining the Hamming distance between the best and second-best solutions vectors \hat{n}_B and \hat{n}_S , respectively, as follows

$$D_h = ||i|\hat{n}_{Bi} \neq \hat{n}_{Si}|| \quad (2)$$

In this way, a threshold on the maximum acceptable Hamming distance can be set in order to accept only the common ambiguities in both solutions, similar to some approaches for PAR followed in previous studies (e.g. Dai et al., 2007; Kroes, 2006). A threshold of zero Hamming distance implies a larger computational burden but also increases the confidence in the computed solution. On the other hand, given that the subset of ambiguities to fix in the PAR algorithm is not strictly chosen in an optimal way, Hamming distances of one or two might be tolerable in order to reduce the computational burden.

3. Precise baseline determination

3.1. Filtering scheme

With available fixed ambiguities, the precise baseline determination algorithm used in the present study consists of a reduced-dynamic extended Kalman filter/smoothen (EKF), using a SD IF measurement model. An overview of the processing scheme and algorithms is shown in Fig. 2. For the relative trajectory prediction, the algorithm uses a reference orbit from POD and the dynamical model described in Table 1, along with the estimation of relative empirical accelerations in radial, tangential and along-track directions. Thus, the estimation parameters include the relative state vector of the spacecraft's center of gravity, the SD receiver clock offset (denoted as $cdt_{[1]}$) and the relative force parameters between the spacecraft in the formation. In addition, given that carrier phase ambiguities are only known at the DD level, the SD IF biases $b_{[IF]}^i$ for the i -th GPS satellite are also included into the parameters to be estimated.

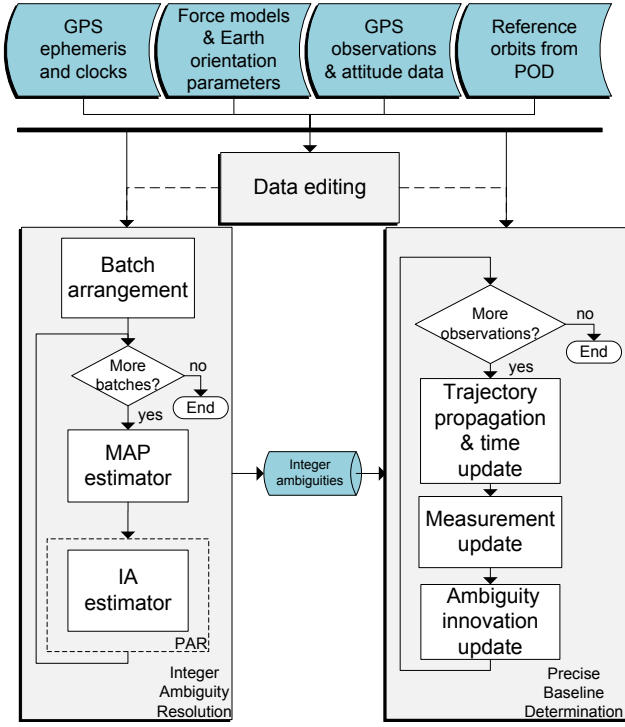


Fig. 2 Processing scheme for GPS-based precise baseline determination. In a first step (left), integer ambiguities are resolved based on GPS observations and a priori orbital constraints obtained from the single-satellite POD using a sliding batch approach. In a second step (right), the relative position is obtained in a reduced-dynamic orbit determination using a sequential filter based on ambiguity resolved single-difference carrier phases.

After the time update, the EKF measurement update is performed by using a SD IF combinations of pseudorange and carrier phase observations, given by

$$P_{[IF]}^i = \rho_{[1]}^i + c\delta t_{[1]} + \epsilon_{[IF]}^i \quad (3a)$$

$$\Phi_{[IF]}^i = \rho_{[1]}^i + c\delta t_{[1]} + \lambda_{IF} b_{[IF]}^i + \varepsilon_{[IF]}^i \quad (3b)$$

where λ_{IF} is the associated wavelength of the IF combination. When a set of rising GPS satellites are introduced into the filter, the measurement update is followed by an ambiguity innovation update (Kroes et al., 2005), in which the available DD integer ambiguities are introduced into the filter by forming a DD IF bias of the i -th and j -th GPS satellites, as follows

$$b_{[IF]}^{ij} = b_{[IF]}^i - b_{[IF]}^j = n_{[1]}^{ij} + \frac{\lambda_{WL}}{\lambda_2} (n_{[1]}^{ij} - n_{[2]}^{ij}) \quad (4)$$

where λ_{WL} is the wavelength of the WL combination. The residuals of this modeled bias and the filter-estimated bias $\hat{b}_{[IF]}^{ij} = \hat{b}_{[IF]}^i - \hat{b}_{[IF]}^j$ are evaluated against a defined threshold. If the test is successfully passed, these residuals are included into the filter with no uncertainty over the modeled bias given by Eq. (4), thus constraining the estimated values of $\hat{b}_{[IF]}^i$ and $\hat{b}_{[IF]}^j$ dur-

ing the complete validity periods of the ambiguities from the i -th and j -th GPS satellites.

3.2. Differential antenna phase pattern calibration

The precise modeling of the GPS carrier phase observations requires the knowledge of the antenna phase center location at the transmitter and receiver antennas, which is typically accounted for by a set of range corrections denoted as the phase center offset (PCO) and the phase center variation (PCV). These quantities cannot be directly measured given that they possess two inherent degrees of freedom (Rothacher et al., 1995), although they can be modeled by defining a set of gauge fixing conditions that must be consistent for all the models involving a given antenna (Rothacher and Schmid, 2006).

The GPS receivers on board the GRACE, TanDEM-X and Swarm missions make use of choke ring antennas in order to minimize the impact of multipath effects. Even though on-ground calibrations of a given antenna model define a set of PCO and PCV corrections, they are not representative of the error sources encountered in the spacecraft environment. These distortions can be partially recovered from an in-flight analysis of carrier phase residuals (Haines et al., 2004; Jäggi et al., 2009; Montenbruck et al., 2009). In POD analysis it is expected that some systematic errors, including PCV distortions, may be absorbed by other estimation parameters, such as float IF biases. This might limit the actual impact of the resulting corrections and therefore an estimation of PCV distortions based on differential carrier phase measurements is expected to better reflect the magnitude of those systematic errors (Jäggi et al., 2009). The method for estimation of differential PCV correction maps used in this study is based on the so-called residuals stacking approach, described in detail by Montenbruck et al. (2009).

Figs. 3, 4 and 5 show the estimated differential PCV correction patterns with a resolution of 1.5° of the IF L1/L2 combination for the GRACE, TanDEM-X and Swarm missions, respectively. The pattern for the main antennas of the GRACE spacecraft was estimated using data covering days 3-30 of 2009 and is expressed in the antenna-fixed coordinate system of GRACE A. The pattern for the POD_MAIN and POD_AUX antennas of TerraSAR-X and TanDEM-X spacecraft, respectively, was estimated using data covering days 1-10 of 2014 and is expressed in the POD_MAIN antenna-fixed coordinate system of TerraSAR-X. Both of these patterns have been estimated on top of patterns from on-ground calibration. Finally, the pattern for the GPS-A antennas of Swarm A and Swarm C spacecraft was estimated using data from the period between days 214 and 229 of 2014. In the absence of available corrections from on-ground calibration, the pattern has been referred to the antenna reference point (ARP) and is expressed in the antenna-fixed coordinate system of Swarm A.

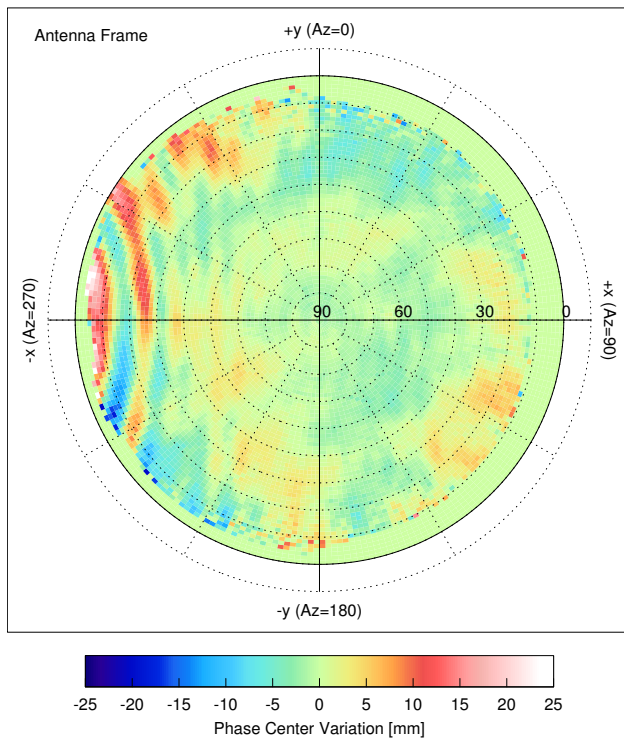


Fig. 3 Differential L1/L2 PCV pattern for the two main antennas on-board the GRACE spacecraft in the antenna-fixed coordinate system of GRACE A.

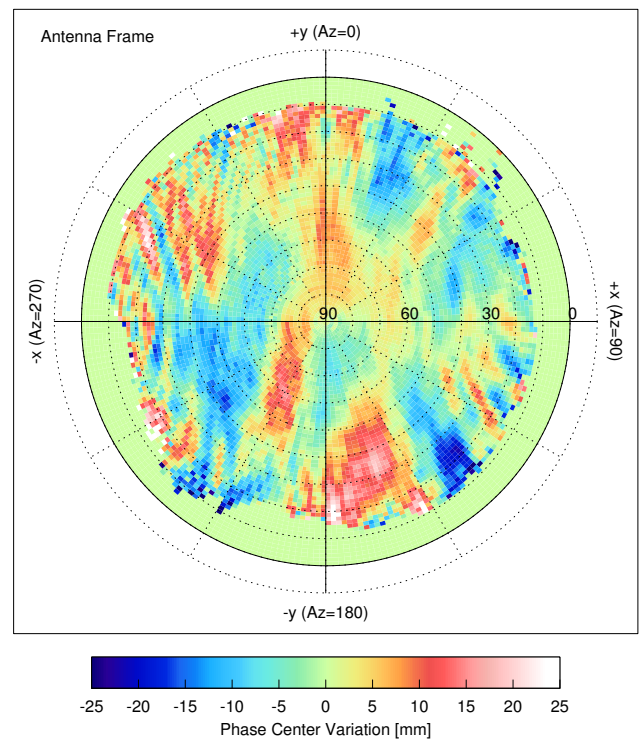


Fig. 4 Differential L1/L2 PCV pattern for the POD_MAIN and POD_AUX antennas on-board the TerraSAR-X and TanDEM-X spacecraft, respectively, in the antenna-fixed coordinate system of TerraSAR-X.

For the case of GRACE, a matching pattern was obtained by Jäggi et al. (2009) using data from year 2007 and an approach based on the direct estimation of the PCV corrections in a relative orbit determination scheme using the Bernese GPS Software (Dach et al., 2007). The pattern shows the small differences between the antennas of both spacecraft, except for the larger multipath error caused by cross-talk of the active occultation antenna of GRACE A shown in the $-x$ direction (Montenbruck and Kroes, 2003). For the case of the TanDEM-X mission, peak phase variations of around 15 mm are visible, mainly at low elevations. The origin of some of these phase variations has been discussed by Montenbruck et al. (2009) in the context of the TerraSAR-X spacecraft.

Other than GRACE and TanDEM-X, the two Swarm spacecraft exhibit small differences in the orientation of the antenna boresight vectors due to the combination of a nadir-pointing attitude control and a non-negligible spacecraft distance. While the relative orientation varies over an orbit, a mean pitch bias at the level of 1° can be observed. The resulting differential pattern is thus essentially equivalent to the difference of the single-satellite PCVs taking into account this mean pitch offset. As such, small fringes (related to multipath effects) are visible in the differential pattern, even though almost identical multipath effects can be observed in the undifferenced patterns of the individual spacecraft.

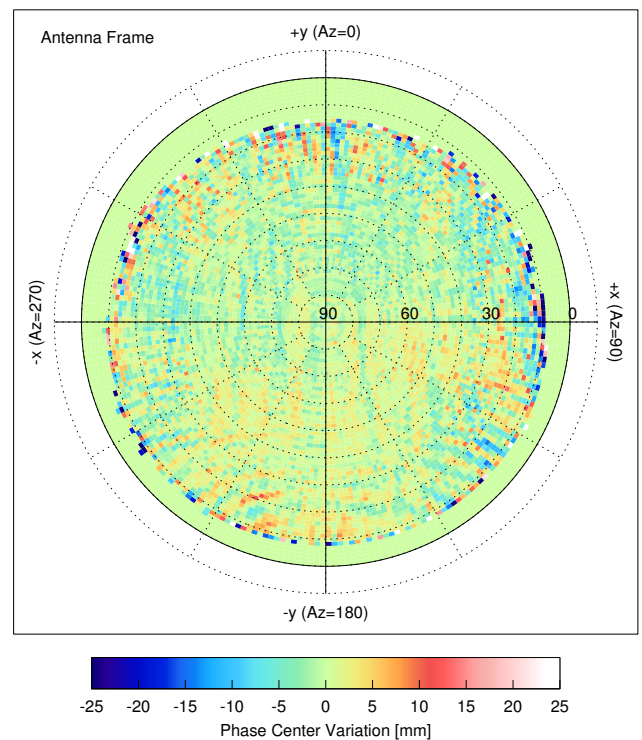


Fig. 5 Differential L1/L2 PCV pattern for the GPS-A antennas on-board the Swarm A and Swarm C spacecraft in the antenna-fixed coordinate system of Swarm A.

4. Flight data analysis

As briefly stated before, the integer ambiguity resolution and precise baseline determination schemes described in Sections 2 and 3 were tested using flight data from the GRACE, TanDEM-X and Swarm missions. These tests allowed to check the overall performance of the proposed algorithms in face of different mission profiles, baseline dimensions and receiver characteristics. The following sections give an introduction to the selected data sets as well as the specific strategies included in the overall proposed scheme for each of the missions under analysis.

4.1. Data sets

For the evaluation of the data sets that have been used in the present study, representative arcs for each mission have been selected. Covering 10-days periods on years 2009 and 2014, Table 2 depicts the measurements statistics for the six GPS receivers under analysis. The GRACE spacecraft have been equipped with two identical 16-channel NASA JPL BlackJack dual-frequency GPS receivers, whereas their commercial version, the Integrated GPS Occultation Receiver (IGOR) manufactured by Broadreach Engineering, has been used to equip the TerraSAR-X and TanDEM-X satellites. On the other hand, each spacecraft in the Swarm mission carries an 8-channel GPSR-G2 dual-frequency receiver manufactured by RUAG Space. For the GRACE mission, the present study makes use of the publicly available Level 1B data obtained from the JPL's Physical Oceanography Distributed Active Archive Center (PODAAC, 2015). Data from the IGOR receivers has been contributed by the GeoForschungsZentrum Postdam (Montenbruck et al., 2011-2012). For the Swarm mission, data has been provided by the European Space Agency (ESA; ESA-EO, 2015).

The depicted error levels in Table 2 for both pseudorange and carrier phase measurements have been obtained from residuals of precise orbit and baseline determination processing using undifferenced and SD formulations of IF combinations. Aside from receiver thermal noise, these error levels reflect the actual flight environment, which includes performance degradation conditions such as multipath, cross-talk between different antenna inputs and/or atmospheric scintillation. In general, the pseudorange error levels from all receivers

lie between 0.5 m and 0.7 m, except for GRACE A, where the effect of cross-talk with the GPS occultation antenna results in slightly higher levels. For carrier phase measurements the residuals from POD processing represent an upper bound of the receiver noise (Montenbruck and Ramos-Bosch, 2008). In the case of SD processing in baseline determination, including the corresponding antenna phase pattern corrections, the residuals from the BlackJack and IGOR receivers closely match the expected performance at 0.5-1 mm levels evaluated in signal simulator tests reported by Williams et al. (2002) and Montenbruck et al. (2006). Aside from exhibiting different noise levels resulting from receiver internal preprocessing for a 1-s sampling, carrier phase measurements from the GPSR receivers are largely affected by atmospheric scintillation (Sust et al., 2014). This situation is reflected both in the POD and SD residuals, which shows an effective receiver noise level of 2-3 mm.

In addition, the last column in Table 2 shows the assessment of dPOD solutions for each Earth-Centered Earth-Fixed (ECEF) coordinate, using reference orbits from precise baseline determination (obtained either with the scheme developed by Kroes (2006) or the scheme developed in Section 3.1). This evaluation provides useful a priori information used in the MAP estimator, as explained in Section 2.3. The resulting accuracies for all three missions show similar typical values (at the 1-2 cm level) for dPOD solutions, as those obtained likewise in previous studies (see e.g. Montenbruck et al., 2011-2012).

4.2. GRACE mission

The GRACE mission, launched in March 2002, consists of two identical spacecraft in a near circular orbit at an initial altitude of almost 500 km and an inclination of 89.5° with a nominal inter-spacecraft separation of 220 km. Its main purpose is the precise measurement of Earth's gravity field anomalies (Tapley et al., 2004). Among other instruments, the two spacecraft have been equipped with a K/Ka-band ranging instrument (KBR), one of the key instruments of the mission whose main objective is the ultra-precise satellite-to-satellite tracking with a precision at the μm -level. This allows to use KBR data for independent validation and precision assessment of baseline solutions obtained from

Table 2 Measurements and dPOD statistics for the GRACE, TanDEM-X and Swarm missions during representative arcs. The receiver error levels are given by the RMS residuals of the ionosphere-free combination in a precise orbit and baseline determination.

Mission	Baseline dimension	Arc (data and POD)	Receiver	Residuals				RMS error dPOD		
				POD		SD	ECEF coordinates			
				PIP2	L12		L12	X	Y	Z
GRACE	220 km	2009/101-110	BlackJack	GR A	0.8 m	<6 mm	2.3 mm	0.7 cm	0.8 cm	0.9 cm
				GR B	0.5 m	<5 mm				
TanDEM-X	500 m	2014/001-010	IGOR	TSX	0.6 m	<6 mm	2.2 mm	1.3 cm	1.0 cm	0.8 cm
				TDX	0.6 m	<6 mm				
Swarm	60-175 km	2014/213-222	GPSR	SW A	0.7 m	<11 mm	8.4 mm	0.7 cm	1.6 cm	0.7 cm
				SW C	0.6 m	<11 mm				

other instruments, such as GPS, as shown in several previous studies (e.g. Jäggi et al., 2007; Kroes et al., 2005; Švehla and Rothacher, 2004).

The nominal space baseline length of the GRACE formation makes it suitable for the analysis of precise relative orbit determination under conditions of long baselines and hence large residual ionospheric delays. To this end, solutions from the entire years 2007 and 2009 as well as one month of year 2011 were obtained. This allows to test the long-term performance of the proposed algorithms under different solar activity periods. In particular, October 2011 represents one of the periods with largest solar activity within the total mission lifetime, a scenario that is well known to be unfavourable for successful integer ambiguity resolution (Richert and El-Sheimy, 2005). A subset of this period has been already analysed by Tancredi et al. (2015) in the context of real-time navigation.

4.2.1. Baseline assessment

The first analysis is focused on the degree of improvement of the solutions taking into account different types of PCV corrections. Fig. 6 shows the KBR-assessment of solutions computed every 10 s during year 2009 (without 3 unprocessed days), depicting a comparison of the different achieved baseline precisions using PCV corrections from on-ground, absolute in-flight and differential in-flight calibrations. As shown by previous studies (Jäggi et al., 2009; Montenbruck et al., 2009) the corrections added by in-flight calibrations of individual antennas contributes to a more accurate carrier phase modeling, hence improving the resulting precision. However, as discussed in Section 3.2, it is possible to further enhance this modeling by including differential PCV corrections from in-flight calibrations and this can be observed in Fig. 6. The average standard deviations from KBR data obtained with on-ground, absolute in-flight and differential in-flight PCV corrections are 1.28 mm, 0.90 mm and 0.73 mm, respectively. The improvement provided by differential PCVs is particularly interesting in periods with good data quality. This effect can be observed during

the first 50 days of this year, where precisions of around 0.37 mm can be achieved.

A second analysis consists in the comparison of the solutions obtained using the proposed scheme for IAR and the solutions obtained using the scheme developed by Kroes (2006) which uses an EKF-based IAR (i.e. sequential IAR), both using differential PCV corrections. In this case, the comparison focuses on the consistency of the final solutions with the KBR data along with a precision-assurance indicator in the form of an availability rate. To this end, a screening threshold can be used in order to discard those solutions with low precision. Although this threshold is arbitrary, the relation of availability rates using different values between both schemes should be proportional.

Fig. 7 (top) shows the daily consistency with KBR data of solutions computed every 10 s for the year 2007. For the analysis of this year, 8 days were excluded due to problems with the processing of GPS measurements or KBR data. Applying a screening threshold of 2.5 mm, the solutions obtained using the EKF-based IAR scheme show an availability of 95.2% and an average standard deviation of 0.95 mm, whereas the solutions from the proposed scheme show an average standard deviation of 0.72 mm with an availability of 99.4%. Provided this availability rate, the value of 0.72 mm is in good agreement with the reported value of 0.81 mm by Jäggi et al. (2009) for the same period and obtained taking into account absolute empirical PCV corrections (with the small difference possibly stemming from the use of a differential PCV). On the other hand, if a sub-millimeter precision must be assured, the availability rate of the solutions using the EKF-based IAR scheme drops to 63.3% with an average standard deviation of 0.76 mm whereas the solutions computed with the proposed scheme achieve an availability rate of 87.6% and an average standard deviation of 0.65 mm. In addition, it is interesting to note that for the period between days 70 and 100 when the data has an excellent quality, both approaches perform very well, achieving precisions of 0.48 mm for the solutions using the EKF-based IAR scheme and 0.36 mm for the solutions using the proposed scheme.

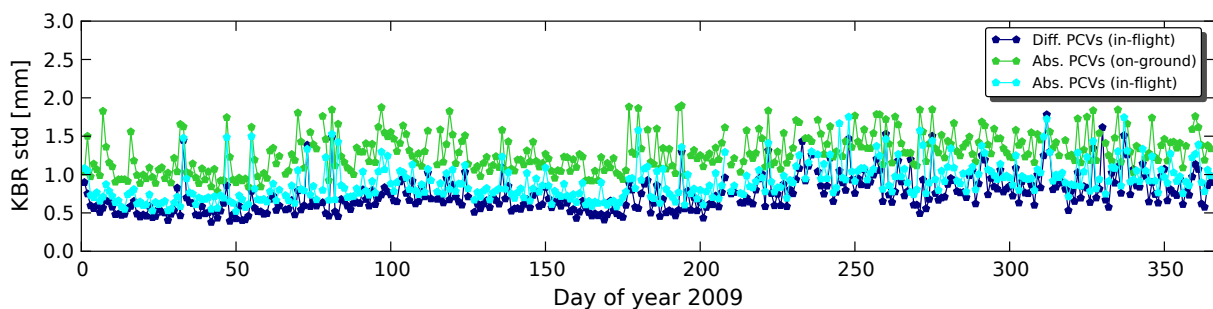


Fig. 6 Assessment using KBR data of the estimated reduced-dynamic GRACE baselines for year 2009 considering different PCV corrections.

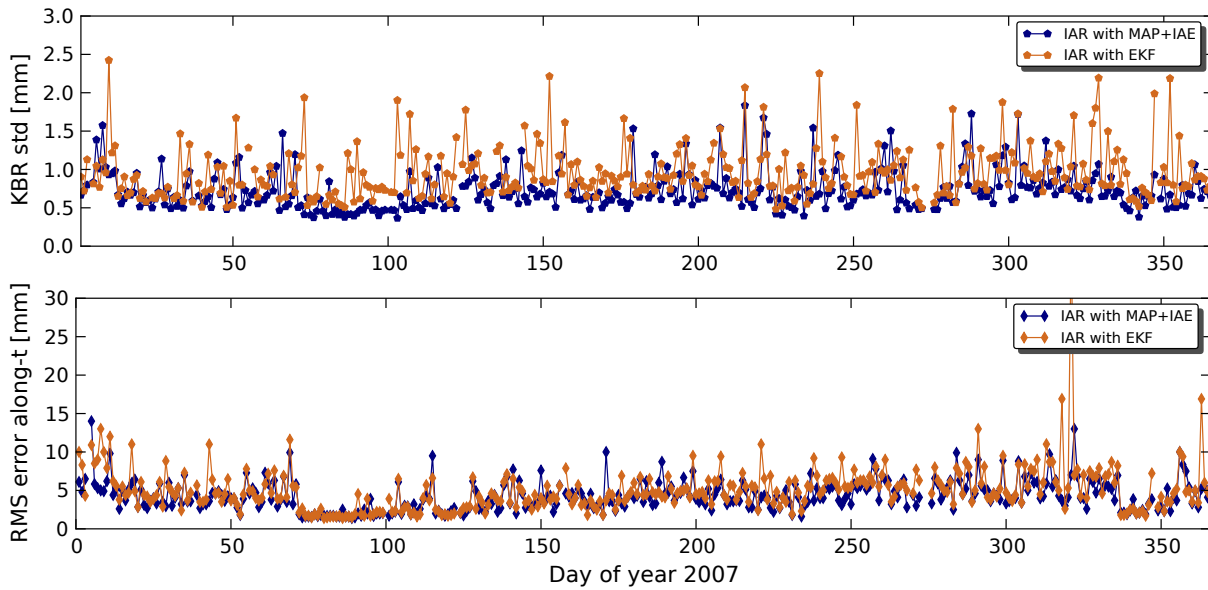


Fig. 7 Comparison of GRACE precise baseline solutions for year 2007 obtained with the proposed scheme (blue curves) and with an EKF-based IAR approach (red curves). The upper plot shows the assessment of reduced-dynamic solutions using KBR data. The lower plot depicts the consistency between precise kinematic and reduced-dynamic solutions in the along-track direction.

A related assessment of the performance of both schemes is provided by the analysis of purely kinematic solutions using only carrier phase measurements with fixed ambiguities. Given that the precise kinematic solution is more prone to errors due to the presence of wrongly fixed ambiguities in comparison with its reduced-dynamic counterpart, the assessment by comparison of these solutions provides an indicator of the quality of fixed ambiguities. Fig. 7 (bottom) shows the consistency in the along-track component between the kinematic and reduced-dynamic solutions from both estimation schemes for the year 2007. The average RMS error from the solutions using the EKF-based IAR is of 5.04 mm whereas the solutions using the proposed scheme show an average RMS error of 4.27 mm. Although in general both schemes seem to perform well, some big outliers are present in solutions using the EKF-based IAR during the last months of the year, which reflect large affections due to the presence of wrongly-fixed ambiguities. Even though the difference in the achieved accuracy of kinematic solutions between both schemes has a correspondence with the observed difference in precision of reduced-dynamic solutions, as shown in Fig. 7 (up), the evaluation of reduced-dynamic solutions using KBR data provides a joint indicator of the number and quality of estimated ambiguities used in the computation of the baseline solution. This situation may be more difficult to grasp in the assessment of kinematic solutions.

A third analysis is focused on the performance of both IAR schemes under intense ionospheric activity. Under such conditions, the correlation among float ambiguity estimates is particularly large, which makes

the integer ambiguity search process more difficult and makes both IAR schemes more prone to an erroneous ambiguity fixing. This is specially important for the EKF-based IAR algorithm, given that erroneous ambiguities are fed into the filter state and used for subsequent ambiguity estimation, leading possibly to more wrongly-fixed ambiguities. In the proposed scheme, aside from a potential larger amount of measurements used for float ambiguity estimation before an attempt of fixing, the independence among processing batches define individual estimation processes each time. This implies that possible wrongly-fixed ambiguities do not take part in the estimation of more ambiguities, leading in general to solutions with an increased precision and lower number of outliers. Fig. 8 depicts the performance of both IAR schemes in terms of assessment with KBR data for daily solutions computed every 10 s obtained during the month of October 2011. Only day of year 301 has shown problems with the ambiguity resolution of both approaches. As can be seen, even during these harsh conditions for successful integer ambiguity resolution, an average standard deviation of 0.86 mm is achieved with the solutions obtained with the proposed scheme. In addition, the number of outliers from these solutions is lower with respect to those obtained with the EKF-based IAR scheme, which has also an impact on the final availability.

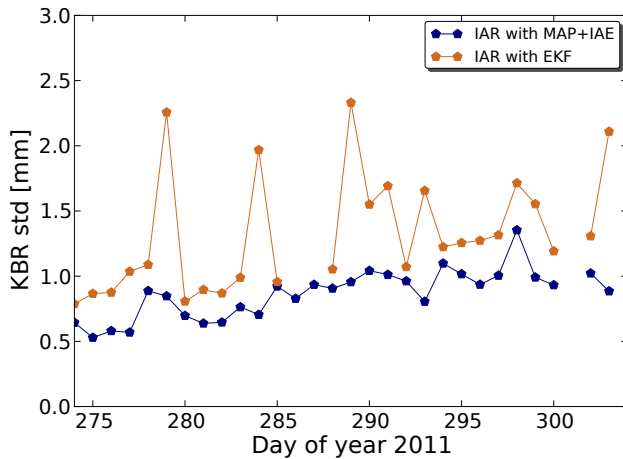


Fig. 8 Assessment using KBR data of the estimated reduced-dynamic GRACE baselines during October 2011 in comparison with solutions obtained with an EKF-based IAR approach.

4.3. TanDEM-X mission

The TanDEM-X spacecraft was launched in June 2010 and its main purpose was to complement the orbiting TerraSAR-X satellite to form the first configurable synthetic aperture radar (SAR) with baselines of a few hundred meters in space (Krieger et al., 2010). As a whole, both spacecraft conform the TanDEM-X mission whose main objective is the generation of a global digital elevation model (DEM). The two spacecraft orbit Earth in a polar dusk-dawn orbit with an altitude of 515 km, keeping the TerraSAR-X controlled to fly in a predefined tube of 250 m radius, though regular control maneuvers have been exercised to maintain specific formation flying geometries according to each mission phase (Montenbruck et al., 2008). For this study, two representative periods of data from the TanDEM-X mission have been used. The first one consists of 10 days at the beginning of January 2014 in which both spacecraft maintain a baseline with a typical dimension of 500 m. The second period under analysis covers a 32-days data arc between September and October 2014, when the two spacecraft broke up the close formation and were brought to an inter-spacecraft separation of around 75 km (M. Wermuth, personal communication). These two periods are representative of short and medium to long baselines for the evaluation of performance of the proposed schemes.

4.3.1. Baseline assessment

Unlike the GRACE mission, there are no direct measures for precision assessment of the resulting baseline with the TanDEM-X mission, although internal consistency checks can be obtained. For this purpose, solutions using the EKF-based IAR scheme have been employed. This type of solutions has been used in comparisons with other estimation schemes and software packages, as shown by Jäggi et al. (2012). All the solutions obtained for this assessment were computed using differential PCV corrections.

The first test consist in the computation (using both schemes) of purely kinematic solutions using carrier phase measurements with fixed ambiguities only. As stated before, these solutions provide an indicator of the quality of fixed ambiguities and thus give a benchmark of the quality of the resulting baseline. Fig. 9 depicts a direct comparison between the assessments of daily solutions computed every 10 s using both the EKF-based IAR and the proposed schemes during the 42 days under analysis, except for day 273 when not enough attitude information for the TanDEM-X spacecraft was available.

As shown in Fig. 9, the performance from both approaches is very similar, though some days required a manual adjustment of wrong-ambiguity detection thresholds in the case of the proposed scheme in order to achieve the best possible performance. This situation was mainly caused by the big number of detected cycle-slips in combination from both receivers (largely driven by the receiver on-board TanDEM-X), which in turn was translated into an increased amount of float ambiguities to fix (per batch) in the MAP estimator. This factor had a direct impact in the proposed scheme in the resulting lower bound of the ILS success rate, mainly due to the large number of ambiguities from very short observation periods. This situation could be partially tackled by selecting heuristic constraints as a priori information for differential ionospheric delays in the short baseline scenario, but this strategy was certainly less effective in the case of medium baselines. On the other hand, the EKF-based IAR appeared to perform reasonably good due to the scheme of sequential ambiguity estimation, for which short-period passes have less impact, although a degraded kinematic solution was obtained on day 285, which could not be corrected by manual adjustments. The resulting RMS errors of kinematic solutions using the EKF-based IAR are 11.4 mm, 3.8 mm and 3.2 mm in the radial, along-track and cross track directions, respectively. Likewise, the RMS errors of solutions using the proposed scheme are 11.5 mm, 3.8 mm and 3.4 mm in the radial, along-track and cross-track directions, respectively. Hence, although the net result is a slightly worse performance in the final kinematic solution of the proposed scheme with respect to the EKF-based IAR, the robustness of the MAP and IA estimators under these particular conditions is fairly good, a feature that can be grasped by looking at the number of provided kinematic solutions with an acceptable accuracy.

A more stringent test consists in the comparison of reduced-dynamic solutions obtained from both schemes, as well as a comparison with single-frequency reduced-dynamic solutions in the short baseline case using the EKF-based IAR. Although all these solutions use the same dynamic modeling strategies, the single- and dual-frequency solutions exhibit a fair degree of statistical independence due to the use of L2 measurements in the dual-frequency case. The RMS differences in the

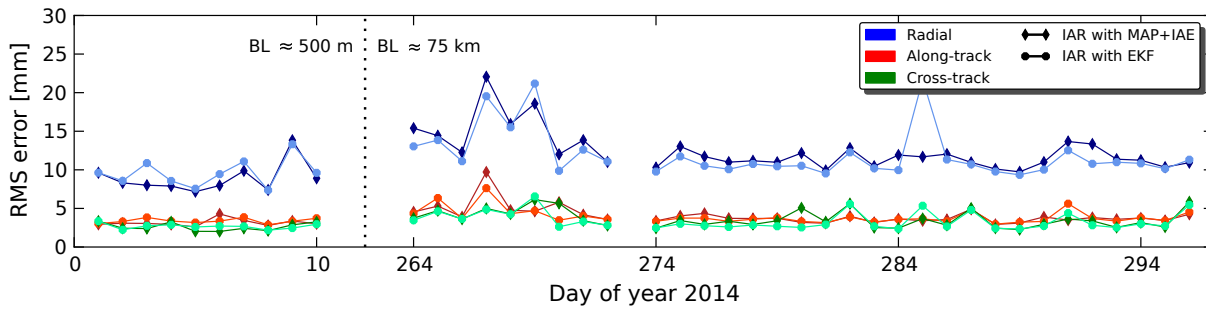


Fig. 9 Consistency between reduced-dynamic solutions and the estimated TanDEM-X precise kinematic baselines using the proposed scheme and those obtained using an EKF-based IAR approach, during 42 days of year 2014. The indication *BL* stands for the baseline dimension at the specified period. Radial (blue tones), along-track (red tones) and cross-track (green tones) directions in the local orbit coordinate frame of the TerraSAR-X spacecraft. The solutions from both schemes are pointed out by a different type of marker.

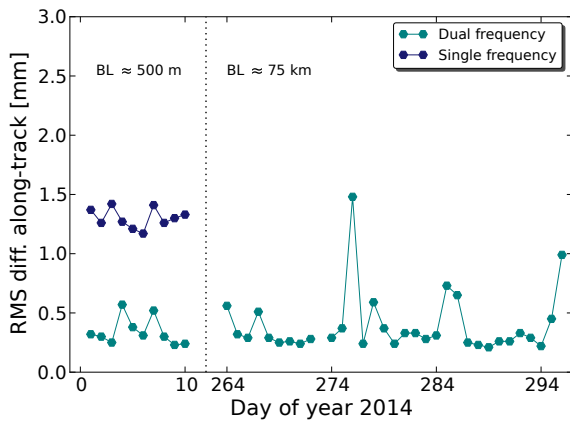


Fig. 10 Consistency in the along-track direction of estimated TanDEM-X reduced-dynamic baselines using the proposed scheme and those obtained using an EKF-based IAR approach in single- and dual-frequency modes, during 41 days of year 2014. The indication *BL* stands for the baseline dimension at the specified period.

along-track component of a daily comparison during the period under analysis is shown in Fig. 10, including maneuver arcs. In general, the solutions using the proposed scheme and single-frequency solutions using the EKF-based IAR in the short baseline case exhibit an agreement of 1.3 mm in the along-track direction, whereas in the radial and cross-track components, the agreement is of 1.1 mm and 1.2 mm, respectively. These differences are highly driven by discrepancies during periods of maneuvers and include systematic biases below 0.5 mm. They provide, in general, a good indication of the quality of solutions from the two schemes provided the degree of statistical independence.

Similarly, the solutions from the two dual-frequency schemes have been compared for both baseline scenarios. As shown in Fig. 10 the solutions obtained from both schemes exhibit an agreement in the 0.3-1.5 mm range, with only one big outlier, which has been likely caused by wrong integer ambiguity estimation from either or both schemes. The resulting average RMS consistency during the period under analysis is of 0.32

mm, 0.38 mm and 0.31 mm in the radial, along-track and cross-track components, respectively. Although the dual-frequency solutions from both schemes have statistical dependence, this cross-validation provides an indication of the performance of the IAR strategies and the consistency of the final solutions given that, in general, the fixed ambiguities used in the baseline determination process in each scheme are different.

The analysis of the TanDEM-X data revealed the problem of a large number of detected cycle slips, in particular from the receiver on-board the TanDEM-X spacecraft. The possible presence of half cycle slips in the data is suspected to be one of the main driving factors and a more complete analysis is left for further investigation.

4.4. Swarm mission

The Swarm mission was launched in November 2013 and consists of three identical spacecraft, flying in different orbital planes. Two satellites (Swarm A and Swarm C at the time of analysis) orbit at an initial altitude of 460 km with a longitudinal separation of 1-1.5°, whereas the third satellite (Swarm B) remains at a higher orbit of around 510 km. The primary goal of the mission is the study of the Earth's magnetic field and its variation over time (Friis-Christensen et al., 2008). The Swarm mission requirements state only the usage of POD products for the generation of scientific data and therefore the synchronization of GPS receivers for baseline reconstruction was not part of the initial characteristics. However, starting from March 2014, the receivers from Swarm A and Swarm C started to deliver measurements at common epochs with a 0.1 Hz delivery rate. Later, in July 2014, it was decided to modify this rate to 1 Hz (Jäggi et al., 2014), which offered the possibility of baseline reconstruction.

As briefly stated in Section 4.1, recent analyses of GPS receivers on-board the Swarm spacecraft have shown a degraded performance in the generated carrier phase measurements due to atmospheric scintillation, an effect that is particularly large in the polar regions

(Sust et al., 2014). Along with the de-synchronization between receivers, this factor has also an impact in the selection of the most suitable data set to analyze. For this study, data from the Swarm A and Swarm C spacecraft for the month of August 2014 have been used, a period with a reasonably good performance of the GPS receivers outside the polar regions. The relative orbital motion of the Swarm A and Swarm C spacecraft creates a variable baseline from approximately 60 km to around 175 km, making it a representative scenario of a variable medium to long baseline for the performance evaluation of the proposed schemes.

4.4.1 Half and full cycle ambiguity resolution

Unlike GRACE and TanDEM-X missions, the GPS receivers on-board the Swarm spacecraft generate carrier phase measurements also at half cycles (M. Sust, personal communication), which necessitates the consideration of half cycle ambiguities in the observation models. This situation, which has been already noted in previous missions such as Jason 2 (Bertiger et al., 2010b), is particularly challenging for IAR algorithms given that a successful integer resolution is highly dependent on the number of half cycle ambiguities.

An initial approach could consist simply in the execution of IAR dismissing the presence of half cycle ambiguities, which may lead to solutions with moderate to high ambiguity resolution rates, depending on the applied model and validation strategy. However, this approach might imply a large number of *forced* ambiguities from half to full cycle, increasing the percentage of wrongly fixed ambiguities. On the other hand, the execution of IAR considering only half cycle ambiguities would complicate the integer search process given the apparent wavelength reduction of carrier phase observables. In this case, the resulting fixing rate is expected to decrease, although this condition is highly dependent on the number of available observations and the validation strategy.

Therefore, in order to increase the performance of the IAR algorithm, it is necessary to consider the inclusion of an extra constraint over the modeled carrier phase observations. To provide such a constraint, the proposed algorithm focuses on a strategy based on the cycle type determination for each ambiguity to be resolved in the MAP and IAR algorithms. To this end, due to the decorrelating property of the WL transformation, it is possible to retrieve important information from WL ambiguities as they possess typically a high degree of discernibility. The set of WL ambiguities to evaluate can be obtained from the estimated L1 and L2 ambiguities in an initial run of the MAP estimator without considering any special constraint. In order to resolve for the cycle type of the estimated WL ambiguity, the probabilities of two hypothesis (one for each cycle type) are compared against each other and

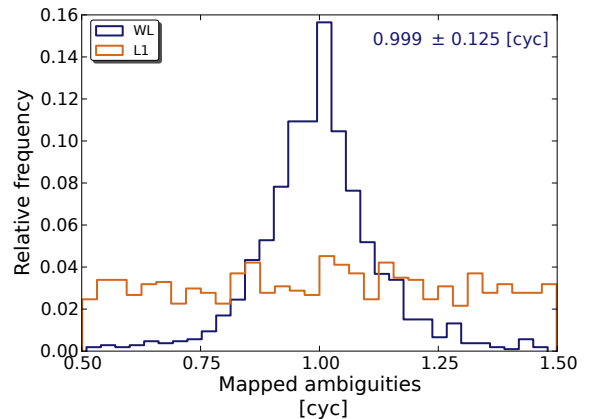


Fig. 11 Frequency distribution of mapped estimated float WL and L1 ambiguities into the interval [0.5, 1.5] on 13 August 2014 for the Swarm A-Swarm C baseline.

resolved based on the resulting variance of such ambiguity. This approach is complemented from the analysis of the frequency distribution of estimated float ambiguities in the data set. As an example, Fig. 11 shows the normalized frequency distribution of mapped WL ambiguities into the interval [0.5, 1.5] on 13 August 2014. Subsequently, depending on the resolved cycle type of the WL ambiguities, these are *frozen* to a half or full integer value by using a variance-controlled rounding estimator. The frozen WL ambiguities $\hat{m}_{[WL]}^{ij}$ are in turn used to perform a rough estimation of L1 float ambiguities, using the reference orbits of the spacecraft as known values, as follows

$$\hat{a}_{[1]}^{ij} \approx \frac{1}{\lambda_{IF}} (\Phi_{[1]}^{ij} - \rho_{[1]}^{ij}) - \frac{\lambda_{WL}}{\lambda_2} \hat{m}_{[WL]}^{ij} \quad (5)$$

These estimates are averaged over the validity period of the DD ambiguity. No attempt of fixing is performed at this point. The resulting value for $\hat{a}_{[1]}^{ij}$ is used for cycle type evaluation in a second hypothesis testing method. By defining a set of boolean variables x_{WL} , x_1 and x_2 with solutions of half or full cycle type for the WL, L1 and L2 ambiguities, respectively, the remaining cycle type for the L2 ambiguity can be obtained from

$$x_{WL} = x_1 \odot x_2 \quad (6)$$

where \odot denotes an exclusive nor (XNOR) operation. In this way, the information about the cycle type in L1 and L2 is considered in the MAP estimator for a proper modeling of the carrier phase measurements. In particular, according to Fig. 11, the distribution of WL ambiguities around a full cycle type has shown to be an advantage for the proposed scheme, given that it represents an effective constraint for the IAR method, resulting in a reduced search space and an expected overall improvement in the performance of the algorithm. Similarly, this reveals that, according

to Eq. (6), the number of individual L1 and L2 float ambiguities of half and full cycle types should be uniformly distributed in the sample space, a fact that is likewise depicted in Fig. 11 in the normalized frequency distribution of estimated L1 float ambiguities mapped into the interval $[0.5, 1.5]$ on 13 August 2014. However, it is important to note that the posterior covariance matrix for every float ambiguity in the MAP solution vector is characterized by the observation model and a priori information.

The distribution of WL float ambiguities around a full cycle type hints at the presence of a degree of correlation between L1 and L2 carrier phase measurements in the GPSR receivers, a situation already found in other geodetic receivers if carrier phases of encrypted codes are tracked with the help of the C/A code (Tiberius et al., 1999). Thus, it can be considered that the current form of the proposed algorithm is better suited for receivers with such characteristics. On the contrary, for receivers with an uncorrelated number of half and full cycle ambiguities in L1 and L2, the WL float ambiguities are expected to have a bimodal distribution in the sample space. This implies that more stringent hypothesis tests for cycle type determination might be necessary (depending on the observation model and available a priori information) in order to provide the proper constraints to the IAR algorithm so as to effectively improve the performance with respect to a half cycle-only ambiguity estimation.

4.4.2 Baseline assessment

In order to be able to form SD of measurements, a preprocessing step has been executed in data provided by ESA in which all observations have been aligned to integer GPS seconds by means of a coarse clock offset estimation using pseudorange measurements. Like in the case of the TanDEM-X mission, in the absence of external baseline solutions, internal consistency checks have been performed in order to assess the accuracy of the estimated baseline between Swarm A and Swarm C spacecraft. However, unlike the TanDEM-X mission,

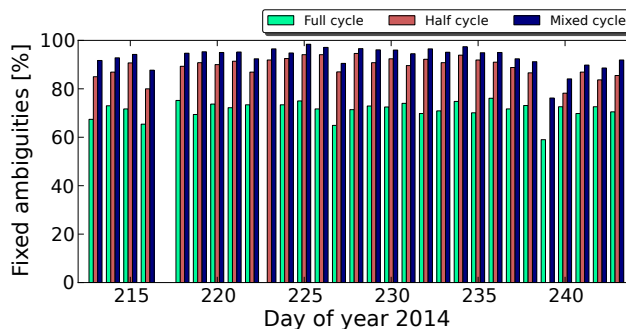


Fig. 13 Fixing ambiguity rates of Swarm A-Swarm C baseline solutions using full, half and mixed cycle IAR schemes during August 2014.

it was not possible to obtain solutions using the EKF-based IAR approach given its current formulation within the baseline determination scheme for the case of half cycle ambiguities. Hence, the baseline analysis using Swarm data is based on the assessment of precise kinematic solutions with respect to the corresponding reduced-dynamic solutions, computed using differential PCV corrections. As part of the test, a second (related) indicator to evaluate is the percentage of fixed ambiguities that were used in the relative orbit determination process. This assessment includes, in addition to the approaches using full or half cycle IAR, the proposed strategy described in Section 4.4.1, denoted here as mixed cycle IAR.

Fig. 12 depicts the assessment of precise kinematic solutions computed every 5 s for the 30 days under analysis, excluding day 217 for which not enough GPS data were available. For simplicity, only RMS errors of the solutions in the radial and along-track components are shown. Additionally, Fig. 13 shows the percentage of fixed ambiguities that were used in the computation of the final baseline solutions taking into account each of the IAR strategies under analysis. As can be seen, the performance of the full cycle IAR scheme is rather poor, both in terms of the fixing rate and the achieved kinematic accuracy. Having measurements with a 0.2 Hz rate provides more evidence of the presence of half cycle ambiguities in the data and hence the estimated

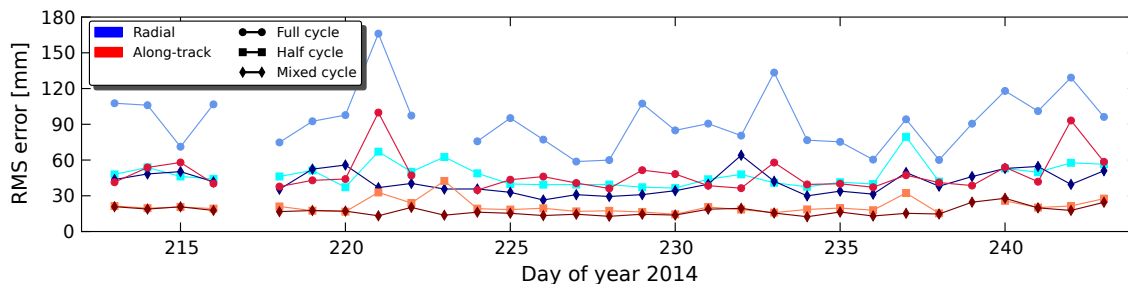


Fig. 12 Consistency between reduced-dynamic solutions and the estimated Swarm A-Swarm C kinematic baselines using the proposed scheme during August 2014. The comparison is done over solutions computed using full, half and mixed cycle IAR schemes, denoted by different markers. Radial and along-track components in the local orbit coordinate frame of the Swarm A spacecraft are indicated by colored lines with blue and red tones, respectively.

float ambiguities cannot not be fixed with enough confidence. On the other hand, the performance of the half and mixed cycle IAR strategies is very similar, both in terms of the number of fixed ambiguities and the achieved accuracy of the kinematic solution. The high availability rate of GPS measurements is particularly helpful for the half cycle IAR approach, given that in the presence of half cycle ambiguities, the algorithm uses enough measurements to resolve them, even in the situation of an apparent reduction of the effective wavelength in the modeled observations. However, as shown in Fig. 13, it is possible to further increase the amount of fixed ambiguities if the specific cycle type for every processed ambiguity is included in the algorithm. This is translated to an overall slight improvement of the accuracy of the kinematic solution using the mixed cycle IAR strategy. In addition, Figs. 12 and 13 show that the full and half cycle estimation schemes failed to provide solutions for days 223 and 239, respectively, whereas the mixed cycle scheme could provide solutions for all processed days, which gives an indication of the robustness of the algorithm.

The RMS errors for the period under analysis of the kinematic solution using the half cycle IAR scheme are 4.7 cm, 2.1 cm and 1.3 cm in the radial, along-track and cross-track components, respectively, with

a mean fixing rate of 89.2%. Similarly, the RMS errors resulting from the mixed cycle IAR scheme are 4.0 cm, 1.7 cm and 1.1 cm in the radial, along-track and cross-track components, respectively, with a mean fixing rate of 93.1%. Similar, albeit slightly lower precisions were obtained by Jäggi et al. (2014) for precise kinematic solutions using data from a one-month period on April-May 2014 and a WL/NL ambiguity resolution technique. In particular, Jäggi et al. (2014) do not report to have used any special strategy for half cycle ambiguity resolution, although a NL ambiguity fixing rate of around 89% was achieved. This situation could be explained by the presence of full cycle WL ambiguities in the data (as depicted in Fig. 11), which means that approximately 95% ($\approx 2\sigma$) of these ambiguities can be fixed to integer values with enough confidence and without any consideration about the cycle type.

Table 3 RMS error of Swarm A-Swarm C precise kinematic baseline with the reduced-dynamic solution as reference, during the period depicted in Fig. 14. Shown are the three IAR strategies under analysis.

IAR strategy	Radial [mm]	Along-track [mm]	Cross-track [mm]
Full cycle	48.9	25.3	34.7
Half cycle	7.7	3.6	3.0
Mixed cycle	7.5	3.0	2.9

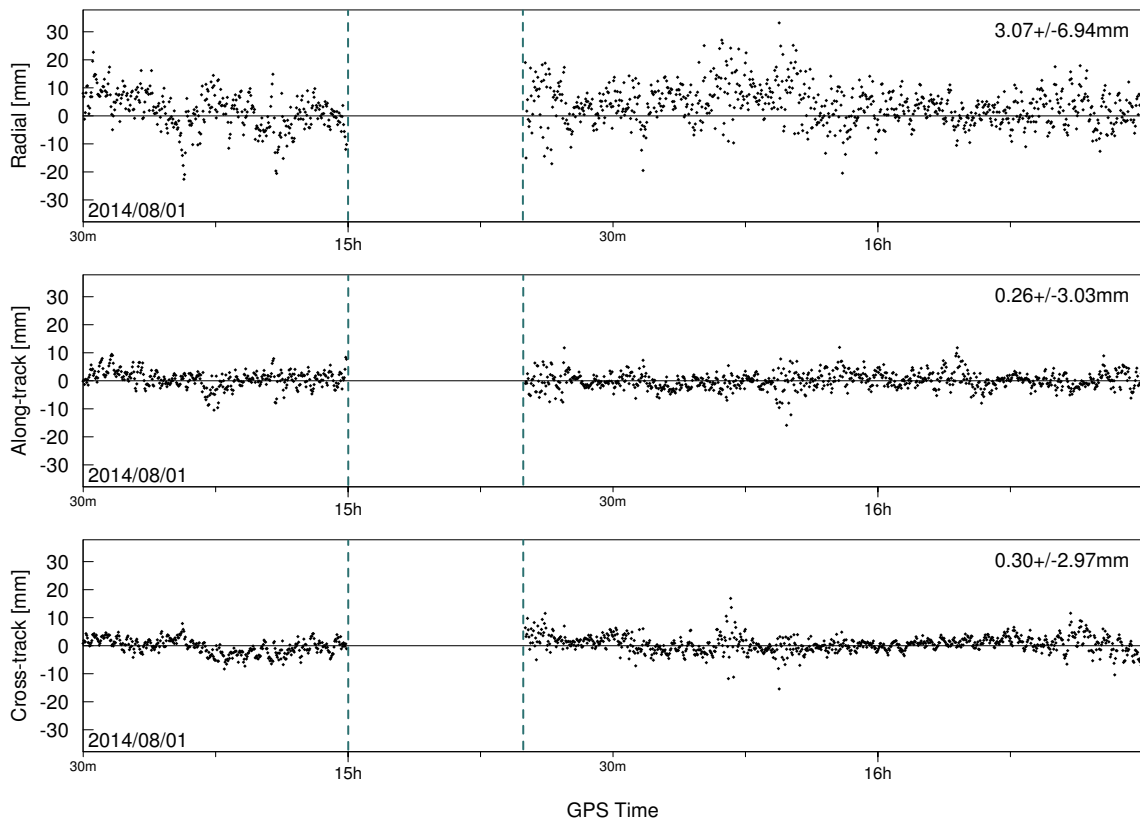


Fig. 14 Consistency between estimated Swarm A-Swarm C precise kinematic and reduced-dynamic baseline solutions during 14:30-16:30 GPST on 1 August 2014. Excluded is the period between dashed lines, where errors due to atmospheric scintillation occur.

Thus, this constraint on WL ambiguities can be further exploited in the fixing process of NL ambiguities, which may be similarly constrained to full cycle values and fixed to integers without any other special analysis, resulting in a fairly good fixing rate.

As briefly stated at the beginning of Section 4.4, carrier phase measurements from the Swarm spacecraft are highly affected by atmospheric scintillation, mainly at the polar regions. Indeed, this can be confirmed in the measurements statistics shown in Table 2. The higher RMS errors from the kinematic solution shown in Fig. 12 (cf. Fig. 9) are mainly driven by this effect (along with a reduced number of channels in the GPSR receivers). As an additional test, in order to better grasp the performance of the different IAR strategies under analysis, Fig. 14 shows the assessment of a precise kinematic solution computed every 5 s during a 100-minutes period (\approx one orbit) from 14:30 to 16:30 GPST on 1 August 2014. This period excludes a stretch between 15:00 and 15:20 GPST where large errors attributed to atmospheric scintillation are present. Depicted is the baseline solution computed using the mixed-cycle IAR strategy but a comparison of assessments of the three IAR schemes is shown in Table 3. In general, this test confirms that the performance of both the mixed- and half-cycle strategies is very similar and that, during this period, a large number of ambiguities ($>95\%$) is fixed in both schemes. Similarly, although the period under analysis is very short, the achieved accuracy of the precise kinematic solution gives a rough indication of the performance of the GPSR receivers in the absence of atmospheric scintillation effects, which is very close to the achieved performance of the BlackJack and IGOR receivers (cf. Figs. 7 (bottom) and 9)

5. Summary and conclusions

A set of algorithms for robust and precise baseline determination using GPS measurements has been presented and analysed. Precise relative navigation has been achieved by using carrier phase measurements, which calls for the implementation of strategies for integer ambiguity resolution. For this purpose, the framework of the presented scheme is based on a dedicated algorithm for the formation of suitable combinations of GPS satellites for the estimation of DD float ambiguities in a MAP estimator. An additional scheme for integer ambiguity fixing based on an IA estimator has been included. Precise baseline determination has been achieved by considering a reduced-dynamic approach and a SD IF observation model in an EKF. To achieve optimal solutions, differential antenna PCV corrections have been estimated and included in the analysis.

The presented algorithms have been tested using data from different periods of the GRACE, TanDEM-X and Swarm missions. The results from the GRACE mission using data sets from years 2007, 2009 and 2011 show an overall consistency with KBR data of 0.7 mm for periods of low and medium solar activity and of 0.8

mm for a period under intense ionospheric activity. For some days within periods of good data quality, precisions of around 0.3 mm could be attained. Likewise, the analysis of long periods allowed to test the availability of solutions with a given required precision. As an example, the results from year 2007 showed an availability rate of 99.4% of solutions with precisions better than 2.5 mm whereas solutions with sub-millimeter precisions could be guaranteed with a 87.6% availability rate.

On the other hand, results from the TanDEM-X mission using data from year 2014 in short and medium-large baseline configurations showed an overall consistency between precise kinematic and reduced-dynamic solutions of 11.4 mm, 3.8 mm and 3.2 mm in the radial, along-track and cross-track components, respectively. In addition, internal consistency checks with reduced-dynamic solutions obtained using an EKF-based IAR, showed a RMS error of around 1.2 mm and 0.3 mm in each component in the single- and dual-frequency modes, respectively. Data from the TanDEM-X mission showed a particular challenge due to the high number of detected cycle slips from common measurements. The possible presence of half cycle slips in the data has been considered as one of the main causes. However, it could be shown that the robustness of the presented algorithms under such conditions was preserved.

Similarly, the present study introduced some strategies for coping with half cycle ambiguities in an IAR scheme and tests using data from the Swarm A and Swarm C spacecraft have been carried out. During a one-month period, the results showed an average fixing rate of around 93% and a consistency between precise kinematic and reduced-dynamic solutions of 4.0 cm, 1.7 cm and 1.1 cm in the radial, along-track and cross-track components, respectively, using an estimation scheme considering concurrent models of full and half cycle ambiguities. In addition, the results suggest the suitability of the proposed scheme for receivers that exhibit correlations between L1 and L2 carrier phase measurements and thus a high number of ambiguities with equal cycle type in both carriers.

In general, the results presented in this study suggest the feasibility of obtaining relative navigation solutions with high precision and good levels of robustness in diverse spacecraft formation flying scenarios, including long, short and variable baseline lengths, as well as different GPS receiver characteristics. This allows a consistent long-term generation of highly-precise GPS-based space baseline products, which may benefit scientific and engineering applications derived from current and future distributed spacecraft missions.

Acknowledgements

The present study makes use of GPS measurements and spacecraft data that have been made available by the JPL's Physical Oceanography Distributed Active Archive Center (PODAAC), the GeoForschungsZen-

trum (GFZ), Postdam and the European Space Agency (ESA/ESTEC), Noordwijk. GPS orbit and clock solutions have been obtained from the Center for Orbit Determination in Europe (CODE). The support of all these institutions has been essential for this work and is gratefully acknowledged. The authors are grateful to M. Wermuth for the provided assistance with TanDEM-X data. In addition, the authors would like to thank to three anonymous reviewers for their valuable remarks that greatly helped to improve the original manuscript. GAA is holder of a fellowship from the Consejo Nacional de Ciencia y Tecnología de México and the Deutscher Akademischer Austauschdienst and wishes to thank the provided financial support.

References

- Altamimi, Z., Collilieux, X., Legrand, B., Garayt, B., Boucher, C., 2007. ITRF2005: a new release of the international terrestrial reference frame based on time series of position stations and Earth orientation parameters. *J. Geophys. Res.* 112 (B9), 401–409. <http://dx.doi.org/10.1029/2007JB004949>.
- Altamimi, Z., Collilieux, X., Métivier, L., 2011. ITRF2008: an improved solution of the international terrestrial reference frame. *J. Geod.* 85 (8), 457–473. <http://dx.doi.org/10.1007/s00190-011-0444-4>.
- Bertiger, W., Desai, S.D., Haines, B., Harvey, N., Moore, A.W., Owen, S., Weiss, J.P., 2010a. Single receiver phase ambiguity resolution with GPS data. *J. Geod.* 84 (5), 327–337. <http://dx.doi.org/10.1007/s00190-010-0371-9>.
- Bertiger, W., Desai, S.D., Dorsey, A., Haines, B., Harvey, N., Kuang, D., Sibthorpe, A., Weiss, J., 2010b. Sub-centimeter precision orbit determination with GPS for ocean altimetry. *Mar. Geod.* 33 (1), 363–378.
- Carlson, J.M., Doyle, J., 2002. Complexity and robustness. *Proc. Natl. Acad. Sci.* 99 (1), 2538–2545.
- Dach, R., Hugentobler, U., Fridez, P., Meindl, M., 2007. Bernese GPS Software Version 5.0. Astronomical Institute, University of Bern.
- Dach, R., Brockmann, E., Schaer, S., Beutler, G., Meindl, M., Prange, L., Bock, H., Jäggi, A., Ostini, L., 2009. GNSS processing at CODE: status report. *J. Geod.* 83 (3–4), 353–365. <http://dx.doi.org/10.1007/s00190-008-0281-2>.
- Dai, L., Eslinger, D., Sharpe, T., 2007. Innovative algorithms to improve long range RTK reliability and availability. In: *Proceedings of ION NTM*, pp 860–872.
- Friis-Christensen, E., Lühr, H., Knudsen, D., Haagmans, R., 2008. Swarm – an Earth observation mission investigating Geospace. *Adv. Space Res.* 41 (1), 210–216. <http://dx.doi.org/10.1016/j.asr.2006.10.008>.
- European Space Agency – Earth Online, 2015. Swarm data access. <<https://earth.esa.int/web/guest/swarm/data-access/>>, last accessed Aug 2015.
- Gill, E., 1996. Smooth Bi-polynomial Interpolation of Jacchia 1971 Atmospheric Densities for Efficient Satellite Drag Computation. DLR-GSOC IB 96-1. Deutsches Zentrum für Luft und Raumfahrt, Oberpfaffenhofen, Germany.
- Haines, B., Bar-Sever, Y., Bertiger, W., Desai, S., Willis, P., 2004. One-centimeter orbit determination for Jason-1: new GPS-based strategies. *Mar. Geod.* 27 (1–2), 299–318.
- Hou, Y., Verhagen, S., 2014. Model and data driven partial ambiguity resolution for multi-constellation GNSS. In: *Proceedings of the China Satellite Navigation Conference (CSNC)*, Vol. 2. In: *Lecture Notes in Electrical Engineering*, Vol. 304, pp 285–302.
- Jäggi, A., Hugentobler, U., Bock, H., Beutler, G., 2007. Precise orbit determination for GRACE using undifferenced or doubly differenced GPS data. *Adv. Space Res.* 39 (10), 1612–1619. <http://dx.doi.org/10.1016/j.asr.2007.03.012>.
- Jäggi, A., Dach, R., Montenbruck, O., Hugentobler, U., Bock, H., Beutler, G., 2009. Phase center modeling for LEO GPS receiver antennas and its impact on precise orbit determination. *J. Geod.* 83, 1145–1162. <http://dx.doi.org/10.1007/s00190-009-0333-2>.
- Jäggi, A., Montenbruck, O., Moon, Y., Wermuth, M., König, R., Michalak, G., Bock, H., Bodenmann, D., 2012. Inter-agency comparison of TanDEM-X baseline solutions. *Adv. Space Res.* 50 (2), 260–271. <http://dx.doi.org/10.1016/j.asr.2012.03.027>.
- Jäggi, A., Dahle, C., Arnold, D., Meyer, U., Bock, H., 2014. Kinematic space-baselines and their use for gravity field recovery. Presented at the 40th COSPAR Scientific Assembly, Moscow, Russia.
- Jaynes, E.T., Bretthorst, G.L., 2003. *Probability Theory: The Logic of Science*, first ed. Cambridge University Press.
- Kihara, M., Okada, T., 1984. A satellite selection method and accuracy for the global positioning system. *Navigation: J. Inst. Navig.* 31 (1), 8–20.
- Krieger, G., Hajnsek, I., Papathanassiou, K.P., Younis, M., Moreira, A., 2010. Interferometric synthetic aperture radar (SAR) missions employing formation flying. *Proc. IEEE* 98 (5), 816–843.
- Kroes, R., Montenbruck, O., Bertiger, W., Visser, P., 2005. Precise GRACE baseline determination using GPS. *GPS Solutions* 9, 21–31.
- Kroes, R., 2006. *Precise Relative Positioning of Formation Flying Spacecraft Using GPS* (Ph.D. Thesis). TU Delft.
- Li, J., Ndili, A., Ward, L., Buchman, S., 1999. GPS receiver satellite/antenna selection algorithm for the stanford gravity probe B relativity mission. In: *Proceedings of the ION National Technical Meeting*, pp 541–550.
- McCarthy, D.D., 1996. *IERS Conventions, 1996*. IERS Technical Note 21. Central Bureau of IERS, Observatoire de Paris, Paris.
- Misra, P., Enge, P., 2006. *Global Positioning System: Signals, Measurements, and Performance*. Ganga-Jamuna Press, Lincoln, MA.
- Montenbruck, O., Kroes, R., 2003. In-flight performance analysis of the CHAMP BlackJack GPS receiver. *GPS Solutions* 7 (2), 74–86. <http://dx.doi.org/10.1007/s10291-003-0055-5>.
- Montenbruck, O., van Helleputte, T., Kroes, R., Gill, E., 2005. Reduced dynamic orbit determination using GPS code and carrier measurements. *Aerosp. Sci. Technol.* 9 (3), 261–271. <http://dx.doi.org/10.1016/j.ast.2005.01.003>.
- Montenbruck, O., Gill, E., 2005. *Satellite Orbits*. Springer-Verlag, Heidelberg.
- Montenbruck, O., Garcia-Fernandez, M., Williams, J., 2006. Performance comparison of semi-codeless GPS receivers for LEO satellites. *GPS Solutions* 10 (4), 249–261. <http://dx.doi.org/10.1007/s10291-006-0025-9>.
- Montenbruck, O., Kahle, R., D’Amico, S., Ardaens, J.S., 2008. Navigation and control of the TanDEM-X formation. *J. Astronaut. Sci.* 56 (3), 341–357.
- Montenbruck, O., Ramos-Bosch, P., 2008. Precision real-time navigation of LEO satellites using global positioning system measurements. *GPS Solutions* 12 (3), 187–198. <http://dx.doi.org/10.1007/s10291-007-0080-x>.
- Montenbruck, O., Garcia-Fernandez, M., Yoon, Y., Schön, S., Jäggi, A., 2009. Antenna phase center calibration for precise positioning of LEO satellites. *GPS Solutions* 13, 23–34. <http://dx.doi.org/10.1007/s10291-008-0094-z>.
- Montenbruck, O., Wermuth, M., Kahle, R., 2011–2012. GPS based relative navigation for the TanDEM-X mission – first flight results. *Navigation: J. Inst. Navig.* 58 (4), 293–304.
- Park, C.W., 2001. *Precise Relative Navigation Using Augmented CDGPS* (Ph.D. Thesis), Stanford University.
- PODAAC, 2015. *Physical Oceanography Distributed Active Archive Center – Gravity Recovery and Climate Experiment*, <<ftp://podaac.jpl.nasa.gov/allData/grace/>>, last accessed March 2015.

- Psiaki, M.L., Mohiuddin, S., 2007. Modeling, analysis, and simulation of GPS carrier phase for spacecraft relative navigation. *J. Guid. Control Dyn.* 30 (6), 1628–1639.
- Richert, T., El-Sheimy, N., 2005. Ionospheric modeling – The Key to GNSS Ambiguity Resolution. *GPS World*, pp. 35–40.
- Rothacher, M., Schaer, S., Mervart, L., Beutler, G., 1995. Determination of antenna phase center variations using GPS data. In: *Proceedings of IGS Workshop*. GeoForschungsZentrum Postdam, pp. 205–220. Rothacher, M., Schmid, R., 2006. ANTEX: The antenna exchange formation version 1.3.
- Shampine, L.F., Gordon, M.K., 1975. *Computer Solution of Ordinary Differential Equations*. Freeman, San Francisco, CA.
- Stone, James V., 2013. *Bayes' Rule: A Tutorial Introduction to Bayesian Analysis*. Sebtel Press.
- Sust, M., Zangerl, F., Montenbruck, O., Buchert, S., Garcia-Rodriguez, A., 2014. Spaceborne GNSS-receiving system performance prediction and validation. In: *NAVITEC: ESA Workshop on Satellite Navigation Technologies and GNSS Signals and Signal Processing*.
- Švehla, D., Rothacher, M., 2004. CHAMP and GRACE in Tandem: POD with GPS and K-band measurements. Presented at the Joint CHAMP/ GRACE Science Meeting, Postdam, Germany.
- Tancredi, U., Renga, A., Grassi, M., 2011. Ionospheric path delay models for spaceborne GPS receivers flying in formation with large baselines. *Adv. Space Res.* 48 (3), 507–520. <http://dx.doi.org/10.1016/j.asr.2011.03.041>.
- Tancredi, U., Renga, A., Grassi, M., 2013. Validation on flight data of a closed-loop approach for GPS-based relative navigation of LEO satellites. *Acta Astronaut.* 86, 126–135.
- Tancredi, U., Allende-Alba, G., Renga, A., Montenbruck, O., Grassi, M., 2015. Relative positioning of spacecraft in intense ionospheric conditions by GPS. *Aerosp. Sci. Technol.* 43, 191–198. <http://dx.doi.org/10.1016/j.ast.2015.02.020>.
- Tapley, B.D., Chambers, D.P., Bettandur, S., Ries, J.C., 2003. Large scale ocean circulation from the GRACE GGM01 geoid. *Geophys. Res. Lett.* 30 (22), 2163. <http://dx.doi.org/10.1029/2003GL018622>.
- Tapley, B.D., Bettadpur, S., Watkins, M., Reigber, C., 2004. The gravity recovery and climate experiment: mission overview and early results. *Geophys. Res. Lett.* 31 (9). <http://dx.doi.org/10.1029/2004GL019920>.
- Teunissen, P.J.G., 1995. The least-squares ambiguity decorrelation adjustment: a method for fast GPS ambiguity resolution. *J. Geod.* 70 (1–2), 65–82.
- Teunissen, P.J.G., 1997. On the GPS widelane and its decorrelating property. *J. Geod.* 71 (9), 577–587.
- Teunissen, P.J.G., 1999. An optimality property of the integer least-squares estimator. *J. Geod.* 73 (11), 587–593.
- Teunissen, P.J.G., 2003. Integer aperture GNSS ambiguity resolution. *Artif. Satell. J. Planet. Geod.* 38 (3), 79–88.
- Teunissen, P.J.G., Verhagen, S., 2009. The GNSS ambiguity ratio-test revisited: a better way of using it. *Surv. Rev.* 41 (312), 138–151.
- Tiberius, C., Jonker, N., Kenselaar, F., 1999. *The Stochastics of GPS Observables*. *GPS World*, pp. 49–54.
- UT/CSR ocean tide models, 2001. University of Texas, Center for Space Research, Austin, Texas. <http://ftp.csr.utexas.edu/pub/grav/OTIDES.TOPEX3.0>.
- van Barneveld, P.W.L., Montenbruck, O., Visser, P.N.A.M., 2009. Epochwise prediction of GPS single differenced ionospheric delays of formation flying spacecraft. *Adv. Space Res.* 44 (9), 987–1001. <http://dx.doi.org/10.1016/j.asr.2009.07.006>.
- Verhagen, S., 2004. *The GNSS Integer Ambiguities: Estimation and Validation (Ph.D. Thesis)*, TU Delft.
- Verhagen, S., Teunissen, P.J.G., Van der Marel, H., Li, B., 2011. GNSS ambiguity resolution: which subset to fix?. In: *Proceedings of International Global Navigation Satellite Systems Society, IGNSS Symposium*, pp. 1–15.
- Verhagen, S., Li, B., 2012. *LAMBDA – Matlab Implementation, Version 3.0*. TU Delft and Curtin University.
- Verhagen, S., Teunissen, P.J.G., 2013. The ratio test for future GNSS ambiguity resolution. *GPS Solutions* 17, 535–548. <http://dx.doi.org/10.1007/s10291-012-0299-z>.
- Williams, J., Lightsey, E.G., Yoon, S.P., Schutz, R.E., 2002. Testing of the ICESat BlackJack GPS receiver engineering model. In: *Proceedings of the ION-GPS-2002*, pp. 703–714.
- Wu, S.C., Yunck, T.P., Thornton, C.L., 1991. Reduced-dynamic technique for precise orbit determination of low Earth satellites. *J. Guid. Control Dyn.* 14 (1), 24–31.

Appendix B

Publication 2

Reduced-dynamic and kinematic baseline determination for the Swarm mission

Gerardo Allende-Alba^{1,2}, Oliver Montenbruck², Adrian Jäggi³, Daniel Arnold³, Franz Zangerl⁴

¹*Institute for Astronomical and Physical Geodesy, Technische Universität München, 80333 München, Germany*

²*Deutsches Zentrum für Luft- und Raumfahrt (DLR), German Space Operations Center (GSOC), 82234 Weßling, Germany*

³*Astronomical Institute, Universität Bern, 3012 Bern, Switzerland*

⁴*RUAG Space GmbH, 1120 Vienna, Austria*

Abstract

The Swarm mission of the European Space Agency was launched in November 2013 with the objective of performing measurements of the earth's magnetic field with unprecedented accuracy. At the beginning of data collection, two satellites started to fly in orbits with a separation in ascending nodes of 1° – 1.5° at an altitude of about 480 km, and a third satellite has been placed in a higher orbit with an altitude of 530 km. The three spacecraft are equipped with dual-frequency eight-channel GPS receivers for the generation of precise orbits. Although such orbits support the fulfillment of the primary objectives of the mission, precise space baselines may be helpful for studying the earth's gravity field, a spin-off application of the Swarm mission. Hitherto, a particular challenge for the computation of precise baselines from Swarm has been the presence of half-cycle ambiguities in GPS carrier phase observations, which complicate the implementation of integer ambiguity resolution methods. The present study shows the feasibility of generating carrier phase observations with full-cycle ambiguities, which in turn has been used to improve the performance of reduced-dynamic and kinematic precise baseline determination schemes. The implemented strategies have been tested in a period of 90 days in 2016. The obtained reduced-dynamic and kinematic baseline products were evaluated by inter-product and inter-agency comparisons using two independent software tools.

Keywords: Swarm; Space baseline determination; Half-cycle ambiguity resolution; GPS

Introduction

The ESA's Swarm mission was successfully launched on November 22, 2013, with the fundamental goal of performing measurements with unprecedented accuracy for the study of earth's magnetic field (Friis-Christensen et al. 2006, 2008). The mission comprises three spacecraft called the Earth's Magnetic Field and Environment Explorers, commonly referred to as Swarm satellites A, B and C. The initial orbit configuration for data collection consists of two spacecraft with east–west separation of 1° – 1.5° and at altitude of about 480 km and a third spacecraft at altitude of about 530 km. Starting from April 2014, the Swarm A and Swarm C were placed in the lower orbits, whereas Swarm B was left in the upper orbit (Mackenzie et al. 2014).

As a spin-off application of the Swarm constellation, data derived from the GPS receivers onboard the

spacecraft can be used for the generation of geodetic products using high–low satellite-to-satellite (hl-SST) data (Gerlach and Visser 2006). Further studies have effectively demonstrated the feasibility of using GPS data from each Swarm spacecraft for earth's gravity field determination (Jäggi et al. (2016); Teixeira da Encarnação et al. (2016) and references within). In this way, the Swarm mission will allow continued monitoring of the earth system for gravity field determination during an intermission gap between of the GRACE mission (Tapley et al. 2004) and the GRACE Follow-On mission, which is expected to be launched after August 2017 (Flechtner et al. 2014).

Unlike some past hl-SST missions (CHAMP, Reigber et al. 2002), the Swarm constellation offers, in addition, the possibility of baseline reconstruction, i.e., low–low satellite-to-satellite or ll-SST data. Such data can provide added information for the refinement of

gravity models. Simulation-based studies have suggested that the use of single-satellite orbits in combination with baseline products can be used for the determination of the static field, offering an improved precision with respect to single-satellite-only solutions (Wang and Rummel 2012). Nevertheless, an in-depth analysis remains to be carried out, as pointed out by Jäggi et al. (2009a), exploring the actual potential benefit of precise kinematic baselines using real data for gravity field determination, now in particular for the Swarm mission.

The key for precise baseline determination (PBD) is the use of carrier phase measurements with fixed integer ambiguities. However, unlike other geodetic-class GPS receivers used in previous formation flying missions, such as GRACE and TanDEM-X (Krieger et al. 2010), the GPS receivers in the Swarm spacecraft generate carrier phase measurements also at half cycles in their default configuration. This fact necessitates the consideration of half-cycle ambiguities in the observation models, which complicates the implementation of integer ambiguity resolution (IAR) strategies. Jäggi et al. (2014) showed first the feasibility of computing precise baselines of Swarm A and Swarm C using fixed ambiguities based on the wide-lane/narrow-lane (WL/NL) approach, as described by Jäggi et al. (2007). Allende-Alba and Montenbruck (2016) and Mao et al. (2016) proposed tailored algorithms for ambiguity resolution on L1 and L2 for coping with the presence of half-cycle ambiguities. A further analysis performed by Jäggi et al. (2016) confirmed the possibility of ambiguity fixing and precise baseline reconstruction, and its possible use for gravity field determination.

Although the described algorithms have demonstrated that IAR can be performed even in the presence of half-cycle ambiguities, the lack of integer ambiguities influences the overall complexity of the algorithms and the capability of a successfully fixing. The present study introduces an alternative strategy to resolve the half-cycle ambiguity during the process of generation of carrier phase observations from raw GPS data. Therefore, the generated observations are guaranteed to have integer-valued double-difference ambiguities, which allow executing IAR schemes without further special considerations or assumptions.

We start with a brief description of the GPS receivers on board the Swarm spacecraft and the process of half-cycle ambiguity resolution during the generation of carrier phase observations. Subsequently, the description is focused on the strategies for IAR and space baseline determination used in the present study, followed by a discussion of results obtained from actual flight data.

GPS receivers and carrier phase observations

For the generation of precise orbit determination (POD) products, each Swarm spacecraft is equipped with a high-end geodetic-type dual-frequency GPS re-

ceiver (called GPSR), manufactured by RUAG Space (Zangerl et al. 2014). The variant of the GPSR receiver onboard the Swarm spacecraft has eight channels and delivers dual-frequency measurements for the legacy signals. During the first months of operation, the three GPSR receivers provided measurements at a rate of 0.1 Hz, which was enough for the generation of POD products, also called precise science orbits (PSOs, van den IJssel et al. 2015). During this period, baseline determination was not possible due to lacking synchronization of the measurement epochs across the different spacecraft. However, on July 15, 2014, the receiver configuration was modified, and the observation-delivery rate changed to 1 Hz (Jäggi et al. 2014), hence offering the possibility of baseline reconstruction.

Signal tracking concepts

The GPSR instrument is based on the space-hardened AGGA-2 (Advanced GPS/GLONASS ASIC) correlator chip, which has been developed in an initiative of the European Space Agency (ESA). It is specifically designed to support semi-codeless tracking of the encrypted P(Y) signal on the L1 and L2 frequencies along with the direct tracking of the L1 C/A code. AGGA-2-based GPS receivers for radio occultation observations and POD have previously been flown on Metop (Silvestrin et al. 2000; Montenbruck et al. 2008), GOCE (Zin et al. 2006; Bock et al. 2011) as well as various other international missions. With a total of two AGGA-2 chips, the Swarm GPSR supports concurrent tracking of L1 C/A, L1 P(Y) and L2 P(Y) for up to eight satellites.

Following the philosophy of the Metop radio occultation receiver, the GPSR does not directly output pseudorange and carrier phase observations as expected in common GPS processing techniques. Instead, the receiver provides a lower-level data set more closely related to the actual tracking process in the receiver. Among others, this includes the code phase as well as the phase of the numerically controlled oscillator (NCO) that is used to remove the residual Doppler shift from the down-converted signal. Traditional pseudorange and carrier phase observations are only generated after data processing on ground. This concept offers a substantially larger flexibility and transparency in the measurement generation, albeit at the expense of a higher operational effort in the ground segment. Among others, different types of receiver time scales can more easily be realized in this approach. A timescale aligned with the estimate of the GPS time determined within the receiver as part of the navigation solution has been used in the present study.

For tracking of the binary phase shift keying (BPSK) modulated L1 C/A signal, a Costas loop with a twoquadrant phase discriminator (Betz 2016) is employed to make the carrier phase tracking independent of the unknown navigation data bits. Depending on the value of the data bit at the start of tracking, the

reported NCO phase and the derived carrier phase observation may thus be affected by a constant 180° phase offset over the entire tracking arc. When forming double differences of L1 phase observations across individual tracking channels, half-cycle ambiguities will thus arise. These are of little concern for the POD but detrimental for carrier phase differential GPS navigation.

For tracking the encrypted P(Y) signal, the Swarm GPSR makes use a patented semi-codeless technique (Silvestrin and Cooper 2000) that resembles the well-known Z-tracking (Woo 2000) but uses an improved decision process for estimating the unknown W-bit as well as different assumption for the W-bit duration. The down-converted L1 and L2 signals are first mixed with the output of distinct L1 and L2 NCOs, then correlated with a P-code replica and subsequently integrated over the assumed duration of a W-bit (22 P-code chips). Subject to a positive decision on the W-bit sign, the estimated L1 W-bit is then used to demodulate the P(Y)-code on L2 and vice versa. The W-bit estimation and stripping induces no sign ambiguity and, in principle, enables recovery of the full L2 carrier phase using a four-quadrant discriminator. On the other hand, the processing makes use of the known L1 NCO phase from the L1 C/A code tracking. The L1 half-cycle ambiguities will thus be inherited to the L2 measurements, while the difference of L1 and L2 NCO phases is ensured to be of integer nature. This is consistent with the empirical observation of half-cycle ambiguities in both L1 and L2 phase measurements reported in Allende-Alba and Montenbruck (2016), while WL ambiguities were always found to be integer valued.

The 180° phase shift in the L1 carrier replica that may be caused by the use of a Costas loop results in an associated inversion of the data bits, which can be detected from an inverted preamble (0111010011 instead of 1000101100) and subsequently be used to invert the decoded data stream. Making use of information on the observed sign of the preamble as reported in the raw receiver telemetry, it is possible to correct the reported L1 and L2 NCO phase by 0.5 cycles before forming the carrier phase observations whenever the preamble is inverted. A corresponding modification of the GPSR preprocessing has been developed for this study and used to obtain observation data with full-cycle ambiguities.

Impact of ionospheric scintillation

Starting from the first assessments of GPS data from the Swarm mission, it was possible to observe the impact of ionospheric scintillation on carrier phase observations, whose effects were mostly noticed in polar regions (Sust et al. 2014; Zangerl et al. 2014). Ionospheric scintillation is caused by irregularities in the ionosphere and affects GPS carrier phase observations mainly as diffraction and refraction, originated from the group delay and phase advance as the GPS signal interacts with free electrons along the transmission

path (Kintner et al. 2007). It can be considered a form of space-based multipath (Kintner and Ledvina 2005). Further analyses also revealed a performance degradation of the GPS receivers at the equatorial region (Buchert et al. 2015; Xiong et al. 2016).

The temporal and regional dependence of scintillation intensity and its impact on PSOs for Swarm has been extensively analyzed by van den IJssel et al. (2015) and van den IJssel et al. (2016). In comparison with previous analyses, data processed for this study benefit from an improved robustness of the Swarm receivers stemming from the modifications on the carrier tracking loops parameters performed during 2015.

Strategies for space baseline determination

For the first part of this study, precise baselines have been computed using the DLR's GPS High-precision Orbit Determination Software Tools (GHOST; Montenbruck et al. 2005). The reduced-dynamic approach (Yunck et al. 1990; Wu et al. 1991) is applied for POD and PBD schemes, making use of highly precise dynamical models for orbit integration (Montenbruck et al. 2005). Carrier phase integer ambiguities are resolved using a dedicated algorithm based on a batch/sequential estimation of float ambiguities using a priori information from previously computed POD solutions. Subsequently, the solved integer ambiguities are introduced as known parameters into reduced-dynamic and kinematic baseline determination schemes using single-difference ionosphere-free (IF) observation models. Reduced-dynamic baselines are determined with an extended Kalman filter/smoothing. Kinematic solutions are computed using only carrier phase observations with fixed ambiguities (Allende-Alba and Montenbruck 2016). Estimated differential phase variation (PV) maps have been used in the computation of both reduced-dynamic and kinematic baselines. Precise GPS clocks and orbit products have been obtained from the Center for Orbit Determination in Europe (CODE, Dach et al. 2016).

The orbital motion of the Swarm A and Swarm C spacecraft creates a baseline of variable dimension with maximum cross-track separation at the equator of about 160 km (Sieg and Diekmann 2016). This type of long baseline represents a challenging situation for IAR, and consequently for PBD, due to the presence of large ionospheric delays in GPS observations. For the assessment of PBD solutions and the performance of algorithms under such conditions, the present study makes use of a series of inter-product comparisons with solutions from GHOST. Additionally, an inter-agency assessment has been carried out using solutions from the Bernese GNSS Software (BSW, Dach et al. 2015) from the Astronomical Institute of the University of Bern (AIUB).

Results and discussion

PBD solutions have been computed for 90 days of data comprising the period of January to March, 2016. Days January 1 and March 3 have been excluded from the analysis due to the presence of large data gaps or maneuvers. On January 26, roughly half a day of data was not considered in the analysis as a result of anomalous UTC-offset values transmitted by the GPS space segment on that day (Kovach et al. 2016).

Integer ambiguity fixing performance

A major aim of this study is to analyze the performance of IAR algorithms when half-cycle ambiguities are resolved during the generation of carrier phase observations. As an example, Fig. 1 shows the level of improvement on float ambiguity estimation. The plot depicts the frequency distribution of mapped L1 and L2 float ambiguities into the interval $[0.5, 1.5]$ on March 20. As observed, float ambiguity estimates are normally distributed around an integer value. For comparison, a bimodal distribution with peaks at full and half cycles results when processing observations with half-cycle ambiguities. Depending on the observation noise, the distribution modes may, however, be difficult to discern. An almost uniform distribution has in fact been obtained in Allende-Alba and Montenbruck (2016) with such observations.

The representative frequency distribution shown in Fig. 1 provides a rough indication about the expected performance of the IAR scheme: approximately 95% of float ambiguity estimates deviate by less than 0.3 cycles from an integer value and can be fixed with good confidence. Figure 2 shows the integer ambiguity fixing performance for the complete period under analysis. On average, 94% of ambiguities were fixed and used for the computation of reduced-dynamic and kinematic baselines. This value represents an improvement with respect to previous analyses with Swarm data (Jäggi et al. 2014, Allende-Alba and Montenbruck 2016, Mao et al. 2016), where values of 88–89% are reported considering carrier phase observations with half-cycle ambiguities.

Reduced-dynamic baselines

An effective assessment of reduced-dynamic baselines is a non-trivial task due to the lack of a reference of any sort. An initial hint of the baseline quality can be obtained by analyzing the goodness-of-fit of modeled and observed carrier phase measurements using post-fit residuals. Figure 3 depicts the frequency distribution of RMS errors of single-difference carrier phase IF residuals from daily baseline solutions, which provide an indication of the effective receiver carrier phase tracking error levels. As observed, most IF residuals exhibit RMS errors at the level of 3.8–4.1 mm, implying error levels of 1.2–1.3 mm of single-difference observations on individual frequencies.

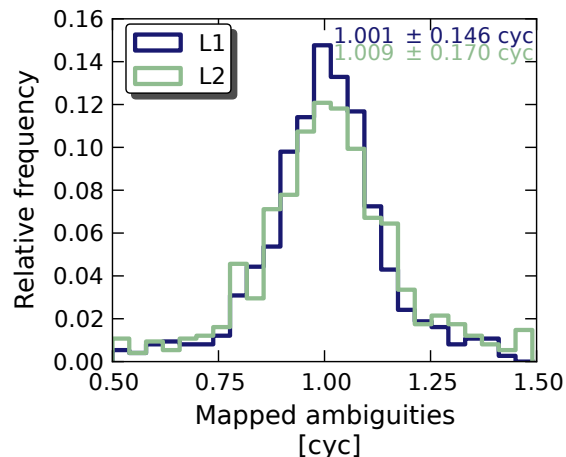


Fig. 1 Frequency distribution of estimated float L1 and L2 ambiguities, mapped into the interval $[0.5, 1.5]$, on March 20, 2016

An external assessment of PBD solutions can be performed by an analysis of satellite laser ranging (SLR, Pearlman et al. 2002) residuals. Such an evaluation provides a tool for a qualitative analysis of the improvement of PBD solutions with respect to their POD counterpart. Figure 4 shows the SLR residuals of normal points from station Yarragadee, Australia, on February 3 and February 26, 2016, using trajectories from POD and PBD solutions. The SLR station tracks in an alternating way each spacecraft as they pass by the station location. Swarm A's trajectory is used as reference for the computation of PBD solutions, and hence, the residuals are the same for both comparisons. In PBD, the relative trajectory of Swarm C with respect to Swarm A is well constrained by differential pseudorange and carrier phase observations. As seen in Fig. 4 (top), SLR residuals of trajectories from POD solutions appear to be unconnected as they are computed independently. In contrast, Swarm C's trajectory from PBD solutions is more tightly constrained to Swarm A's, as evidenced by the better consistency of SLR residuals for the two spacecraft in Fig. 4 (bottom). Obviously, however, SLR measurement and modeling errors are too large to

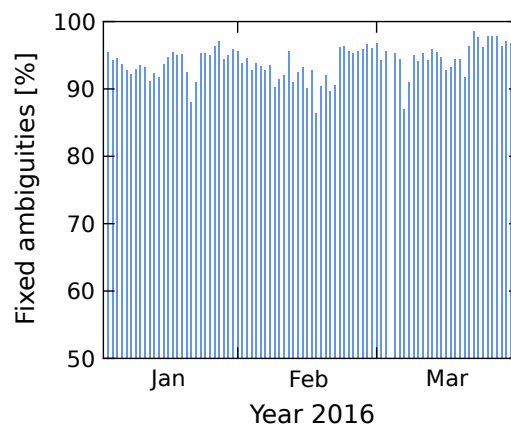


Fig. 2 Carrier phase integer ambiguity fixing performance

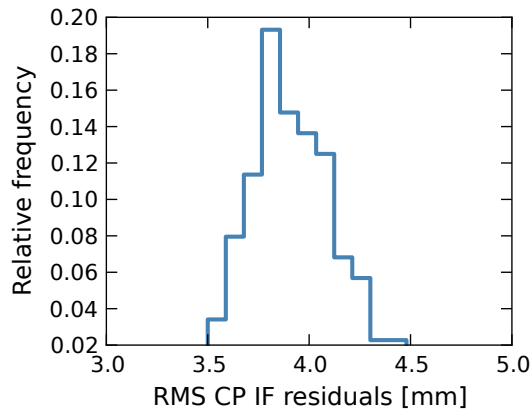


Fig. 3 Frequency distribution of daily RMS error of single-difference carrier phase ionosphere-free (CP IF) residuals from reduced-dynamic baseline determination

allow a quantitative assessment of the baseline accuracy at the mm level.

A further evaluation of PBD solutions can be obtained in an inter-product assessment using differential POD (dPOD) solutions, i.e., the difference of individual POD solutions from each spacecraft. This assessment is useful to establish a coarse quality check of baseline products. Figure 5 depicts the comparison of daily dPOD and PBD solutions for the entire period under analysis. On average, RMS errors of 3.3, 7.4 and 4.9 mm could be achieved in the radial, along-track and cross-track directions, respectively. The values obtained are in good accord with similar dPODPBD assessments for other formation flying missions such as GRACE (Kroes 2006) and TanDEM-X (Montenbruck et al. 2011).

Kinematic baselines

The overall quality of kinematic baselines can be evaluated in comparison with reduced-dynamic solutions. Kinematic solutions are more influenced by the quality of GPS observations and possible wrongly fixed ambiguities, than their reduced-dynamic counterpart. For this assessment, a simple threshold of 50 cm has been selected to discard outlier point solutions stemming from bad data points. The resulting reduction in average number of solutions has been less than 1 difference between kinematic and reduced-dynamic baseline components. This assessment mainly depicts the effect of the observation geometry and GPS carrier phase effective receiver error levels on the resulting kinematic solutions. In general, there is no apparent variation in time during the period under analysis regarding measurement errors. On average, RMS errors of 18.36, 6.25 and 5.08 mm can be achieved in the radial, along-track and cross-track directions, respectively. In comparison with baseline analyses with data from 2014 (see Jäggi et al. (2014, 2016) and Allende-Alba and Montenbruck (2016)) the obtained error levels mainly suggest an improvement of the ambiguity fixing rate and the quality of carrier phase observations stemming from receiver configuration changes during 2015.

Aside from an analysis in time, an inspection of the spatial distribution of errors in kinematic solutions is useful to observe the geographical dependency of the impact of ionospheric scintillation on carrier phase observations and baseline solutions. Figure 7 shows the global distribution of bin-wise RMS errors of kinematic solutions in each baseline component. As observed, the quality of kinematic baselines is highly affected in the polar regions, particularly in the radial direction. Solutions over these regions dominate the RMS values

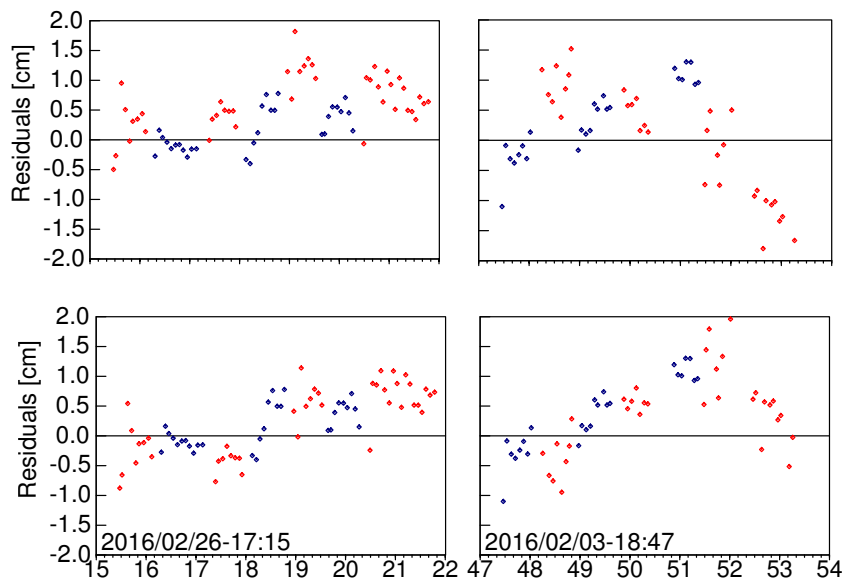


Fig. 4 SLR residuals of POD (top) and PBD (bottom) solutions of Swarm A (blue) and Swarm C (red) at station Yarragadee, Australia, on February 3 (right) and February 26 (left), 2016, as a function of time. The units are minutes

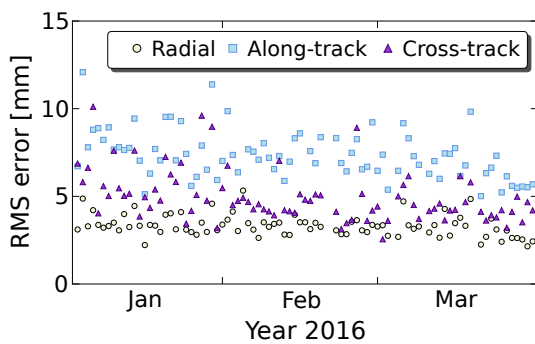


Fig. 5 Daily RMS errors of the difference between dPOD and PBD solutions

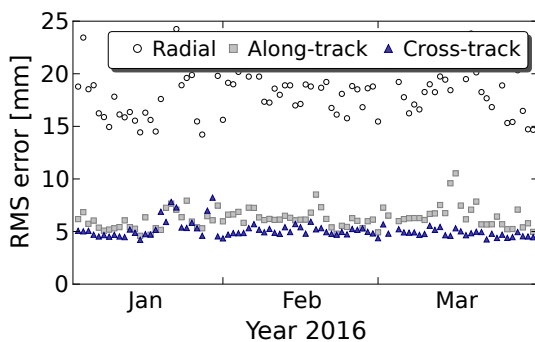


Fig. 6 Daily RMS errors of the differences between kinematic and reduced-dynamic baselines

derived from Fig. 6. For the radial component, the average RMS errors in the polar regions exceed those in midlatitude regions by a factor of about 2.5, whereas the vertical dilution of precision (VDOP) is, on average, only larger by 0.8. This suggests that the observed solution degradation on latitudes higher than $\pm 60^\circ$ is mostly caused by increased effective observation error levels due to ionospheric scintillation. Noticeable is the absence of large error signatures that have been observed along the (magnetic) equatorial region in previous POD studies during 2014 (van den IJssel et al. 2015). Although the occurrence and intensity of ionospheric scintillations have a strong dependency on geomagnetic and solar activity, part of the improvement of kinematic solutions may also be attributed to the widening of GPSR carrier tracking loop bandwidths during 2015; see van den IJssel et al. (2016) for a POD analysis in 2015.

Impact of half-cycle ambiguities

When half-cycle ambiguities are present in carrier phase observations, POD solutions are virtually not affected, with changes at the 0.1 mm level in dPOD solutions. However, baseline solutions from standard IAR/PBD schemes may be degraded if no adaptation or tailoring strategies are applied. A comparison of baseline solutions using different approaches can be

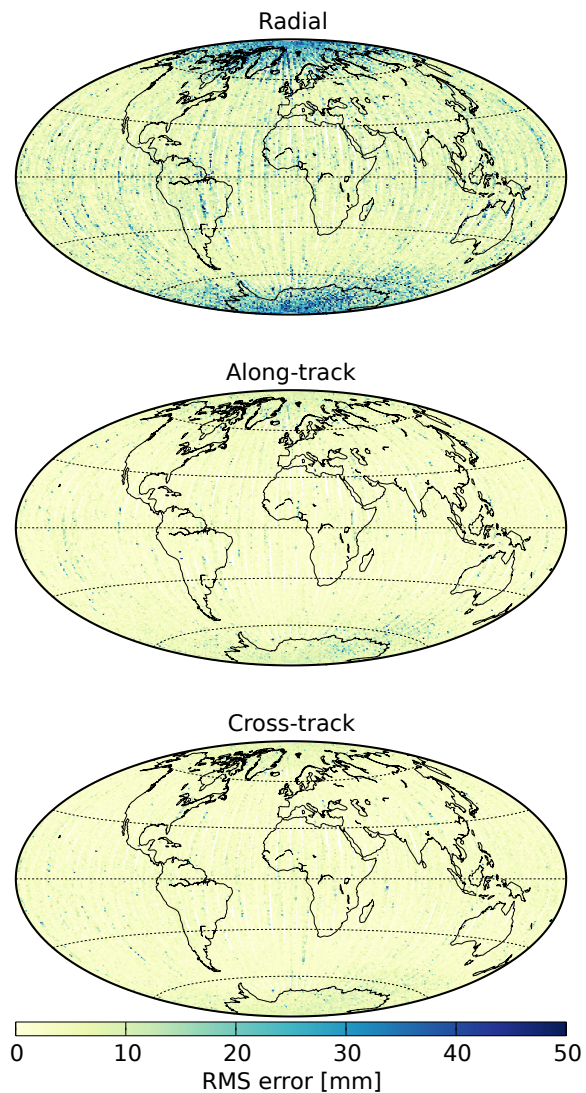


Fig. 7 Global distribution of RMS errors of the differences between kinematic and reduced-dynamic baselines. Swarm A's trajectory has been used for spatial mapping of errors

evaluated to observe the impact of half-cycle ambiguities in PBD. For this test, kinematic baselines are computed using all available carrier phase observations with float and fixed ambiguities. Reduced-dynamic baseline solutions are used as reference for assessment.

If half-cycle ambiguities are not resolved during preprocessing of GPSR data, the PBD algorithm has to cope with carrier phase observations with the same statistical distribution of half- and full-cycle ambiguities. Figure 8 (top and middle) shows an example assessment of kinematic baselines in the along-track direction on February 29. The solutions are computed using the methods developed in Allende-Alba and Montenbruck (2016), denoted as "half-cycle" and "mixed-cycle" IAR schemes. As observed, by taking into account such adaptation techniques, it is possible to obtain baselines with reasonable quality, at the expense of an increased complexity in the processing algorithms. During this

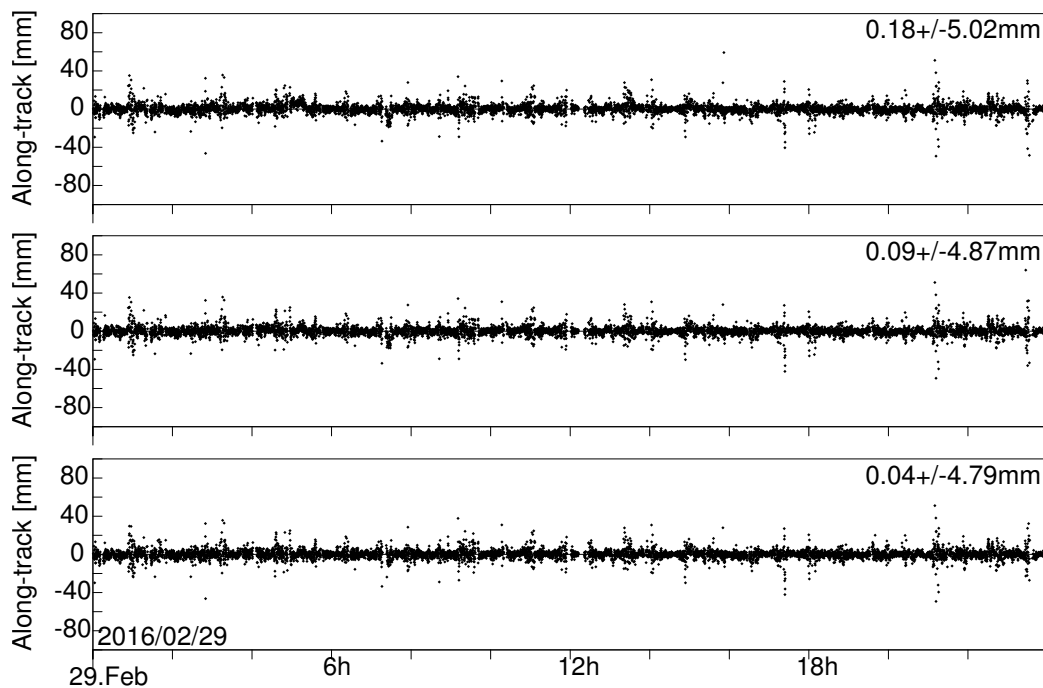


Fig. 8 Assessment of kinematic baselines on February 29. Solutions shown in *top* and *middle* plots have been computed using uncorrected (with half-cycle ambiguities) observation files, employing the "half-cycle" and "mixed-cycle" IAR approaches, respectively. The solution shown in the *bottom plot* has been computed using carrier phase observations with full-cycle ambiguities only

day, the obtained ambiguity fixing rates for each scheme are 92 and 95%, respectively. Figure 8 (bottom) shows the corresponding assessment of a solution computed using carrier phase observations with full-cycle ambiguities only. The achieved ambiguity fixing rate with this approach is of 97%.

Apart from a slight overall improvement of kinematic solutions provided by carrier phase observations with full-cycle ambiguities, a further benefit lies in the performance of IAR/PBD algorithms. In particular, the scheme denoted as "mixed-cycle" IAR requires a $2\text{--}2.5 \times$ increase in processing time in comparison with an IAR processing of full-cycle ambiguities only. This suggests that the strategy presented in this study allows an overall improvement of the performance of standard IAR/PBD schemes and quality of baseline solutions without requiring any adaptation or special consideration in the processing algorithms.

Inter-agency baseline comparison

Baselines from the GHOST software have been further assessed using external and independent solutions computed using the BSW at AIUB. In BSW, reduced-dynamic and kinematic solutions are computed using a batch least-squares estimation scheme using double-difference IF GPS observations with fixed carrier phase integer ambiguities, resolved using the WL/NL approach. See Jäggi et al. (2007) for details.

The comparison of reduced-dynamic baselines is shown in Fig. 9. Table 1 depicts the resulting average values of the comparison. In this assessment, some hours during days 50, 51 and 79 have been excluded due to the presence of large data gaps. As observed in Fig. 9 (top), the biases among solutions are well confined below 1 mm, providing an indication of low systematic errors in the solutions. Additionally, regarding average standard deviation [Table 1; Fig. 9 (bottom)], the achieved consistency of solutions lies in the 1–2 mm range. In comparison with similar assessments using data from the GRACE and TanDEM-X missions (Jäggi et al. 2009b, 2012), reduced-dynamic baseline solutions from Swarm appear to be slightly degraded. This may be attributed mainly to both the larger carrier phase errors in the observations and the reduced number of available tracking channels in the GPSR instruments.

Similar to the assessment shown in Fig. 6, for the comparison of kinematic baselines from GHOST and BSW, a simple threshold has been used to discard outlier solutions. Figure 10 shows the resulting comparison. As in the case of reduced-dynamic solutions, most of the biases of kinematic baselines are below 1 mm [Fig. 10 (top)]. However, a relatively large average bias in the radial direction between both kinematic solution types is present (Table 1). The main cause for this is still under investigation. The consistency of solutions shown in Fig. 10 (bottom) is in good agreement with the values obtained in the inter-product assessment

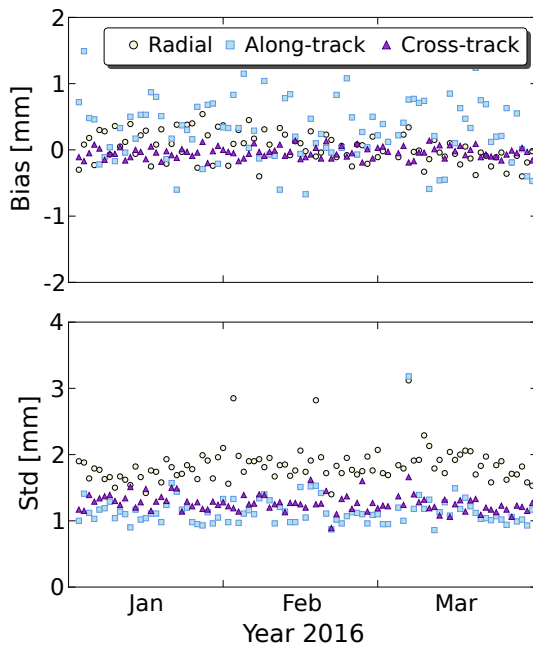


Fig. 9 Comparison of daily reduced-dynamic baseline solutions from GHOST and BSW

of GHOST solutions (Fig. 6). On average, standard deviations are obtained in the range of 5–6 mm for the horizontal components and around 17 mm in the radial direction, as shown in Table 1.

Conclusions

The present study has shown the feasibility of generating carrier phase observations with full-cycle ambiguities from the GPSR receivers onboard the Swarm spacecraft. The resulting observation files have helped to improve the performance of IAR, reduced-dynamic and kinematic baseline determination schemes. Precise baseline products have been computed using the GHOST software, and they have been assessed using inter-product and inter-agency comparisons. The results show an average integer ambiguity fixing rate of around 94%. A consistency of reduced-dynamic baselines and dPOD solutions of better than 1 cm (3D RMS) has been achieved. Average errors of kinematic baselines of around 5–6 and 18 mm have been achieved in the horizontal and vertical components, respectively. The inter-agency assessment using solutions from the AIUB's BSW shows a consistency of reduced-dynamic baselines at the level of 1–2 mm (3D RMS). Similarly, kinematic baselines are consistent at the 5 and 17 mm level in the horizontal and vertical components, respectively. Altogether, these results suggest the feasibility of generating precise reduced-dynamic and kinematic baselines for the Swarm mission, being of particular interest for applications on earth system monitoring and gravity field determination.

Table 1 Average values of reduced-dynamic and kinematic baseline comparison using solutions from GHOST and BSW

Component	Reduced-dynamic (mm)		Kinematic (mm)	
	Bias	Std	Bias	Std
Radial	0.03	1.83	0.53	17.17
Along-track	0.29	1.15	-0.32	5.83
Cross-track	-0.04	1.26	0.10	5.07

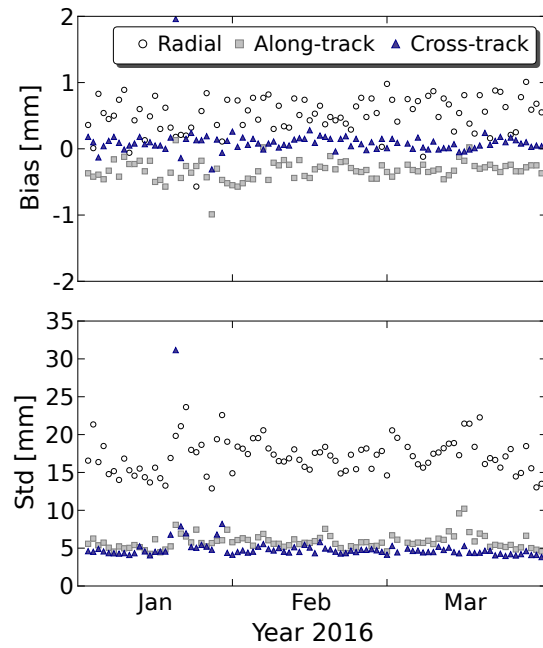


Fig. 10 Comparison of daily kinematic baseline solutions from GHOST and BSW

Acknowledgments

The present study uses data made available by the European Space Agency (ESA/ESTEC), Noordwijk, the Center for Orbit Determination in Europe (CODE) and the International Laser Ranging Service (ILRS). The support of these institutions is gratefully acknowledged. The authors acknowledge the reviewers for their valuable remarks that helped to improve the original manuscript. GAA wishes to thank the support provided by the Consejo Nacional de Ciencia y Tecnología de México, the Deutscher Akademischer Austauschdienst (Grant No. 213633 - A/10/72692) and the TU München Graduate School.

References

- Allende-Alba G, Montenbruck O (2016) Robust and precise baseline determination of distributed spacecraft in LEO. *Adv Space Res* 57(1):46–63. doi:10.1016/j.asr.2015.09.034.
- Betz J (2016) Engineering satellite-based navigation and timing— global navigation satellite systems, signals, and receivers. Wiley- IEEE Press, Hoboken.
- Bock H, Jäggi A, Meyer U, Visser P, van den IJssel J, van Helleputte T, Heinze M, Hugentobler U (2011) GPS-derived orbits for the GOCE satellite. *J Geodesy* 85(11):807–818.
- Buchert S, Zangerl F, Sust M, André M, Eriksson A, Wahlund JE, Opgenoorth H (2015) SWARM observations of equatorial electron densities and topside GPS track losses. *Geophys Res Lett* 42(7):2008–2092. doi:10.1002/2015GL063121.

- Dach R, Lutz S, Walser P, Fridez P (eds) (2015) Bernese GNSS Software version 5.2. User manual. Astronomical Institute, University of Bern, Bern Open Publishing. doi: 10.7892/boris.72297.
- Dach R, Schaer S, Arnold D, Orliac E, Prange L, Sušnik A, Villiger A, Jäggi A (2016) CODE final product series for the IGS. Published by Astronomical Institute, University of Bern. doi: 10.7892/boris.75876.
- Flechtner F, Morton P, Watkins P, Webb F (2014) Status of the GRACE Follow-on mission. In: Gravity, geoid and height systems, IAG symposia, vol. 141. pp 117–121. doi: 10.1007/978-3-319-10837-715.
- Friis-Christensen E, Lühr H, Hulot G (2006) Swarm: a constellation to study the Earth's magnetic field. *Earth Planets Space* 58(4):351–358. doi:10.1186/BF03351933.
- Friis-Christensen E, Lühr H, Knudsen D, Haagmans R (2008) Swarm—an earth observation mission investigating geospace. *Adv Space Res* 41(1):210–216. doi:10.1016/j.asr.2006.10.008.
- Gerlach C, Visser P (2006) SWARM and gravity: possibilities and expectations for gravity field recovery. In: Proceedings of the first international science meeting, SWARM, ESA WPP-261.
- Jäggi A, Hugentobler U, Bock H, Beutler G (2007) Precise orbit determination for GRACE using undifferenced or doubly differenced GPS data. *Adv Space Res* 39(10):1612–1619. doi:10.1016/j.asr.2007.03.012.
- Jäggi A, Beutler G, Prange L, Dach R (2009a) Assessment of GPS-only observables for gravity field recovery from GRACE. In: Sideris MG (ed) Observing our changing earth. IAG symposia, vol. 33. pp 113–123. doi: 10.1007/978-3-540-85426-514.
- Jäggi A, Dach R, Montenbruck O, Hugentobler U, Bock H, Beutler G (2009b) Phase center modeling for LEO GPS receiver antennas and its impact on precise orbit determination. *J Geodesy* 83:1145–1162. doi:10.1007/s00190-009-0333-2.
- Jäggi A, Montenbruck O, Moon Y, Wermuth M, König R, Michalak G, Bock H, Bodenmann D (2012) Inter-agency comparison of TanDEM-X baseline solutions. *Adv Space Res* 50(2):260–271. doi:10.1016/j.asr.2012.03.027.
- Jäggi A, Dahle C, Arnold D, Meyer U, Bock H (2014) Kinematic space-baselines and their use for gravity field recovery. Presented at the 40th COSPAR Scientific Assembly, Moscow, Russia, Aug 2014. doi: 10.7892/boris.58970.
- Jäggi A, Dahle C, Arnold D, Bock H, Meyer U, Beutler G, van den IJssel J (2016) Swarm kinematic orbits and gravity fields from 18 months of GPS data. *Adv Space Res* 57(1):218–233. doi:10.1016/j.asr.2015.10.035.
- Kintner PM, Ledvina BM (2005) The ionosphere, radio navigation, and global navigation satellite systems. *Adv Space Res* 35(5):788–811. doi:10.1016/j.asr.2004.12.076.
- Kintner PM, Ledvina BM, de Paula ER (2007) GPS and ionospheric scintillations. *Space Weather* 5:S09003.
- Kovach K, Mendicki PJ, Powers E, Renfro B (2016) GPS receiver impact from the UTC Offset (UTCO) Anomaly of 25–26 Jan 2016. In: Proceedings of ION GNSS?, Institute of Navigation, Portland, Oregon, Sept 12–13, pp 2887–2895.
- Krieger G, Hajnsek I, Papathanassiou KP, Younis M, Moreira A (2010) Interferometric synthetic aperture radar (SAR) missions employing formation flying. *Proc IEEE* 98(5):816–843.
- Kroes R (2006) Precise relative positioning of formation flying spacecraft using GPS. Ph.D. thesis, TU Delft.
- Mackenzie R, Bock R, Kuijper D, Ramos-Bosch P, Sieg D, Ziegler G (2014) A review of Swarm flight dynamics operations from launch to routine phase. In: Proceedings of the 24th international symposium on space flight dynamics, May 2014.
- Mao X, Visser P (2016) Swarm absolute and relative orbit determination. Presented at: living planet symposium, ESA SP-740, May 2016. http://lps16.esa.int/posterfiles/paper1458/ID1458_Mao_Swarm_Orbit_Determination.pdf.
- Montenbruck O, van Helleputte T, Kroes R, Gill E (2005) Reduced-dynamic orbit determination using GPS code and carrier measurements. *Aerosp Sci Technol* 9(3):261–271. doi:10.1016/j.ast.2005.01.003.
- Montenbruck O, Andres Y, Bock H, van Helleputte T, van den IJssel J, Loiselet M, Marquardt C, Silvestrin P, Visser P, Yoon Y (2008) Tracking and orbit determination performance of the GRAS instrument on MetOp-A. *GPS Solut* 12(4):289–299. doi:10.1007/s10291-008-0091-2.
- Montenbruck O, Wermuth M, Kahle R (2011–2012) GPS based relative navigation for the TanDEM-X mission—first flight results. *Navigation*, 58(4):293–304. doi: 10.1002/j.2161-4296.2011.tb02587.x.
- Pearlman MR, Degnan JJ, Bosworth JM (2002) The international laser ranging service. *Adv Space Res* 30(2):135–143. doi:10.1016/S0273-1177(02)00277-6.
- Reigber Ch, Lühr H, Schwintzer P (2002) CHAMP mission status. *Adv Space Res* 30(2):129–134. doi:10.1016/S0273-1177(02)00276-4.
- Sieg D, Diekmann FJ (2016) Options for the further orbit evolution of the Swarm mission. In: Proceedings of the living planet symposium, ESA SP-740, August.
- Silvestrin P, Cooper J (2000) Method of processing of signals of a satellite positioning system. US Patent 6 157 341, Dec 5.
- Silvestrin P, Bagge P, Bonnedal M, Carlstrom A, Christensen J, Hagg M, Lindgren T, Zangerl F (2000) Spaceborne GNSS radio occultation instrumentation for operational applications. In: Proceedings ION GPS, Institute of Navigation, Salt Lake City, UT, Sept 19–22, pp 872–880.
- Sust M, Zangerl F, Montenbruck O, Buchert S, Garcia-Rodriguez A (2014) Spaceborne GNSS receiving system performance prediction and validation. In: NAVITEC: ESA workshop on satellite navigation technologies and GNSS Signals and signal processing.
- Tapley BD, Bettadpur S, Watkins M, Reigber C (2004) The gravity recovery and climate experiment: mission overview and early results. *Geophys Res Lett.* doi:10.1029/2004GL019920.
- Teixeira da Encarnação J, Arnold D, Bezděk A, Dahle C, Doornbos E, van den IJssel J, Jäggi A, Mayer-Gürr T, Sebera J, Visser P (2016) Gravity field models derived from Swarm GPS data. *Earth Planets Space* 68:27.
- van den IJssel J, Encarnação J, Doornbos E, Visser P (2015) Precise science orbits for the Swarm satellite constellation. *Adv Space Res* 56(6):1042–1055. doi:10.1016/j.asr.2015.06.002.
- van den IJssel J, Forte B, Montenbruck O (2016) Impact of swarm GPS receiver updates on POD performance. *Earth Planets Space* 68(1):1–17. doi:10.1186/s40623-016-0459-4.
- Wang X, Rummel R (2012) Using Swarm for gravity field recovery: first simulation results. In: Sneeuw N, Novák P, Crespi M, Sansò F (eds) VII Hotine-Marussi symposium on mathematical geodesy, IAG Symposia, vol. 137, pp 301–306. doi: 10.1007/978-3-642-22078-4_45.
- Woo KT (2000) Optimum semi-codeless carrier phase tracking of L2. *Navigation* 47(2):82.
- Wu SC, Yunck TP, Thornton CL (1991) Reduced-dynamic technique for precise orbit determination of low Earth satellites. *J Guid Control Dyn* 14(1):24–31.
- Xiong C, Stolle C, Lühr H (2016) The Swarm satellite loss of GPS signal and its relation to ionospheric plasma irregularities. *Space Weather* 14(8):563–577. doi:10.1002/2016SW001439.
- Yunck TP, Wu SC, Wu JT, Thornton CL (1990) Tracking of remote satellites with the global positioning system. *IEEE Trans Geosci Remote Sens* 28(1):108–116.
- Zangerl F, Griesauer F, Sust M, Montenbruck O, Buchert B, Garcia A (2014) SWARM GPS precise orbit determination receiver initial in orbit performance evaluation. In: Proceedings ION GNSS?, Institute of Navigation, Tampa, Florida, Sept 8–12, pp 1459–1468.
- Zin A, Landenna S, Conti A (2006) Satellite-to-satellite tracking instrument—design and performance. Presented at the 3rd international GOCE user workshop, Nov 6–8 Nov 2006, ESA-ESRIN, Frascati, Italy.

Appendix C

Publication 3

Estimating maneuvers for precise relative orbit determination using GPS

Gerardo Allende-Alba^{a,b}, Oliver Montenbruck^b, Jean-Sébastien Ardaens^b, Martin Wermuth^b,
Urs Hugentobler^a

^a*Institute for Astronomical and Physical Geodesy, Technische Universität München, Arcisstraße 21, 80333 München, Germany*

^b*Deutsches Zentrum für Luft- und Raumfahrt (DLR), German Space Operations Center (GSOC), Münchner Straße 20, 82234 Weßling, Germany*

Abstract

Precise relative orbit determination is an essential element for the generation of science products from distributed instrumentation of formation flying satellites in low Earth orbit. According to the mission profile, the required formation is typically maintained and/or controlled by executing maneuvers. In order to generate consistent and precise orbit products, a strategy for maneuver handling is mandatory in order to avoid discontinuities or precision degradation before, after and during maneuver execution. Precise orbit determination offers the possibility of maneuver estimation in an adjustment of single-satellite trajectories using GPS measurements. However, a consistent formulation of a precise relative orbit determination scheme requires the implementation of a maneuver estimation strategy which can be used, in addition, to improve the precision of maneuver estimates by drawing upon the use of differential GPS measurements. The present study introduces a method for precise relative orbit determination based on a reduced-dynamic batch processing of differential GPS pseudorange and carrier phase measurements, which includes maneuver estimation as part of the relative orbit adjustment. The proposed method has been validated using flight data from space missions with different rates of maneuvering activity, including the GRACE, TanDEM-X and PRISMA missions. The results show the feasibility of obtaining precise relative orbits without degradation in the vicinity of maneuvers as well as improved maneuver estimates that can be used for better maneuver planning in flight dynamics operations.

Keywords: Precise relative orbit determination; Maneuver estimation; GPS; GRACE; TanDEM-X; PRISMA

1. Introduction

The formation flying technology has been successfully applied in remote sensing and Earth observation missions during the last years. Notable examples include GRACE and TanDEM-X (Tapley et al., 2004; Krieger et al., 2010) and it represents similarly a fundamental part of future missions, such as GRACE Follow-On and SAOCOM-CS (Flechtner et al., 2012; Barbier et al., 2014). For the generation of scientific and engineering products, the precise relative orbit determination (PROD) of spacecraft in the formation is a key element. The use of the Global Positioning System (GPS) has allowed to achieve millimeter and sub-millimeter precision in kinematic and reduced-dynamic baseline solutions, particularly for the GRACE and TanDEM-X missions (Jäggi et al., 2009; Montenbruck et al., 2011-2012).

As part of the formation constraints imposed by specific mission profiles, control maneuvers are typically executed. These maneuvers may be sparse as in the case of the GRACE mission (e.g. 2–4 per year (Yoon et al., 2006)) or executed at rates of several maneuvers per day (depending on the formation configuration) as in the case of the TanDEM-X and PRISMA missions (Kahle et al., 2012; Ardaens et al., 2011). A consistent generation of PROD products from these missions calls for the implementation of a maneuver handling strategy in order to avoid discontinuities or precision degradation before, after and during maneuver execution.

In an effort to overcome the difficulties added by the presence of control maneuvers, various maneuver handling strategies have been implemented in renowned orbit determination software packages. In the Bernese GNSS Software (BSW, Dach et al. (2015)) and the

Earth Parameter and Orbit System - Orbit Computation (EPOS-OC, Zhu et al. (2004)) used at the German Research Center for Geoscience (GFZ), maneuvers are taken as a series of instantaneous velocity changes (pulses) at specific epochs based on known maneuver execution times in the radial, along-track and cross-track directions. These parameters are estimated in both precise and relative orbit adjustments using a batch least squares processing (Jäggi et al., 2012). The GPS High-precision Orbit determination Software Tools (GHOST, Montenbruck et al. (2005)) used at DLR's German Space Operations Center (GSOC) follow a two step strategy. First, maneuvers are treated as constant thrusts over intervals according to known burn start time and duration. Total Dv maneuvers in radial, along-track and cross-track directions associated with these thrust events are estimated in single-satellite precise orbit determination (POD) using a batch least squares processing. Thereafter, these estimated values are used as known parameters in PROD using an extended Kalman filter (EKF). Uncertainties in the estimated values are compensated by adding process noise in the filter time update (Montenbruck et al., 2011-2012).

The present study introduces a scheme for maneuver estimation as part of a batch relative orbit determination process, using differential GPS pseudorange and carrier phase measurements. In the proposed scheme, maneuvers are considered as constant thrust accelerations in the local spacecraft's radial, along-track and cross-track directions over the total burn duration. The implementation of a batch relative orbit determination scheme adds robustness to the provided solution as well as the capability of direct estimation of maneuvers, in contrast to a sequential orbit adjustment, as used by Kroes et al. (2005) and Montenbruck et al. (2011-2012). In addition, the estimation of maneuvers using a differential GPS approach benefits from common error cancellation in the observations. By using a constant thrust model, not only the resulting relative trajectory but also the relative velocity solution is differentiable over the entire orbital arc, which cannot be attained when maneuvers are estimated as instantaneous pulses. The constant thrust model results in a smoother and more realistic description of the satellite orbit which benefits the analysis of remote sensing data (from line scanners, synthetic aperture radars, etc.) in the vicinity of maneuvers.

In a recent study of Ju et al. (2015), a similar strategy was implemented in the National University of Defense Technology orbit determination ToolKit (NUDTTK). However, the analysis was limited to sparse data from only one mission and did not address the maneuver estimation accuracy. In contrast, the scheme presented in this study has been tested using flight data from missions with different maneuvering rates and GPS receiver characteristics, including GRACE, TanDEM-X and PRISMA. In addition, a

more thorough analysis of results has been carried out, which includes not only an assessment of resulting precise relative orbit products but also an evaluation of the maneuver estimation capabilities of the presented algorithms.

The paper starts with the development of a PROD scheme, including maneuver estimation and carrier phase integer ambiguity resolution. Subsequently, flight data and formation configurations of the missions under analysis are briefly described and, finally, the PROD and maneuver estimation results are evaluated using various criteria according to the mission profiles.

2. Relative orbit and maneuver adjustment

The present section provides a description of the overall proposed scheme for reduced-dynamic PROD. It consists of an interplay of strategies including single-satellite POD, maneuver estimation, GPS carrier phase integer ambiguity estimation and relative orbit dynamic integration. The scheme has been implemented and integrated into DLR's GHOST.

2.1. GPS observation models

According to the processing strategy and availability of measurements, different observation models are employed. For this study, three main processing schemes are analyzed. Current POD (Montenbruck et al., 2005) and PROD (Kroes et al., 2005) (henceforth denoted as PROD A) strategies implemented in GHOST are used as reference for analysis of the proposed PROD method (henceforth denoted as PROD B). Table 1 shows a summary of GPS models and estimation strategies used in the present study.

For dual-frequency processing, PROD B makes use of single-difference ionosphere-free (IF) combinations of pseudorange (P) and carrier phase observations (U), which are modeled as

$$P_{D,IF}^i = \rho_D^i + c\delta t_D + \epsilon_{D,IF}^i \quad (1a)$$

$$\Phi_{D,IF}^i = \rho_D^i + c\delta t_D + \lambda_{IF} b_{D,IF}^i + \epsilon_{D,IF}^i \quad (1b)$$

where the notation \square_D denotes any relative quantity of spacecraft B with respect to reference spacecraft A. Thus, ρ_D^i represents the single-difference of geometric ranges between both receivers and the i -th GPS satellite. In addition, $c\delta t_D$ depicts the difference of receiver clock offsets from both spacecraft (where c is the speed of light in vacuum) and $b_{D,IF}^i$ gives the IF bias of single-difference carrier phase observations. The terms $\epsilon_{D,IF}^i$ and $\epsilon_{D,IF}^i$ denote un-modeled errors (including receiver thermal noise) of single-difference IF pseudorange and carrier phase observations, respectively.

For the case of single-frequency processing (applicable to TanDEM-X and PRISMA), the present study has been focused on short baselines (in the order of <5 km) where the spatial correlation of ionospheric delays in observations from each spacecraft allows a high de-

Table 1 Summary of GPS models and estimation strategies used in the present study for POD and PROD

Item	PROD (Scheme A) ^a	PROD (Scheme B)	POD ^b
GPS measurement model	Single-difference pseudorange and carrier phase observations 5°/10° cut-off elevation w.r.t. local horizon Differential phase center offset and variations of receiver antenna *		Un-differenced pseudorange and carrier phase observations Phase center offset and variations of receiver antenna *
(Dual-frequency)	Estimated differential ionospheric delays	Ionosphere-free combination	Ionosphere-free combination
(Single-frequency)	Lear model and estimated differential zenith ionospheric delays Phase center offset and variations of transmitter antenna; phase wind-up; GPS orbits and clock solutions	Dismissed differential ionospheric delays for short baselines	GRAPHIC combination
Estimation method	Extended Kalman Filter/smoothing (EKF)	Batch least-squares (LSQ)	Batch least-squares (LSQ)
Numerical integration	Fourth-order single-step Runge-Kutta method	Variable-order variable step-size DE method	multi-step Shampine-Gordon
Integer ambiguity resolution scheme	Sequential EKF-based + ILSQ	A priori-constrained sequential/batch + ILSQ/IA	Not applied
Maneuver handling	Applied constant thrust arcs. Increase of process noise	Estimated constant thrust arcs	Estimated constant thrust arcs

^a Kroes et al. (2005).

^b Montenbruck et al. (2005).

* Except from PRISMA.

gree of reduction of errors when using single-difference observations. For the estimation of the reference trajectory in PROD B (see Section 2.2), the GRAPHIC combination (Yunck, 1993) is used.

2.2. Orbit determination and maneuver estimation

The key task in reduced-dynamic orbit determination is the application of pseudo-stochastic/empirical parameters that are used to correct deficiencies and/or a mismodeling of the dynamics used for orbit integration (Yunck et al., 1990). These parameters can be included in the estimation algorithm in the form of an added process noise (e.g. selected heuristically) on the propagated orbit state. Alternatively, in order to avoid any discontinuity in the estimated state resulting from this approach, empirical accelerations can be applied directly in the force model (Wu et al., 1991). In a GPS-based estimation method, these parameters can be estimated from measurements and they can be conveniently modeled to be applied in the spacecraft's radial, along-track and cross-track directions. The proposed reduced-dynamic relative orbit determination method described in the present study follows this approach. Empirical accelerations are considered to be piecewise constant in predefined time intervals (typically 400–600 s) and are estimated together with other solve- for parameters in a least-squares (LSQ) estimation method. For the computation of a reference trajectory (i.e. for spacecraft A) it is important to consider that in a reduced-dynamic approach, the

provided corrections to the force model are applied locally within the bounds of the predefined intervals. A PROD strategy based on a previously estimated reference trajectory (see e.g. Kroes et al. (2005)) may not be a suitable approach due to a possible mismatching definition of intervals for empirical accelerations in both PROD and POD. Although such inconsistencies could be avoided by a proper management of tuning parameters in the cross-estimation of absolute and relative orbits, such an approach fails (in addition) to take advantage of the relation between the absolute and relative dynamics. Thus, a more unified approach is implemented in the proposed scheme, consisting of a concurrent adjustment (i.e. in the same algorithm) of a relative trajectory along with the reference spacecraft's absolute orbit. In this way, a congruent grid of intervals for both trajectories can be guaranteed for proper estimation of relative empirical accelerations.

The LSQ algorithm starts with a set of initial approximate estimates and performs an iterative orbit adjustment by making use of GPS observations (see Table 1 and Section 2.1) and precise dynamical models (Montenbruck et al., 2005, 2011–2012). With a data set of duration T and defined intervals of duration Δt (assuming momentarily an absence of maneuvers for simplicity), the estimation vectors in both concurrent estimation schemes comprise the same corresponding set of parameters for absolute and relative orbit determination, as follows: a 6-dimensional spacecraft state vector at the reference epoch $\mathbf{y}(t_0) = \mathbf{y}_0 = (\mathbf{x}_0, \mathbf{v}_0)$, a solar

radiation pressure coefficient C_R , an air drag coefficient C_D , empirical accelerations $\alpha_k = (a_R, a_T, a_N)_k$ at intervals defined with $\{k \in \mathbb{N} \mid t_0 + k\Delta t \leq t < t_0 + (k+1)\Delta t\}$, epochwise receiver clock offsets $c\delta t_h$ at the h -th observation epoch as well as a set of ionosphere-free biases b_{IF}^i for the i -th continuous tracking arc of a GPS satellite (for the single-frequency case, see Table 1).

At each iteration, the reference and relative trajectories are numerically integrated across the entire data arc in order to compute residuals from observations and modeled measurements. The concurrent integration of the absolute and relative state vectors from observation epoch t_h to epoch t_{h+1} can be expressed as

$$\begin{pmatrix} \mathbf{x}_A \\ \mathbf{v}_A \\ \mathbf{x}_D \\ \mathbf{v}_D \end{pmatrix} = \int_{t_h}^{t_{h+1}} \begin{pmatrix} \mathbf{v}_A \\ \mathbf{a}_A(\tau, \mathbf{x}_A, \mathbf{v}_A) \\ \mathbf{v}_D \\ \mathbf{a}_B(\tau, \mathbf{x}_A + \mathbf{x}_D, \mathbf{v}_A + \mathbf{v}_D) - \mathbf{a}_A(\tau, \mathbf{x}_A, \mathbf{v}_A) \end{pmatrix} d\tau \quad (2)$$

By having a congruent grid of intervals for empirical accelerations, it is possible to apply a proper correction in the integration of $\mathbf{a}_D = \mathbf{a}_B - \mathbf{a}_A$ with the corresponding estimated relative empirical accelerations $\alpha_{D,k}$ at interval k . Given that each piecewise constant acceleration represents a discontinuity in the dynamics, the numerical integrator must be restarted at the beginning of each interval. Typically, 2-3 iterations are required to adjust the absolute reference trajectory and an equal number of iterations are required in order to adjust the relative trajectory (see Fig. 1).

Maneuvers are considered as constant thrust arcs in the local spacecraft's radial, along-track and cross-track directions $\mathbf{F} = (F_R, F_T, F_N)$ over the maneuver duration interval δt_m . If short duration and small magnitude maneuvers are considered, the total mass flow can be neglected from the analysis (Montenbruck and Gill, 2005), and thus, the total applied $\Delta \mathbf{v} = (\Delta v_R, \Delta v_T, \Delta v_N)$ can be approximated as

$$\Delta \mathbf{v} = \int_{t_s}^{t_s + \delta t_m} \frac{\mathbf{F}}{m} d\tau \approx \frac{\mathbf{F}}{m} \delta t_m \quad (3)$$

which is adjusted as part of the orbit determination process. The proper correction for state vector integration in Eq. (2) during maneuver execution can be applied considering the knowledge of δt_m .

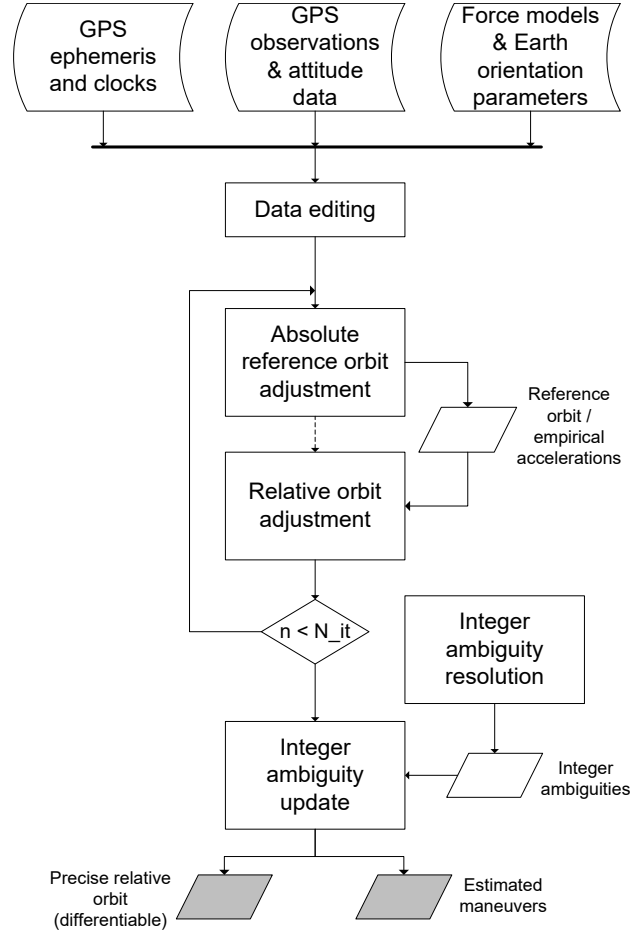


Fig. 1 Block diagram for the computation of PROD B solutions. The adjustment of absolute reference and relative orbits can be performed (equivalently) in different stages or in the same iteration block.

With the above considerations, the resulting estimation vector for the reference trajectory is given by

$$\begin{pmatrix} \mathbf{T}_A \\ \mathbf{X}_A \\ \mathbf{B}_A \end{pmatrix} = \begin{pmatrix} c\delta t_{0,A}, \dots, c\delta t_{n_T-1,A} \\ \mathbf{y}_{0,A}; C_{R,A}; C_{D,A}; (\Delta \mathbf{v}_A); (\alpha_A) \\ b_{A,IF}^0, \dots, b_{A,IF}^{s-1} \end{pmatrix} \quad (4)$$

whereas the estimation vector for the relative orbit yields

$$\begin{pmatrix} \mathbf{T}_D \\ \mathbf{X}_D \\ \mathbf{B}_D \end{pmatrix} = \begin{pmatrix} c\delta t_{0,D}, \dots, c\delta t_{n_T-1,D} \\ \mathbf{y}_{0,D}; C_{R,D}; C_{D,D}; (\Delta \mathbf{v}_D); (\alpha_D) \\ b_{D,IF}^0, \dots, b_{D,IF}^{s-1} \end{pmatrix} \quad (5)$$

where (α_A) and (α_D) denote the set of empirical accelerations vectors to estimate for the reference and relative trajectories, respectively. Similarly, $(\Delta \mathbf{v}_A)$ and $(\Delta \mathbf{v}_D)$ denote the set of $\Delta \mathbf{v}$ vectors to estimate for each spacecraft. In this way, the estimation scheme is able to handle scenarios where both spacecraft perform

maneuvers (e.g. TanDEM-X mission, see Section 3.2) without affection to the structure and/or robustness of the overall system.

2.3. Maneuver data from telemetry

The maneuver model described in Section 2.2 consists of a $\Delta\mathbf{v}$ vector (to be estimated) and takes into account the knowledge of the maneuver duration δt_m as well as the start time of burn t_s . The latter values can be obtained from telemetry data and correspond to a center-of-burn time $t_{cob} = t_s + 0.5\delta t_m$ as used in the maneuver planning (Chatel, 2015) under the assumption of a constant thrust profile. Due to diverse delays in maneuver execution (or maneuver time-tagging) by the on-board computer as well as from the actual thrusters, these data contain uncertainties. This may lead to increased (though subtle) error levels in the final relative position solution in the vicinity of t_{cob} if both parameters are introduced as known parameters in the estimation process. An effective shift in the value of t_{cob} can be performed by a manual adjustment of the input parameters or by direct estimation of either t_s or δt_m in the orbit determination scheme. However, the latter approach turns out to be less effective in scenarios with several maneuvers per day given that the degree of freedom is reduced, which has an impact on the overall estimation process.

2.4. Ambiguity-fixed solution

The float ambiguity solution provided by the scheme described in Section 2.2 can be further improved by making use of fixed carrier phase ambiguities. As an alternative to common widelane/narrowlane (WL/NL) ambiguity resolution techniques used by some software packages (see e.g. Jäggi et al. (2007)), the present study makes use of the scheme developed in (Allende-Alba and Montenbruck, 2016). This scheme is based on an a priori-constrained sequential/batch LSQ method for float ambiguity estimation and integer least-squares (ILSQ) and integer aperture (IA) estimation methods for ambiguity resolution. The underlying strategy consists of a kinematic relative positioning model with constraints from pre-processed reduced-dynamic orbit solutions. This implies that, aside from the possible presence of multipath errors in the observations, the overall ambiguity resolution scheme is not affected by the presence of maneuvers (granted that a maneuver handling strategy is used also for estimation of reference trajectories). The resulting integer ambiguities are included as known parameters in the estimation system as a constraint for the computation of the ambiguity fixed relative orbit solution (see Fig. 1).

3. Formation flying missions

The relative orbit determination scheme discussed above has been tested using flight data from formation flying missions with different maneuver-execution rates. The next sections provide a brief overview of the

spacecraft propulsion and formation control strategies as well as a short description of the data sets under analysis.

3.1. Spacecraft propulsion

For the GRACE mission, each of the two spacecraft is equipped with two 40 mN cold gas nitrogen (GN_2) thrusters located in the anti-flight direction (Schelkle, 2000). The TerraSAR-X and TanDEM-X spacecraft (TSX and TDX, respectively) have four 1 N hydrazine (N_2H_4) thrusters installed in anti-flight direction. In addition, two 40 mN GN_2 thrusters in each flight and anti-flight direction have been added to the TDX spacecraft (Kahle et al., 2012). For the case of the PRISMA mission, the active orbit control system was installed only on the Mango spacecraft. It consists of six 1 N N_2H_4 thrusters distributed on the spacecraft body (D'Amico et al., 2013a). In addition, two experimental propulsion systems have been included in the mission, but these are not considered in this study. The reader is referred to Anflo and Möllerberg (2009) and Rangsten et al. (2011) for details.

3.2. Formation control strategies

The main operative objective of the GRACE formation, launched on March 2002, is to maintain a relative along-track separation of 220 ± 50 km in order to provide the proper configuration for measuring high-order harmonic coefficients of the Earth's gravity field (Tapley et al., 2004). The orbit maintenance strategy has been to maximize the time between maneuvers in order to counteract the effects of conservative and non-conservative perturbations on the spacecraft trajectories. Based on the characteristics of the designed relative trajectories and the ballistic coefficients of the spacecraft (differing mainly due to the different pitch angle and orientation of each satellite to ensure a line-of-sight orientation), these maintenance maneuvers have been planned to be executed with a maximum rate of 12 maneuvers per year (Kirschner et al., 2001), although the actual maneuvering rate during the mission has been 2–4 maneuvers per year.

The TSX spacecraft was inserted in a sun-synchronous dusk-dawn orbit on June 2007, which has been maintained within a maximum absolute radial/cross-track distance of 250 m from a target Earth-fixed trajectory (Arbinger et al., 2004; D'Amico et al., 2004). Orbit maneuvers to counteract luni-solar and atmospheric drag perturbations are performed 3–5 times per year (out-of-plane) except during periods of high solar activity, for which a rate of up to 3 maneuvers per week (in-plane) is necessary (Kahle et al., 2012). On June 2010, the TDX spacecraft was launched in order to create a closed formation with TSX for Synthetic Aperture Radar (SAR) interferometry. The formation geometry has been designed in order to guarantee a maximum cross-track separation at the equator and maximum radial separation at the poles by using

the concept of relative eccentricity/inclination vectors (D’Amico and Montenbruck, 2006). For the task of formation maintenance to meet tight relative control requirements, the TDX spacecraft must execute daily in-plane maneuver pairs (using GN2 thrusters) to compensate the natural eccentricity vector drift and control the along-track separation perturbed mainly by atmospheric drag. In addition, H₂N₄ thrusters are used to replicate maneuvers executed by TSX as well as to perform out-of-plane maneuvers so as to counteract the natural drift of the inclination vector (Kahle et al., 2012).

The period under analysis for the PRISMA mission covers part of the Spaceborne Autonomous Formation-flying Experiment (SAFE) which consists of two operational slots called Autonomous Formation Control (AFC) 1 and 2 (D’Amico et al., 2013b). During both AFC periods, the formation was mainly operated in closed-loop mode with in-plane control strategies realized by the execution of maneuvers in either radial or along-track direction (D’Amico et al., 2012). Several close formation configurations were exercised during this experiment, most of them characterized by (anti-) parallel relative eccentricity and inclination vectors in order to provide increased safety and to remove out-of-plane J_2 secular effects (D’Amico and Montenbruck, 2006). The number of maneuvers for the execution of each formation configuration varies according to the specific characteristic of each one. For the case of the period under analysis, approximately 150 maneuvers using primarily H₂N₄ thrusters were executed.

3.3. Data sets

In total, data from six spacecraft from the GRACE, TanDEM-X and PRISMA missions have been used. As maneuvers for the GRACE mission have been sparse, for evaluation of baseline precision and maneuver estimation, a set of 10 days distributed from 2004 to 2012 has been used. In addition, a 10-days period from year 2009 has been selected for a statistical assessment of maneuver estimation performance, as further described

in Section 4.2.2. For the TanDEM-X mission, a 10-days data set from 2014 has been selected for both baseline estimation and maneuver estimation analysis. During this period the formation is maintained in cross-track interferometry mode with a baseline dimension of around 500 m (Krieger et al., 2010). For the PRISMA mission, a total of 14 days during 2010 and 2011 have been analyzed. These days are contained in the execution periods of the AFC operational slots (D’Amico et al., 2012). Table 2 depicts an overview of the spacecraft characteristics as well as the observation statistics of representative data arcs under analysis.

4. Results and discussion

The evaluation of performance of the presented algorithms has been focused mainly on two factors. The first one consists of an assessment of relative orbit solutions in order to observe the impact of maneuver estimation on the final trajectory precision. The second factor is the evaluation of the actual maneuver estimation. The following sections present and discuss the results obtained using flight data from the formation flying missions described in Section 3.

4.1. Relative orbit assessment

The assessment of final solutions has been performed according to the available tools and products for each mission. For GRACE, the availability of KBR measurements allows a direct assessment of precision of the GPS-based relative orbit solution (as already shown in several previous studies, see e.g. Bertiger et al. (2010), Jäggi et al. (2007), Kroes (2006)). For the TanDEM-X and PRISMA missions this assessment consists of an inter-product consistency check using solutions from the PROD A scheme, which has been used for routine baseline generation in such missions (Ardaens et al., 2010; Montenbruck et al., 2011- 2012). All the solutions used in this assessment have been computed using carrier phase observations with fixed integer ambiguities.

Table 2 Spacecraft characteristics and data statistics. The RMS residuals of IF combinations (single- and dual-frequency) in precise absolute and relative orbit determination provide an indication of the effective receiver error levels. In the case of single-frequency processing in PROD (scheme B), these values include non-modeled differential ionospheric errors in short baselines (< 5 km). IF combinations are denoted as P12, L12 and G1 for pseudorange, carrier phase and GRAPHIC observations, respectively.

Mission	Spacecraft	Propulsion system (orbit control)	GPS receiver	Data arc	Residuals				
					POD		PROD		
					P12 (m)	L12 (mm)	G1 (m)	L12 (mm)	L1 (mm)
GRACE	GRACE A	2 x 40mN (GN ₂)	BlackJack (JPL)	2009/030-040	0.80	6.7	0.17	1.3	—
	GRACE B				0.47	5.6	0.16		
TanDEM-X	TSX	4 x 1N (H ₂ N ₄)	IGOR (BRE,GFZ)	2014/001-010	0.60	6.3	0.11	2.2	5.0
	TDX	4 x 1N (H ₂ N ₄), 2 x 40mN (GN ₂)			0.68	7.2	0.12		
PRISMA	Tango	—	Phoenix (DLR)	2010/258-263	—	—	0.24	—	6.0
	Mango	6 x 1N (H ₂ N ₄)			—	—	0.21	—	

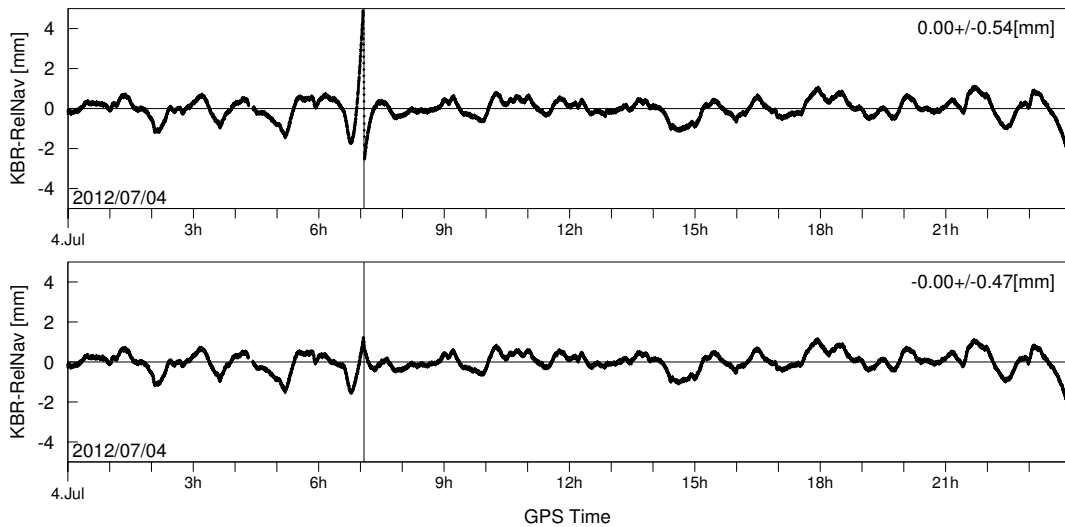


Fig. 2 KBR residuals of precise relative orbit solutions for the GRACE formation, computed with the PROD B scheme during 4 July 2012, using values $[t_s, \delta t_m]$ from telemetry (top) and a corrected value for t_{cob} (bottom). Gray bars denote maneuver execution periods.

4.1.1. Precision evaluation

The KBR data from the GRACE mission provide a biased estimate of the inter-spacecraft separation in along-track direction with μm precision. From the days under analysis, three days have been excluded from this assessment, due to the unavailability of KBR measurements during yaw-steering and cross-track maneuvers. The precision provided by the KBR measurements is particularly useful in order to evaluate the impact of maneuver execution and estimation at mm and sub-mm precision levels and, in particular, to observe the effect of a proper setting of t_{cob} . As an example, Fig. 2 shows the KBR residuals of precise relative orbit solutions on 4 July 2012. The top plot shows the impact of using the values $[t_s, \delta t_m]$ from telemetry. As stated, the uncertainty on t_{cob} depends on several factors (e.g. on-board computer task scheduling, thrust profile). Typically, this uncertainty may be at the 1-2 s level, which leads to (additional) relative positioning errors. Fig. 2 shows the effect of shifting the telemetry value for t_{cob} considering an estimated value for t_s (from POD solution) and using δt_m from telemetry (see Section 2.3). For the days under analysis, the estimated shifts applied to telemetry values for t_s are located in the range of 0.04 s to 0.9 s. Aside from the subtle improvement in the overall precision of the solution, Fig. 2 mainly depicts a representative expected local error reduction (at the level of 4-5 mm) in the vicinity of a maneuver when a slightly corrected value for t_{cob} is used. Similarly, Fig. 2 (bottom) shows that, when properly handled, the presence of a maneuver does not have a major impact on the overall statistics of the solution.

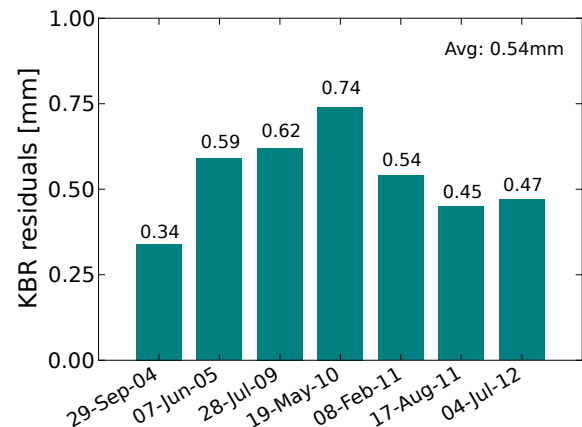


Fig. 3 KBR residuals of precise relative orbit solutions for the GRACE formation, computed using the PROD B scheme and corrected t_{cob} values for 7 days distributed from 2004 to 2012. During these days, one maneuver per day has been executed.

In general, an average precision of 0.54 mm in terms of KBR residuals has been obtained for 7 days within the period of analysis (see Fig. 3). These tests provide an indication of the capabilities of the presented algorithms for achieving sub-mm precision levels during days with maneuvering activities. The obtained precision is comparable with nominal days without maneuvers (e.g. Jäggi et al. (2009) and Allende-Alba and Montenbruck (2016) report average precision values of 0.81 mm and 0.72 mm in a one-year analysis using BSW and GHOST, respectively). Likewise, the obtained precision confirms the recent results obtained by Ju et al. (2015) for the same days under analysis, using a different precise baseline determination strategy for the GRACE mission.

Table 3 Inter-product consistency of precise relative orbit solutions using PROD schemes A and B for the TanDEM-X formation for a 10-days period. In the main text, reference is made to the four columns displaying the maximum absolute errors (R: Radial, T: Along-track, N: Cross-track; 1F: Single-frequency, 2F: Dual-frequency).

DOY 2014	Maneuvers per day	Maximum absolute error (mm)											
		PROD A (2F - 1F)			PROD B (2F - 1F)			PROD B (2F) - PROD A (1F)			PROD B (2F) - PROD A (2F)		
		R	T	N	R	T	N	R	T	N	R	T	N
1	2	27.7	18.2	10.4	6.1	10.5	2.4	24.9	19.2	12.1	16.1	4.8	7.9
2	3 + 1	18.5	5.8	6.8	3.8	8.3	1.9	24.5	6.8	5.8	16.0	6.7	2.7
3	2	30.6	9.1	9.2	4.6	7.3	3.5	25.2	9.8	12.4	10.8	6.4	9.7
4	2	15.1	5.7	6.2	2.3	3.7	2.4	12.1	6.4	8.3	13.5	5.6	2.0
5	3 + 1	26.7	7.5	9.6	3.5	3.7	2.0	19.9	14.7	10.1	11.9	17.5	5.2
6	2	24.8	19.7	10.5	4.0	3.3	2.7	24.1	19.0	10.4	8.0	5.5	2.1
7	3	35.8	12.7	8.3	6.2	8.7	4.1	33.8	12.5	10.9	17.3	9.6	7.5
8	2	14.1	6.7	12.8	6.4	3.2	2.4	21.0	8.1	18.8	9.3	7.3	5.9
9	2	22.0	8.1	13.7	3.5	3.6	3.1	29.4	6.7	12.7	20.3	5.6	6.2
10	3 + 1	59.7	22.0	13.6	5.2	5.9	2.3	52.0	15.5	15.2	48.2	14.8	4.8

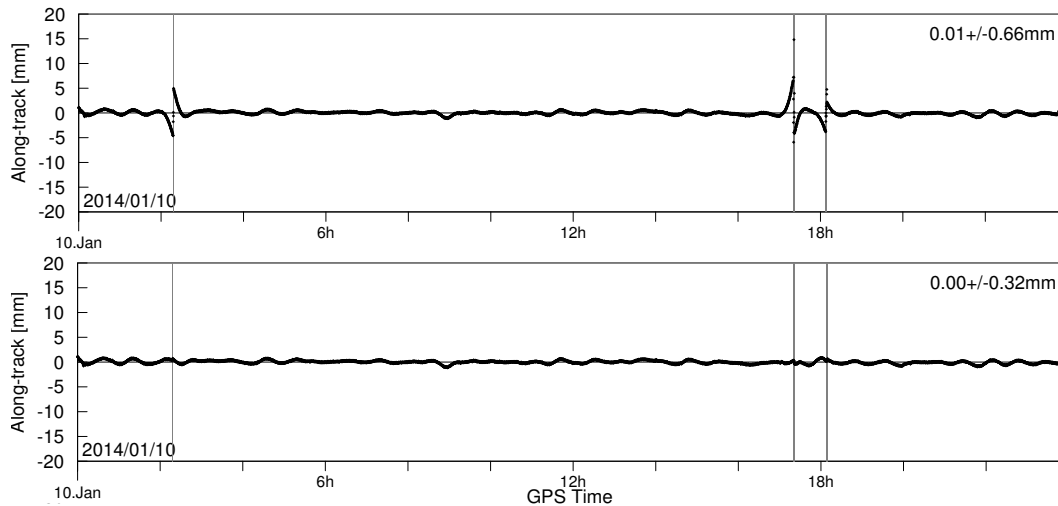


Fig. 4 Inter-product consistency in the along-track direction of dual-frequency relative orbit solutions using PROD schemes A and B for the TanDEM-X formation on 10 January 2014. Depicted are the differences before (top) and after (bottom) modification of added process noise during maneuver execution in PROD A. Gray bars denote maneuver execution periods.

4.1.2. Inter-product consistency

In the case of the TanDEM-X and PRISMA missions, relative orbit solutions can be evaluated by means of an inter-product consistency analysis. This comparison aims at the validation of the algorithms described in Section 2 with products computed using the PROD A scheme (see Table 1). As stated, in this scheme maneuvers are applied as constant thrust arcs with information from telemetry data or POD. The uncertainty of the applied maneuvers is introduced as additional process noise during the time update of the EKF. In routine operations, the absence of a suitable reference for these solutions prevents the evaluation of the actual impact of uncertainties during maneuver execution. Therefore, a general process noise model is used for the introduced thrust arcs. Similarly, unlike

GRACE, for the TanDEM-X and PRISMA missions it is difficult to assess the actual impact of errors of t_{cob} values reconstructed from telemetry data. Hence, no further efforts have been done to apply corrections (manual or estimated) to such values in tests with data from those missions.

For TanDEM-X, the period under analysis lies within a mission phase with close formation operations. This scenario allows the computation of single-frequency solutions that can be used in the overall analysis due to their degree of statistical independence with dual-frequency solutions. Table 3 depicts the maximum absolute errors of inter-product comparisons for the TanDEM-X mission, using both PROD schemes in dual- and single-frequency modes. In particular, from the first and third columns in Table 3 it is possible to

observe peak errors of up to 6 cm, which are mostly present around executed maneuvers. In PROD A, the increased process noise during maneuvering periods leads to an estimated trajectory with reduced stiffness in the vicinity of maneuvers. During such periods, the solution approximates more narrowly to the observations. This may result in enlarged local error levels, which in general are different for the single- and dual-frequency cases. On the other hand, PROD B solutions exhibit a better consistency, with most peak errors below 1 cm. Comparing the consistency of solutions from each individual scheme (first and second columns in Table 3) provides a hint of the benefits of maneuver estimation in PROD B.

Likewise, the comparison of dual-frequency solutions from PROD A and B (fourth column in Table 3) shows that peak errors are present predominantly around maneuvers. Provided that both solutions have statistical dependence due to the use of the same set of observations, such inconsistencies mainly reveal the differences of maneuver handling strategies in both schemes. As an example, Fig. 4 (top) shows the differences in the along-track direction of dual-frequency solutions from both PROD schemes on 10 January, 2014. On this day at around 2:15 h, TSX performed an orbital correction maneuver which was replicated (after few seconds) by TDX. In PROD A, after increasing the state covariance during maneuvering periods, the filter may require several updates to achieve steady error bounds again. This may result in characteristic error signatures in the solution, as shown in Fig. 4 (top). In addition, given that the PROD A scheme is based on an EKF/ smoother (i.e. dual-direction execution), the displayed error signatures exhibit some degree of symmetry around the period of maneuver execution.

In general, the resulting peak errors of solutions from PROD A (first, third and fourth columns in Table 3) provide an indication of uncertainties around maneuver execution stemming from the implemented maneuver handling strategy. To a large degree, this factor has prevented the use of baseline products from routine operations for remote sensing applications during maneuvering periods.

For the PRISMA mission, the maneuvering activity is much more intense in comparison with TanDEM-X. Given that precise relative orbit products are mainly used for the evaluation of other on-orbit-generated products (Ardaens et al., 2010, 2011), an evaluation of the impact of specific maneuver events is of less importance in comparison with an assessment of the overall quality of the resulting solutions. Such an assessment can be based on an inter-product consistency check of solutions from both PROD schemes. Table 4 shows the RMS errors in consistency of solutions from both PROD schemes under analysis during 10 days within the SAFE (see Section 3.2). This period is characterized by the large number of executed maneuvers and, similarly, the differences between the two orbit

Table 4 Inter-product consistency of precise relative orbit solutions using PROD schemes A and B for the PRISMA formation for a 10-days period (R: Radial, T: Along-track, N: Cross-track).

DOY 2010	Maneuvers per day	RMS error (mm)		
		PROD B - PROD A (Single-frequency)		
		R	T	N
263	7	4.24	3.47	1.93
267	11	3.16	4.59	2.16
268	20	8.03	6.53	2.33
269	16	2.98	2.31	1.58
270	20	2.58	2.47	3.77
DOY 2011				
84	14	3.07	3.29	2.21
85	27	6.88	4.18	1.55
86	16	4.44	3.50	1.59
88	13	5.93	4.64	2.85
89	15	3.79	2.66	1.44

products consist mainly of discrepancies during maneuver execution. An example of these differences is shown in Fig. 5 (top) for the radial component on 26 March, 2011, depicting the execution of 27 maneuvers. In general, it is expected that the maneuver estimation strategy used by PROD B provides relative orbit estimates with reduced error levels during maneuver execution intervals. So, as in the case of TanDEM-X, the depicted comparison appears to indicate that discrepancies during maneuver execution are due to increased error levels in solutions from PROD A. Indeed, because of the maneuver handling strategy used by PROD A, periods with frequent maneuver execution (such as the interval between 18:00 and 22:00 h in Fig. 5 (top)) are difficult to handle by the EKF due to the constant increment of the state covariance.

4.1.3. Inter-product precision evaluation

Although so far it has been argued that most of the inconsistencies of solutions from both PROD schemes for TanDEM-X and PRISMA are founded on the maneuver handling strategy, a more general comparison of strategies used by each scheme requires the evaluation of solutions by using an external validation tool. In particular, this evaluation may be applied in a more effective way if true values of executed maneuvers were known. Due to the difficulty to achieve this requirement, an alternative approach used in the present study is the inclusion of dummy maneuvers into the data processing. In this procedure, the presence of a maneuver is indicated as input parameter to both PROD schemes during a true-maneuver-free period. Dummy maneuvers have the same characterization as real maneuvers (i.e. start/stop times, duration, standard deviation) but they have a (true known) magnitude of zero.

In order to evaluate the impact of maneuver handling strategies in the baseline solution, data from the GRACE mission has been used for this test as it provides an external validation tool for baseline assessment.

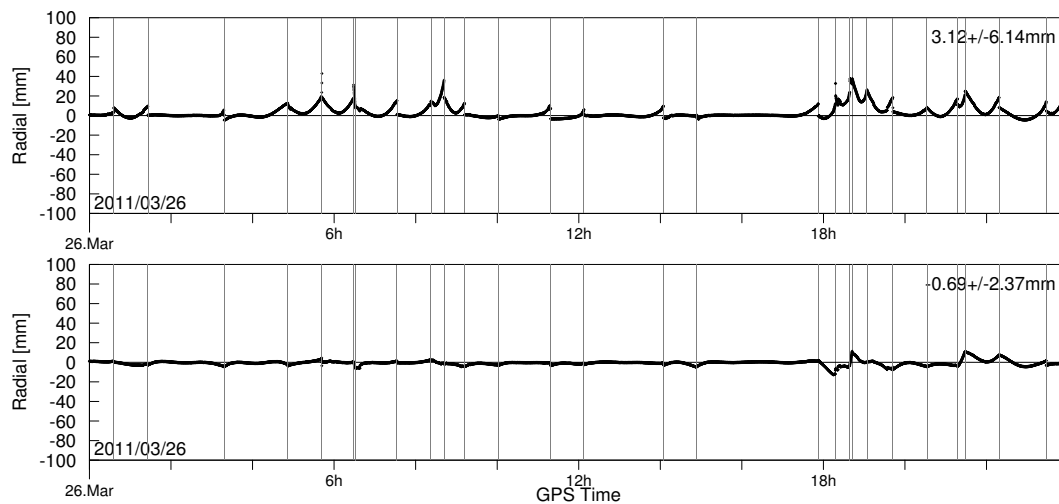


Fig. 5 Inter-product consistency of precise relative orbit solutions in the radial direction using PROD schemes A and B for the PRISMA formation on 26 March 2011. Depicted are the differences before (top) and after (bottom) modification of added process noise during maneuver execution in PROD A. Gray bars denote maneuver execution periods.

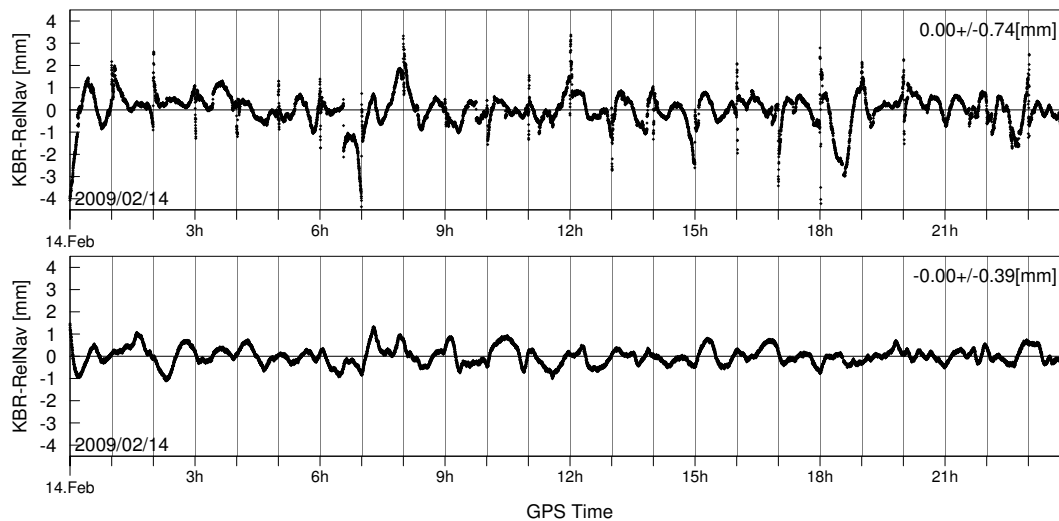


Fig. 6 KBR residuals of precise relative orbit solutions for the GRACE formation, computed with the PROD A (top) and B (bottom) schemes on 14 February 2009, using the concept of dummy maneuvers (denoted with gray bars).

Thus, a set of 22 dummy maneuvers with duration of 60 s has been applied at a rate of one maneuver per hour to the GRACE data set on 14 February, 2009. Fig. 6 shows the KBR residuals of solutions from PROD A (top) and PROD B (bottom). Although, in general, both solutions achieve a sub-mm precision, they exhibit different statistical characteristics (aside from features related to the estimation scheme). In the case of the solution from PROD A, even if maneuvers are modeled with true values (in this case maneuvers of magnitude zero), the impact of increasing the EKF state covariance during maneuver execution is evident, as already hinted in the tests with TanDEM-X and PRISMA. In contrast, the resulting trajectory from PROD B is smoother and continuous for the complete period under

analysis, which provides an indication of the performance of the maneuver estimation capabilities of the algorithm.

Similarly, for TanDEM-X and PRISMA, dummy maneuvers can be a useful resource for evaluation of the impact of each maneuver strategy, supporting the discussion of results in Section 4.1.2. In this case, solutions obtained during maneuver-free periods can be used for the assessment of solutions with introduced dummy maneuvers. Alternatively, based on the results with GRACE data, solutions from PROD B can be used as reference for evaluating the impact of uncertainties in the modeling of true maneuvers in solutions from PROD A. Such an evaluation may provide, in addition, an indication of the capabilities of the PROD

A scheme and add quantitative evidence regarding its maneuver handling strategy.

To this end, several solutions are computed with PROD A using different values of added process noise during maneuver execution, until a good agreement with PROD B solutions is achieved by trial and error. As an example, Figs. 4 (bottom) and 5 (bottom) show the resulting assessment of the corresponding TanDEM-X and PRISMA solutions, respectively. As observed, the overall consistency in both cases has been improved during maneuver periods. However, some large differences remain during periods of intense maneuvering activity in the case of PRISMA. These results suggest that the used maneuver modeling strategy in PROD A may perform reasonably well in terms of relative orbit determination, subject to a proper configuration. Nevertheless, finding the best maneuver modeling values in more general cases might prove to be a very difficult task, which represents a potential disadvantage of such a strategy.

4.2. Maneuver estimation assessment

Aside from the benefits of maneuver estimation on relative orbit solutions, the resulting estimated values may represent an important asset for an improved maneuver planning in flight dynamics operations. In this way, an evaluation of the resulting maneuver estimates from the orbit determination schemes under analysis is of major importance. The present section elaborates on two assessment strategies based on a comparison with telemetry-reconstructed values and a statistical analysis of estimates.

4.2.1. Telemetry data

Precise maneuver planning typically requires an interplay of several factors, including flight dynamics operations and propulsion systems. Although Δv and t_{cob} are parameters that can be planned based only on the current and final orbits (from orbit determination), the actual delivered Δv depends on the knowledge of

the mass flow rate and specific impulse within the propulsion system. In addition to errors stemming from the applied maneuver models, telemetry-reconstructed maneuvers are subject to errors due to inaccurate predicted pressure and temperature values from the propulsion system. In addition, autonomous attitude control schemes may cause an unpredictable contribution to the final Δv (Chatel, 2015). Consequently, such maneuvers are typically compared with estimates from POD in order to evaluate their performance, as POD processing benefits from GPS measurements and typically delivers more accurate values. For the present purposes, an inter-product consistency check of estimated maneuvers from the schemes under analysis can be carried out by computing the relative errors with respect to (or equivalently the performance of) telemetry-reconstructed maneuvers. Given that POD solutions are available from routine operations, maneuver estimates from both POD and PROD are compared in this assessment. In addition to values from fixed solutions, this analysis includes estimates from PROD float solutions, which are typically more robust (less vulnerable to wrong ambiguity estimates) and already benefit from differential GPS techniques.

Fig. 7 shows the relative error of 10 estimated maneuvers with respect to telemetry-reconstructed values for the GRACE B spacecraft, as a function of maneuver magnitude. In general, the three orbit determination schemes show consistent relative error values below 3%. As the maneuver estimation performance is directly determined by GPS observations and the estimation scheme, maneuvers with smaller magnitude tend to exhibit higher relative errors. In contrast, for example, the difference between estimates and reconstructed values for the large swap maneuver (executed on 12 December, 2005) with magnitude of about 10 cm/s, has a relative error well below 1%. In general, the average relative error for the sample under analysis is about 1.14% for both PROD solutions and 1.17% for POD

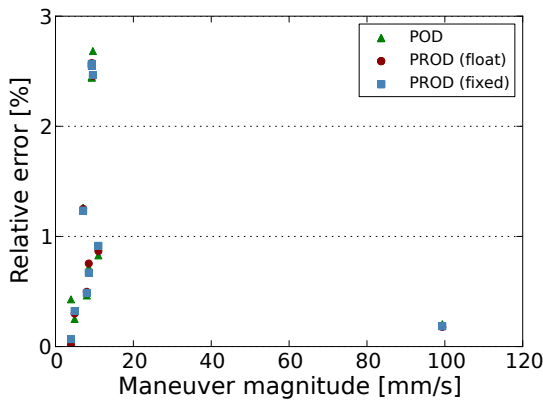


Fig. 7 Relative errors of estimated maneuvers from POD and PROD (float and fixed) solutions for the GRACE B spacecraft as a function of maneuver magnitude. Telemetry-reconstructed maneuvers are used as reference.

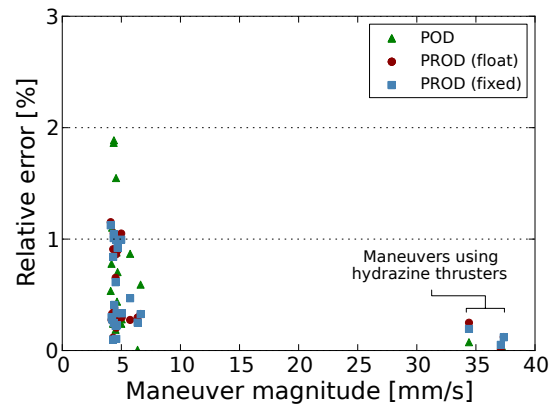


Fig. 8 Relative errors of estimated maneuvers from POD and PROD (float and fixed) solutions for the TDX spacecraft as a function of maneuver magnitude. Telemetry-reconstructed maneuvers are used as reference.

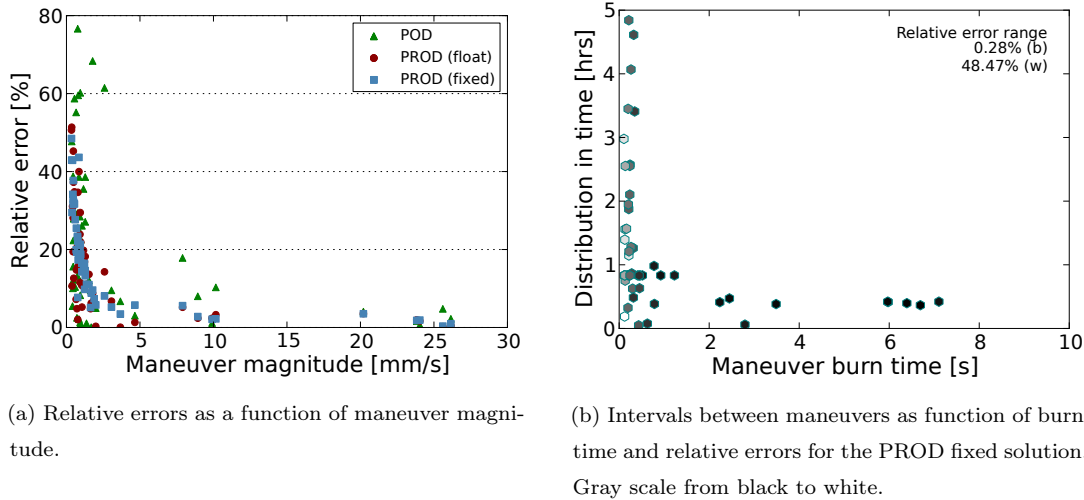


Fig. 9 Analysis of estimated maneuvers from POD and PROD (float and fixed) solutions for the Mango spacecraft, using telemetry-reconstructed maneuvers as reference. Only maneuvers below 30 mm/s and 10 s are shown for clarity.

solutions.

For the TDX spacecraft, Fig. 8 shows the relative error of 24 estimated maneuvers, again with respect to telemetry-reconstructed values and as a function of maneuver magnitude. As with the case of GRACE B, small maneuvers exhibit larger relative errors, which are similarly executed by GN_2 thrusters. Three larger maneuvers of about 35 mm/s using H_2N_4 thrusters are executed within the period under analysis, which show relative errors below 0.5%. In general, all three orbit determination schemes exhibit relative errors below 2% with average values of 0.47% for both PROD solutions and of 0.56% for POD solutions.

The analysis for the Mango spacecraft has been done with 61 maneuvers executed during the AFC 2 operation slot of the SAFE (see Section 3.2). At the beginning of mission, the achievable minimum impulse bit (MIB) amounted to 0.1 Ns (which translates to 0.7 mm/s), which decreased with time due to its dependency on tank pressure. As the MIB determines directly the minimum achievable Δv that can be executed by the propulsion system, by the time of implementation of AFC 2, the minimum achievable Δv reached the level of about 0.3 mm/s. Given the maneuver estimation capabilities in single-frequency orbit determination, the relative error of estimates for such small maneuvers with respect to telemetry-reconstructed values is expected to increase to different levels in comparison to what has been obtained with GRACE B and TDX.

Table 5 RMS errors of differences between estimated maneuvers from POD and PROD (float and fixed) solutions and telemetry-reconstructed maneuvers for the PRISMA mission.

	RMS error (mm/s)		
	Radial	Along-track	Cross-track
POD	0.59	0.47	0.40
PROD float	0.17	0.25	0.30
PROD fixed	0.18	0.24	0.30

Fig. 9a shows the relative errors with respect to telemetry-reconstructed values of estimated maneuvers as a function of maneuver magnitude. In this case, the difference in performance of the three orbit determination schemes is more pronounced as relative errors reach levels beyond 10%. On average, the resulting relative error values are 21.52% for POD solutions and 15.20% and 16.84% for PROD float and fixed solutions, respectively. In addition, due to the number of maneuvers under analysis, it is possible to retrieve some statistical information about the differences between estimated and reconstructed maneuvers, as shown in Table 5. As hinted from the analysis depicted in Fig. 9a, estimates from POD exhibit larger RMS errors in comparison with PROD-estimated values, whose error levels are below 0.3 mm/s for the three orbital directions and both types of solutions.

At this point, it must be noted that the obtained relative errors mostly denote discrepancies between estimated and reconstructed values from each method. As such, each of the discussed approaches has different sources of errors that are being reflected in this assessment. On one hand, as briefly stated before, inexact models and predicted values from the propulsion system may lead to an inaccurate reconstruction of delivered thrust from telemetry data, being particularly noticeable for small and short duration maneuvers (as in the case of Mango). On the other hand, the precise estimation of small thrust maneuvers in orbit determination is much more dependent on the available data in order to be able to properly discriminate them from other non-modeled non-conservative perturbations. This interplay of factors may be grasped from Fig. 9b. The plot depicts the distribution of maneuvers in time (i.e. the relative distance between consecutive maneuvers), as a function of maneuver burn time and relative error of PROD fixed solutions. As observed,

many maneuvers with short burn times (below 1 s) and small inter-maneuver distances (below 1 h) show large relative errors. This might suggest that accurate reconstructed and/or estimated values for small, short duration maneuvers with high execution rates are particularly difficult to obtain. However, from a relative error analysis it is not completely possible to discuss the actual performance of each individual strategy.

4.2.2. Statistical analysis

Although the analysis of relative errors carried out in Section 4.2.1 is a useful tool as an inter-product consistency check, it is difficult to separate errors stemming from orbit determination and telemetry data in order to effectively assess estimated maneuvers. An analysis of absolute errors requires the use of reference (*true*) values, which is not possible for actual executed maneuvers. However, such an analysis can be carried out by using the concept of dummy maneuvers, as introduced in Section 4.1.3. The key idea for these tests is to intro-

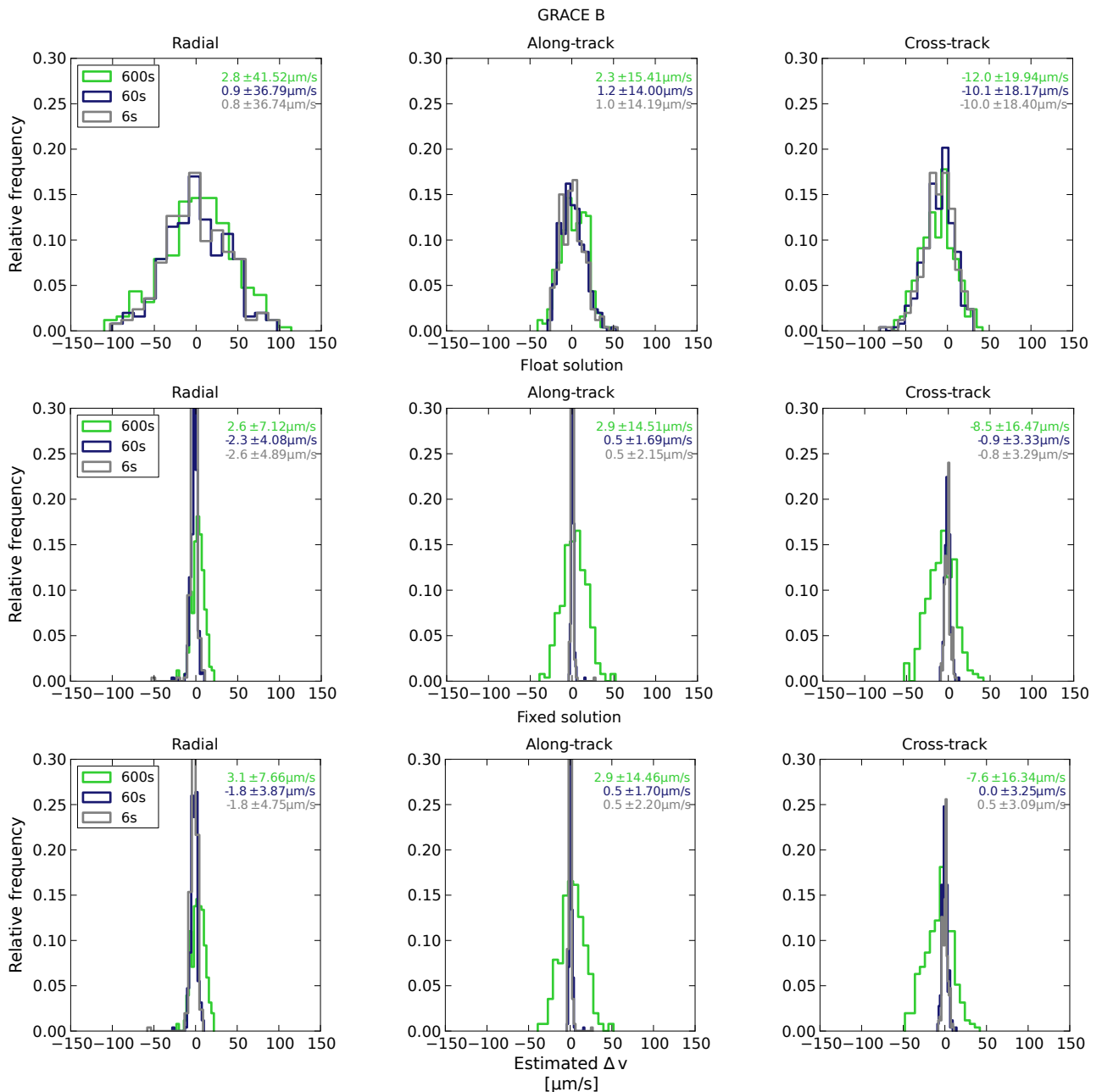


Fig. 10 Frequency distribution of estimated maneuvers from POD (top), PROD float (middle) and fixed (bottom) solutions in dual-frequency mode for the GRACE formation.

duce zero-valued maneuvers into the estimation scheme at regular intervals during maneuver-free periods, with initial constraints of 1 m/s (i.e. for *quasi*-free maneuver estimation). Given that dummy maneuvers have an exactly known true magnitude of zero, they can be used for comparison with the estimated values. If this test is run for a large number of maneuvers, it is possible to perform an analysis on the statistical distribution of estimates. Three representative duration-sets for each mission are used during these tests in order to assess the performance of the estimation methods to different

duration values. In the absence of other sources of information, the obtained distributions provide a good characterization of the statistical properties of each maneuver estimate.

For the GRACE mission, a 10-days period of year 2009 has been analyzed. During this period, daily POD and PROD (float and fixed) solutions are computed using three maneuver-duration sets of 6, 60 and 600 s introduced at one-hour intervals, except for the initial and final points of the orbit, giving a total of more than 250 maneuvers. For simplicity, the analysis is

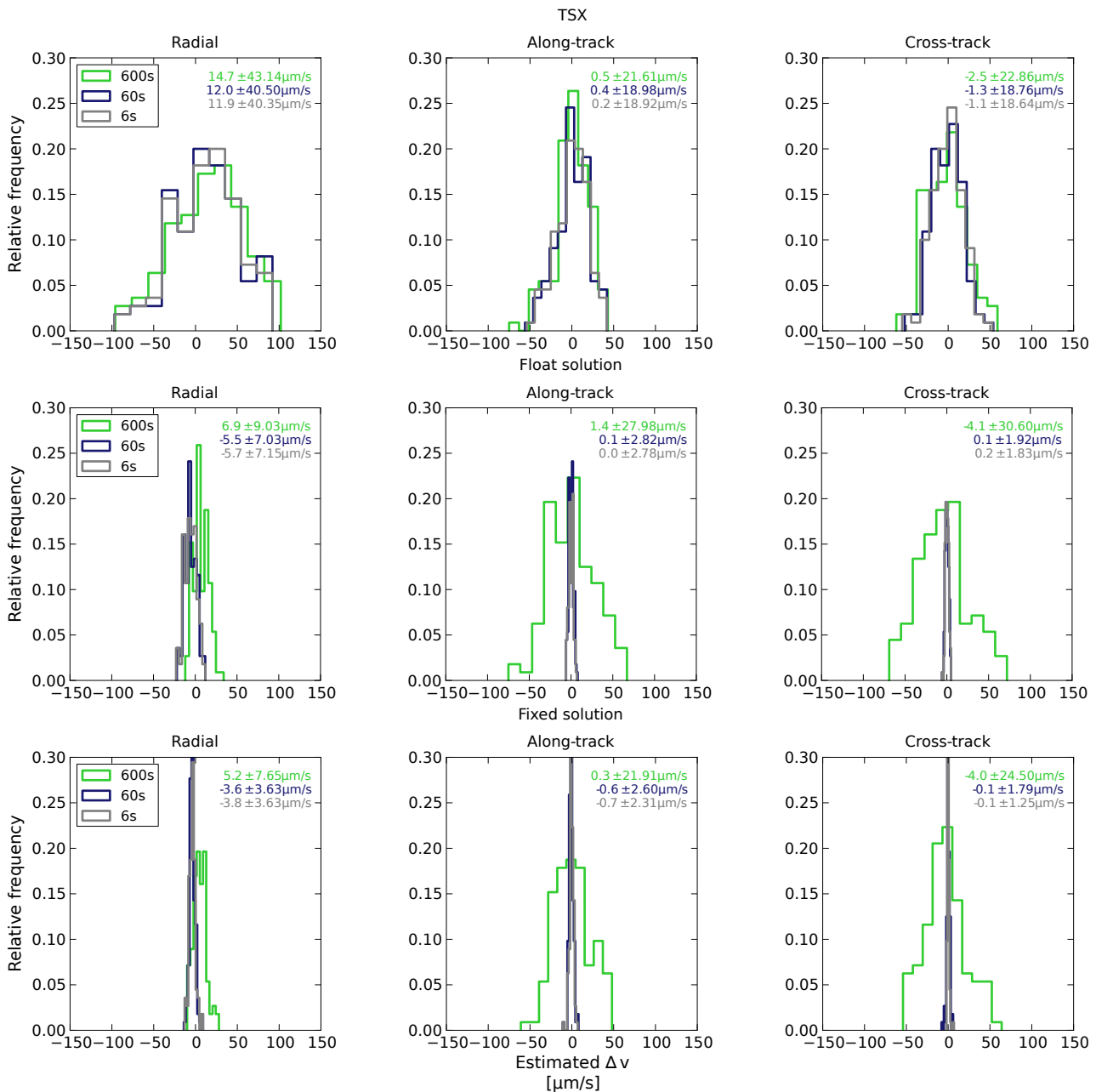


Fig. 11 Frequency distribution of estimated maneuvers from POD (top), PROD float (middle) and fixed (bottom) solutions in dual-frequency mode for the TanDEM-X formation.

limited to the GRACE B spacecraft. As illustrated in Fig. 10 (top), the frequency distribution of maneuver estimates from POD depicts a (quasi-) normal distribution for the three local orbital components for the maneuver-duration sets under test. The estimates in the along-track and cross-track directions exhibit 1σ errors in the range of 14–20 $\mu\text{m/s}$ and slightly biased estimates in the cross-track direction are present. In comparison, estimates in the radial component exhibit around twice as large errors. The observed maneuver estimation errors can be understood by correlation with the estimation of empirical accelerations in the POD process. A priori uncertainties in the dynamical model (as reflected in the estimated empirical accelerations) result in a reduced stiffness of the modeled trajectory and render the detection/estimation of maneuver-induced orbit changes more difficult.

In the case of PROD, uncertainties in the relative dynamics are lower than those in the absolute accelerations given that both spacecraft experience almost the same orbital perturbations. Hence, tighter constraints on the estimated relative empirical accelerations make it possible to estimate changes in the dynamics of the formation with higher precision. Such improvement on maneuver estimates can be grasped in the frequency distributions depicted in Fig. 10 (middle and bottom). Estimates of relative empirical accelerations from float and fixed solutions benefit from common error reduction/cancellation when processing single-difference GPS observations. In particular, it can be noticed that float solutions already provide an approximate sixfold improvement of estimates in the along-track and cross-track directions with respect to values from POD for maneuver-duration sets of 6 and 60 s, which is roughly consistent with the ratio of empirical accelerations in the relative and absolute orbit models. This improvement is much more conservative for the case of 600-s maneuvers, which mainly reflects the uncertainties in the dynamical model, absorbed by such estimates dur-

ing this (larger) period. In contrast, the approximate sixfold improvement of estimates in the radial direction is kept for all three maneuver-duration sets mostly due to the tighter constraints used for estimation of relative radial empirical accelerations.

In general, maneuver estimates from fixed solutions are only slightly better than those from float solutions, which reflects that although estimates of relative empirical accelerations are improved, maneuver estimates still absorb uncertainties in the dynamical model for GRACE B. For maneuver-duration sets of 6 and 60 s, 1σ errors lie in the range of 1.7–5 $\mu\text{m/s}$. The overall improvement in estimates of 600-s maneuvers from fixed solutions is much smaller.

For the case of the TanDEM-X mission, a series of similar tests were conducted. Introducing dummy maneuvers with duration sets of 6, 60 and 600 s during the 10-days period under analysis, a total of more than 110 maneuvers (due to the lower number of maneuver-free periods) could be used for this statistical test. Fig. 11 (top) shows the frequency distribution of maneuver estimates from POD for the TSX spacecraft. In the along-track and cross-track directions, the estimates exhibit 1σ errors in the range of 18–22 $\mu\text{m/s}$. As in the case of GRACE B (cf. Fig. 10 (top)), the largest uncertainties are obtained in the radial direction. Similar to tests with GRACE, PROD float and fixed solutions provide improved maneuver estimates due to the lower uncertainty on relative dynamics. Particularly, float solutions give estimates with 1σ precision in the range of 1.8–7.2 $\mu\text{m/s}$ in the three directions for 6 and 60 s of maneuver duration, as shown in Fig. 11 (middle). Fixed solutions provide slightly better estimates (1σ precision in the range of 1.3–3.7 $\mu\text{m/s}$) for all three directions for duration-sets of 6 and 60 s. The overall largest amelioration with respect to POD and PROD float solutions occurs in the radial direction, even for 600-s maneuvers.

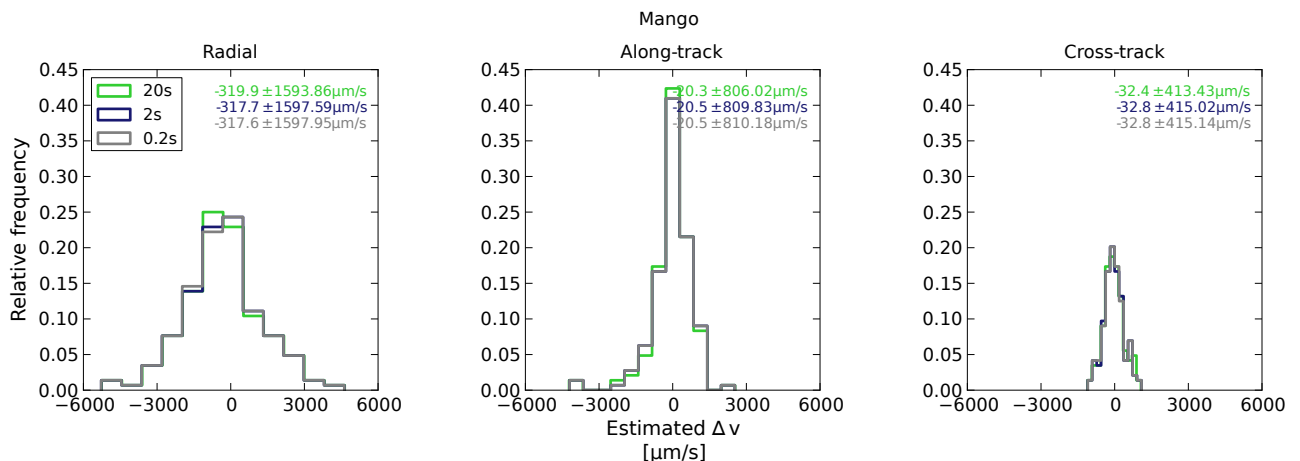


Fig. 12 Frequency distribution of estimated maneuvers from POD solutions for the Mango spacecraft.

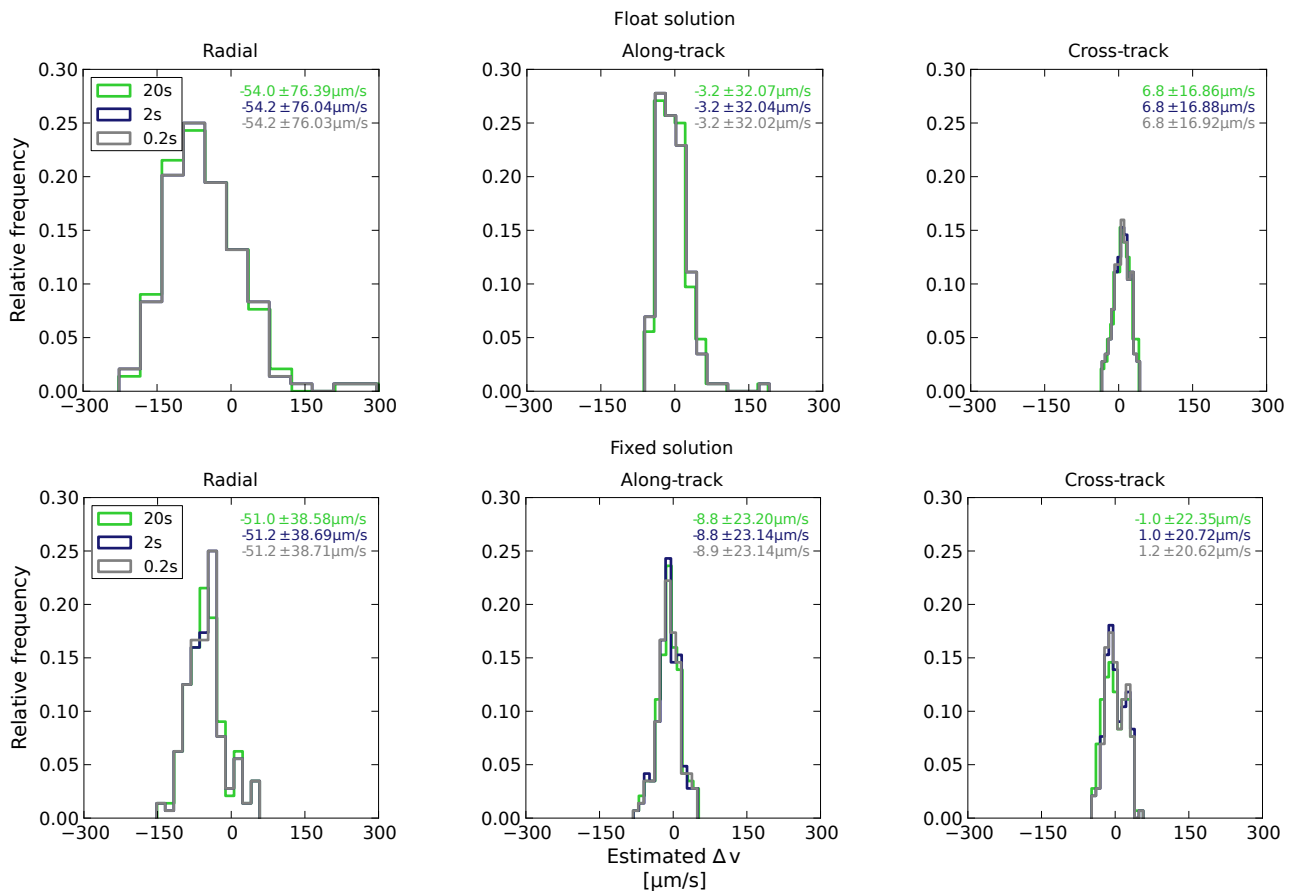


Fig. 13 Frequency distribution of estimated maneuvers from PROD float (top) and fixed (bottom) solutions for the PRISMA formation (Mango spacecraft).

For the PRISMA mission, the statistical analysis of maneuver estimates was conducted for the Mango spacecraft. For these tests, more representative maneuver-duration sets of 0.2, 2 and 20 s were selected. Given that maneuver-free periods with short baselines are much more scarce, and considering the selected duration sets, dummy maneuvers were inserted at 15 min intervals in a period of 4 days, giving a total of more than 140 maneuvers for analysis. Fig. 12 depicts the frequency distribution of maneuver estimates from POD for the Mango spacecraft. As expected from the quality of observations (see Table 2), the initial uncertainty of the introduced maneuvers and the use of single-frequency observations, the resulting estimates exhibit a much larger dispersion in comparison with the GRACE B and TSX cases. For all three components and maneuver-duration sets, 1σ -error estimates are located in the range of 0.41–1.6 mm/s with non-negligible biases of up to -0.32 mm/s in the radial direction. While not immediately obvious, this bias can be readily explained by a radial error (with an inferred size of about 1.8 cm) in the adopted GPS antenna location. Within the orbit determination process, the measurement residuals are minimized by shifting the center of mass by a

corresponding amount relative to the true trajectory. This shift can either be accomplished by a constant empirical acceleration of about 90 nm/s² in radial direction, or alternatively, by radial velocity increments of about 0.32 mm/s once every hour. Since no phase patterns calibrations could be obtained in the PRISMA mission, all POD and PROD solutions make use of an antenna reference point close to the geometric antenna center. As such, a phase center error of the aforementioned magnitude is highly plausible and constitutes the most likely explanation for the observed maneuver estimation error.

Maneuver estimates from PROD float solutions are notably improved with respect to values from POD, exhibiting 1σ errors in the range of 0.02–0.08 mm/s for all three components and maneuver-duration sets with biases up to -0.05 mm/s, as shown in Fig. 13 (top). Compared to POD, the radial maneuver estimation error is notably smaller since both Mango and Tango use identical antennas. The differential phase center error introduced by the different accommodation is therefore substantially smaller than the absolute error, which ultimately reduces the systematic error in the maneuver estimation. Although the benefit on along-track and

cross-track components is larger in comparison with the radial direction, the impact of using differential carrier phase observations leads to an overall twenty-fold improvement in the precision of maneuver estimates. On the other hand, a further slight improvement from the fixed solution has been achieved, particularly in estimates in the along-track and radial directions, as depicted in Fig. 13 (bottom), achieving 1σ errors in the range of 0.02–0.04 mm/s. In contrast, estimates in the cross-track direction are slightly worse in comparison with values from the float solution. Given that integer ambiguities are introduced as known quantities into the relative orbit adjustment for the fixed solution, errors due to unaccounted differential ionospheric delays can no longer be absorbed by float ambiguities and hence may be reflected in other estimates. In the case of maneuver estimates, this affection is reflected particularly in the cross-track direction due to its uncoupling from in-plane components.

In general, the error levels of estimates from PROD solutions hinted by these statistical tests suggest the suitability of using such estimates for maneuver evaluation and calibration in flight dynamics operations. Similarly, such an analysis also indicates that the tests described in Section 4.2.1 provide representative values of the actual achieved performance (and error levels) of telemetry-reconstructed maneuvers for the three missions examined in this study.

5. Summary and conclusions

The present study introduced a method for precise relative orbit determination and maneuver estimation for distributed spacecraft missions using GPS data. The estimation strategy consists of a batch adjustment of absolute reference and relative trajectories using a reduced-dynamics approach. In addition, the scheme makes use of a dedicated algorithm for integer ambiguity resolution. Maneuver estimates are generated as part of the relative orbit solution.

The method has been tested using flight data from the GRACE, TanDEM-X and PRISMA missions. An assessment of baseline precision using GRACE data during periods with maneuvering activity suggests the feasibility of generating solutions with precision comparable to maneuver-free periods. For TanDEM-X and PRISMA, an inter-product consistency check with solutions from a PROD estimation scheme used in routine operations has shown that the presented scheme generates solutions with improved quality during periods with maneuvering activity.

An evaluation of (relative errors of) maneuver estimates using telemetry-reconstructed maneuvers has shown that for maneuvers of GRACE and TanDEM-X, an inter-product consistency below 3% can be achieved. For PRISMA, a much larger uncertainty among estimates from orbit determination and telemetry data was found. In order to evaluate absolute errors of maneuver estimates, a series of statistical tests have been

performed, using the concept of dummy maneuvers. Overall, these statistical tests provide an indication of the expected accuracy of estimated maneuvers using POD and PROD strategies. Without loss of generality, the formation control requirements of most remote sensing missions impose the implementation of maneuvers with magnitudes ranging from 0.5–1 mm/s to 10–20 cm/s, for which the presented PROD algorithm may provide estimates with rough error levels in the range of 10% (worst case for small maneuvers and single-frequency processing) to 0.1–0.01% (best case for large maneuvers and dual-frequency processing).

Acknowledgments

The present study makes use of data that have been made available by the JPL's Physical Oceanography Distributed Active Archive Center (PODAAC), the GeoForschungsZentrum (GFZ) Postdam, the European Space Agency (ESA/ESTEC) Noordwijk, the Center for Orbit Determination in Europe (CODE) and the International GNSS Service (IGS). The support of all these institutions has been essential for this work and is gratefully acknowledged. The authors thank Stefan Hackel for his assistance during the analysis of data from the TanDEM-X mission. Additionally, the authors are grateful to three anonymous reviewers for the provided comments that helped to enhance the original manuscript. GAA wishes to thank the support provided by the Consejo Nacional de Ciencia y Tecnología de México, the Deutscher Akademischer Austauschdienst and the TUM Graduate School.

References

- Allende-Alba, G., Montenbruck, O., 2016. Robust and precise baseline determination of distributed spacecraft in LEO. *Adv. Space Res.* 57 (1), 46–63. <http://dx.doi.org/10.1016/j.asr.2015.09.034>.
- Anflo, K., Möllerberg, R., 2009. Flight demonstration of new thruster and green propellant technology on the PRISMA satellite. *Acta Astronaut.* 65 (9–10), 1238–1249.
- Arbinger, C., D'Amico, S., Eineder, M., 2004. Precise ground-in-the-loop orbit control for low earth observation satellites. In: *Proceedings of the 18th International Symposium on Spaceflight Dynamics*, Munich, Germany.
- Ardaens, J.-S., Montenbruck, O., D'Amico, S., 2010. Functional and performance validation of the PRISMA precise orbit determination facility. In: *Presented at the ION International Technical Meeting*, San Diego, California, Jan 25–27.
- Ardaens, J.-S., D'Amico, S., Montenbruck, O., 2011. Final commissioning of the PRISMA GPS navigations system. In: *Presented at the 22nd International Symposium on Spaceflight Dynamics*, Sao Jose dos Campos, Brazil, Feb 28–Mar 4.
- Barbier, C., Derauw, D., Orban, A., Davidson, M.W.J., 2014. Study of a passive companion microsatellite to the SAOCOM-1B satellite of Argentina, for bistatic and interferometric SAR applications. In: *Proceedings SPIE 9241, Sensors, Systems and Next-Generation Satellites XVII*, Nov 11.
- Bertiger, W., Desai, S.D., Haines, B., Harvey, N., Moore, A.W., Owen, S., Weiss, J.P., 2010. Single receiver phase ambiguity resolution with GPS data. *J. Geodesy* 84 (5), 327–337. <http://dx.doi.org/10.1007/s00190-010-0371-9>.
- Chatel, F., 2015. Propulsion Subsystem Operations. In: Uhlig, T., Sellmaier, F., Schmidhuber, M. (Eds.), *Spacecraft Operations*. Springer.

- D'Amico, S., Arbinger, S., Kirschner, M., Campagnola, S., 2004. Generation of an optimum target trajectory for the TerraSAR-X repeat observation satellite. In: Proceedings of the 18th International Symposium on Spaceflight Dynamics, Munich, Germany.
- D'Amico, S., Montenbruck, O., 2006. Proximity operations of formation-flying spacecraft using an eccentricity/inclination vector separation. *J. Guid. Contr. Dynam.* 29 (3), 554–563. <http://dx.doi.org/10.2514/1.15114>.
- D'Amico, S., Ardaens, J.-S., Larsson, R., 2012. Spaceborne autonomous formation-flying experiment on the PRISMA mission. *J. Guid. Contr. Dynam.* 35 (3), 834–850. <http://dx.doi.org/10.2514/1.55638>.
- D'Amico, S., Bodin, P., Delpech, M., Noteborn, R., 2013a. PRISMA. In: D'Errico, M. (Ed.), *Distributed Space Missions for Earth System Monitoring*. Springer.
- D'Amico, S., Ardaens, J.-S., De Florio, S., 2013b. Autonomous formation flying based on GPS - PRISMA flight results. *Acta Astronaut.* 82 (1), 69–79.
- Dach, R., Lutz, S., Walser, P., Fridez, P. (Eds.), 2015. *Bernese GNSS Software Version 5.2. User manual*. Astronomical Institute, University of Bern, Bern Open Publishing. <http://dx.doi.org/10.7892/boris.72297>.
- Flechtner, F., Watkins, M., Morton, P., Webb, F., 2012. Status of the GRACE Follow-on mission. In: Presented at the Joint GSTM/SPP Final Colloquium, Postdam, Germany, Sep 17.
- Jäggi, A., Hugentobler, U., Bock, H., Beutler, G., 2007. Precise orbit determination for GRACE using undifferenced or doubly differenced GPS data. *Adv. Space Res.* 39 (10), 1612–1619. <http://dx.doi.org/10.1016/j.asr.2007.03.012>, 2007.
- Jäggi, A., Dach, R., Montenbruck, O., Hugentobler, U., Bock, H., Beutler, G., 2009. Phase center modeling for LEO GPS receiver antennas and its impact on precise orbit determination. *J. Geodesy* 83, 1145–1162. <http://dx.doi.org/10.1007/s00190-009-0333-2>.
- Jäggi, A., Montenbruck, O., Moon, Y., Wermuth, M., König, R., Michalak, G., Bock, H., Bodenmann, D., 2012. Inter-agency comparison of TanDEM-X baseline solutions. *Adv. Space Res.* 50 (2), 260–271. <http://dx.doi.org/10.1016/j.asr.2012.03.027>.
- Ju, B., Gu, D., Herring, T.A., Allende-Alba, G., Montenbruck, O., Wang, Z., 2015. Precise orbit and baseline determination for maneuvering low Earth orbiters. *GPS Solut.* <http://dx.doi.org/10.1007/s10291-015-0505-x>, On press.
- Kahle, R., Schlepp, B., Saika, A., Kirschner, M., Wermuth, M., 2012. Flight dynamics operations of the TanDEM-X formation. In: Presented in SpaceOps Conference, Stockholm, Sweden, Jun 11–15.
- Kirschner, M., Montenbruck, O., Bettadpur, S., 2001. Flight dynamics aspects of the GRACE formation flying. In: Presented at the 16th International Symposium on Spaceflight Dynamics, Pasadena, California, Dec 3–7.
- Krieger, G., Hajnsek, I., Papathanassiou, K.P., Younis, M., Moreira, A., 2010. Interferometric synthetic aperture radar (SAR) missions employing formation flying. *Proc. IEEE* 98 (5), 816–843.
- Kroes, R., Montenbruck, O., Bertiger, W., Visser, P., 2005. Precise GRACE baseline determination using GPS. *GPS Solut.* 9, 21–31.
- Kroes, R., Precise relative positioning of formation flying spacecraft using GPS. PhD Thesis, TU Delft, 2006.
- Montenbruck, O., van Helleputte, T., Kroes, R., Gill, E., 2005. Reduced dynamic orbit determination using GPS code and carrier measurements. *Aerosp. Sci. Technol.* 9 (3), 261–271. <http://dx.doi.org/10.1016/j.ast.2005.01.003>.
- Montenbruck, O., Gill, E., 2005. *Satellite Orbits*. Springer-Verlag, Heidelberg.
- Montenbruck, O., Wermuth, M., Kahle, R., 2011–2012. GPS based relative navigation for the TanDEM-X mission – first flight results. *NAVIG.: J. Inst. Navig.* 58 (4), 293–304, Winter.
- Rangsten, P., Johansson, H., Bendixen, M., Jonsson, K., Bejhed, J., Grönland, T.-A., 2011. MEMS Micropropulsion Components for Small Spacecraft. In: Proceedings of the 25th Annual AIAA/USU Conference on Small Satellites, Logan, UT, USA, Aug 8–11.
- Schelkle, M., 2000. The GRACE cold gas attitude and orbit control system. In: Proceedings of 3rd International Conference on Spacecraft Propulsion, Cannes, France, Dec.
- Tapley, B.D., Bettadpur, S., Watkins, M., Reigber, C., 2004. The gravity recovery and climate experiment: mission overview and early results. *Geophys. Res. Lett.* 31 (9). <http://dx.doi.org/10.1029/2004GL019920>.
- Wu, S.C., Yunck, T.P., Thornton, C.L., 1991. Reduced-dynamic technique for precise orbit determination of low Earth satellites. *J. Guid. Contr. Dynam.* 14 (1), 24–31.
- Yoon, Y., Montenbruck, O., Kirschner, M., 2006. Precise maneuver calibration for remote sensing satellites. In: Presented at the 19th International Symposium on Space Flight Dynamics, Kanazawa, Japan, Jun 4–11.
- Yunck, T.P., Wu, S.C., Wu, J.T., Thornton, C.L., 1990. Tracking of Remote Satellites with the Global Positioning System. *IEEE Trans. Geosci. Rem. Sens.* GE-28 (1), 108–116.
- Yunck, T.P., 1993. Coping with the atmosphere and ionosphere in precise satellite and ground positioning. In: Valance-Jones, A. (Ed.), *Environmental Effects on Spacecraft Trajectories and Positioning*, AGU monograph.
- Zhu, S., Reigber, Ch., König, R., 2004. Integrated adjustment of CHAMP, GRACE and GPS data. *J. Geodesy* 78 (1), 103–108.

Acknowledgements

The long to road to start learning to do research cannot be walked without a guidance. It is for this invaluable guidance that I would like to express my gratitude to Oliver Montenbruck, who gave me the opportunity to begin this journey with such an interesting topic. Likewise, I want to gratefully acknowledge Urs Hugentobler and Pieter Visser for their valuable review for this dissertation.

I would like to particularly express my thankfulness to Oliver Montenbruck for his support during all the stages of this research. During this time, the conversation sessions and uncountable discussions with him were always very fruitful and thought-provoking, which allowed me to learn a lot. I want to extend my gratitude to Urs Hugentobler for the many interesting discussions that helped me during this research. His support throughout this period was essential for the completion of this work. Likewise, I want to acknowledge the assistance provided by Annette Spengler at the TUM Graduate School. I also would like to thank all my colleagues in the GNSS technology and navigation group at GSOC for their kindness and support during my research and my overall stay at the institute. My gratitude also to all the co-authors of the publications included in this dissertation for the very interesting discussions that were carried out during the preparation of each paper.

Thanks to the communities of the GRACE, TanDEM-X, Swarm and PRISMA missions for their incredible work in the generation of data products, which were fundamental for this dissertation. Likewise, I would like to thank the Center for Orbit Determination in Europe for the generation of GNSS products that were heavily used during this research.

The visualization of many results in this dissertation was possible thanks to the remarkable tools created by the open source community of the C++ and Python languages. I would like to acknowledge their work and effort to produce high quality software that is used everyday to support all kinds of applications and research around the world.

This research was mostly funded by the Mexican National Council for Science and Technology (CONACYT) and the German Academic Exchange Service (DAAD). The support of these institutions is gratefully acknowledged.

Infinitas gracias a Verence, mi compañera de mil batallas. Gracias por su incansable apoyo en cada uno de los días, meses y años de esta travesía. Este logro es nuestro.

Finalmente, quiero agradecer de manera muy especial a mis padres, hermanos y amigos por su gran apoyo y comprensión durante este largo camino recorrido. Todo esto es gracias a ustedes.

